Titre: Title:	Morphological and mechanical study of injection molded HDPE/PA6 blends
Auteur: Author:	Said Fellahi
Date:	1994
Type:	Mémoire ou thèse / Dissertation or Thesis
Référence: Citation:	Fellahi, S. (1994). Morphological and mechanical study of injection molded HDPE/PA6 blends [Thèse de doctorat, École Polytechnique de Montréal]. PolyPublie. https://publications.polymtl.ca/33325/

UNIVERSITÉ DE MONTRÉAL

MORPHOLOGICAL AND MECHANICAL STUDY OF INJECTION MOLDED HDPE/PA6 BLENDS

par

Said FELLAHI

DÉPARTEMENT DE GÉNIE MÉCANIQUE

ÉCOLE POLYTECHNIQUE

THÈSE PRÉSENTÉE EN VUE DE L'OBTENION

DU GRADE DE PHILOSOPHIAE DOCTOR (Ph.D.)

(GÉNIE MÉCANIQUE)

Juin 1994

ISBN 0-315-97139-8

UNIVERSITÉ DE MONTRÉAL

ÉCOLE POLYTECHNIQUE

Cette thèse intitulée :

MORPHOLOGICAL AND MECHANICAL STUDY OF INJECTION MOLDED HDPE/PA6 BLENDS

présentée par Said Fellahi

en vue de l'obtention du grade de : Philosophiae Doctor (Ph.D.)

a été dûment acceptée par le jury d'examen constitué de :

M. SANSCHAGRIN, Bernard, D.Ing., président

M. FISA, Bohuslav, Ph.D., membre et directeur de recherche

M. FAVIS, Basil D., Ph.D., membre et codirecteur de recherche

M. BAKER, Warren E., Ph.D., membre

M. BOUKHILI, Rachid, Ph.D., membre

À mes parents

À mes frères et soeurs

À ma femme et mes enfants Reda, Redouane et Sarah

À mon pays l'ALGÉRIE

en signe d'affection et de reconnaissance

À tous mes amis

SOMMAIRE

Malgré le grand essor dans le développement des mélanges et alliages de polymères, il semble que le moulage par injection de ces matériaux n'a pas été étudié considérablement. On a remarqué également qu'il n'y a pas eu d'études potentielles sur l'effet de lignes de soudure dans les mélanges polymères, ainsi que la relation entre la morphologie, la mise en forme, et les propriétés mécaniques. L'étude entreprise par ce projet se veut une continuité dans la recherche de la compréhension des phénomènes conduisant au développement de morphologies de mélanges de polymères compatibilisés ou non, moulés par injection, et de les relier aux propriétés mécaniques du produit. La présence de lignes de soudure dans ces articles est courante, l'étude de la structure de cette région va être considérée extensivement.

Une étude morphologique très détaillée des mélanges polyethylene haute densité/polyamide-6 (25/75 vol%) moulés par injection, avec et sans compatibilisant, est entreprise, avec un fort accent sur la zone de ligne de soudure plus particulièrement. Un insert peut être installé pour produire la ligne de soudure. Les points essentiels de ces résultats basés sur la microscopie électronique à balayage, l'analyse d'image, la spectroscopie photoelectrons à rayons X (XPS), la microscopie à transmission (TEM) et l'analyse calorimétrique (DSC) sont les suivants : a) existence d'un effet peau/coeur important manifesté sous forme de variation morphologique à travers l'épaisseur i.e phase dispersée très fine dans la peau, très orientée dans la sous-peau et sphérique dans le

coeur. Une analyse de la composition a révélé la présence des deux phases (HDPE et PA-6) sur la surface des plaques et des fronts d'écoulement obtenus à partir des expérience de "sort-shot", avec approximativement la même composition que le mélange original, b) une morphologie plus stable et diminution de l'épaisseur de la peau et de la largeur de la ligne de soudure avec l'ajout d'un compatibilisant. L'apparente absence de la phase dispersée au niveau de la peau ainsi que dans la ligne de soudure n'est qu'un artefact et a été démistifié dans cette étude. Le mécanisme responsable de cette importante réduction de la taille de la phase dispersée observée au niveau du front d'écoulement, de la peau et de la ligne de soudure a été attribué à une rupture des particules à cause de l'écoulement élongationel et à la déformation biaxiale subies par les particules de la phase dispersée au niveau du front d'écoulement.

L'évaluation de l'effet du compatibilisant sur les propriétés mécaniques des mélanges HDPE/PA-6 dépend énormément du type de moule et des conditions du test. Dans les éprouvettes moulées directement sans ligne de soudure, la phase dispersée très orientée dans la direction de sollicitation supporte sa part de chargement. L'effet du compatibilisant sur les propriétés mécaniques est mineure : il est masqué par l'orientation induite par l'écoulement. En présence d'une ligne de soudure, une réduction de 40 % dans les propriétés mécaniques du système non compatibilisé est observée. L'addition d'un compatibilisant permet au matériau de récupérer sa capacité à s'écouler et les propriétés mécaniques sont très proches de celles des échantillons sans ligne de soudure. Pour le deuxième type de moule (plaque), l'effet de la ligne de soudure est moins

prononcé ainsi que l'effet de la distance après l'insert est négligeable. Par conséquent, on peut questionner l'utilité des éprouvettes moulées directement pour étudier les differents aspects reliés aux propriétés mécaniques des systèmes multiphasés surtout en présence de ligne de soudure.

Finalement, les mécanismes de déformation de ces mêmes mélanges moulés par injection ont été étudié en mesurant le changement de volume grâce à la technique de dilatométrie durant un test de traction. Le résultat le plus important de cette étude indique que le mécanisme de déformation qui prédomine dans le mélange non compatibilisé est largement controlé par l'orientation induite par l'écoulement. Les éprouvettes testées dans la direction d'orientation se déforment par écoulement par cisaillement et l'effet du compatibilisant est masqué. L'effet de l'orientation est bien mis en évidence en variant l'épaisseur de la plaque où le rapport peau/coeur est modifié ainsi que la différence très prononcée dans les directions longitudinale est transversale. Les observations microscopiques montrent clairement l'importante orientation dans ces systèmes. Ce phénomène semble être dû principalement à l'orientation de la phase dispersée puisque le polyamide-6 est isotropique.

ABSTRACT

During this last decade there has been an intense activity to tailor new plastics materials in the form of blends and alloys not in polymerization plant which need considerable investment but in conventional processing equipment. During processing, the dispersed phase is deformed and acquire an anisometric configuration. This will result in an anisotropic structure characterised by a distribution of shape factors, concentration and orientation of the dispersed phase throughout the thickness of the molded part.

Injection molding is widely used in plastics processing. It is characterized by a a non-isothermal and complex flow in a closed and cooled mold cavity. This results in an anisotropic skin/core structure. This structure will be even more complicated when the cavity is either double gated, in the presence of an insert or with variable thickness giving bearth to weldlines.

The first part of this study deals with a review on the origin of weldlines, their effects in injection molded neat, filled or reinforced plastics, as well as polymer blends and finally the methods developped to aleviate this weakness. The aspect of weldline in polymer blends was found to be less and the least documented.

The morphology of immiscible polymer blends in injection molding remains a largely unexplored area. The presence of weldlines in injection molded articles is a well-known defect, which limits the use of plastic materials. This weakness is even more serious with polymer blends. The second part of this study deals with a detailed morphological investigation of injection molded high density polyethylene/polyamide-6 (25/75 vol%) blends, with and without compatibilizer, especially at the weldline region. An insert was used to generate the weldline, and short shots were performed in order to observe the evolution of the morphology as the mold is filled. A detailed morphological analysis of the skin and weldline region was undertaken using scanning electron microscopy and image analysis. The results evidenced the following features: a) significant skin-core effect, b) diminution of the thickness of the skin and weldline regions with interfacial modification and c) apparent absence of the minor phase in the skin and weldline region. The existence of a morphological variation with respect to the thickness, dispersed phase is highly oriented in the subskin and spherical in the core, is clearly shown in this study. Additional characterisation techniques; X-ray photoelectron spectroscopy (XPS) and differential scanning microscopy (DSC) of microtomed layers from the surface of the plaques revealed that the surface and the weldline region composition of dispersed phase to be very close to the original, as prepared, composition (25/75 vol%). There is therefore no absence of the minor phase in the skin region. Transmission electron microscopy (TEM) reveals the presence of a very fine dispersed phase in the skin with particle dimensions almost one order of magnitude smaller than in the core. The interfacial modifier, a polyethylene methacrylic acid isobutyl acrylate

ionomer, was found to reduce the size of the dispersed phase, the skin thickness, and the width of the weldline. The dimensions of the regions with very fine dispersed phase (skin and weldline) correlate well with those observed in the advancing melt front as analyzed in the short-shot samples. Less coalescence and a more stable morphology is observed. The mechanism responsible for the dramatic dispersed phase reduction observed in the flow front, the skin and the weldline region may be attributed to particle break up resulting from the elongational flow and biaxial stretching that the dispersed phase particles undergo in the melt front.

The third part of the study deals with relationships between the structure and the mechanical properties of the above injection molded blends blends. The weldline effect is investigated in a detailed manner. A double gated tensile bar cavity (type I) and a rectangular plaque mold (type II) with a circular insert were used to produce the weldline. In the directly molded tensile bar the minor phase is strongly oriented parallel to flow. Only in the core, which represents about 10% of the sample thickness, do the dispersed phase particles assume spherical shape. The morphology of the weldline is closely related to that of the skin: the elongated structures are oriented parallel to the weldline plane. The effect of the compatibilizer on the mechanical properties (without the weldline) of the directly molded tensile bars is minor: it is overshadowed by the flow induced morphology. The weldline strength loss is about 40% in the non-compatibilized blend. The introduction of the compatibilizer has restored the material's ability to yield and the properties are close to those measured without the weldline. For the second type

mold, the effect of the weldline is less pronounced and the effect of the distance from the insert is negligible. The anisotropy is quite pronounced in the non-compatibilized blend. In compatibilized blends, all tensile properties are unaffected by the presence of weldline, except for the 2 mm thick plaque in the position close to the insert. The properties in the direction parallel to flow are similar to the type I mold as influenced by flow induced oritation and not affected by the increase of plaque thickness.

Finally as a fourth part of this study, the mechanism of deformation of the above mentioned blends is investigated by monitoring the volume change using tensile dilatometry. Dog-bone specimens were either directly molded or cut from rectangular plaques. Both neat materials and their blends were tested. The most striking results in this study indicate that the deformation mechanism in injection molded non-compatibilized blends is largely controlled by orientation phenomena. Tensile dilatometry experiments taken in the direction of orientation display a predominantly shear yielding process and mimic the behavior of compatibilized systems. The importance of orientation is confirmed in studies varying the plaque thickness where the skin/core ratio is modified and also by the significant difference in longitudinal vs transverse properties. SEM micrographs clearly show the significant orientation in these systems. This phenomena appears to be principally related to the orientation of the dispersed phase since neat PA-6 is isotropic.

RÉSUMÉ

Durant cette dernière décennie, il y a eu une intense activité à confectionner de nouveaux matériaux plastiques sous forme d'alliages et de mélanges de polymères traditionnels, non pas dans des usines de polymérisation qui nécessitent des investissements considérables pour être rentables, mais de préférence sur des équipements de mise en forme existants dans un atelier de transformation régulier. Lors de la mise en oeuvre de ces matériaux, par extrusion ou par injection par exemple, la phase dispersée peut subir des déformations plus ou moins importantes et acquérir une configuration anisométrique. Ceci va résulter en une structure anisotropique caractérisée par une distribution de rapport de forme, de la concentration et de l'orientation de la phase dispersée à travers l'épaisseur de la pièce moulée ou extrudée.

Le moulage par injection est très répandu dans l'industrie de transformation des matières plastiques. Il est caractérisé par un écoulement complexe, et non-isotherme dans une cavité de moule fermé et refroidis. Ceci résulte en une structure peau/coeur anisotropique. Cette dernière va se compliquer davantage lors de la rencontre de fronts d'écoulement issus de différents seuils d'alimentation, à travers un obstacle ou dans un moule ayant des épaisseurs variables, donnant naissance aux lignes de soudures.

Malgré le grand essor dans le développement des mélanges et alliages de polymères, il semble que le moulage par injection de ces matériaux n'a pas été étudié considérablement. On a remarqué également qu'il n'y a pas eu d'études potentielles sur l'effet de lignes de soudure dans les mélanges polymères, ainsi que la relation entre la morphologie, la mise en forme, et les propriétés mécaniques.

Des variations de compositions au voisinage de la ligne de soudure ont été observées, mais non expliquées. Par conséquent, il est nécessaire d'entreprendre une étude afin d'établir une relation entre les morphologies observées et les propriétés mécaniques résultantes, et parer ainsi à cette lacune.

L'étude entreprise par ce projet se veut une continuité dans la recherche de la compréhension des phénomènes conduisant au développement de morphologies de mélanges de polymères compatibilisés ou non, moulés par injection, et de les relier aux propriétés mécaniques du produit. La présence de lignes de soudure dans ces articles est courante, l'étude de la structure de cette région va être considérée extensivement.

Une analyse de la microstructure d'échantillons découpés à plusieurs positions nous procure une idée sur l'effet de chaque paramètre dans le développement d'une morphologie donnée. Nous tentons de fournir des explications concernant la présence ou l'absence des variations de la composition dans le voisinage de la ligne de soudure et établir une relation entre la structure et les propriétés mécaniques.

Le système utilisé dans cette étude est le HDPE/PA6 (25/75 vol %) avec ou sans compatibilisant préparé au préalable sur une extrudeuse à double vis. Les différentes formulations seront soumises à une étude rhéologique dans un viscosimètre capillaire. Par la suite, elles seront moulées par injection suivant différentes conditions telles que, le type d'écoulement (plaque ou moulé directement), les paramètres géométriques (diamètre de l'insert, et épaisseur de la plaque), la modification interfaciale (avec ou sans compatibilisant). Des échantillons seront découpés à des positions bien données, puis préparés (microtome et extraction de la phase dispersée par un solvant approprié) afin d'étudier leurs morphologies sous un microscope électronique à balayage ou à transmission en plus de l'analyse calorimétrique et la spectroscopie photoélectrons à rayons X.

Finalement, une caractérisation mécanique, où les tests de traction (caractérisation mécanique classique) et le changement de volume grâce à la dilatométrie (pour déterminer les mécanismes de déformation mis en jeux) sera entreprise.

La première partie de cette étude consiste en une revue bibliographique exhaustive résumant l'origine des lignes de soudure, leurs effets dans les plastiques vierges, chargés ou renforcés, les mélanges polymères moulés par injection et finalement les méthodes disponibles pour les traiter. Il faut noter qu'un manque flagrant d'information sur l'aspect des lignes de soudure dans les mélanges polymères a été observé.

La morphologie des mélanges polymères immiscibles moulés par injection reste encore un domaine de recherche vièrge. La présence de ligne de soudure dans les objets moulés par injection est un défaut reconnu depuis longtemps, ce qui limite leur domaine d'application. Cette faiblesse est plus accentuée encore avec les mélanges polymères. Dans cette deuxième partie, une étude morphologique très détaillée des mélanges polyéthylene haute densité/polyamide-6 (25/75 vol%) avec et sans compatibilisant, est entreprise, avec un fort accent sur la zone de ligne de soudure plus particulièrement. Un insert peut être installé dans la cavité pour divisé le front d'écoulement en deux, conduisant à la formation d'une ligne de soudure ainsi que des expériences de "short-shot" afin de suivre l'évolution de la morphologie pendant le remplissage du moule. Les points essentiels de ces résultats sont les suivants : a) existence d'un effet peau/coeur important, b) diminution de l'épaisseur de la peau et de la largeur de la ligne de soudure avec l'ajout d'un compatibilisant et c) une semblante absence de la phase dispersée au niveau de la peau ainsi que dans la ligne de soudure. Des techniques additionelles telles que la spectroscopie photoelectrons à rayons X (XPS), l'analyse calorimétrique (DSC) d'échantillons microtomés de la surface ont été utilisées pour caractériser quantitativement la composition de la surface des plaques ainsi que celles du front d'écoulement et aussi pour valider l'hypothèse de l'absence de la phase mineure sur la peau et dans la ligne de soudure. Les résultats montrent que la composition de la surface et celle de la ligne de soudure est très proche de celle du mélange d'origine (25/75 vol%). La phase dispersée est bien présente dans la peau de l'échantillon. La microscopie électronique à transmission revelle la présence d'une phase dispersée très

fine dans la peau ayant des dimensions presque 10 fois plus petites que celles dans le coeur de l'échantillon. L'agent interfacial utilisé, un ionomère à base d'acrylate d'isobutyle et d'acide méthacrylique de polyéthylène, avait pour effet de réduire la taille de la phase dispersée, l'épaisseur de la peau et la largeur de la ligne de soudure. Les dimensions des régions contenant une phase dipersée très fine (peau et ligne de soudure) correspondent bien avec celles observées dans le front d'écoulement analysés à partir des échantillons de "short-shot". Une morphologie plus stable et moins de coalescence ont été observé. Le mécanisme responsable de cette importante reduction de la taille de la phase dispersée observé au niveau du front d'écoulement, de la peau et de la ligne de soudure a été attribué à une rupture des particules à cause de l'écoulement élongationel et à la déformation biaxiale subies par les particules de la phase dispersée au niveau du front d'écoulement.

La troisième partie de cette étude traite de l'effet de la ligne de soudure sur les propriétés mécaniques des mélanges mentionnés ci-dessus. Des éprouvettes moulées directement avec un ou deux seuils d'alimentation (type I) ou bien découpées à partir de plaques avec ou sans insert (type II) ont été utilisées. Dans le cas des éprouvettes du type I, la phase dispersée est orientée parallèlement à l'écoulement. Dans le coeur qui représente uniquement 10% de l'épaisseur de l'échantillon, la phase dispersée adopte une forme plus sphérique. La morphologie de la ligne de soudure est très similaire à celle de la peau de l'éprouvette, les structures allongées sont orientées parallèlement au plan de la ligne de soudure. L'effet du compatibilisant sur les propriétés mécaniques (sans

ligne de soudure) des éprouvettes moulés directement est mineure : il est masqué par l'orientation induite par l'écoulement. En présence d'une ligne de soudure, une réduction de 40 % dans les propriétés mécaniques du système non compatibilisé est observée. L'addition d'un compatibilisant permet au matériau de récupérer sa capacité à s'écouler et les propriétés mécaniques sont très proches de celles des échantillons sans ligne de soudure. Pour le deuxième type de moule (plaque), l'effet de la ligne de soudure est moins prononcé ainsi que l'effet de la distance après l'insert est négligeable. L'anisotropie est très prononcée avec le mélange non compatibilisé. Dans le cas où il est compatibilisé, toutes les propriétés mécaniques en tension ne sont pas affectées par la présence de ligne de soudure, excèption faite pour les plaques de 2 mm d'épaisseur dans la position très proche de l'insert. Les propriétés dans la direction longitudinale (parallèle à l'écoulement) sont similaires à celles des échantillons du type I et ne sont pas affectées par une augmentation de l'épaisseur de la plaque. Par conséquent, on peut questionner l'utilité des éprouvettes moulées directement pour étudier les differents aspects reliés aux propriétés mécaniques des systèmes multiphasés surtout en présence de ligne de soudure.

Finalement, dans cette dernière partie de cette étude et afin de mieux comprendre les mécanismes de déformation des mélanges HDPE/ PA-6 (25 vol % / 75 vol %) (compatibilisé ou non) moulés par injection, le changement de volume a été mesuré grâce à la technique de dilatométrie durant un test de traction. Des éprouvettes de traction (dogbone) ont été soit découpées à partir de plaques soit moulées directement. Il faut

noter que ces mélanges ainsi que les matériaux vièrges qui les constituent ont été testés. Pour les éprouvettes moulées directement, tous les matériaux considérés dans cette étude : PA-6, HDPE et leurs mélanges dans les mêmes proportions que ci-dessus, se déforment par écoulement par cisaillement. La nature de la phase dispersée a permis de mettre en évidence l'effet de l'orientation induite par l'écoulement. Dans le cas d'une phase dispersée souple (HDPE), elle n'a d'autres choix que de se déformer en supportant une part des contraintes appliquées et l'effet du compatibilisant est mimé par cette orientation. Par contre, dans le cas d'une phase dispersée rigide (billes de verre) dans les même proportions qu'avant, l'effet du traitement de l'interface est très évident. On passe d'un mode cavitation (45 %)/écoulement par cisaillement à un processus de déformation presque par pur écoulement en cisaillement (85 %). Pour les éprouvettes découpées à partir de plaques de PA-6 ou HDPE, elles se déforment principalement par écoulement par cisaillement. Dans la direction transversale à l'écoulement et pour le mélange non compatibilisé, le mécanisme de déformation est un mélange de cavitation (55 %)/écoulement par cisaillement; par contre, dans la direction longitudinale, c'est un mécanisme par écoulement par cisaillement (80 %). Ceci peut être attribué à l'orientation induite par l'écoulement comme mentionné ci-dessus. L'addition d'un compatibilisant transforme le mécanisme de déformation en écoulement par cisaillement (85 %). Le même comportement est observé dans la direction longitudinale pour les deux mélanges avec ou sans compatibilisant. L'épaisseur de la plaque semble avoir un effet appréciable sur le processus de déformation. Le comportement dilatationnel dépend énormément du type de morphologie engendrée par l'orientation induite par l'écoulement.

Le rapport peau/coeur, qui est une indication de la proportion de la phase dispersée orientée par rapport à celle non orientée, joue un rôle déterminant dans le mécanisme de déformation mis en jeux.

ACKNOWLEDGEMENTS

I would like to take this opportunity to express my deep gratitude and acknowledgements to both my supervisors: Profs B. Fisa and B.D. Favis, for the endless help, support, encouragement and understanding they have given me. Their outstanding teaching and supervising ability is unquestionable and I have learned a lot from them. May they find their effort in this manuscript.

Many thanks go to jury members who accepted to read this thesis: Profs B. Sanschagrin, W.E. Baker and R. Boukhili.

This work would not have been accomplished without the collaboration of the following persons: Prof. R. Boukhili for the numerous discussions I had with him, Prof. A. Selmani, Dr. N. Mekhilef, A. Meddad, R. Adimi, the technical staff of the following laboratories: IMI (C. Degrandprès, M. Carmel), CRASP (L. Loiselle, F. Vachon, H. Ould Brahim, F. St-Louis, L. Parent), chemical (A. Lachapelle and S. Pastuch), mechanical (F. Morin, J. Beausoleil, Jean-Marie Béland), metallurgical (J. Claudinon, R. Veillette, and J. Laviolette) and physics (S. Poulain) departments. Many thanks go to Miss J. Dugas for typing this manuscript.

I would like to thank the Algerian Institute of Petroleum for giving me the opportunity to pursue my doctoral studies.

Last but not least my sincere thanks go to all my friends and my family for their understanding, support and compassion.

TABLE DES MATIÈRES

SOMMAIRE v

ABSTRACT viii

RÉSUMÉ xii

ACKNOWLEDGEMENTS xx

TABLE DES MATIÈRES xxii

LIST OF FIGURES xxvi

LIST OF TABLES xxxvi

INTRODUCTION xxxix

CHAPTER 1 - WELDLINE IN INJECTION MOLDED PARTS: A REVIEW . . 1

1.1 Introduction 3

1.2 Origin of weldline 4

1.3 Methods used to study weldlines 17

1.4 Weldline in neat polymers 25

1.5 Reinforced plastics 47

1.6 Polymer blends 59

1.7 How to deal with weldline 71

1.8 References 79

CHAPTER 2 - MORPHOLOGICAL STABILITY IN INJECTION MOLDED HDPE/PA6 BLENDS 91

2.1 Introduction 93

2.1.1 Weldlines 95

2.2 Experimental 98

2.2.1 Materials 98

2.2.2 Compounding 99

2.2.3 Rheology 100

2.2.4 Injection molding 101

2.2.5 Morphological analysis 103

2.2.5.1 Electron microscopy 103

2.2.5.2 Image analysis 104

2.2.5.3 Transmission electron microscopy (TEM) 104

2.2.6 Differential scanning calorimetry (DSC) 105

2.3.7 X-ray photoelectron spectroscopy (XPS) 105

2.3 Results and discussion 106

2.3.1 Rheology 106

2.3.2 Morphology 106

2.3.2.1 Twin screw extrusion 109

2.3.2.2 Injection molding 110

2.3.2.2.1 Sprue area 110

2.3.2.2.2 Inside the mold cavity 111

2.4 Conclusion 137

2.5 References 138

CHAPTER 3 - WELDLINE STRENGTH IN INJECTION MOLDED HDPE/ PA6 BLENDS: INFLUENCE OF INTERFACIAL MODIFICATION 141

3.1 Introduction 143

3.2 Experimental 148

3.2.1 Materials 148

3.2.2 Compounding 149

3.2.3 Injection molding 149

3.2.4 Tensile testing 150

3.2.5 Tensile dilatometry 152

3.2.6 Scanning electron microscopy 152

3.3 Results and discussion 153

3.3.1 Double gated (type I mold) 153

3.3.2 Plaques (type II) 171

3.4 Conclusion 186

3.5 References 187

CHAPTER 4 - TENSILE DILATOMETRY INJECTION MOLDED HDPE/PA6 190

4.1 Introduction 191

4.2 Experimental 195

4.2.1 Materials 195

4.2.2 Compounding 196

4.2.3 Injection molding 196

4.2.4 Tensile testing 197

4.2.5 Tensile dilatometry 197

4.2.6 Scanning electron microscopy 199

4.3 Results and discussion 200

4.3.1 Directly molded dogbone specimens (type I) 200

4.3.2 Machined from plaque (type II) specimens 209

4.4 Conclusion 223

4.5 References 224

LIST OF FIGURES

Figure 1.1 Fountain flow in an injection mold cavity[14]. A - Progress of the fountain flow; B- Movement of a tracer particle 7

Figure 1.2 Two common causes of weldlines in injection molded parts (mold filling patterns in rectangular cavities) - A: double gated mold; B: mold with two gates side by side. Weldlines are indicated by dashed lines, gates by arrows 11

Figure 1.3 Standard test mold cavity (ASTM-D647)[173] - A: "cold weld"; B: "hot weld" 12

Figure 1.4 Mold cavity with variable thickness[174] - A: Gate located in the thinner section; B: Formation of a pocket of entrapped air 14

Figure 1.5 Weldlines detected by visual inspection in an experimental simple gated mold representing half of a passenger vehicle instrument panel[175] 15

Figure 1.6 Topography of the weldline in time of the mold filling process[154]. A: Straight at time t_1; B: Deformed at time t_2 16

Figure 1.7 Model of a material with a weldline 20

Figure 1.8A Stress/strain curves of directly molded (type I) samples with or without a weldline. An extensometer is placed either on or outside the weldline. A: Polystyrene (PS); Polyamide-6 (PA) and high density polyethylene (PE) 23

Figure 1.8B Cont'd - B: Polycarbonate (PC) and polypropylene (PP), the top curve corresponds to the without weldline case followed by the out of WL then the ON-WL cases 24

Figure 1.9 Healing process of two opposing melt fronts - a: Before contact; b: Onset of molecular diffusion; c: Disappearance of the interface with complete healing 27

Figure 1.10 Compression molding of PS pellets[43] - a: Before molding; b: After molding 28

Figure 1.11 Stress at break vs processing time ($s^{1/4}$) of compression molded PS[43] 29

Figure 1.12 Weldline factor vs T_p-T_g (°C) for directly molded specimens: PS, PP and HIPS[3], PC[53,54] 33

Figure 1.13 The different zones in a weldline, i.e, V-notch, strong weld and poor weld[54] 34

Figure 1.14 Stress at break vs machining depth (poorly bounded layer) for PS and PC[54] 35

Figure 1.15 Fracture surfaces of a whole type I PS sample (perpendicular to flow view) a: No weldline; b: With weldline 38

Figure 1.16 Fracture surfaces of a whole type II sample (perpendicular to flow view) a: No weldline; b: With weldline, right behind the insert 39

Figure 1.16 Cont'd - c: With weldline, 10 mm away from the insert; d: With weldline, 40 mm away from the insert 40

Figure 1.17 Fibre orientation in and away from the weldline in glass reinforced polypropylene, type II plaque[1]. B: Perpendicular to flow view, C: Parallel to flow view 48

Figure 1.18 Flow in the center of a centrally gated disc mold cavity assuming pure elongational flow. If an insert is located at a distance r_0 from the gate, the element of the weldline having an area of A_0 (at r_0) will be reduced to r_0A_0/r at a distance (r-r_0) from the insert[2] . 49

Figure 1.19 Strain as a function of time, recorded by a 10 mm gage length extensometer, in the 33 wt.% type I samples; ON-WL: on the weldline; NO-WL: no weldline; OUT-WL: strain measured outside the weldline 54

Figure 1.20 Tensile strength as a function of volume fraction Φ, for type I and type II without (I,II) and with weldline (I-II-WL) specimens. PP:(---); PA66:(-) 55

Figure 1.21 Schematic illustration of the skin/core structure in injection molded polymer blends - a: Without compatibilizer; b: With compatibilizer 63

Figure 1.22 Schematic illustration of the weldline structure in injection molded polymer blends - a: without compatibilizer; b: with compatibilizer 65

Figure 1.23 Stress/strain curves for non-compatibilized HDPE/PA6 (25/75 vol%) blends measured using a 10 mm gage length extensometer. No-WL: no weldline; OUT-WL or ON-WL: the extensometer is either placed 10 mm away from or on the weldline respectively 69

Figure 1.24 Stress/strain curves for compatibilized HDPE/PA6 (25/75 vol %) blends with an ionomer. The same notation is used as in Fig. 1.23 70

Figure 1.25 The push-pull molding process[154]; A: Left unit forward, right unit forward; B: Left unit forward, right unit backward; C: Left unit backward, right unit forward 77

Figure 1.26 Weldline factor versus weldline displacement during a Simultaneous Composite Injection molding of glass fiber reinforced polycarbonate[160] 78

Figure 2.1 Injection molded plaques, shape and positions at which samples were taken 102

Figure 2.2 Apparent viscosity vs shear rate of neat HDPE, PA-6 and Surlyn . 107

Figure 2.3 Apparent viscosity vs shear rate of neat PA-6, uncompatibilized (PEPA) and compatibilized (PEIPA) 108

Figure 2.4 Schematic representation of the fountain flow 112

Figure 2.5 Morphology of non-compatibilized sample - a) Morphological change throught the thickness in complete sample at position 4 (parallel to flow view), b) Shear induced coalescence in the subskin region of a non-compatibilized sample (perpendicular to flow view) 113

Figure 2.6 Morphological change throughout the thickness - a) compatibilized complete sample at position 4 (parallel to flow view), b) compatibilized complete sample at position 2 (perpendicular to flow view) 114

Figure 2.6 Cont'd - c) magnification in the subskin of Fig. 2.6b 115

Figure 2.7 Schematic of the skin/core structure of injection molded parts - a) non-compatibilized blend, b) compatibilized blend 117

Figure 2.8 DSC thermograms for: HDPE (1), PA-6 (2) and PEPA (3) (samples taken from the skin) 118

Figure 2.9 XPS spectrums from the surface of: PA-6 (1), HDPE (2) and Surlyn (3) plaques 121

Figure 2.10 XPS spectrum from the surface of non-compatibilized blend 122

Figure 2.11 XPS spectrum from the surface of compatibilized blend 123

Figure 2.12 TEM micrographs of samples taken from the skin region of: a) PEPA transverse view, b) PEPA longitudinal view 125

Figure 2.13 SEM micrographs of samples containing a weldline - a) non-compatibilized blend, b) compatibilized blend 128

Figure 2.14 Schematic representation of weldline structure - a) non-compatibilizer blend, b) compatibilized blend 129

Figure 2.15 SEM micrographs of short-shot samples taken at position 1, and showing the skin thickness in the flow front (perpendicular to flow view): a) with compatibilizer, b) without compatibilizer 131

Figure 2.16 XPS spectrum of the flow front surface of PEPA blend 133

Figure 2.17 SEM micrographs of the weldline region in non-compatibilized blend - a) inside the weldline, b) outside the weldline region 134

Figure 3.1 Mold cavities used in this work. Type I-directly molded tensile specimens. Type II-Rectangular plaque with locations at which samples were machined. Plaques thickness: (t): 2, 4 and 6 mm, insert diameter (d): 6, 12 and 18 mm 151

Figure 3.2 Micrographs of type I non-compatibilized blend (NC)-perpendicular to flow view - A) no weldline B) with weldline . . . 155

Figure 3.3 Stress/strain curves of type I samples with (WL) and without weldline PA6, compatibilized (C) and non-compatibilized (NC) blends 157

Figure 3.4 Micrograph of non-compatibilized (NC) blends type I specimens. Fracture surface at the weldline. General view perpendicular to flow 160

Figure 3.5 Micrographs of fractured surfaces of tested type I non-compatibilized (NC) specimens containing a weldline (perpendicular to flow view). A) skin, B and C) core 161

Figure 3.5 Cont'd - c) core 162

Figure 3.6 Micrographs of fractured surfaces of compatibilized (C) blends type I specimens containing a weldline (perpendicular to flow view). A) skin, B) core 163

Figure 3.7 Stress vs axial strain curves of type I samples. Neat HDPE (PE), PA6, compatibilized (C) non-compatibilized (NC), filled PA6 with treated (GB-T) and untreated (GB-NT) glass beads and (---) equation 2 165

Figure 3.8 Volume change versus axial strain of type I specimens (notation same as in Fig. 3.7) 166

Figure 3.9 Effect of the weldline and of the extensometer location on the stress/strain curve for type I specimens of non-compatibilized blends: without weldline position 1 (NC), with a weldline position 1 (NC-WL), with but outside the weldline positions 2 and 3 (NC-out- WL) 168

Figure 3.10 Effect of the weldline and the location of the extensometer on the stress/strain curves of type I specimens of compatibilized (C) blends (notation same as in Fig. 3.9) 170

Figure 3.11 Short-shots of type II mold with 4 mm thickness and 12 mm insert diameter, obtained with: A) neat PA6 and B) compatibilized blends (HDPE/Ionomer/PA6) 172

Figure 3.12 Stress/strain curves for non-compatibilized blends (NC) type II specimens. Plaque thickness: 2, 4 and 6 mm, insert diameter: 12 mm. Transverse direction (M). Weldline in the 4 mm thick plaque: 4-WL 176

Figure 3.13 Stress/strain curves for compatibilized blends type II specimens. Plaque thickness: 2, 4, 6 mm, insert diameter: 12 mm. Weldline in the 4 mm thick plaque: 4-WL 177

Figure 3.14 Stress/strain curves for non-compatibilized (NC) and compatibilized (C) blends type II specimens. Plaque thickness: 2, 4 and 6 mm. In the longitudinal direction (—— with compatibilizer, --- without compatibilizer) 178

Figure 3.15 Micrographs of freeze fractured untested 4 mm thick samples. A) non-compatibilized (NC) parallel to flow view, B) compatibilized (C) blend perpendicular to flow view 180

Figure 3.15 Cont'd - c) magnification (x 25000) 181

Figure 3.16 Micrographs of rupture surfaces perpendicular to flow view of tested non-compatibilized type II specimens containing a weldline (position M). A) whole cross-section, B) skin 182

Figure 3.16 Cont'd - c) core 183

Figure 3.17 Micrographs of fracture surfaces (perpendicular to flow view) of tested compatibilized blends type II specimens containing a weldline at position M. A) whole crossection, B) skin 184

Figure 3.17 Cont'd - c) core 185

Figure 4.1 Mold cavities used in this work. Type I molded tensile specimens. Type II- rectangular plaque with location at which samples were machined 198

Figure 4.2 Stress versus strain curves for type I specimens for different materials: PA-6; HDPE; GB-T: treated glass beads filled PA-6; GB-NT: untreated glass-beads filled PA-6; C and NC: with and without compatiblizer respectively for HDPE/PA-6 blends 201

Figure 4.3 Volume change versus axial strain of type I specimen. Same notation as in Fig. 4.2 202

Figure 4.4 Micrograph of fracture surface of type I glass bead filled PA-6 (transverse to flow view) - a: untreated; b: treated glass beads . . 205

Figure 4.5 Micrograph of fracture surface of type I non-compatibilized blend (transverse to flow view) 207

Figure 4.6 Volume change versus axial strain for 4 mm type II specimens. Neat PA6 and non-compatibilized (NC) are compared in the transverse (at position M) and the longitudinal direction (L) 210

Figure 4.7 Volume change versus axial strain of 4 mm thick type II specimens. Compatibilized (C) and non-compatibilized (NC) samples are compared in the transverse (at position M) and the longitudinal direction (L) 212

Figure 4.8 Volume change versus axial strain of 4mm thick type II specimens. Non-compatibilized (NC) samples taken at positions: B, M, E, L (see Fig. 4.1) 215

Figure 4.9 Volume change versus axial strain of non-compatibilized (NC) type II specimens with variable plaque thickness (2, 4, 6 mm), compared in the transverse direction (at position M) and longitudinally (L) 216

Figure 4.10 Non-compatibilized type II samples (longitudinal to flow view) - a) in the skin, b) subskin 218

Figure 4.10 Cont'd - c) core 219

Figure 4.10 Cont'd (transverse to flow view) - d) and e) fracture surfaces of a 2 mm and 4 mm thick samples 220

Figure 4.11 Volume change versus axial strain of non-compatibilized (NC) blends. Comparison between type I and type II specimens (4 mm thick), taken at positions M and L 222

LIST OF TABLES

Table 1.1 Weldline strength of reinforced thermoplastics[23]. GL:glass fiber, GB:glass beads, SAN:styrene acrylonitrile, PP:polypropylene, PPS:polyphenylene sulfide 18

Table 1.2 Values of angle ψ calculated using equation (8) as a function of the convergence ratio r_0/r and the angle ψ_0. A high aspect ratio p is assumed $(x=1)^2$ 51

Table 1.3 Tensile properties of Neat and Glass fiber Reinforced Polycarbonate (ASTM-D647 Shape samples machined from double-gated rectangular plaques 32 mm wide x 127 mm long, 3 mm thick; samples without weldline were produced by blocking one of the gates). Values represent properties at yield for neat and at break for reinforced polycarbonate[102] 56

Table 1.4 Weldline strength of long fiber reinforced polypropylene. Tensile bars were cut from 4 mm thick plaque in transverse direction[103] . . . 57

Table 1.5 Effect of various filler and reinforcements on the weldline strength (stress at break) of directly molded PP specimens[90] (NWL and WWL stand for without and with weldline) 58

Table 1.6 Weldline strength factor (%) for ABS with and without lubricants at different cross head speeds[140] 73

Table 1.7 Dependence of weldline strength on Mica concentration and interfacial modification[9] 74

Table 2.1 Compounding conditions 100

Table 2.2 Comparison of the dispersed phase size (μm): d_n and d_v 109

Table 2.3 Composition (atom %) of the surface of the plaques as revealed by X-ray Photoelectron Spectroscopy (XPS) 120

Table 3.1 Tensile properties for type I samples; NC-without compatibilizer, C-with compatibilizer, NC-WL: with weldline, and C-WL: with weldline. Standard deviations are: modulus, E-3%; yield stress, σ_y-3%; stress-at-break, σ_b-5%, elongation at yield, ϵ_y-15%; and elongation at break, ϵ_b-25% of reported values. NA:not available. (*):PA6 twin screw extruded 158

Table 3.2 Tensile properties of type II samples as functions of positions B, M, E, and L (see Fig. 3.1); sample thickness - t; C and NC with and without compatibilizer respectively. In each column the first/ second values are for samples with and without weldlines respectively. The average standard deviations are similar to those reported in Table 3.1 174

Table 4.1 Post-yield slope and Poisson ratio (ν) at 0.5% axial deformation. Directly molded (Type I) specimens. (C and NC): with and without compatibilizer respectively. (*): 25 vol% glass bead filled PA-6, (T) treated and (NT) non-treated 203

Table 4.2 Post-yield slope and Poisson ratio at 0.5% axial deformation for Type II specimens with 2, 4, 6 mm thickness. (C and NC): with and without compatibilizer respectively. Samples were taken longitudinally (L) and transversally at position (B,M,E) 213

INTRODUCTION

During this last decade there has been an intense activity to tailor new plastics materials in the form of blends and alloys not in polymerization plant which need considerable investment but in conventional processing equipment. There is 4500 patents produced annually devoted to polymer blends and alloys, with an annual growth of 9-11%, against 2-4% for neat resins.

Polymer blends are physical or chemical mixtures of homopolymers (having different molecular weight or structure) or copolymers having different structures. They are therefore multiphase systems. In the past there has been a growing interest in developing filled or reinforced materials, where the matrix properties are improved through the use of a rigid non-deformable dispersed phase. This is not the case with polymer blends where in addition to the matrix, the dispersed phase is deformable and orientable. During processing (extrusion or injection molding), the dispersed phase may be deformed and acquire an anisometric configuration. This will result in an anisotropic structure characterised by a distribution of shape factors, concentration and orientation of the dispersed phase throughout the thickness of the extruded or molded part.

From a miscibility point of view, polymer blends can be classified into three categories. The first category includes miscible blends such as polyoxyphenylene (PPO)/polystyrene (PS). It is characterized by a single glass transition temperature (T_g).

The second category includes the partially miscible blends such as polycarbonate (PC)/polybutylene terephtalate (PBT). This system combines the properties of PC (high impact strength but weak resistance to solvant and chemicals) and those of PBT (excellent chemical resistance but weak impact strength). This blend is manufactured by GE and used in bumpers. Finally the third category includes most of the industrial blends which are immiscible such as HDPE/PMMA.

Polyolefins/polyamides blends belong to the third category. Polyethylene (PE) is often used to modify and widen the range of the polyamide (PA) properties. But there has been a special interest when the PE is the matrix and modified by a more costly and performing engineering plastic such as PA. Permeability was the property of interest. Using an appropriate molding process which produces a lamelar morphology, the permeability was found to be highly reduced. This was attributed to the fact that the diffusion path (tortuosity) becomes more complicated.

The use of a third agent (compatibilizer) at a reduced concentration is necessary to improve the interface, reduce the interfacial tension as well as the dispersed phase size and a better adhesion between the components. This will result in a stable morphology. As stated earlier, PE/PA blend has been used in the packaging industry of hydrocarbons by developping a lamelar morphology during injection or extrusion blow molding. This system has also been studied extensively during sheet or fibre extrusion where the processing/structure relationship is more or less established. But unfortunately there is

great lack of literature when this blend (HDPE/PA-6) is injection molded as well as on the resulting morphology.

Injection molding is widely used in plastics processing. It is characterized by a a non-isothermal and complex flow in a closed and cooled mold cavity. This results in an anisotropic skin/core structure. This structure will be even more complicated when the cavity is either double gated, in the presence of an insert or with variable thickness giving bearth to weldlines.

Despite the great developement of polymer blends, there is a great lack of studies when these materials are injection molded. Studies on polymer blends containing weldlines are even more rare. The morphology/processing/mechanical properties relationship is not well established. Compositional variations near the weldline have been observed, but not explained. Consequently, it is necessary to undertake a study to establish the relationship between the morphology and the resulting mechanical properties, and fill this gap of knowledge.

The study undertaken by this project is aimed to be a continuity of the research seeking to understand the phenomena leading to morphology development in injection molded polymer blends with or without compatibilizer, and to relate them to the mechanical properties. Since weldlines are often present in such articles, the structure of the weldline region will be considered extensively.

A microstructural analysis of samples taken at various positions give informations on the effect of each parameter in the development of a given morphology. I will attempt to give explanations concerning the compositional variations (if any) of the dispersed phase in the skin and in the vicinity of the weldline region and establish a structure/mechanical properties relationship.

The system used in this study is HDPE/PA6 (25/75 vol %) with or without a ompatibilizer compounded in a twin screw-extruder. Rheological charaterization of the different formulations was undertaken on a capillary viscosimeter. Then they were injection molded under various conditions such as the flow type (plaque ou directly molded), geometrical parameters (insert diameter and plaque thickness), interfacial modification (with and without compatibilizer). Samples will be cut at specified positions, then prepared (microtome and dispersed phase extraction with an appropriate solvent) to study their morphologies using scanning or transmission electron microscopy in addition to calorimetry analysis (DSC) and X-rays photoelectron spectroscopy (XPS).

Finally a mechanical characterization, where tensile tests (clasical mechanical characterization) and the volume change through the use of tensile dilatometry (to determine the mechanism of deformation involved) will be undertaken.

In the following, I start with an exhaustive literature review on the origin of weldlines, their effect in neat, filled or reinforced, as well as in polymer blends and

finally methods to alleviate their effect on the performance of injection molded parts in chapter 1. Chapter 2 deals with the morphology of injection molded HDPE/PA-6, with and without weldlines and the effect of a compatibilizer on the stability of the morphology. Chapter 3 deals with the effect of weldlines on the mechanical properties of the above blends when injection molded under various conditions. Finally, chapter 4 deals with the mechanism of deformation of the same above system (HDPE/PA-6 with or without compatibilizer) using tensile dilatometry. It has to be mentionned that all chapters constituting this thesis have been submitted for publication. Chapter 1 was submitted to "Advances in Polymer Technology", chapter 2 to "Polymer", chapter 3 to "Journal of Applied Polymer science" and chapter 4 to "Journal of Materials Science".

CHAPTER 1

WELDLINES IN INJECTION MOLDED PARTS:

A REVIEW

SOMMAIRE

La présence des lignes de soudure dans les pièces moulées par injection est devenue une réalité incontournable. Il est intéressant de remarquer que le développement de nouveaux matériaux a été handicapé par des lignes de soudure faibles. Parmi ces matériaux, on peut citer les polymères à cristaux liquides, les plastiques à renforts plaquettaire et les mélange de polymères. Il a même été dit que les lignes de soudure sont «le talon d'Achille» pour ces matériaux.

Dans ce chapitre, l'origine des lignes de soudure, leur influence sur les performances des plastiques vierges, chargés ou renforcés, des mélanges polymères ainsi que les méthodes utilisées pour minimiser leurs effets sont revues en détail. L'origine des lignes de soudure et leur effet sur les performances des plastiques vierges et charges ou renforcés est un sujet bien documenté. La seule exception est le manque d'information sur l'effet de la modification interfaciale. Mais c'est surprenant que malgré le grand essor de développement des mélanges de polymères et considérant l'importance du procédé de moulage par injection, il y a très peu d'études sur l'effet des lignes de soudure sur les mélanges de polymères moulés par injection.

Il a été reconnu depuis longtemps que les éprouvettes de traction moulées directement (conçues pour les plastiques vierges pour étudier l'effet des lignes de soudure) sont inadéquates pour les plastiques chargés et par conséquent d'autres configurations ont été essayées, soit l'utilisation d'un insert qui divise l'écoulement en deux ou bien deux seuils d'alimentation placés côte à côte. D'autres méthodes pour évaluer les propriétés mécaniques des plastiques ont été occasionnellement utilisées dans le cas des lignes de soudure : le choc, la fatigue, le fluage, la mécanique de la rupture, l'analyse viscoélastique et l'émission acoustique.

Finalement, la question qui peut se poser est comment traiter les lignes de soudure? Les premières publications avaient pour but d'alléger l'effet des lignes de soudure par l'optimisation des paramètres de mise en oeuvre mais malheureusement la marge de manoeuvre est plus ou moins limitée. Différentes approches sont disponibles maintenant, plusieurs d'entre eux se trouvent sous forme de brevets, et sont passés en revue dans ce chapitre.

Ils peuvent être divisés en quatre catégories : traitement postmoulage (chauffage, solvent), modification de la composition de matériau (modification de l'interface dans le cas de systèmes multiphasés), le design de moule (localisation de la ligne de soudure dans des zones non critiques, chauffage de l'insert) et le développement de nouveaux procédés ayant pour but de mieux contrôler la topographie des lignes de soudure.

1.1 INTRODUCTION

In early stages of the design procedure, designers of fabricated parts made of any modern material use, data sheets provided by suppliers. With plastics, particularly with those containing more than one phase, the usual molding and testing procedures for generation of these data yield samples with structures and properties which may differ significantly from those found in parts made of the same material. For example, with fiber reinforced materials, this approach gives the best possible values of mechanical properties since in specimens molded according to standard methods (e.g ASTM D 638) the predominant fiber orientation is parallel to the applied stress. In "real" parts the fiber orientation is not so favourable and consequently the properties such as strength and stiffness are lower.[1,2] In addition, various molding defects are possible in finished parts. One such type of flaw is due to the presence of weldlines which are observed in parts made by several processes (injection molding, blow molding, extrusion, compression molding). It has often been suggested that the process and the part be designed in such a way that the weldlines are avoided or if possible, located in non-critical areas of the parts. However, it is a known fact that weldlines are unavoidable in most commercial products of even moderate complexity.[3,4] It is interesting to note that the development of many otherwise exciting materials has been hampered by weak weldlines. Among such liquid crystal polymers[5,6,7] are plastics reinforced with high aspect ratio platelets,[8,9] and multiphase polymer blends.[10,11] Weldlines have even been called the "Achilles' heel" of these materials.[11]

Since the pioneering paper published in 1951 by Spencer and Gilmore[12] describing weldline formation, in which the authors state that weldlines present a difficult problem in terms of appearance and strength, an impressive body of literature on this subject has accumulated. The objective of this paper is to review the literature dealing with weldlines in polymer materials fabricated by the injection molding process. It is divided into five parts. We begin by a brief description of the phenomena important for the part formation in the mold which include those leading to weldlines, in addition to the techniques used to characterize weldline containing parts. The following three sections consider the structure and properties of weldlines in neat amorphous and semicrystalline polymers, filled and reinforced plastics, and finally in polymer blends and alloys. In the last section methods developed for increasing the weldline strength are discussed.

1.2 ORIGIN OF WELDLINES

In injection molding the term "weldline" is used to designate the interface created when two streams of molten plastic, flowing to fill the mold are brought into contact. Other words used in the literature to identify the weldline phenomenon are "knitline" or "meldline". These terms were initially devised to describe surface imperfections in injection molded parts. In today's context the word "weldline" may appear misleading since, as results of numerous investigations published over the past 40 years have shown, these are much more than simple unsightly superficial flaws. What we call a weldline

is typically a zone extending throughout the entire part thickness in which many structural features differ from those away from the weldline.

Although the weldlines are formed as the mold is being filled, their structure, shapes and properties are affected by the entire injection molding cycle. It is therefore useful to review briefly the events leading to the part formation in the mold and those which affect the material structure both in and away from the weldline. The principle of injection molding is simple: fill a cold mold with molten plastic, compress it and wait until it solidifies. Considering only the closed mold, the molding cycle can be divided into three stages: filling, packing and cooling; the latter one begins when the first melt penetrates into the mold. As the plastic flows into the mold, the first melt to contact the cold mold wall solidifies instantaneously, forming an immobile "frozen layer". Additional flow then takes place within the envelope created by the frozen layer. A key aspect of the mold filling is the so-called "fountain-flow": the streamlines of a fluid advancing between the mold walls appear as a fountain to an observer moving with the flow front.[13] The fountain flow which has a major effect on the microstructure of all injection molded objects is illustrated in Fig. 1.1. The melt flows from left to right between two immobile frozen layers. Because of the shape of the velocity profile, the fluid elements in the core will move at a faster velocity until they reach the melt front zone. There, assuming a constant shape of the melt front profile, they will expand and flow to the wall, where solidification takes place. As the streamlines indicate, considerable stretching takes place in the melt front area and the fluid that has stretched

most is the one to contact the cold mold wall. Because of the viscoelastic character of the fluid, the orientation generated by stretching is frozen, forming an oriented skin that is part and parcel of all-injection molded articles molded by currently available technology. Schmidt,[14] has used a colour tracer technique to demonstrate the fountain flow. His results are summarized in Figure 1.1B. The tracer particle (a coloured droplet of the same melt), which enters the mold as a sphere, gradually deforms into a circular arc with a U-shaped cross-section. The flow and deformation continue until the tracer reaches the melt front where the material flowing on the midplane at the highest velocity splits the tracer and forces the leading edges to the mold wall. The first tracer particles to enter the mold will solidify closest to the gate. Similar techniques were also applied to more complex molds.[15]

An injection-molded article can then be said to consist of a skin, which emanates from the continuously regenerated melt front surfaces, and a core, which is a result of a more or less fully developed flow behind the melt front.

The velocity profile in the core is quite flat because polymer melts are pseudo-plastic: the apparent viscosity is highest where the shear rate is lowest, i.e., in the core. It follows that the intermediate layer between the immobile frozen skin and the relatively undeformed core undergoes most intensive shearing and the heat generated further reduces the viscosity and further contributes to the flattening of the velocity profile.

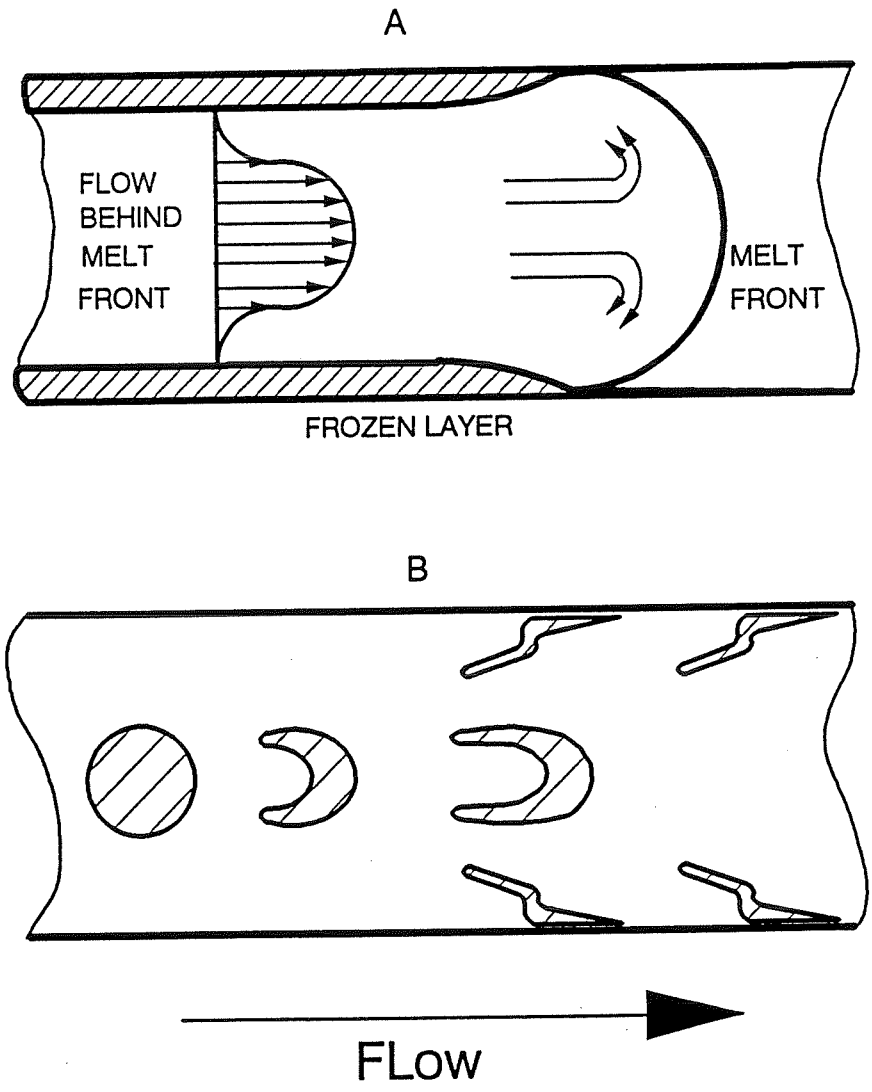

Figure 1.1 - Fountain flow in an injection mold cavity[14]. A- Progress of the fountain flow, B- Movement of a tracer particle

When the mold is filled the solid skin envelops a core of still molten plastic which, having a density (at atmospheric pressure) 10% to 25% lower than the solid polymer, needs to be compressed to compensate for the shrinkage the polymer undergoes during cooling. Since the mold volume is constant, the compression is accomplished by injecting more polymer into the mold. This second part of the molding cycle, called "packing" stage, begins when the mold has been filled with the melt and ends when solidified polymer completely obstructs the path between the mold and the injection unit (source of pressure). The additional flow during the packing stage is most important in the area close to the gate and is limited to the still molten layers in the mold.

Given the nature of the molten polymers the weldline strength will depend on whether the polymer chains had enough time to diffuse across the interface to form a strong bond. The rate of cooling in the mold will therefore have a strong bearing on the bond development. When the molten polymer contacts the mold, the temperature at the polymer/mold boundary T_i is given by equation 1[16]:

$$T_i = \frac{b_m T_m + b_p T_p}{b_m + b_p} \quad (1)$$

where T_m and T_p on one hand and b_m and b_p on the other hand denote temperatures and thermal effusivities of the mold and the polymer respectively. For example, in the case of molten polystyrene at T_p = 200°C and a stainless steel mold at 40°C the temperature

at the steel/polymer interface is (b_p = 5.02 x 10^2 J/°Cms$^{1/2}$ and b_m = 7.52.10^3 J/°Cms$^{1/2}$) about 50°C, i.e., close to the mold temperature before the contact with the polymer. Considering that cooling an amorphous polymer solidifies when it reaches its glass transition temperature (T_g), the thickness of the solid layer (y) can be calculated from the equation 2[16]:

$$\frac{T_g - T_p}{T_i - T_p} = erf \frac{y}{2\sqrt{at}} \qquad (1.2)$$

where a is the thermal diffusivity of the polymer. For the above example of polystyrene (T_g = 100°C, a = 8.6 x 10^{-8} m^2/s) and with T_i = 50°C the time required to freeze the outermost 10 μm is only 0.04 s. Within 1 s the solid front will have reached a depth of 150 μm.

There are numerous situations that can lead to weldlines in injection molds. It is often stated in the literature that weldlines can be divided into two categories (Fig. 1.2). In Figure 1.2A, two melt fronts flowing in opposite directions collide and become rapidly immobilized. The last area to be filled is close to the mold surface often, but not always,[17,18] leading to a V-shaped ridge on the surface. Given the high rate of cooling, the "V-notch" may contain poorly bonded areas besides being a source of stress concentration in the part. The problem of two impinging melt fronts, was studied by Mavridis et al.[19] They have shown that the orientation of material elements in the

weldline zone induced during the collision phase is relatively small and that the anisotropy is mainly due to the fountain flow. The weldline formation is fast: with an average velocity of 0.1 m/s and cavity thickness of 2.10^{-3} m, the weldline forms in about 2 milliseconds. Figure 1.2B illustrates a situation where the molten plastic penetrates into the mold via two gates located side by side. In the beginning the melt spreads around in a semicircular fashion until the melt fronts meet halfway along the shorter side of the mold-forming weldline which is, in this area, similar to that of Fig. 1.2A. As the recombined front advances one expects the polymer to "forget" the initial division and the weldline to disappear. Menges et al.[20] and Yokoi et al.[21] have related the recovery of the "without weldline" structure to the value of the melt front angle α (see Fig. 1.2B) and state that the weldline effectively disappears when the angle α has reached a value of the "weldline vanishing angle". With PS the weldline vanishing angle was found to be between 140 and 150 degrees.[21] Three-dimensional flow analysis of the weldline formation process carried out by Yokoi et al.[21] shows that, since the weldline plane is formed by the meeting of two curved surfaces there is a surplus area which folds into the weldline. As the melt front angle increases the surplus area decreases. It is interesting to note that the weldline types shown in Fig. 1.2 have been translated into standard mold cavity shapes for weldline strength evaluation. The ASTM D 647 method suggests a cavity shown in Fig. 1.3A to give a "cold" or "butt" weld, and another one (Fig. 1.3B) to produce a "hot" or "streaming" weldline.

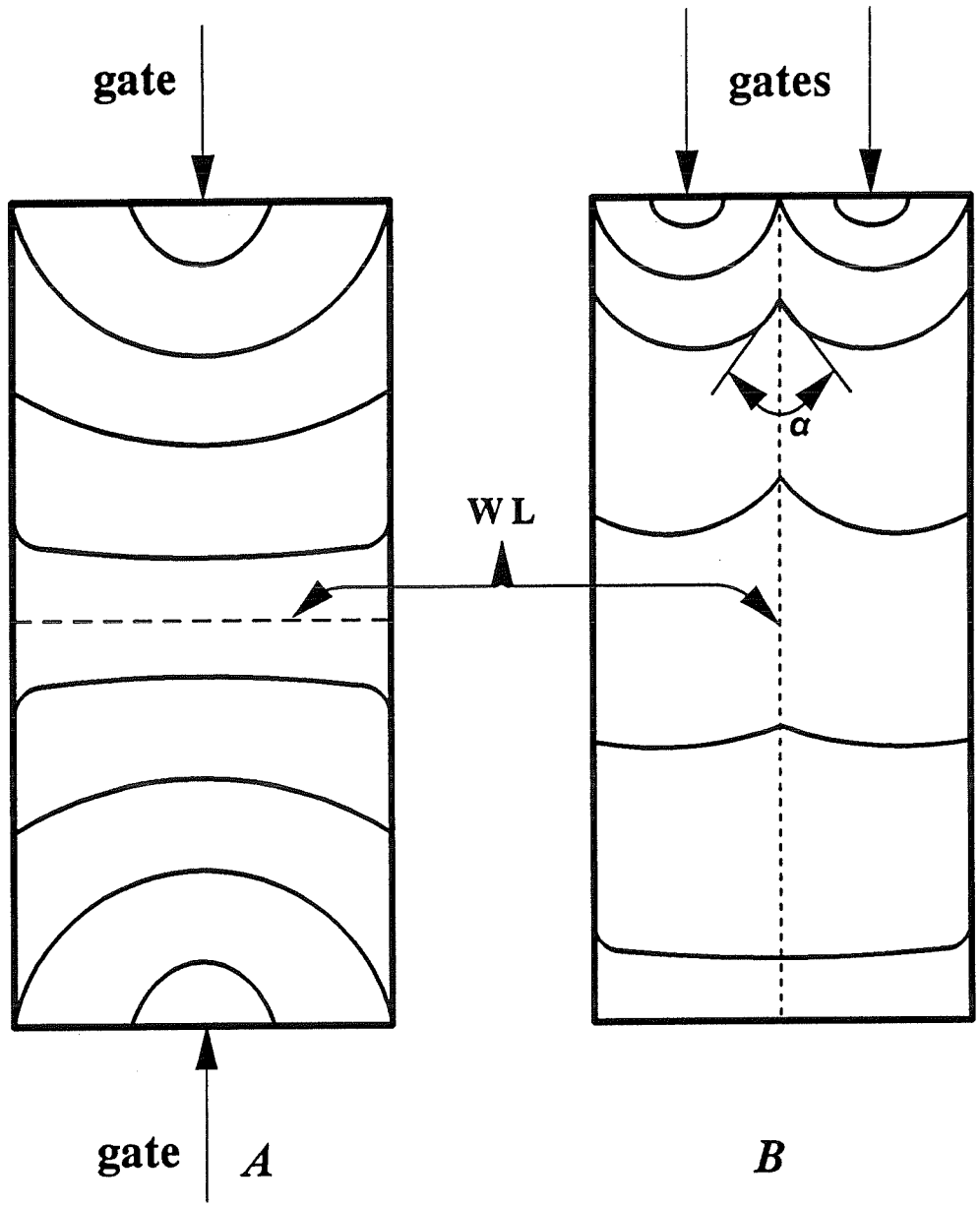

Figure 1.2 - Two common causes of weldlines in injection molded parts (mold filling patterns in rectangular cavities). A- double gated mold, B- mold with two gates side by side. Weldlines are indicated by dashed lines, gates by arrows

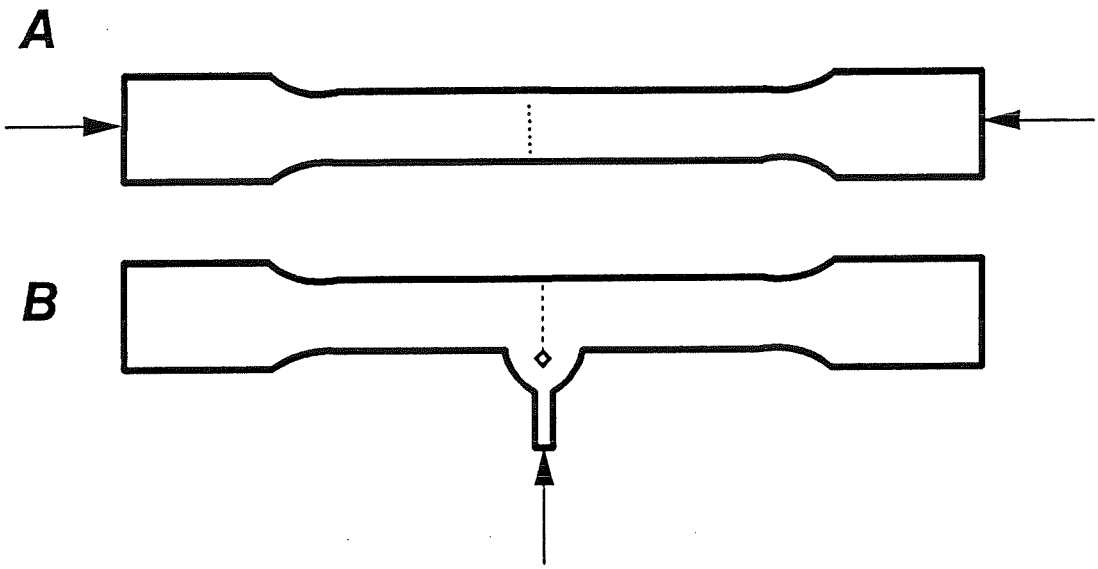

Figure 1.3 - Standard test mold cavity (ASTM-D647)[173]. A- "cold weld", B- "hot weld"

Weldlines are also observed in molds of variable depth. In such cases the melt advances faster in thicker sections. For example, when the gate is located in the thinner section (Fig. 1.4A) the melt will flow into the thick section, accelerate compared to the thinner one, and flow partly back leading to a weldline. For the panel in Fig. 1.4B, where an edge gate is located in the thinner section, a pocket of entrapped air may form in addition to the weldlines. In moldings containing holes, weldlines are formed when the melt stream, divided as it flows around the insert, recombines. An example of this situation is shown in Fig. 1.5. In this part, a half dashboard, weldlines of varying lengths were drawn following a simple visual inspection.

When the flow in the mold is perfectly symmetrical during both the filling and the packing stage, as is the case in Figs. 1.2 and 1.3, the weldline will be planar across the part thickness. However in most "real" parts the weldline topography will not be planar. Consider a relatively simple molding shown in Fig. 1.6. When the left side of the mold is filled (at time t_1) the weldline has already formed and is perpendicular to the panel surface. The melt required to fill the rest of the mold will be supplied from both gates and as a result, the initially planar weldline will assume a shape shown in Fig. 1.6B. It follows that, in order to estimate the strength loss due to the presence of weldlines in injection molded parts information about the weldline topography is required. It is worth noting that the control of the weldline topography during the molding cycle has become one of the preferred methods of dealing with deleterious effect of the weldlines.

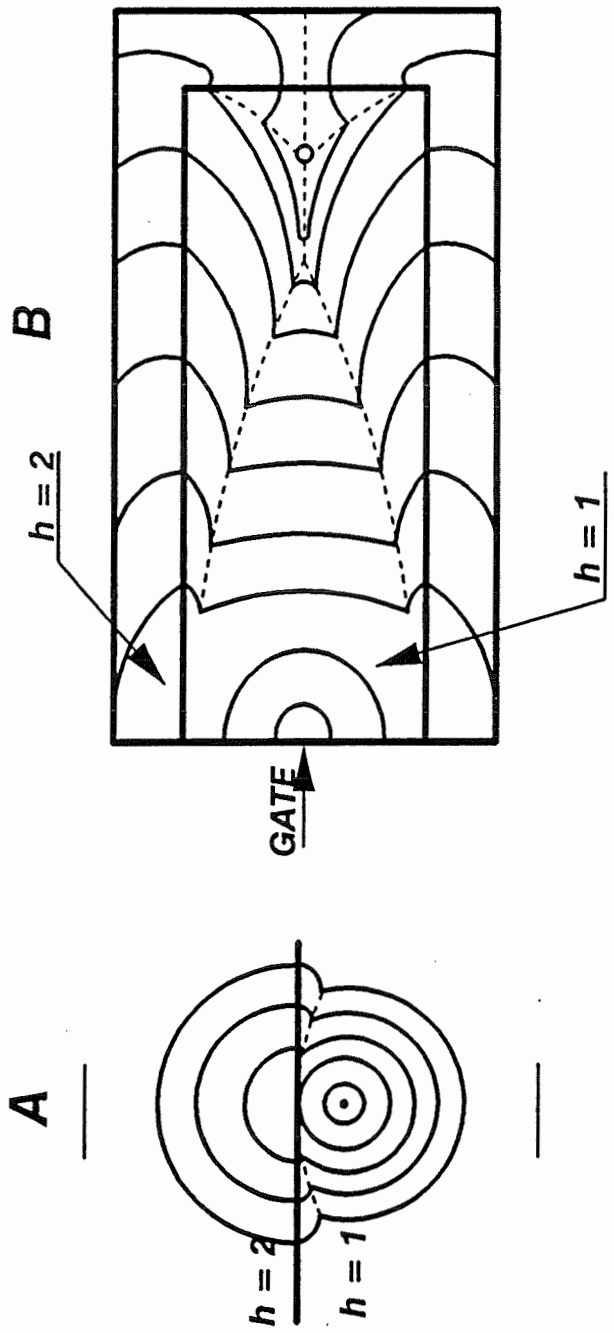

Figure 1.4 - Mold cavity with variable thickness[174]. A- gate located in the thinner section, B- formation of a pocket of entrapped air

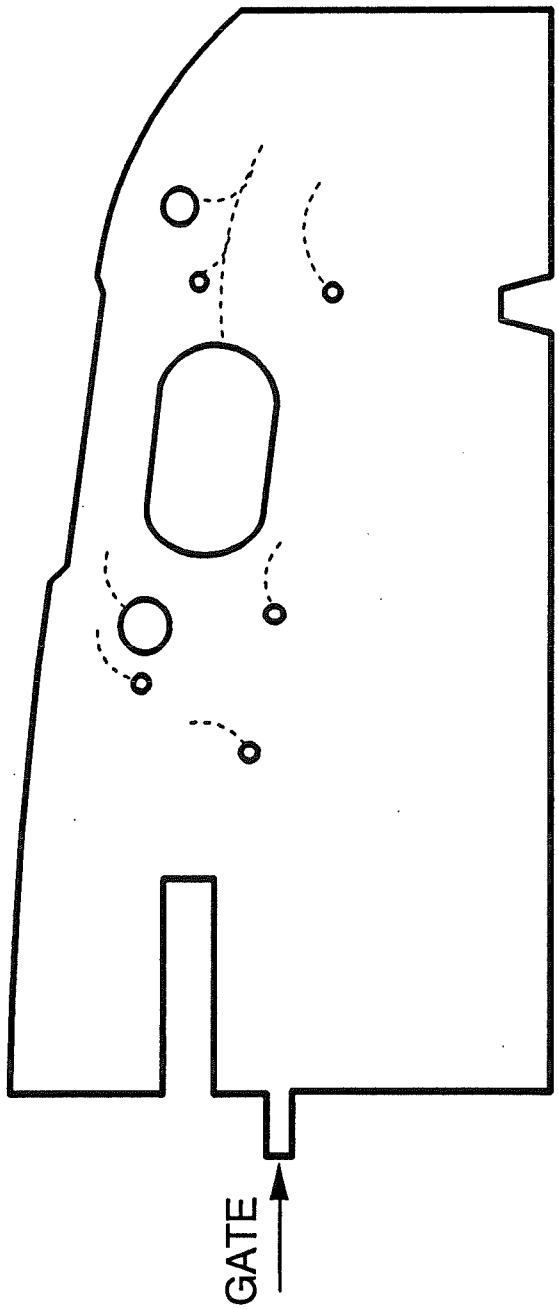

Figure 1.5 - Weldlines detected by visual inspection in an experimental simple gated mold representing half of a passenger vehicle instrument panel[175]

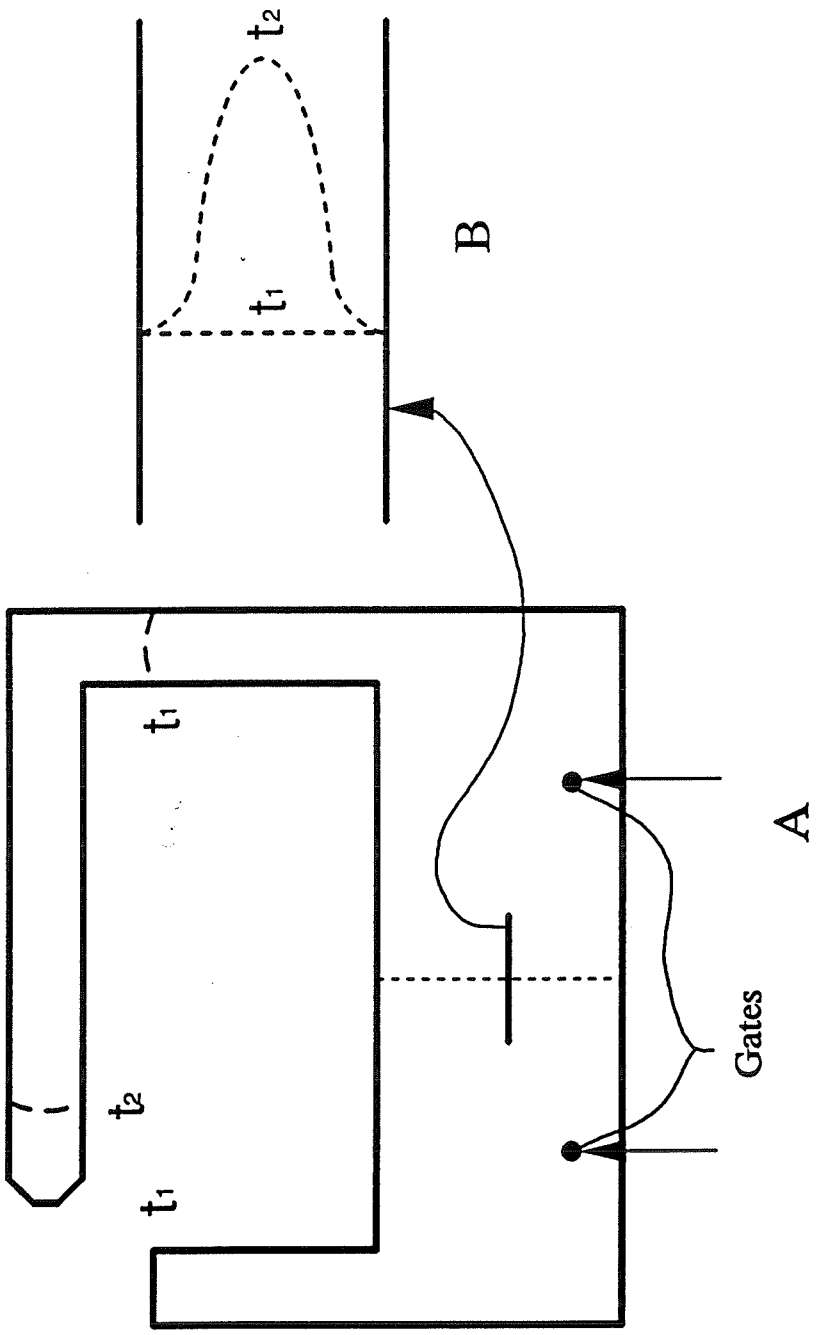

Figure 1.6 - Topography of the weldline in time of the mold filling process[154]. A- straight at time t_1, B- deformed at time t_2

1.3 METHODS USED TO STUDY WELDLINES

The effect of the weldline on the mechanical behaviour of a given resin is usually estimated by testing simple shaped specimens molded with and without a weldline. A weldline strength (or other property) "retention factor" is then obtained by dividing the strength of a sample with a weldline by that of an equivalent weldline free specimen. This information is sometimes considered in handbooks[22] and trade literature[23] as an indication of the weldline strength in injection molded parts (Table 1.1).

An overwhelming majority of the results published on weldlines was produced using a directly molded double gated tensile sample such as the one shown in Fig. 1.3A. This mold was conceived to as a part of a simple and above all fast method for evaluation of weldlines in unfilled polymers in which the strength loss is determined primarily by the incomplete bonding at the interface of the two flow fronts. This plays an important role in some thermoplastics particularly those in which the mold temperature is so low that the "instantaneous polymer temperature" T_i as it touches the mold wall [equ. 1] is below the glass transition temperature. This is for example the case of polystyrene[24] or styrene-acrylonitrile copolymer.[25]

Table 1.1 Weldline strength of reinforced thermoplastics[23]. GF:Glass fiber, GB:glass beads, SAN:styrene acrylonitrile, PP:polypropylene, PPS:polyphenylene sulfide.

Resin	Reinforced	Tensile Strength (MPa)		
		No Weldline	Weldline	WL-Factor (%)
Polysulfone	None	65	65	100
Polysulfone	30 % GF	115	70	62
SAN	None	80	60	80
SAN	30 % GF	110	45	40
PP	None	35	34	86
PP	20 % GF	65	30	47
PP	30 % GF	67	23	34
PP	15 % GF + 15% GB	45	19	42
PPS	None	60	50	83
PPS	10 % GF	70	25	38
PPS	40 % GF	140	28	20

Different molecular orientation and the presence of V-notch in the weldline zone may also affect the weldline strength. The directly molded tensile sample with a weldline in the middle may yield information about the materials ability to form a strong bond across a rapidly cooling interface. However the values of properties other than strength usually obtained from tensile tests are affected not only by the weldline but also by the material away from the weldline. For example consider the idealized situation in the

Fig. 1.7. A rectangular bar of material of length L_o, with a weldline whose length is $X.L_o$, both materials being perfectly elastic until fracture, is subjected to tensile or bending loads. The bulk of the material (away from the weldline) has a modulus E_1, and strength σ_1. The weldline has a modulus E_2 and strength σ_2. In the tensile mode the apparent (average) modulus of the structure $\bar{E}_t$ is:[2]

$$\bar{E}_t = \frac{E_1 E_2}{E_2 + (E_1 - E_2)x} \tag{1.3}$$

Assuming that $\sigma_2 < \sigma_1$, the bar will break at a stress σ_t:

$$\sigma_t = \sigma_2 \tag{1.4}$$

at an elongation at break given by:

$$\epsilon_t = \frac{\sigma_2}{E_t} \tag{1.5}$$

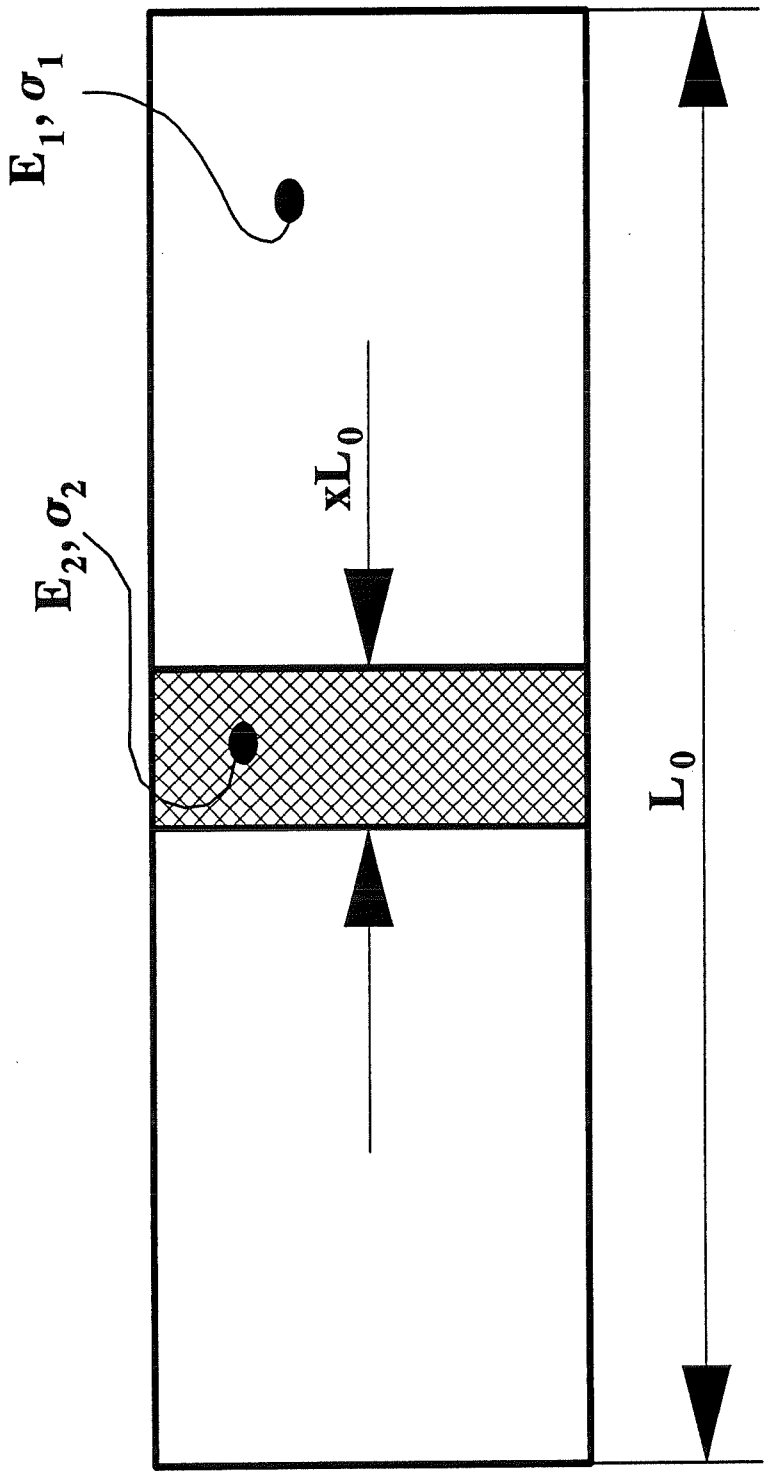

Figure 1.7 - Model of a material with a weldline

The strain energy (or energy to break) W_t is equal to:

$$W_t = \int_0^{\epsilon_t} \bar{E}_t \cdot \epsilon \cdot d\epsilon = \frac{\bar{E}_t \cdot \epsilon_t^2}{2} = \frac{\sigma_2^2}{2\bar{E}_t} \qquad (1.6)$$

Considering the weldline structure described above ($x << 1$) the modulus $\bar{E}_t$ will be then close to E_1 while the strength of the sample is equal to that of the weldline. As a result the breaking elongation, ϵ_t, and the strain energy, W_t, are affected not only by the properties of the weldline itself but by the stiffness of the material away from the weldline.

To illustrate this idea, a tensile test was performed on samples with and without weldline. The strain measuring device can be placed either on or outside of the weldline and the load displacement data compared. Testing conditions are given elsewhere.[124] Fig. 1.8 shows the results for neat amorphous or semi-crystalline resins, i.e., PS, PP, PC, HDPE and PA6, when the gage length of the strain indicator is 10 mm. In polystyrene both curves are superimposed until the weldline sample breaks (Fig. 1.8a). This can be considered as an indication that the weldline zone, regardless of its weakness, is narrow relative to the gage length of the extensometer. In other polymers such as PA6 and HDPE the weldline effect, if any, is simply not detectable, all curves being superimposed well beyond yield. Yet other polymers show small, but significant

differences (PC and PP), as shown in Fig. 1.8b. In PP, for example, the load displacement curve of the weldline zone is slightly below that of the outside of the weldline tested at the same time (the process is also accompanied by the stress whitening of the weldline zone) (see insert Fig. 1.8b). It is conceivable that these small differences in the strain-strain behaviour are related to much larger effects determined in longer term tests (e.g., fatigue) on these same materials.[26]

If the structure in Fig. 1.7 is subjected to a flexural test with the load applied at the weldline (e.g., ASTM D-790), analogous results are obtained; in this case the average flexural modulus $\bar{E}_f$ is more sensible to the relative weldline width x than the tensile modulus $\bar{E}_t$:[2]

$$\bar{E}_f = \frac{E_1 E_2}{E_1 - (E_1 - E_2)(1 - x)^3} \qquad (1.7)$$

For materials in which the flow in the mold induces mechanical anisotropy (filled and reinforced polymers, LCP's, certain polymer blends and alloys), the measured weldline effect will appear much greater than what would be observed in a typical molded part such as the one shown in Fig. 1.2.

The inadequacy of the specimens in Fig. 1.3, for reinforced plastics, has been recognized for some time[27] and various other testing configurations were tried.[20,25,27-29]

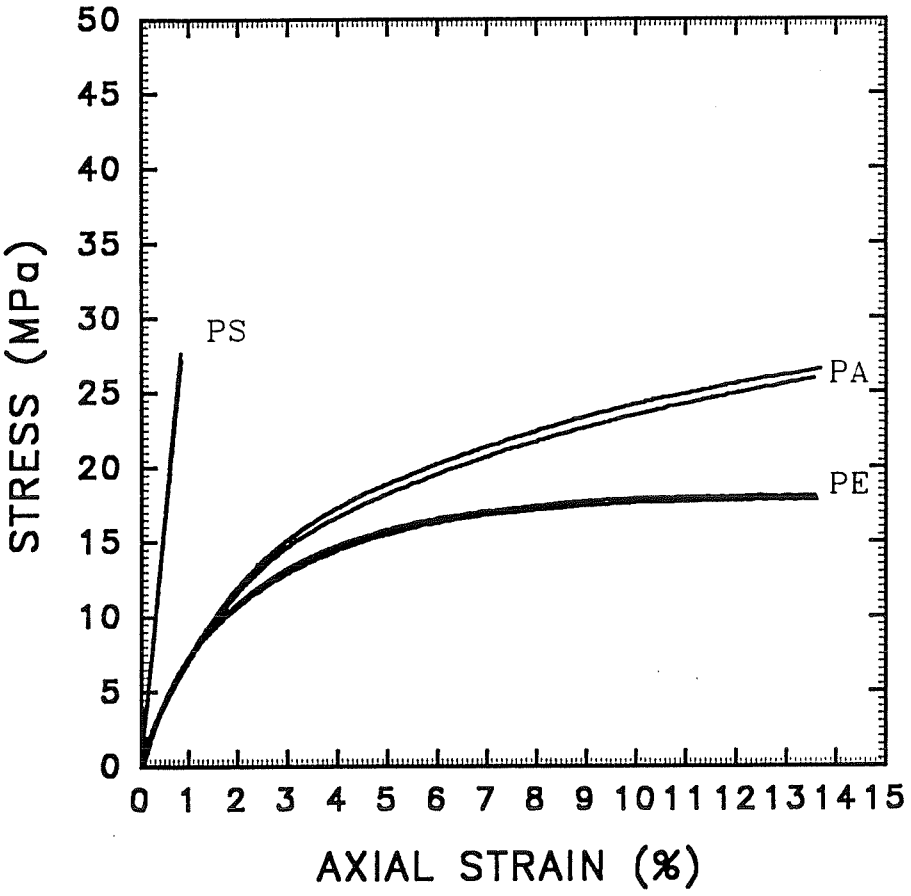

Figure 1.8 - Stress/strain curves of directly molded (type I) samples with or without a weldline. An extensometer is placed either on or outside the weldline. A- Polystyrene (PS), Polyamide-6 (PA) and high density polyethylene (PE)

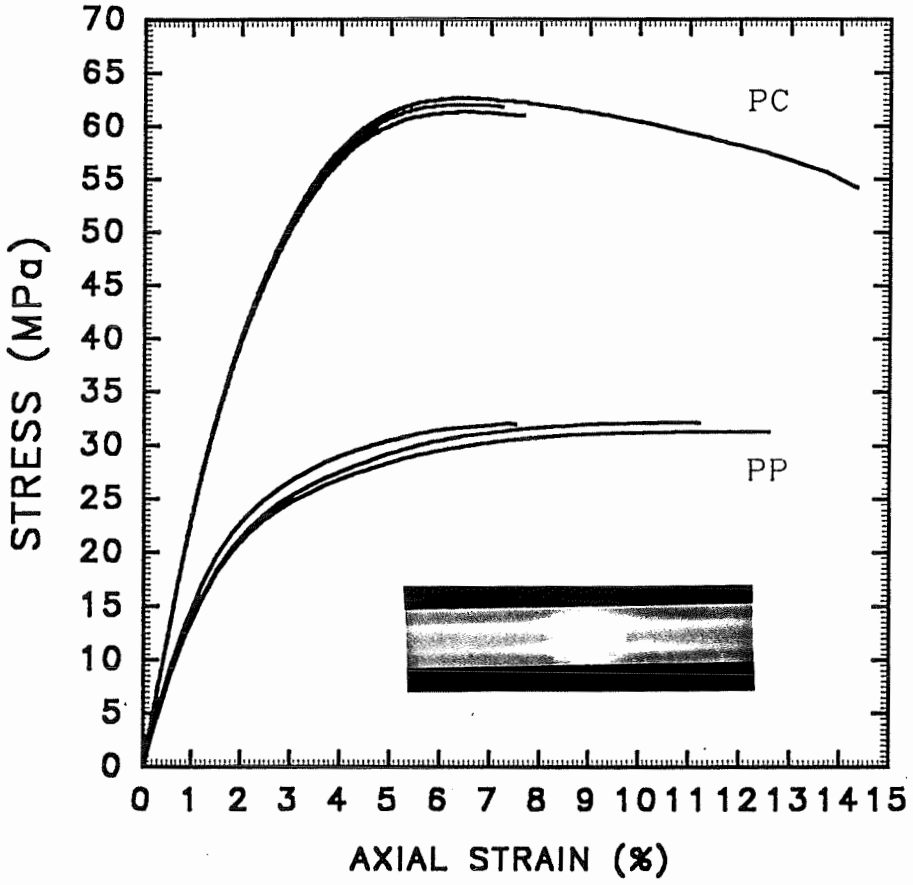

Figure 1.8 - Cont'd
B- Polycarbonate (PC) and polypropylene (PP), the top curve correspond to the without weldline case followed by the out of WL then the ON-WL cases

Most of them use flow conditions analogous to those shown in Fig. 1.3 either by the use of an insert, which divides the flow front into two[20,28] or by the use of two gates located side by side.[29,30] Other methods and approaches used to study mechanical properties of polymers have also been occasionally applied to weldlines: fatigue[31-34] and creep[34] fracture mechanics,[35-37] viscoelastic analysis,[29,38] acoustic emission etc.[39] Other authors suggest the use of impact testing rather than tensile testing to characterize the weldline strength of rubber-modified polymers.[25,29,30,40,41]

1.4 WELDLINE IN NEAT POLYMERS

The welding process has been studied previously through two different approaches: the first is the measurement of engineering properties of samples containing weldlines and their dependence on processing conditions,[42] the second is on the molecular diffusion across a static polymer-polymer interface.[43,44] However, in polymer processing operations, the welding process takes place with an initial condition of highly oriented molecular chains on both sides of the interface. This orientation of macromolecules plays an important role in determining the mechanical properties of the part, and it is not evident whether it enhances or reduces the diffusion process of polymer molecules across the weld interface.[45]

The concept of polymer chain reptation has been developed to describe the diffusion process across the interface between two polymer surfaces brought together at

a temperature greater than their T_g. The interface disappears gradually and the bond strength is developed as the time passes. The stages of this healing process are schematized in Fig. 1.9. Immediately following the contact (at time zero) there are no chains that have crossed the interface (Fig. 1.9a). As the time of contact increases the chain reptates across the interface leading eventually to its disappearance (Fig. 1.9c). It has been suggested that the bond strength is proportional to the number of chains having diffused from one side of the interface to the other. This approach is attributed to De Gennes[44] and has been used to study welding[45], crack healing[43,46-48] and other aspects of polymer behaviour involving interfaces.[49] At constant temperature and molecular weight (M_w), the bond strength (σ_u) develops with time (t) according to equation 11[43]:

$$\sigma_u = At^{1/4} \tag{11}$$

The parameter A being proportional to $M_w^{1/2}$.

To simulate the welding process, Wool and O'Connor[47] have compression molded polystyrene pellets where the interfaces (weldlines) form when the pellet surfaces contact in the mold as shown in Fig. 1.10a. With the appropriate combination of time, temperature, and pressure, the interfaces wet, the diffusion occurs. If sufficient time is

allowed the interface disappears (Fig. 1.10b). A plot of the stress at break vs processing time ($t^{1/4}$) is shown in Fig. 1.11. The processing time (duration the material is kept inside the press) to reach the virgin state near $\sigma_{+\infty}$ was between 10-20 min and the authors suggest that it is close to an estimated reptation time (20 min). In addition to the chain diffusion across the weldline other factors play a role in the bond development across the interface. In the aforementioned review,[43] Wool described the interface formation in terms of the following stages:

- surface rearrangement: describes the roughness or the topography of surfaces and how they change with time, temperature and pressure following contact, i.e., chain end distribution, spatial change, chemical reaction;
- surface approach: represents the time dependent contact of the parts, surface roughness (impurities play an important role in determining the rate of wetting and contact of the surfaces to form the interface);
- wetting: can occur in a time dependent fashion but can be hindered by a rough surface;
- diffusion: with respect to instantaneous wetting conditions;
- randomization: refers to equilibrium of the non-equilibrium conformations of the chains near the surface.

It is extremely difficult to analyze the bond development in an injection mold principally because of the non-isothermal character of the process which adds to the

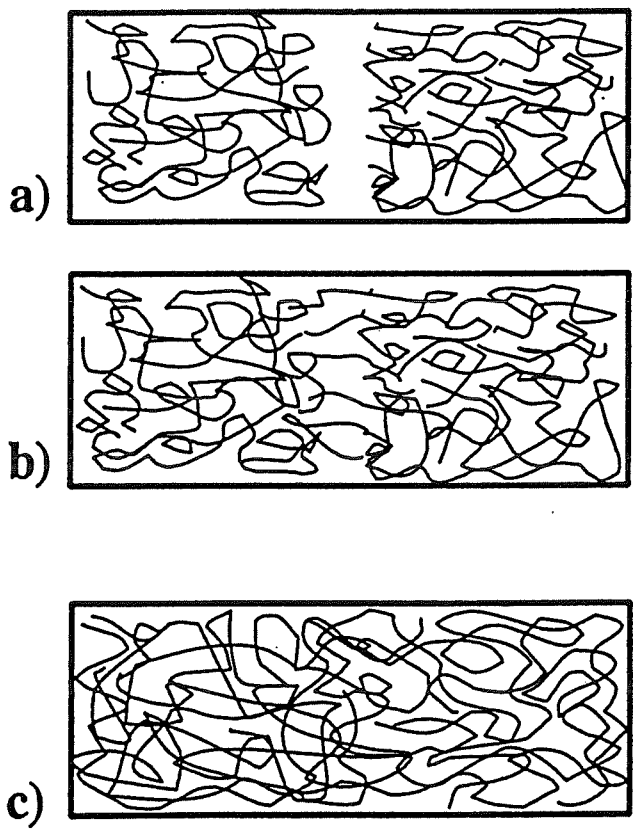

Figure 1.10 - Healing process of two opposing melt fronts - a) before contact, b) onset of molelcular diffusion, c) disappearance of the interface with complete healing

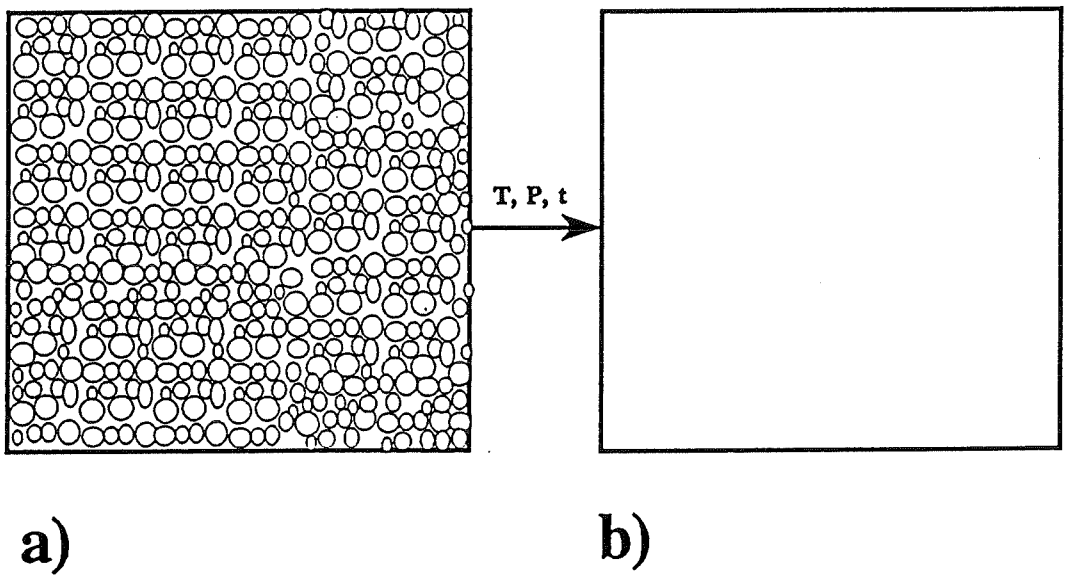

Figure 1.11 - Compression molding of PS pellets[43] - a) before molding, b) after molding

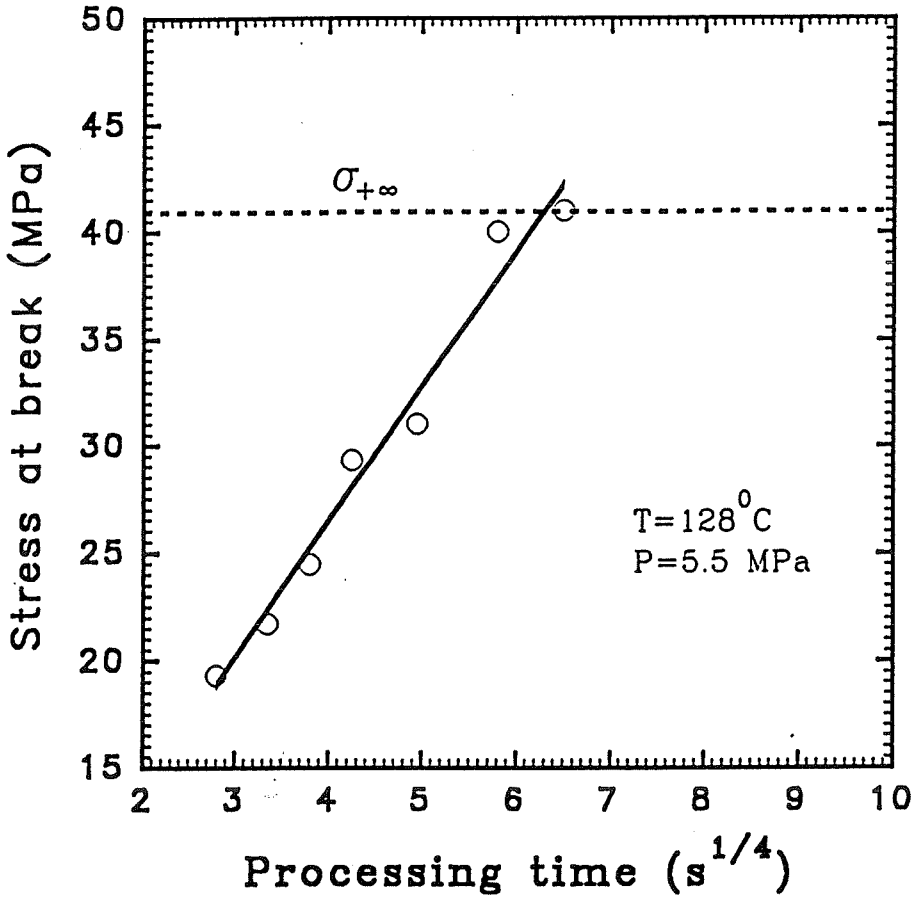

Figure 1.9 - Stress at break vs processing time ($s^{1/4}$) of compression molded PS[43]

complexity of the problem. The theoretical studies dealing with weldline neglect the existence of the temperature gradient across the part thickness as it cools down. Kim and Suh[50] based their theoretical model for the strength of the weldline on the self-diffusion of molecular chains across the polymer-polymer interface and on the frozen molecular orientation parallel to the weldline plane. The solidification time which is the duration for the average melt temperature to drop below T_g is determined as a function of the depth from the surface. Then the amount of relaxation and the thicknesswise frozen-in birefringence index can be obtained. The tensile strength can be obtained from the stress-birefringence experiment. The main parameters controlling the degree of bonding are assumed to be the initial melt temperature rather than the contact time. Mekhilef[51] has developed an analogous model to predict the weldline strength of injection molded samples based on the Flory theory of lattices. It is expressed in terms of the coefficient of diffusion, as well as the operating parameters, i.e., temperature and contact time. The author does not take into account the orientation difference, but suggests that the weldline strength is attributed to a diffusion phenomena. His model was developed in terms of the diffusion coefficients and the operating variables (temperature and contact time). The model was tested with polycarbonate. Some theoretical work on the prediction of the weldline appearance has been done using computer simulation software such as MOLDFLOW.[52]

According to conventional wisdom, the brittle-amorphous plastics, e.g., polystyrene (PS) and styrene acrylo-nitrile (SAN) tend to give a weak weldline, while in

the ductile -amorphous, i.e., polycarbonate (PC) and the semi-crystalline family of polymers, weldlines are nearly as strong as the material without the weldline. However, the time the polymer has to spend to diffuse across the interface, relative to relaxation or re-entanglement time, appears to determine the weldline strength. Fig. 1.12 shows weldline factor vs T_p-T_g where T_p represents the melt temperature and T_g the glass transition temperature of the polymer. For polystyrene (Fig. 1.12), which is typically molded at a value of (T_p-T_g) = 100°C, the weldlines tend to be effectively weak. Polycarbonate molded at about (T_p-T_g) = 150°C will give this polymer more time to diffuse, and when (T_p-T_g) for polycarbonate is brought down to the same value as those used with polystyrene, weak weldlines are obtained. Semi-crystalline polypropylene (T_g = -10°C) is molded at a mold temperature above the glass transition of the polymer. In this case, polymer chains maintain their mobility until they become incorporated into a crystallite.

Even when the weldlines are weak, the weak zone is usually limited to the outer layers of moldings (Fig. 1.13). Tomari et al.[53,54] measured the strength of samples from which the surface layers were machined away (Fig. 1.14). With polystyrene ((T_p-T_g) = 100°C) the "without weldline strength" was recovered at the depth of 150 μm (dotted line in Fig. 1.14). With polycarbonate ((T_p-T_g) = 150°C) the poorly bonded layer was only about 50 μm deep (dotted line in Fig. 1.14). The experimental results of Tomari et al.[54] are in broad agreement with those predicted by the theoretical models[50,51] despite their shortcomings.

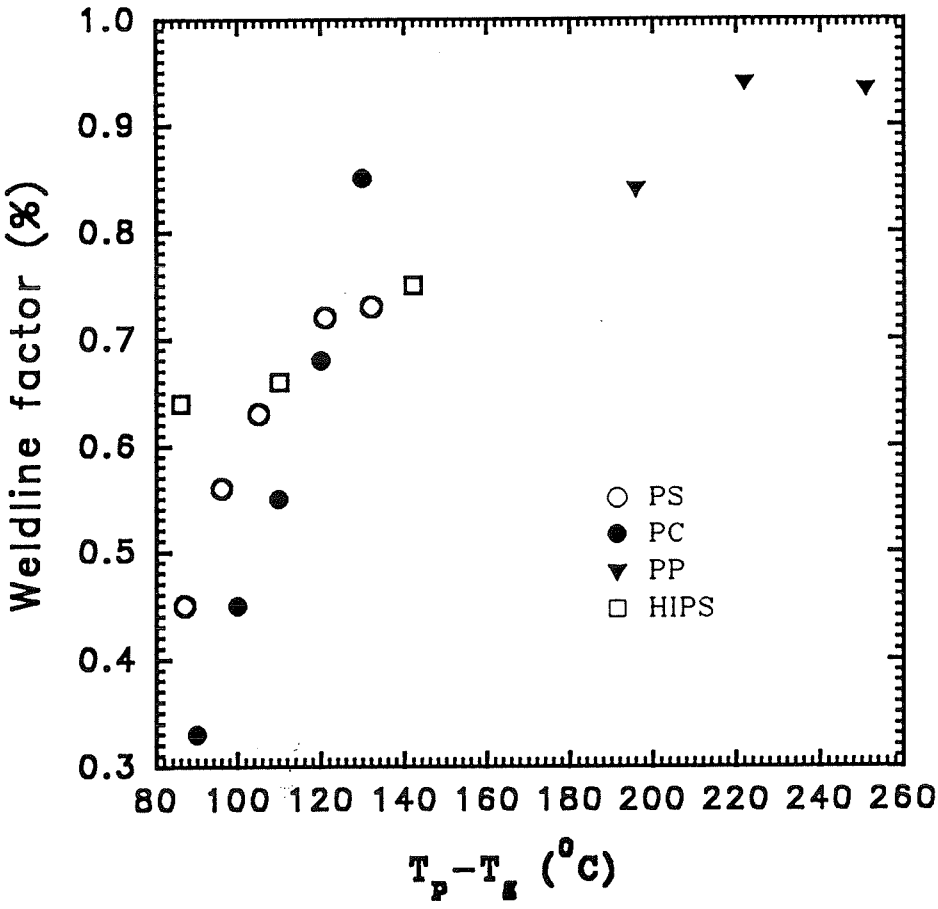

Figure 1.12 - Weldline factor vs T_p-T_g (C°) for directly molded specimens: PS, PP and HIPS[3], PC[53,54]

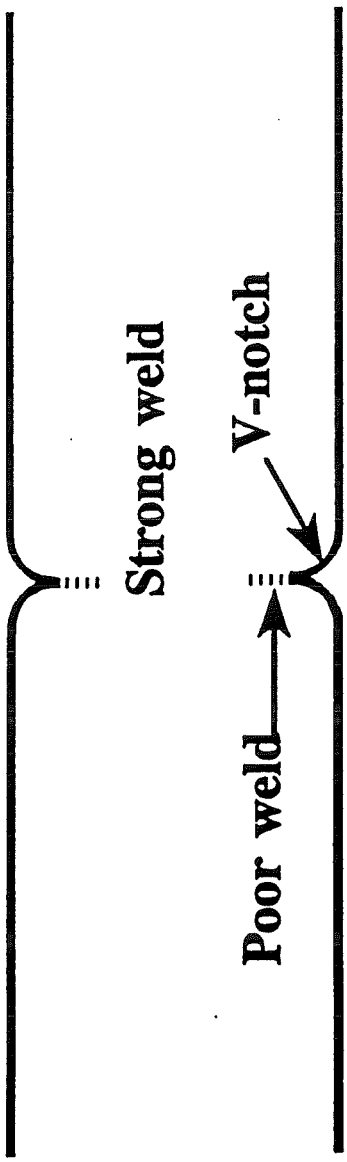

Figure 1.13 - The different zones in a weldline i.e. V-notch, strong weld and poor weld[54]

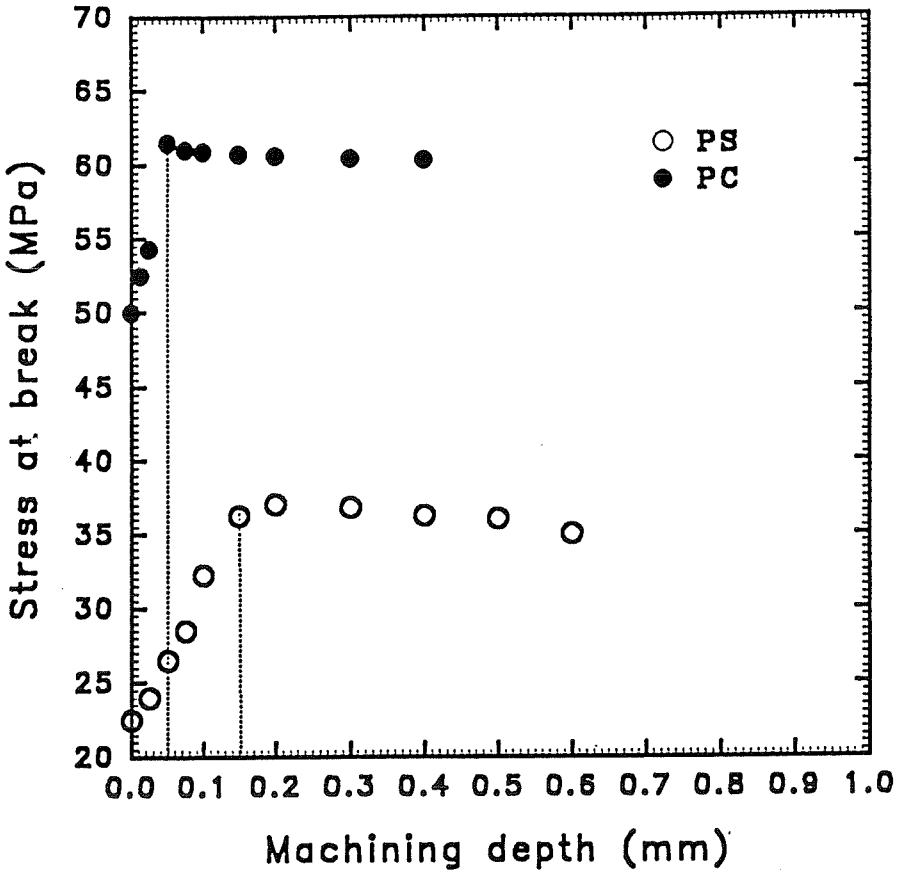

Figure 1.14 - Stress at break vs machining depth (poorly bounded layer) for PS and PC[54]

Other studies in which the weldline strength is related to the molecular mobility are those of Pisipati and Baird[55] and of Menning.[56] Pissipati et al. measured "the re-entanglement time" using an experiment in which the polystyrene melt is deformed and its relaxation characterized. The speed at which the initial melt conformation is recovered is related to the material's ability to diffuse across the interface. Factors increasing the re-entanglement time, such as molecular weight, decrease the weldline strength. Menning,[56] working with PMMA of varying molecular weight, also observed that the weldline strength decreases with increasing molecular weight. However, if the melt temperature is adjusted so that the viscosity is constant the weldline strength becomes independent of the molecular weight.

Nadkarni et al.[57] reported that unfilled PP, PBT, and PET are not influenced by the presence of weldline. This was explained in terms of relaxation of induced stresses and diffusion processes which have enough time to take place adequately above T_g in the double gated specimens. By contrast, PS showed the lowest weldline strength. The above processes are hindered by the high T_g of this material, so only minor relaxation and diffusion will take place, consequently reduced properties are observed for PS.

The structure of the weldline region in amorphous polymers as proposed by Tomari et al.[54] is shown in the Fig. 1.13. The V-notch may or may not be present depending on the venting situation of the weldline area, and on other factors.[58] There is also a "poorly bounded layer" where the two interfaces are in contact but the adhesion

is weak. Fig. 1.15 shows a micrograph of fracture surfaces of directly molded PS samples without (a) and with (b) a weldline. A shiny surface with a smooth topography is observed in the absence of a weldline, but is somewhat rougher in the presence of the weldline. Similar observations have already been reported.[59] A 200 μm thick V-notch is clearly visible in Fig. 1.15b. When the weldline is produced through the use of an insert, and fracture surfaces observed under a scanning electron microscope (Fig. 1.16), it is interesting to note that right behind the insert (Fig. 1.16b), there is a poorly bounded layer, similar to the one obtained in directly molded samples, which persists for a few millimetres behind the insert (Fig. 1.16c) but vanishes afterwards (Fig. 1.16d).

In addition to these contributions to weldline weakness, other factors are worth mentioning, namely trapped air and volume shrinkage. Spencer et al.[12] and Hagerman[4] and others[54] attributed the weakness due to the presence of a weldline to the air trapped at the interface between two opposing or adjacent flow fronts. This will act as a stress concentrator leading to catastrophic failure. This action has been minimized through the use of venting zone to allow the air to escape. Piccarolo et al.[58] suggested that either local sample thickening or grooves form at the weldline when complete solidification takes place and related it to a volume shrinkage.

In the semi-crystalline family, PP is the most studied polymer because of its wide use in the plastics industry. In addition to orientation, the degree of crystallization as well the size of the crystal aggregates depend on the cooling rate. The cooling rate is

dependent on melt temperature, mold temperature, method of cooling and cooling time. Slow cooling favors crystal growth, resulting in a greater crystalline content and larger spherulites. The coarse morphology thus developed contains some defaults such as voids and cracks at the interface between crystals which generally lead to inferior mechanical properties. On the other hand, rapid cooling tends to lower degree of crystallisation, smaller crystallites and spherulites, and large amorphous domains. The structure tends to distribute the stress more uniformly leading to superior mechanical properties.[3]

The combined effect of temperature, pressure and molecular chain orientation was considered by Trotignon et al.[60] who divided the solidification process of a crystallizable polymer (polypropylene) melt into four stages, and reviewed by Fisa[61]:

- Mold filling: during this stage the melt temperature is above the crystallization range except in the immediate vicinity of the mold wall where a highly oriented layer of low crystallinity formed. The pressure is low.

- Filling-packing transition: When the mold is filled, the melt velocity drops but the pressure remains low. The flow induced orientation starts to relax in the subskin layer until the temperature at which the polymer starts to crystallize is reached. The rate of crystallization is high because it is favored by the chain orientation. A crystalline form of polypropylene (α-form) is known to crystallize at low pressure.

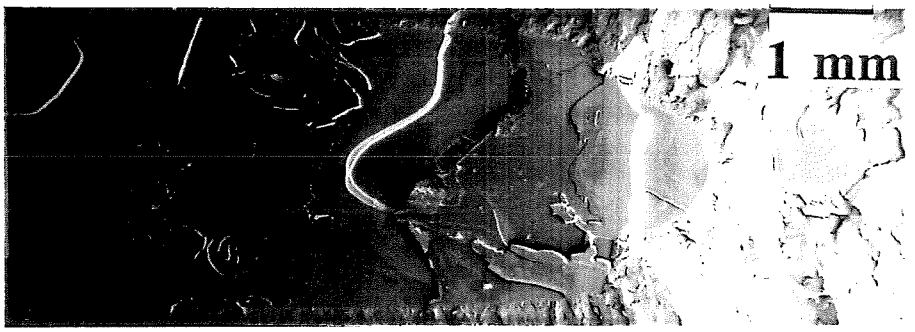

a)

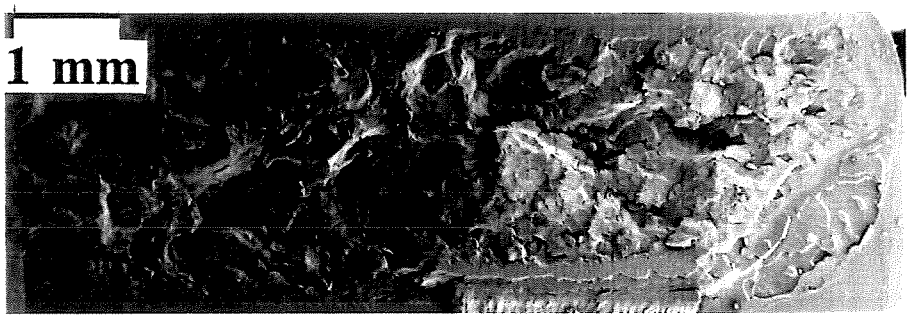

b)

Figure 1.15 - Fracture surfaces of a whole type I PS sample (perpendicular to flow view) - a) no weldline, b) with weldline

a)

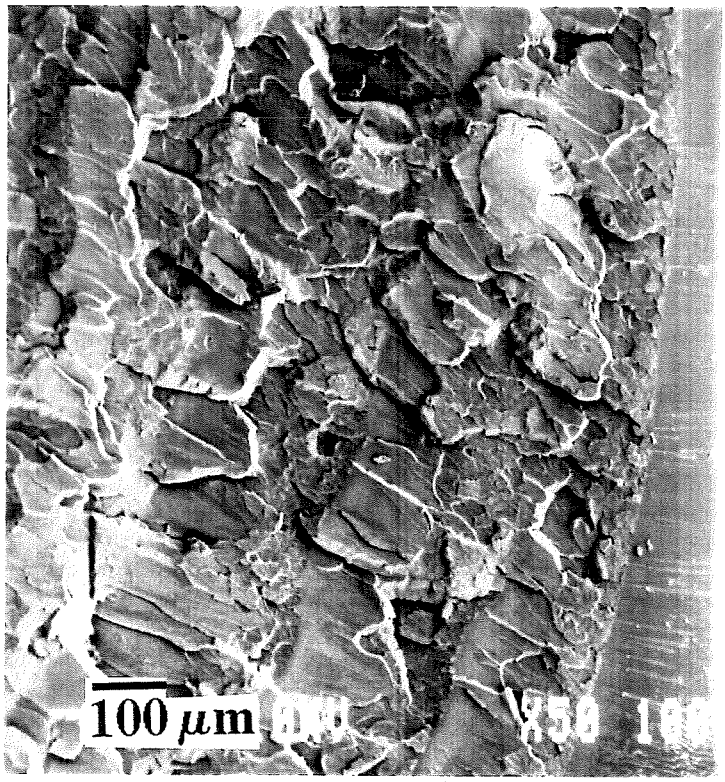

b)

Figure 1.16 - Fracture surfaces of a whole type II sample (perpendicular to flow view) - a) no weldline, b) with weldline, right behind the insert

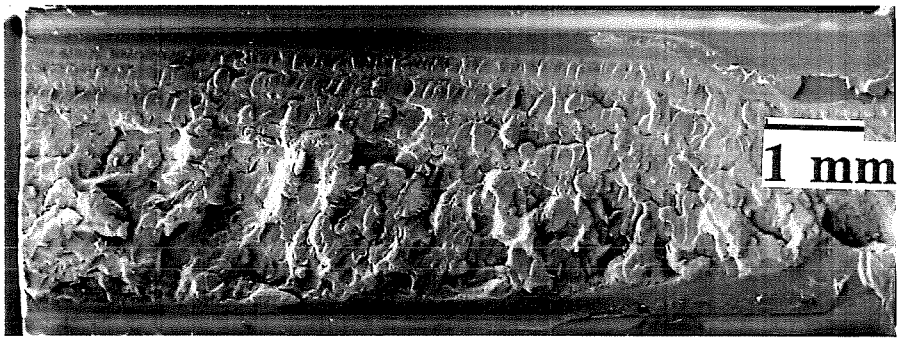

c)

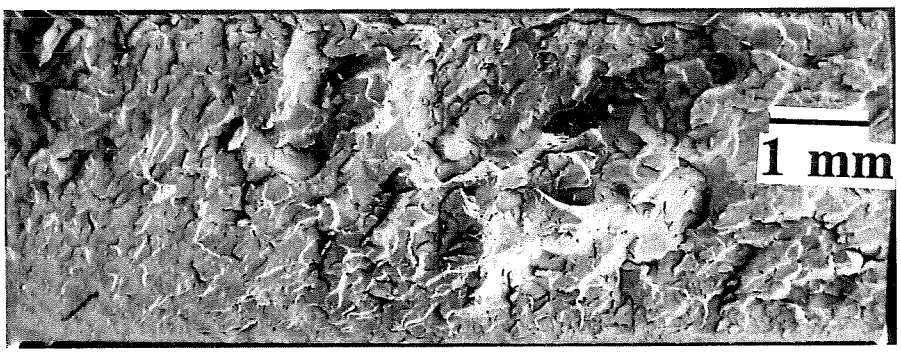

Figure 1.16 - Cont'd
c) with weldline, 10 mm away from the insert, d) with weldline, 40 mm away from the insert

- Packing stage: a sudden increase in pressure during this stage produces an effect similar to quenching (fast cooling). Thus, the front of crystallization (position of significant rate of crystallization) jumps towards the core leaving behind a layer of low degree of crystallinity. The packing pressure also affects the orientation distribution across the thickness. The melt compressed by the packing pressure has lower free volume and, as a result, the rate of orientation relaxation is considerably reduced. This contributes to higher levels of orientation close to the gate where the pressure is highest.

- End of molding: once the front of crystallization has reached the unoriented core ($\sim$ 500 μm from the surface for polypropylene), the α form of crystallization becomes largely predominant.

Microscopic examination of injection molded semicrystalline polymers confirms the existence of a layered structure, i.e., skin, subskin, and core. A highly oriented skin, where the crystallinity depends on the crystallization behaviour of the polymer. In the intermediate layer the crystallization is dominated by the matrix orientation and high temperature gradients. Nuclei are formed in the zone near the skin where the temperature is lower and crystallization then proceeds towards the core. The term transcrystallization is used to describe the crystal growth in one direction. Finally, the core contains randomly nucleated structures which grow in all directions. The layered

structure described above has been reported for a wide variety of semicrystalline polymers.[62-75]

Mechanical properties of injection molded semicrystalline thermoplastics are affected by the variations in crystallinity and orientation. Typically, the oriented but less crystalline skin and the unoriented, albeit more crystalline, core will be more ductile than the subskin layer.[69,70] As a result, fracture will often initiate in this intermediate layer in objects loaded parallel to the injection direction.[76]

It follows that the morphology of weldlines in semi-crystalline materials is more complex than that of a purely amorphous polymer. Hobbs,[77] using scanning electron microscopy on thin sections cut perpendicular to the weldline in polypropylene samples, concluded that while the surface notch at the weldline surface can act as a stress concentrator and initiate failure, the deformation is propagated through weaker regions which border rather than form the weldline. Similar results have also been reported.[38,78] For Trotignon et al.[79], Singh et al.,[80] Wenig et al.[81] the weldline zone is characterized by a low crystalline ratio, the absence of ß crystalline phase, and the lack of orientation along melt-flow direction, all of which may contribute to the lower strength and stiffness.

In addition to orientation and crystallization behaviour, two other influencing factors have been recognized: the notch effect, which as the molding shrinks form a

sharp ridge; and the concentration of inhomogeneities (abraded particles, impurities, mold release agent, and so on) in the weldline.[82,83]

The mechanical properties of the weldline are influenced by the material characteristics and by the processing conditions. In practical terms the freedom one has to improve the weldline strength by changing processing parameters such as the melt and mold temperatures to favor chain diffusion is limited (polymer degradation and longer cycle time).

Several investigators[3,84] have reported the beneficial effect of an increase in melt temperature on the weldline strength in amorphous polymers. According to Malguarnera[3] melt temperature in glassy polymers is the most important injection molding process parameter. It affects both the strength and elongation at break of samples with weldlines. Criens and et al.[84] recognized that the effect of melt temperature may vary from polymer to polymer. For PS, the weldline strength increases with increasing melt temperature. For PC no influence of the weldline on the yield strength could be found, but a significant reduction of both the ultimate strength and elongation was observed. In another paper, Criens[85] reported that the same tendency in impact strength is observed for the styrene based plastics (PS, SAN, and ABS). The impact strength of these material is reduced by the presence of a weldline. While for samples with weldlines the impact force at fracture increases with higher melt temperature (better diffusion across the weldline), it decreases in samples without weldlines (lower chain orientation).

Hubbauer[86] reported that the presence of a weldline in polycarbonate has a minor effect on their impact properties, while PVC loses half of its impact strength at the weldlines area. Increasing the melt temperature enhances the weldline strength. In the case of PS,[78,86] only sharp V-notch were observed and their dimensions are mainly related to the operating variables (melt temperature, mold temperature and injection rate) which influence the temperature of the flow front. The mechanism for weldline formation is attributed to a viscosity increase in the solid layer.

In semi-crystalline polymers (PP) the effect of processing parameters (mold and melt temperatures, cooling rate and injection pressure) is similar to that observed for their amorphous counterpart.[87,88] Criens[85] and Rosato[40] reported that the impact properties of POM samples with weldline are most affected by the melt and mold temperatures. Rallis et al[78] working with PA-6 recognized the formation of a V-notch in a double gated cavity, mostly affected by the mold temperature in addition to melt temperature, time and holding pressure. Singh and Mosle[89] have studied the structure/property relationship of double gated injection molded PP sample containing weldline. A slower cooling rate allows the molding to crystallize more thoroughly, as indicated by an increase in the degree of crystallinity and spherulite size, and leads to better mechanical properties. The opposite is true for higher mold temperature. The V-notch angle was found to decrease with an increase in the melt temperature. Impact strength was found to increase with melt temperature. In a tensile test, the sample broke at the weldline. The weldline region was less crystalline.

Watkinson et al.,[33] studying the effect of melt temperature on dynamic fatigue performance of PP, found that increasing melt temperature improves the load-bearing ability by up to 25%. The effect of a merging weldline (2 gates side by side) on fatigue caused a reduction of only 5%. The weldline region microstructure varied with melt temperature at low temperatures. It is characterized by the formation of columnar growth along the weldline which acts as a site for nucleation; at higher temperature, the weldline could only be identified by a change in the size of the spherulites. Examination of fatigue specimens showed that damage initiated in the shear zone. No appreciable damage occurs in the skin. In double gated specimens the effect of the weldline on the fatigue performance is more pronounced; 40% loss is observed.

Most of the literature dealing with the study of weldline used directly molded specimens.[3,84] In reality, the most frequently encountered weldline is the one obtained through the use of an insert. The effect of weldline produced in polystyrene double gated cavity (type I) is more pronounced than in type II specimens (weldline obtained through the use of an insert).[90] Under similar processing conditions, the weldline factor is 70% for type I compared to 90% for type II. Malguernera et al.[3] found a weldline factor of 70% for PS and HIPS and 90% for PP. For type II specimens, Menges et al.[20] found a weldline factor of 92% for PP and 90% for HIPS. These results again confirm that the results obtained on double gated specimens offer a general idea about a material's sensitivity to the weldline rather than an evaluation of the weldline strength in a molded part.

1.5 REINFORCED PLASTICS

Most of the results published on weldlines in reinforced plastics were also obtained using some sort of double gated dogbone shaped tensile bar mold in which the gates are located in the end of the dogbone (e.g., ASTM-D647). With this type of mold the fibers in the weldline possess a random-in-plane orientation, the plane of orientation being parallel to the plane of the weldline. There is no evidence that the fibers cross the weldline plane. Away from the weldline fibers are oriented parallel to flow. With the weldlines formed by flow around an insert the fibers acquire a parallel-to-flow orientation throughout the entire thickness[29,91-93] and keep it for a considerable distance from the insert. Fig. 1.17 shows the fiber orientation (Fig. 1.17B perpendicular to flow and Fig. 1.17C parallel to flow) observed in a rectangular mold cavity with short glass fiber reinforced polypropylene in the presence of an insert.[1] The weldline width depends on the type of material, cavity depth and the insert diameter but is essentially independent of the distance from the insert. It lies between 2000-8000 μm wide.[29,94,95] Away from the weldline zone the well known skin-core structure is observed. In this case the fibers in the skin are oriented parallel to flow and perpendicular to flow in the core. The question that must be asked is how far from the insert will the weldline disappear and the weldline zone fibers adapt the same orientation pattern as those away from it. Since a general answer is yet to be found, let us consider two simple mold shapes that are often used to study the flow generated fiber orientation for an edge gated rectangular plaque (Fig. 1.2A) and a centrally gated disc (Fig. 1.18).

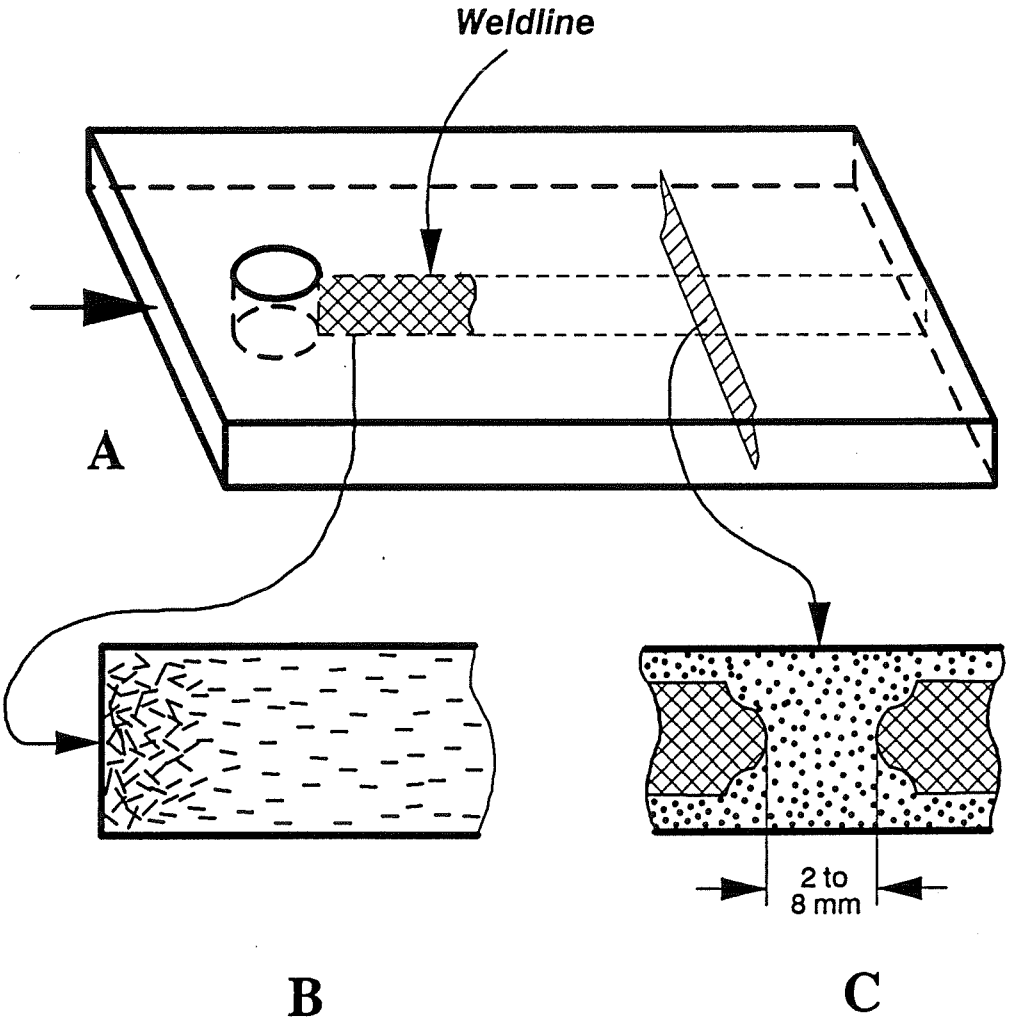

Figure 1.17 - Fibre orientation in the and away from the weldline in glass reinforced polypropylene, type II plaque[1] - B- perpendicular to flow view, C- parallel to flow view

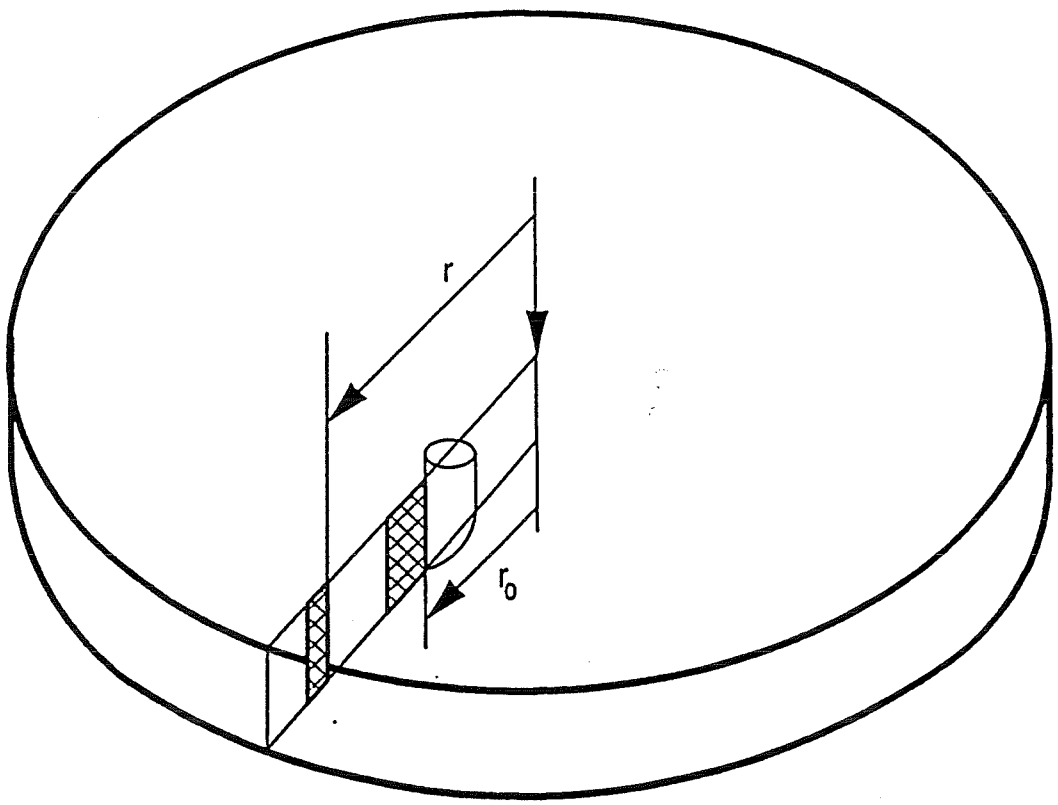

Figure 1.18 Flow in the center of a centrally gated disc mold cavity assuming pure elongational flow. If an insert is located at a distance r_0 from the gate, the element of the weldline having an area of A_0 (at r_0) will be reduced to r_0A_0/r at a distance $(r\text{-}r_0)$ from the insert[2] .

In an edge gated mold the melt first spreads around in a semicircular fashion until the longer of the mold cavity side is reached (see Fig. 1.2A). At this stage the fiber orientation will be similar to that observed in centrally gated disk molds, i.e., flow parallel to the skin where the shear rate is high and perpendicular to flow in the core because of the lateral expansion of the melt front. When the longer side is reached the principal flow direction then changes to follow the longer axis until the mold is filled. Because the molten plastics are highly pseudoplastic the velocity profile across the thickness is generally quite flat. Therefore the core layer where the shear rate is very low will keep the fiber orientation acquired close to the gate for a considerable distance. However, after a sufficiently long flow the fiber orientation should coincide with the flow direction even in the core.[96] In the weldline zone the flow around the insert has already generated fiber orientation parallel to flow. It follows that the difference between the weldline and the rest of the sample will disappear only when the fibers possessing an orientation different from parallel-to-flow (i.e., core fibers away from the weldline) realign to the same orientation as the one in the weldline zone.

In the centrally gated disk mold (Fig. 1.18) the perpendicular-to-flow orientation in the core is also due to the tangential stretching of the melt front as it flows outward. Since the tangential component of the velocity at the melt front is 2π times larger than the radial component the fibers in the weldline should eventually realign and adapt the same orientation as those away from it (i.e., perpendicular to flow). The orientation process in elongational flow can be described by Equation (1.8)[97-99]:

$$\tan \psi \; / \; \tan \psi_o = (A/A_o)^{3x/2} \qquad (1.8)$$

A fiber having an aspect ratio p, oriented at an angle ψ_0 to the local streamline, will reorient to an angle ψ in an elongational flow characterized by the convergence ratio A/A_o. The orientability parameter χ is given by:

$$\chi = (p^2 - 1) \; / \; (p^2 + 1) \qquad (1.9)$$

Assuming a pure elongational flow in the core the convergence ratio A/A_o at a distance r from the gate is equal to r_o/r, r_o being the distance of insert from the gate. It follows that a fiber having a perfect radial orientation ($\psi_0 = 90°$) should never reorient. However, since all fibers deviate from this perfect orientation a gradual reorientation will take place (Table 1.2).

Table 1.2 Values of angle ψ calculated using Equation (8) as a function of the convergence ratio r_0/r and the angle ψ_0. A high aspect ratio p is assumed $(x=1)^2$.

r_0/r	0.5	0.2	0.1
ψ_0 (deg)	ψ (deg)		
89	87	79	70
85	76	46	20
80	63	27	10
45	19	5	2

The disappearance of the weldline may be hampered by the effect of fiber orientation on melt viscosity which leads to the unusual mold filling pattern observed with fiber filled resins. The junction of two fronts persists for a long distance (Fig. 1.2B). It is to be noted that with neat or glass bead filled resin the junction vanishes shortly after the two fronts have met. A theoretical analysis of flow around a circular insert[100] also predicts a fast disappearance of the junction. This observation indicates that with fiber filled resins the melt in the already formed weldline does advance at a substantially lower velocity than the one adjacent to it. It appears that, when filled with fibers, the melt in the weldline advances at a slower pace than in other areas of the plaque. The viscosity of suspensions η_s can be interpreted using one of the many empirical relations such as the Mooney equation:

$$ln\ (\ \eta_s\ /\ \eta_0\ )\ =\ k_E\ \phi\ /\ [\ 1\ -\ \phi\ /\ \phi_m\ ] \qquad (1.10)$$

where η_0 is the viscosity of the suspending liquid, k_E Einstein coefficient, ϕ the volume fraction of the filler and ϕ_m the maximum packing fraction. Nielsen[101] gives the following values of k_E for fibers of aspect ratio p: oriented parallel to flow (k_E = 2p); perpendicular to flow (k_E = 1.5). This suggests that in the weldline, where the flow around the insert has generated fiber orientation parallel to flow, the effective viscosity is higher and the melt advances at a lower velocity than that away from the weldline where at least a portion of fibers (those in the core) offers a reduced resistance to flow.

As a result the stagnating weldline zone plays a role similar to that of the mold wall, i.e., fibers are deposited onto it from both sides by the lateral expansion of the advancing front generating the essentially unidirectional structure in the area.

The same approach as used for neat resins, i.e., testing directly molded samples on and outside the weldline is illustrated in Fig. 1.19. The curves were obtained by placing an extensometer (10 mm gage length) on the weldline (curve ON-WL) and 20 mm away from the weldline (curve OUT-WL) and compared to a sample without the weldline (No-WL). The average local strain rate in the weldline area (whose width was estimated to be about 2000 μm) is 3 times that of the material away from the weldline in the same sample tested at the same time. It is also higher than that of the weldline free sample tested under identical conditions. These local strain rate differences reflect local variations in the stiffness which are lowest in the weldline zone.[94]

Fisa and Rahmani[1] and Meddad and Fisa[94] studied the effect of cavity shape, i.e., directly molded (type I) and plaque (type II) with insert, on the weldline strength in glass fiber reinforced polypropylene as a function of fiber concentration. Some of their results are shown in Fig. 1.20. While significant differences in strength are observed in samples of different shapes without weldlines (curves I and II), the weldline strength is independent of the cavity shape and is a function of fiber concentration only (Fig. 1.20). In the case of glass-fiber reinforced polypropylene the weldline strength, σ_W, obeys the equation:

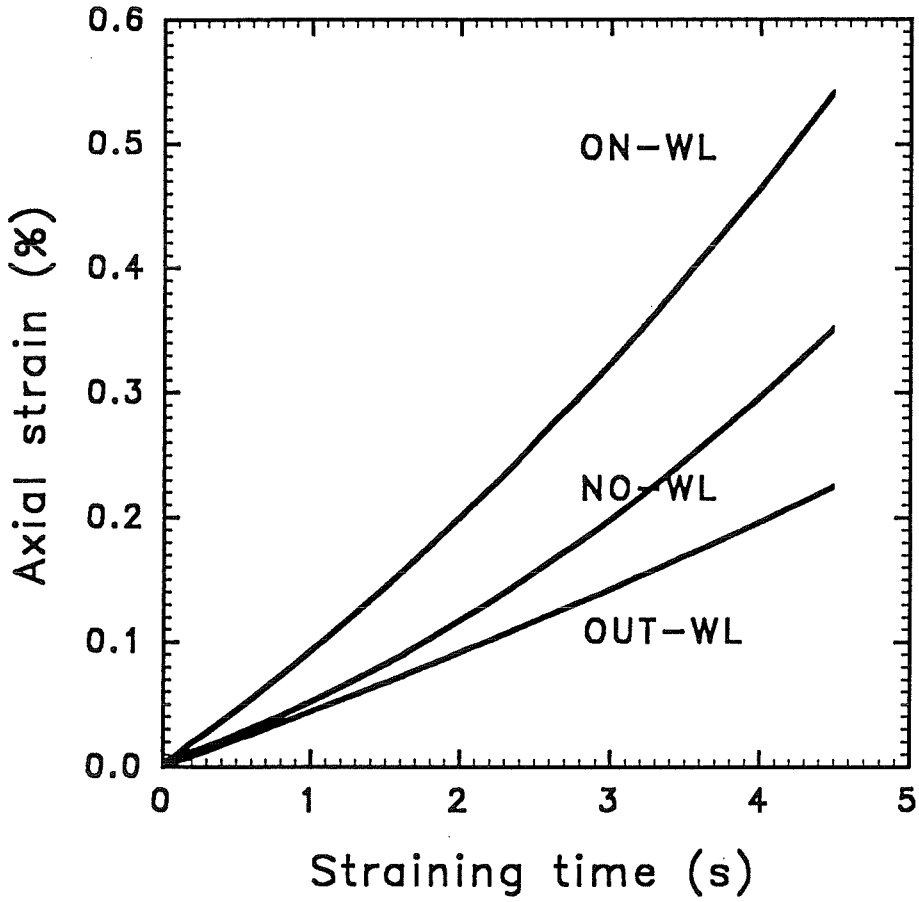

Figure 1.19 - Strain as a function of time, recorded by a 10 mm gage length extensometer, in the 33 wt.% type I samples; ON-WL: on the weldline; NO-WL: no weldline; OUT-WL: strain measured outside the weldline

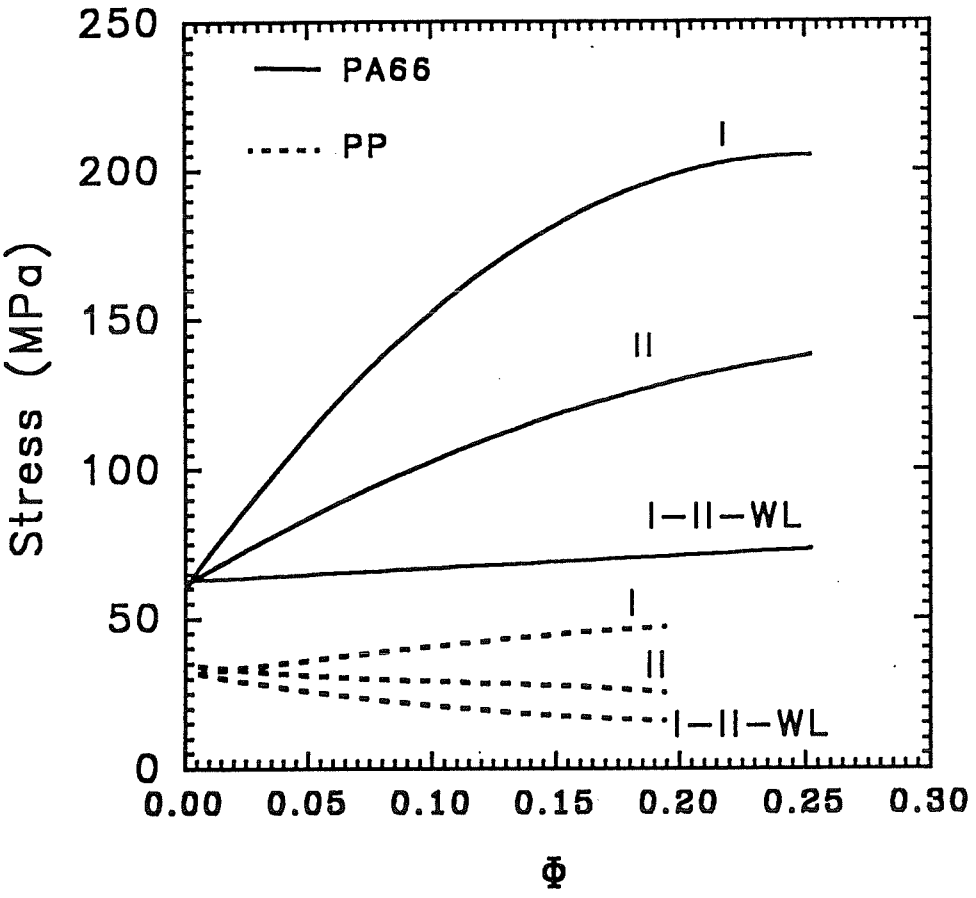

Figure 1.20 - Tensile strength as a function of fibre volume ϕ, for type I and type II without (I,II) and with weldline (I-II-WL) specimens - PP: (---); PA66: (-)

$$\sigma_w = \sigma_M \left[1 - \left(\frac{4\phi}{\pi} \right)^{1/2} \right] \qquad (1.11)$$

where σ_M represents the matrix strength, and Φ is the fiber volume fraction. This equation assumes that the fiber orientation in the weldline is perpendicular to the applied stress and that the fiber-matrix interface has been entirely debonded prior to fracture. With engineering plastics such as nylon[23,94] and polycarbonate[102] the weldline strength is higher than that predicted by Equation (1.11), indicating that the fiber-matrix interfacial strength cannot be neglected. The weldline strength is approximately equal to that of the unreinforced matrix. Table 1.3 resumes the results obtained with glass-fiber reinforced polycarbonate.[102]

Table 1.3 Tensile properties of Neat and Glass fiber Reinforced Polycarbonate (ASTM-D647 Shape samples machined from double-gated rectangular plaques 32 mm wide x 127 mm long, 3 mm thick; samples without weldline were produced by blocking one of the gates). Values represent properties at yield for neat and at break for reinforced polycarbonate[102].

	Polycarbonate		Polycarbonate (30% glass fiber)	
	No-weldline	weldline	No-weldline	Weldline
ϵ (%)	6.5	6.5	2.3	0.9
σ (MPa)	60	60	111	47
E (GPa)	2.4	2.2	6.6	5.3

In long-fiber reinforced plastics the weldlines are even weaker. For instance, Bouti and Fisa[103] and Lalande[104] reported that the weldline strength in long-fiber reinforced PP is extremely poor and decreases with fiber concentration (Table 1.4). Akay et al.[29] reported that impacted long-glass-fiber polypropylene plaque showed fracture by delamination of the core layer from the surface layers, akin to the delamination of plies in continuous fiber-thermosetting systems. Higher impact values and isotropic fracture were observed for twin gated plaques. This was attributed to the enhanced mixing and randomization of orientation because of the head-on collision. Short-fiber filled PP observe lower impact properties. Recently Akay et al.[105] reported that long-fiber reinforced polyamide suffers further weakness because of its vulnerability to melt-fracture induced voiding in the thicker molds where flow divergence may occur. The voiding appears to be eliminated in the thin moldings (2 mm thickness) and as a result the weldline strength becomes at least comparable with that of the short-fiber filled grade.

Table 1.4 Weldline strength of long fiber reinforced polypropylene. Tensile bars were cut from 4 mm thick plaque in transverse direction[103].

	30 % G.F	40 % G.F	50 % G.F
σ (MPa)	70	66	64
σ_{WL} (MPa)	17	12	10
σ_{WL} / σ	0.24	0.18	0.16

The effect of platelet-reinforcement on weldline strength is less documented. The weldline integrity of mica-filled polypropylene was found to be greatly influenced by flake concentration, flake size and surface treatment.[9] Weldline weakness is due to orientation of mica flakes parallel to the weld plane. Similar results have been reported for mica-filled nylon 66 in addition to the fact that molding conditions have little effect on the weldline strength[106] as well as for talc-filled polypropylene.[107,108] Table 1.5 summarizes the effect of various reinforcements and filler on the weldline strength of directly molded PP samples.[90]

Table 1.5 Effect of various filler and reinforcements on the weldline strength (stress at break) of directly molded PP specimens[90] (NWL and WWL stand for without and with weldline).

		σ (MPa)	Weldline factor (%)	E (GPa)
PP	NWL	33	90	1.80
	WWL	30		1.60
PP + 30% Short Glass Fiber	NWL	50	44	6.40
	WWL	22		2.80
PP +30% Long Glass Fiber	NWL	78	23	6.60
	WWL	18		2.80
PP + 30% Glass Beads	NWL	21	100	2.00
	WWL	21		2.00
PP + 30% Talc	NWL	32	34	3.80
	WWL	11		2.00

Finally let us mention the weldlines in the reinforced structural foams. The term "structural foam" refers to materials which consist of a foamed core surrounded by a solid skin. The core and the skin are from the same material and are molded on a modified injection machine. The fiber orientation is similar to that observed in other injection molded composites. In structural foams the weldline zone consists of a higher density material than the one away from the weldline. The density fluctuation may overshadow the effect of fiber orientation on the mechanical behaviour of the weldline.[100,109]

1.6 POLYMER BLENDS

During this last decade, polymer blends have been a new area of growing interest to both industrial and scientific communities. It is now possible to tailor new plastic materials in conventional processing equipment rather than in the costly polymerization plants.

The influence of morphology on physical properties of immiscible polymer blends is very important. In such systems both phases are deformable and orientable so when injection molded they result in a complex morphology. The most common structure is the usual skin core morphology as a result of the fountain flow.[13] Therefore the size and the shape of the minor phase plays a major role particularly with respect to impact strength, elongation at break, barrier properties, and flow properties. The morphology

of the dispersed phase is controlled to varying degrees by interfacial modification, viscosity ratio, elasticity ratio, composition, shear rate and/or shear stress, and processing conditions.[10] Among these parameters, interfacial modification appears to be the dominant one in controlling the dispersed phase size.[110] This is due to the fact that it can minimize the influence of composition, and can significantly moderate the viscosity ratio effect. The term used for this operation is called compatibilization. It is any of the several techniques used to improve the interfacial adhesion in multiphase systems. This is achieved through the use of a third component (copolymers, ionomers) which are capable of physical and/or chemical interactions with the individual component of the system.[111,112] The surface tension is reduced as well as the dispersed phase particle size. A more stable morphology and improved mechanical properties are obtained.

One of the main concerns in the processing of polymer blends is the stability of the morphology. It is generally believed that the addition of an interfacial modifier leads to a better stabilization of the morphology. Despite this fact, little detailed work has been undertaken on both compatibilized and non-compatibilized blends during injection molding, and particularly in the presence of weldline.[113] Lindsay et al.[114] reported that interfacial modification may bring a significant improvement to the weldline strength. It is somewhat surprising that despite the substantial growth of polymer blends, and considering the importance of the injection molding process, there are only a few studies on the structure/mechanical properties relationship of injection molded polymer blends. As mentioned above, the presence of weldlines in injection molded parts are almost

inevitable. The objective of the present section is to review the few studies on the mechanical and the morphological characteristics including weld lines of injection molded polymer blends.

In polymer blends, the morphology of injection molded parts is characterized in general by three distinct layers, i.e., the skin, the sub-skin and the core. The work of Thamm[115] on high impact strength blends of PP and EPDM is among the early studies on the effect of weldlines in polymer blends. A clear difference in crystallinity between the skin and the core is observed. Near the mold surface, PP molecules are highly oriented in the flow direction and are non-spherulitic. The core has a spherulitic crystallinity. The dispersed phase is oriented in the flow direction and is larger in the skin than in the core. By contrast, in the core it has a globular shape. This is further supported by another study[116] on injection molded PP blends modified with ethylene/ propylene/diene terpolymer (EPDM) and thermoplastic polyolefins rubber (TPO). A skin-core morphology is formed in both the continuous PP matrix as well as in the modified PP blends containing rubber particles of various deformation.

A common finding is the existence of an anisotropic distribution of the dispersed phase throughout the thickness of the sample. The apparent absence of the dispersed phase in the outer skin should also be noted.[115,116] In a recent study, Fellahi et al.,[117] through a detailed morphological investigation. showed the presence of the dispersed phase in the skin with almost the same composition as in the as prepared blend. For the

non-compatibilized systems (Fig. 1.21a) a highly oriented sub-skin region with a high dispersed phase concentration, and shear induced coalescence are observed. When a compatibilizer is used, the morphology is more stable and lower elongation is observed in the sub-skin region (Fig. 1.21b). A similar morphology is observed for the non-compatibilized PP/PC blends when injection molded. It was found to exhibit a complex skin-core morphology which evolves with composition.[118]

Weldline in injection molded polymer blends is not well documented. In his review paper on the application of polymer blends, Robeson,[11] reported that with complex molds, the elimination of weldlines is virtually impossible, and very poor retention of strength (especially impact strength) is observed. This problem is often the "Achilles's heel" of immiscible polymer blends and is much more severe in injection molding than in extrusion applications. Weldline strength and toughness are often a problem in homogeneous materials. However, it is a particularly serious problem in heterogeneous blends. Moreover, this region is known to be structurally different from the rest of the sample.[2,35] In the case of the PP/PC system, the weldline appears to consist of deformed PC particles oriented parallel to the weldline.[118] While for the compatibilized system HDPE/PA6 with an ionomer, the weldline produced through the use of an insert has a much finer morphology than the bulk of the sample and is about 200 μm wide, for a non-compatibilized samples the weldline is 600 μm wide. Furthermore and as a result of the fountain flow, it is reported that the weldline region consists mainly of the matrix with an apparent absence of the dispersed phase.[59,115,116]

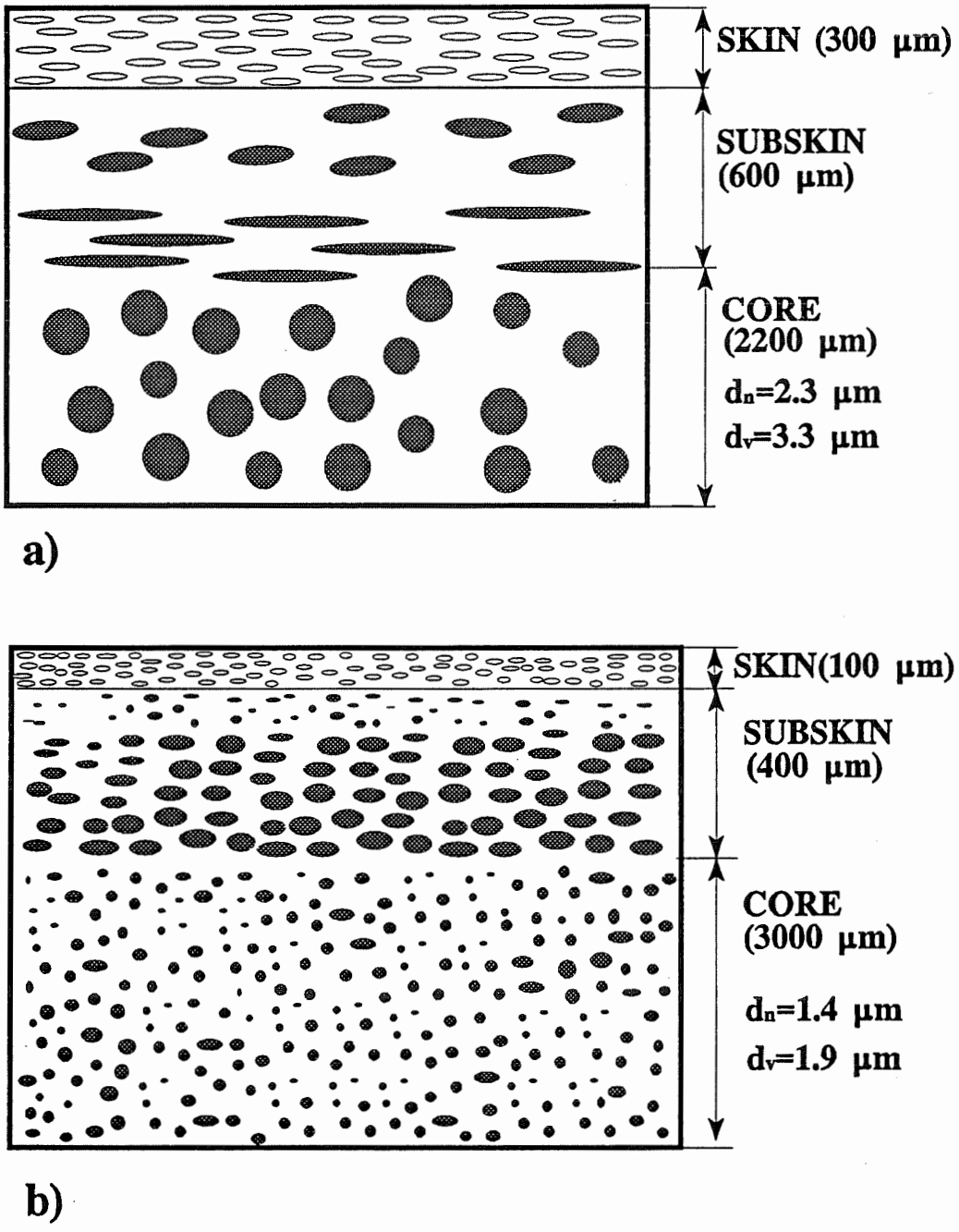

Figure 1.21 - Schematic illustration of the skin/core structure in injection molded polymer blends - a) without compatibilizer, b) with compatibilizer

Fellahi et al.,[117] using an ionomer as a compatibilizer for HDPE/PA6 blends, showed that what seemed to be an apparent absence of the minor phase in the skin and weldline region is only an artifact. In fact, X-ray electron spectroscopy, differential scanning calorimetry and transmission electron microscopy analysis revealed the presence of the minor phase on both skin and weldline regions at almost the same concentration as the prepared blend. The overall behaviour is similar for both systems, without (Fig. 1.22a) and with (Fig. 1.22b) compatibilizer, although there is a difference in the size of the dispersed phase, and the width of the weldline. The compatibilizer causes a reduction of the dispersed phase size and a narrower weldline region.

Mechanical properties of injection molded parts were mostly studied using dogbone shaped specimens. The observed structure in such items has a profound effect on their mechanical behaviour. For instance, and as was reported earlier,[116] during tensile and tensile impact loading failure is initiated in the shear zone along the skin core boundary. This zone has a transcrystalline character and favours the formation of crazing. Final fracture depends on the simultaneous interaction of crazing and shear yielding which is closely related to the dispersed phase average particle size.

In a series of publications by Paul and co-workers on several immiscible blends, HDPE/PS,[114] PP/LDPE[119] and HDPE/PP[120] reported that generally speaking the mechanical properties of such systems are quite poor. Measures of ductility like impact strength or elongation at break always show negative departures from additivity and

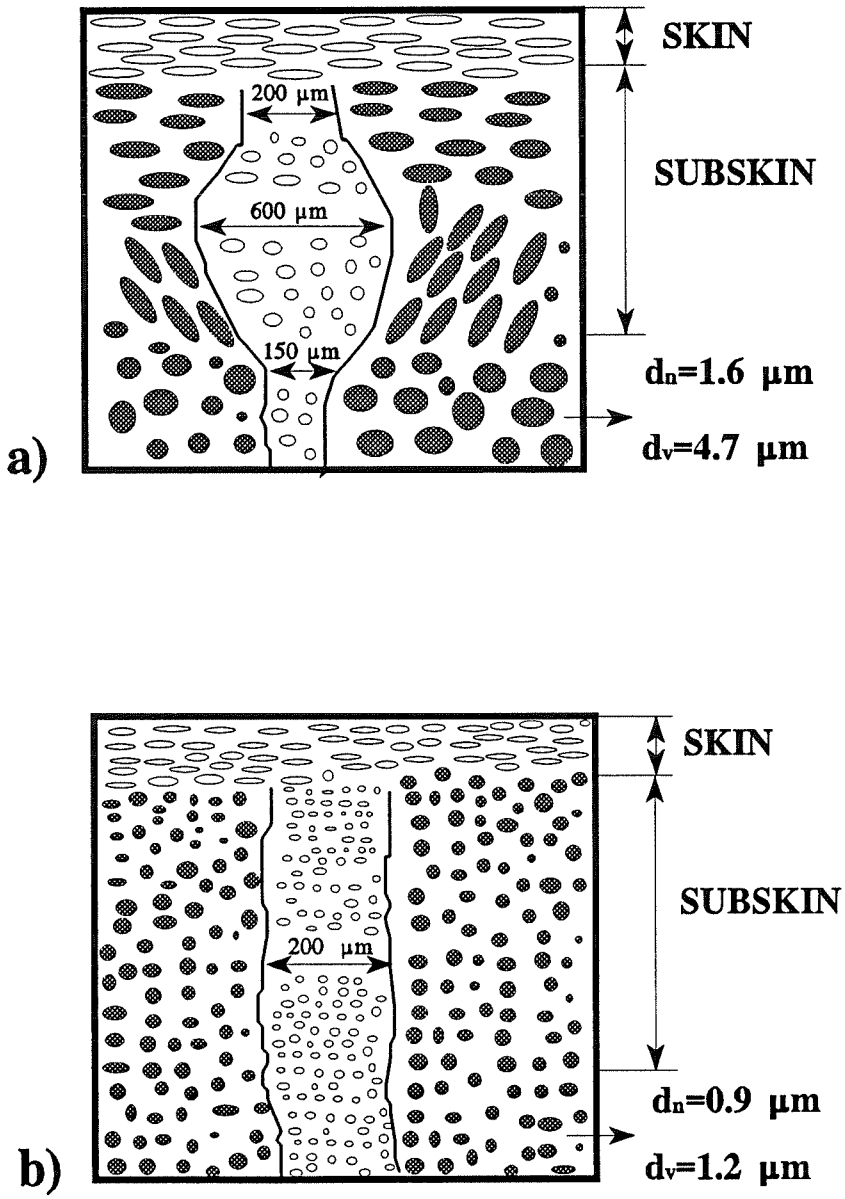

Figure 1.22 - Schematic illustration of the weldline structure in injection molded polymer blends - a) without compatibilizer, b) with compatibilizer

exhibit minima in some cases, although no morphological study was undertaken to support these results. Fisa et al.[118] have undertaken a similar comparative study on PP/PC. The hypothesis of flow induced dispersed orientation can be used to explain the differences observed between the properties of the samples machined from plaques and those directly molded into the dogbone shape. The machined samples exhibit lower modulus and yield strength. In the end gated dogbone shaped cavity the melt convergence, as it enters the narrower section, must impart additional orientation and elongation to the dispersed phase. Fracture occurs in the area where the melt exits from the narrow section, where the diverging flow starts to orient the elongated structure in the direction perpendicular to flow.

The measured effect of the compatibilizer on the mechanical properties of injection molded HDPE/PA-6 depends greatly on the mold shape and on testing conditions.[117] In directly molded tensile samples, the highly stretched polyethylene particles oriented parallel to the applied stress bear their fraction of stress and the yield stress is independent of the presence of the compatibilizer. When test specimens are machined from molded plaques, the properties in the direction parallel to flow were found to be similar to the type I mold and not affected by the increase of plaque thickness. The anisotropy is quite pronounced in the non-compatibilized blend and the effect of the distance from the insert is negligible.[124]

Weldlines are almost always significantly weaker in tension and flexural stress than material molded straight through. In the case of double gated specimens of EPDM/PP, knit lines are especially weak when the dispersed phase has a low viscosity. This is attributed to a very characteristic dispersion of the elastomer phase at the weldline in the form of thin sheets perpendicular to the melt flow direction and parallel to the weldline. This will prevent adequate bonding across the weldline region and probably act as internal stress concentrators as well.[116] These findings support the already reported results by several authors.[4,7,59]

A common feature for injection molded blends (at least semi-crystalline) is that when loaded in tension, failure initiates in the weldline at the edges of the cold welded samples.[77] Crazes initiate from the weldline edges in the inner skin layer (shear zone), and propagate inside.[116] Watkinson et al.[33] established that during fatigue tests of injection molded PP copolymer specimens, damage occurs initially in the sub-skin (shear zone) region.

Rosato[40] and Remaly et al.[121] reported that flame retardant ABS is very sensitive weldline material especially during impact testing. Rubber particles were severely elongated parallel to the weldline and might be the cause of this weakness.

In the already mentioned series of articles published by Paul and co-workers,[114,119,120] only dogbone shaped specimens were used. In every case, failure

occurred at the weldline. Blends with a weldline showed very poor elongation at break, but their strength and elongation at break were improved with the addition of an appropriate compatibilizer. Similar observations were reported for HDPE/PS systems.[122,123] The mechanical properties are generally lower when weldlines are present. The addition of a copolymer significantly improves the strength and the elongation at break of this blend. An important effect of the injection temperature on the tensile strength and the elongation at break of welded samples with copolymer modified blends was observed. The effect of mold temperature on these properties was less important mainly at low temperature. Similarly, Fisa et al.[118] have studied the effect of weldline in non-compatibilized PP/PC blends and observed no difference between machined and molded samples with weldline prepared from non-modified PP/PC. Fellahi et al.,[124] studying injection molded HDPE/PA-6, reported that in directly molded samples, the weldline strength loss is about 40% in the non-compatibilized blends. The introduction of the compatibilizer has restored the material's ability to yield and the properties are close to those measured without weldline. Using the same approach as before, i.e., testing on and outside the weldline, the results are shown in Figs. 1.23 and 1.24. In the non-compatibilized blend, the weldline region has a lower stiffness compared to the outside of the weldline region material (Fig. 1.23). When a compatibilizer is added, this difference is attenuated (Fig. 1.24). For the second type of mold, where an insert was used to produce a weldline, the effect of the weldline is less pronounced, and the effect of the distance from the insert is negligible. In the absence of a compatibilizer a strength loss of about 15% is recorded compared to samples machined from the plaque without

an insert. In compatibilized blends, all tensile properties are unaffected by the presence of weldline, except for the 2 mm thick plaque in the position close to the insert. Finally, there is an interesting, although incomplete,[125] study where the effect of injection speed, hold pressure, mold and injection temperatures on the weldline strength of dogbone bars made of PC/ABS blends were investigated. Parameters which affect the molecular diffusion (melt and mold temperature) seem to have the most important effect in the sense that they help restore the strength loss due to the presence of weldline.

Menning[126] reported the effect of weldline on mechanical properties of injection molded PP/EPDM and PBT/Polybutadiene blends. All characteristics values show very little or no effect of processing parameters, i.e., melt and mold temperatures, and holding pressure on the strength of specimens with weldline. PP/EPDM blends were found to be more sensitive to the presence of weldline than the PBT/polybutadiene in the conventional tensile test; however, a pronounced weakness of the weldline was found in dynamic test (Impact).

1.7 HOW TO DEAL WITH WELDLINES

The early literature on weldlines aimed at alleviating the strength loss via the optimization of processing parameters has shown that the room for improvement was rather limited. Various approaches are now available and many of them can be found in the patent literature. They can be divided into four categories: processing

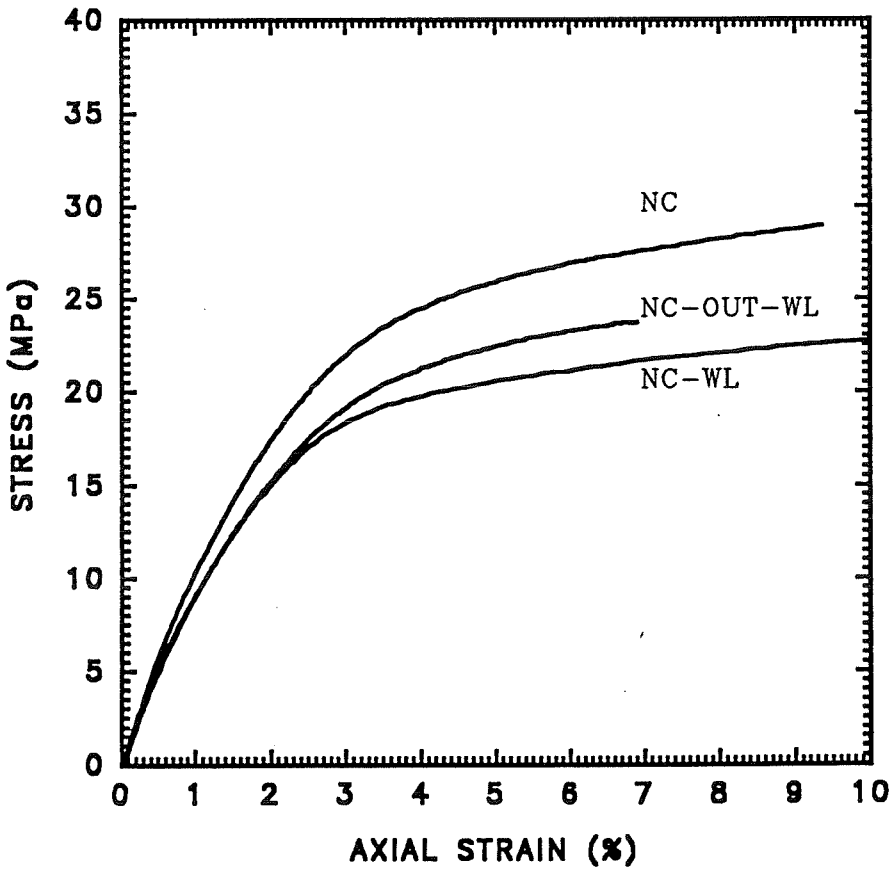

Figure 1.23 - Stress/strain curves for non-compatibilized HDPE/PA6 (25/75 vol%) blends measured using a 10 mm gage length extensometer. No WL:no weldline, OUT-WL or ON-WL:the extensometer is either placed 10 mm away from or on the weldline respectively

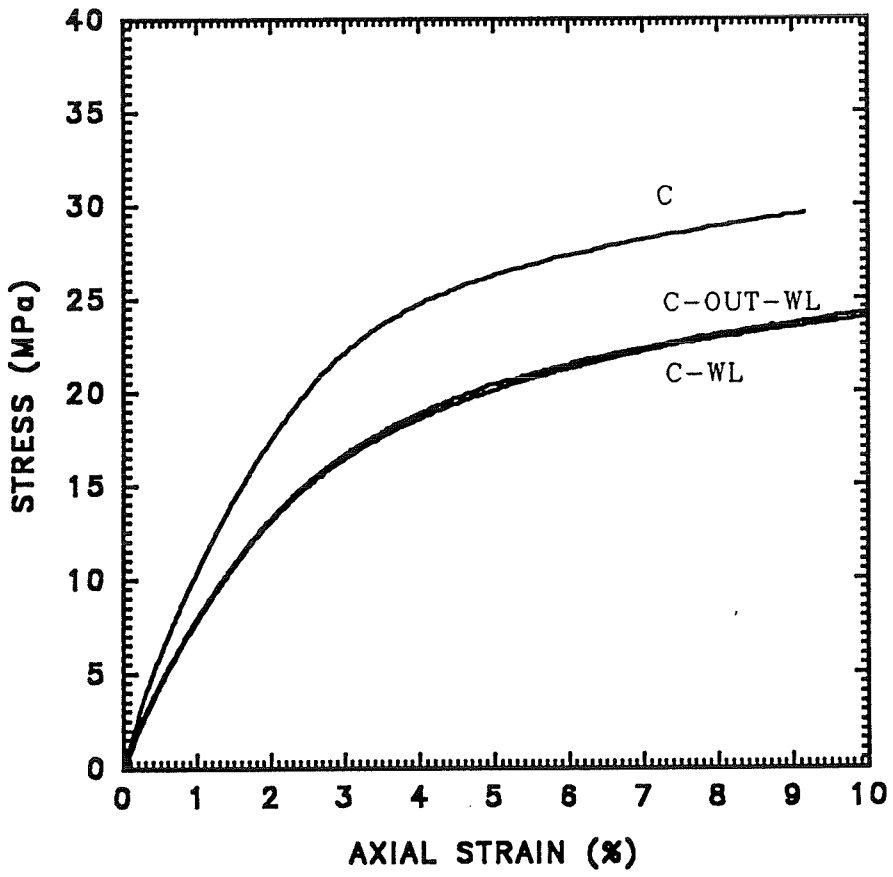

Figure 1.24 - Stress/strain curves for compatibilized HDPE/PA6 (25/75 vol%) blends with an ionomer. The same notation is used as in Fig. 1.23

parameters, material parameters, machinery parameters and break-away techniques.

1) Processing parameters: this aspect has already been discussed in the previous sections, although in practice the room for manoeuvre is rather limited.

2) Material parameters

a) Postmolding treatment: in an effort to strengthen weldlines, Brewer[127] suggested three types of treatment. Two of the methods, i.e., mechanical removal of the notch and heat treatment above the heat distortion temperature of the material resulted in only marginal improvements in weldline strength. Controlled solvent exposure of ABS materials containing weldline did result in significantly improved strength.

b) material composition: this method was mainly developed for multiphase systems where component mismatch can cause problems at the interface of two flow fronts. Through the control of morphology and the improvement of the interface between the various components, researchers were able to find great improvement in the strength of parts containing weldlines.[38,128-138] The interfacial modifier is known to reduce the interfacial tension, the size of the dispersed phase, improve the interfacial adhesion and stabilize the morphology. Therefore the morphology is more or less uniform in the weldline region as well as elsewhere in the sample and matching the viscosities of both phases is found to bring beneficial effects to the weldline strength. It is also known that

a viscosity ratio close to one, favours a fine dispersion and a more uniform stress distribution. The use of endothermic blowing agents for strengthening weldlines in foamed products is also reported[139] as well as the use of an external lubricant in ABS formulations.[140] In this case the use of lubricants promotes the plug-like flow in the mold which reduces the deformation of the rubber particles in the melt front (Table 1.6). In materials containing anisometric particles (fibers, platelets), reduction of the aspect ratio and the use of interface adhesion promoters can also have a beneficial effect (results are shown in Table 1.7).

Table 1.6 Weldline strength factor (%) for ABS with and without lubricants at different cross head speeds[140].

Composition	Weldline strength factor (%)	
	Low cross head speed (5 mm/min)	High cross head speed (50 mm/min)
ABS (no lubricant)	30	26
ABS + 1.25% A-C	100	99
ABS + 2.5% A-C	100	98
ABS + 1.5% EBS	50	53
ABS + 3.0% EBS	79	77
ABS + 1.5% hydrogenated glyceride	68	72

A-C: different oxidized low molecular weight polyethylenes, ZnSt, CaSt, St:stearic acid, EBS:ethylene-bistearamide.

Table 1.7 Dependence of weldline strength on Mica concentration and interfacial modification[9].

Mica type	Weight fraction (%)	Weldline factor (%)
Mica-filled PP	5	86
	20	50
	40	31
Treated mica-filled PP	5	85
	20	55
	40	40

3) Machinery parameters

a) mold design: Several techniques were developed using different approaches such as positioning the weldline in a non-critical position of the part[141-148] or improving the mixing at the weldline.[149] This is achieved through the use of flow diverters (having different dimensions) on both sides of the mold cavity. By creating this difference in size, the flow front hesitates and shifts to the larger diameter runner side causing an initial transient flow, then reverses the flow in the opposite direction, and finally reverses the flow once again to its original direction. These changes in flow direction are expected to increase weldline strength. Another approach reported recently by Gardner et al.[150] consists of an in-mold moving boundary system that promotes local mixing in the weldline area during mold filling. The process utilizes one or more cam operated reciprocating pins that promotes lateral displacement of the melt during mold filling.

The use of a heated insert has also been suggested and was found to improve weldline strength in unfilled PP, but when reinforced with glass fiber no effect was observed.[151] Another method has also been proposed, i.e., an overflow tab installed at the weldline to help sweep the melt fronts through the seam and improve mixing. The tab is later cut from the molded part.[152,153]

b) machine design: the basic idea behind the development of such a process lies in how the weldline topography is influenced. There are several processes in which the weldline is made to be non-planar. By various means the weldline, instead of appearing like a butt joint, is made to be analogous to a tongue and groove. This can be achieved by:

i) influencing the weldline topography through sequential filling; Michaeli et al.[154] suggest doing this through an appropriate control of the shut-off system of the hot runner nozzles. At the start of the mold filling operation, the melt first flows uniformly through the two nozzles until such time as one of the nozzles is shut. Following this, the remainder of the cavity is filled via the second nozzle still open, causing the weldline to be displaced. A similar approach has been reported by Nguyen et al.[155] and employs sequential filling during which the injection gates are opened at different times leading to a relocation or complete elimination of the weldline.

ii) influencing the weldline topography through appropriate gating[154]: the principle of this method is shown in Fig. 1.6. The melt flows uniformly into the cavity via both gates, such that the weldline forms in the middle between the two gates at time t_1 (Fig. 1.6a). After the weldline has fully formed, the upper part of the molding still has to be filled. The prevailing pressure distribution pushes the melt to flow through the weldline and causing its displacement, thus making it less vulnerable (Fig. 1.6b).

iii) the push-pull injection molding process exploits the machine technology of multi-color injection molding with modified control system. The machine is made up of two injection units which are controlled completely independently of each other (Fig. 1.25). The cavity is filled simultaneously by both units via two separate gates (Fig. 1.25A). After the flow fronts meet, the cavity is full and the weldline is formed, the control electronics permits one unit at a time to be retracted, while the second continues to inject the molten material (Fig. 1.25B and C) and reverses the flow of the still molten core to move it in the reverse direction, pushing it through the more viscous barrier of material at the flow joint, thus providing an enlarged area and improved strength in the joint.[154,156-159] Tomari et al.[160] used this approach to mold fiber reinforced polycarbonate (FRPC) and improve weldline strength. Their results are summarized in Fig. 1.26. The weldline topography and the weldline strength (weldline factor) of FRPC as a function of weldline displacement (see insert in Fig. 1.26) are shown in Fig. 1.26. The longer the weldline displacement, the stronger the structure. Another variation of this method is the so-called double or multiple live-feed injection molding developed by Bevis et

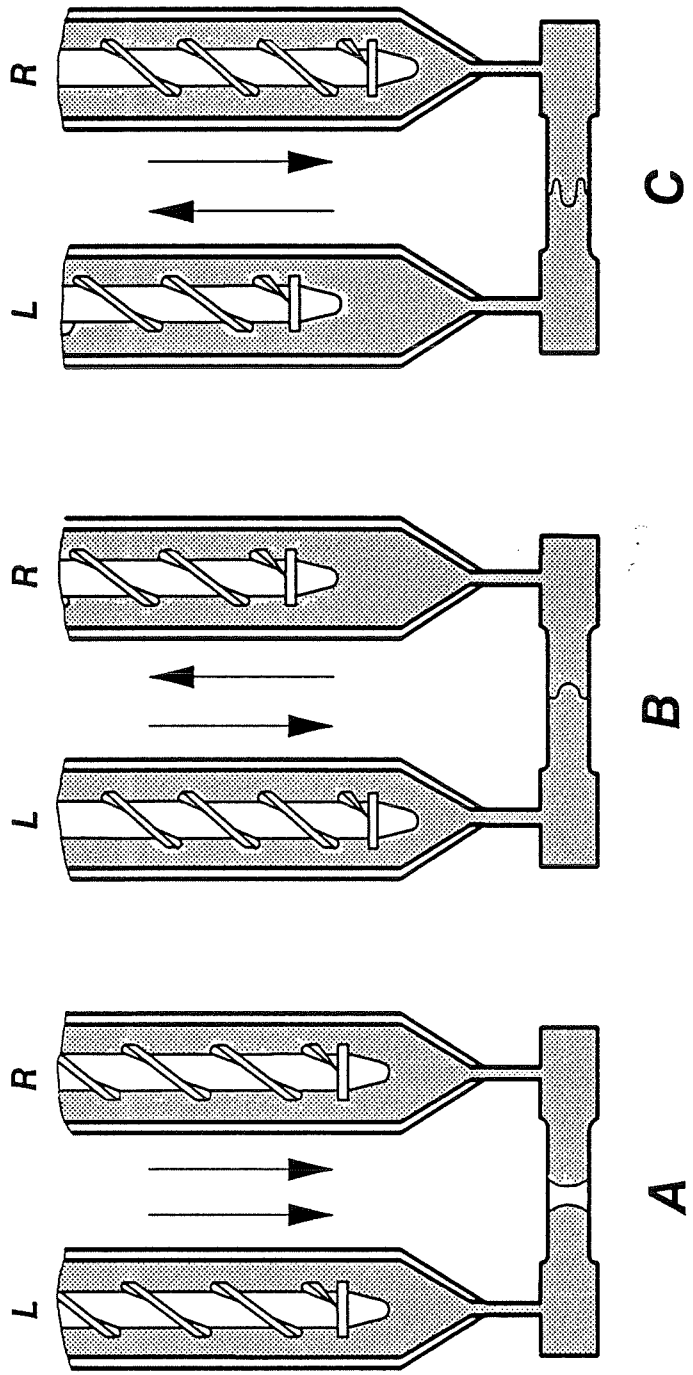

Figure 1.25 - The push-pull molding process[154] - A) left unit forwards, right unit forwards, B) left unit forwards, right unit backwards, C) left unit backward, right unit forwards

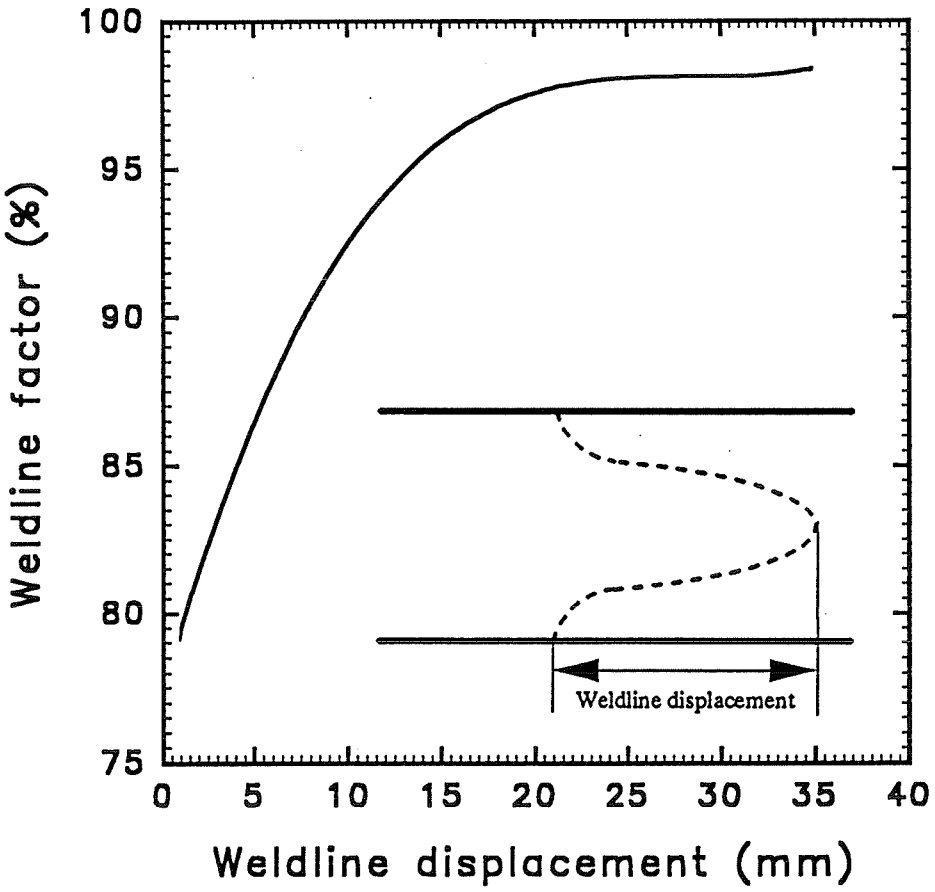

Figure 1.26 - Weldline factor versus weldline displacement during a Simultaneous Composite Injection molding of glass fiber reinforced polycarbonate[160]

al.[161,162] and used by other researchers.[163-167] The single feed molding compound is split into two identical feeds. The sprue consists of a packing head containing two packing pistons which are activated separately to induce fiber alignment inside the mold cavity and thus modify internal weldlines. Of course the outermost layers of the weldline zone, having solidified before the onset of pressure cycling may remain weak. In this case it is conceivable that emerging technologies such as[168] where the mold surface in contact with the polymer is briefly heated to reduce the chain orientation will bring further progress.

4) Break-away: finally, it is possible to make use of the weldline induced weakness to make moldings in which the weldline is located in such a way that an easy to ''break away'' station of a part is defined by the weldline.[169-172]

1.8 REFERENCES

1. B. Fisa and M. Rahmani, *Composites-90*, IMI, November, 23 (1990).
2. B. Fisa, B. Sanschagrin and R. Gauvin, *SPI, 46th conference preprints*, Session 9-C (1991).
3. S.C. Malguarnera, *Polym. Plast. Technol. Eng.*, **18**, 1 (1982).
4. E.M. Hagerman, *Plast. Eng.*, **29**, 67 (1973).
5. K. Engberg, A. Knutsson, P. E. Werner and U. W. Gedde, *Polym.Eng.Sci*, **30**, 1620 (1990).

6. P.R. Lantos, *Polym. Plast. Technol. Eng.*, **26**, 313 (1987).

7. G. Menges, T. Schacht, H. Becker and S. Ott, *Int. Polym. Process.*, **2**, 77 (1987).

8. F. Bataille, T. Vu-Khanh and B. Fisa, *SPE ANTEC Tech. Papers*, **31**, 1174 (1985).

9. M. Christie, *Plast.Eng.*, **7**, 41 (1986).

10. L.A. Utracki, *Polymer Alloys and Blends,* Hanser Publishers, Munich, 1989. Chap I.

11. L.M. Robeson, *Polym.Eng.Sci.*, **24**, 587 (1984).

12. G.D. Gilmore and R.S. Spencer, *Modern Plastics*, **4**, 117 (1951).

13. Z. Tadmor, *J. Appl. Polym. Sci.*, **18**, 1753 (1974).

14. L.R. Schmidt, *Polym. Eng. Sci.*, **14**, 797 (1974).

15. H. Yokoi, S. Kamata and T. Kanematsu, *SPE ANTEC Tech Papers*, **37**, 358 (1991).

16. J.F. Agassant, P. Avenas and J.P. Sergent, *La mise en forme des matières plastiques, Technique & Documentation* - Lavoisier, Paris (France), 96 (1986).

17. Anonymous, Celstran Application Profile, Internal Product Information, Hoechest AG, Frankfurt (1990).

18. Anonymous, European Patent Application EP 0 120 003 B1, Bayer AG, Leverkusen, (1989).

19. H. Mavridis, A.N. Hrymak and J. Vlachopoulos, *AICHE J.*, **34**, 403 (1988).

20. V.G. Menges, T. Schacht and S. Ott, *Kunststoffberater*, **4**, 54 (1988).

21. H. Yokoi, Y. Murata, H. Watanabe and K.Oka, *SPE Antec Tech. Papers*, **37**, 367 (1991).

22. D.R. Tushie, G.A. Jensen and N.F. Beasly, *Engineered Materials Handbook*, **2**, Engineering Plastics, ASMInternational, Metals Park Oh. (1988).

23. P.J. Cloud, F. McDowell and S. Gerarakis, *Plast. Technol.*, **22**, 48 (1986).

24. S.C. Malguarnera and A.I. Manisali, *Polym. Eng. Sci.*, **21**, 586 (1981).

25. R.M. Criens, *Mater. Chem. Phys.*, **14**, 69 (1986).

26. M.M. Hall, D.I. James and K.M. Watkinson, *SPE ANTEC Tech. Papers*, **24**, 369 (1978).

27. B. Fisa, J. Dufour and T. Vu-Khanh, *Polym. Comp.*, **8**, 408 (1987).

28. B. Fisa and M. Rahmani, *Polym. Eng. Sci.*, **31**, 1330 (1991).

29. M. Akay and D. Barklay, *Compos. Struct.*, **3**, 269 (1985).

30. A. Gennaro, Plast. *Rubb. Process. Appl.*, **13**, 251 (1990).

31. R. Boukhili, R. Gauvin and M. Gosselin, *SPE Antec Tech. Papers*, **35**, 1566 (1989).

32. R. Boukhili, R. Gauvin and M. Gosselin, *J. Thermoplast. Compos. Mater.*, **2**, 78 (1989).

33. K. Watkinson, A. Thomas and M. Bevis, *J. Mat. Sci.*, **17**, 347 (1982).

34. R.J. Crawford and P.P. Benham, *J. Mech. Eng. Sci.*, **16**, 178 (1974).

35. R. Boukhili and R. Gauvin, *Plast. Rubb. Process. Appl.*, **11**, 17 (1989).

36. J.M. Hodgkinson, *Polym. Preprints, ACS*, **29**, 143 (1988).

37. C.B. Bucknall, *Pure and Appl. Chem.* (IUPAC), **58**, 999 (1986).

38. M. Kodama and K.Abe, *Mat. Proces. Prod in interior trim, SAE special publ. #* 860 (1991).

39. B. Bruehl and U. Delpy, *Kunstst. Germ. Plast.*, **77**, 439 (1987).

40. D.V. Rosato and D.V. Rosato, *Injection molding Handbook*, Chap. 18, Van Nostrand Reinhold, NY (1986).

41. W.J. Hall and R.D. Burk, *SAE Special Publications*, **SP-710**, 49 (1987).

42. S.C. Malguarnera and A. Manisali, *SPE Antec Tech. Papers*, **26**, 124 (1980).

43. R.P. Wool, B.L. Yuan and O.J. McGarel, *Polym. Eng. Sci.*, **29**, 1340 (1989).

44. P.G. DE Gennes, *J. Chem. Phys.*, **55**, 572 (1971).

45. K.H. Kwei, M.F. Malone and H.H. Winter, *Polym. Eng. Sci.*, **26**, 1012 (1986).

46. S. Prager and M. Thirrel, *J. Appl. Phys.*, **75**, 5194 (1981).

47. R.P. Wool and K.M. Oconnor, *J. Appl. Phys.*, **52**, 5953 (1981).

48. K. Jud, H.H. Kausch and J.G. Williams, *J. Mat. Sci.*, **16**, 204 (1981).

49. N. Avramova, *Polymer*, **34**, 1905 (1993).

50. S.G. Kim and N.P. Suh, *Polym. Eng. Sci.*, **26**, 1200 (1986).

51. N. Mekhilef, *PhD Thesis*, Laval University, Québec (1994).

52. D. Krasnecky, *SPE Antec Tech. Papers*, **37**, 363 (1991).

53. K. Tomari, S. Tonagai, T. Harada, H. Hamada, K. Lee, T. Morii and Z. Maekawa, *Polym. Eng. Sci.*, **30**, 931 (1990).

54. K. Tomari, T. Harada, Z. Maekawa, H. Hamada, M. Iwamoto and A. Ukai, *Polym. Eng. Sci.*, **33**, 996 (1993).

55. R. Pisipati and D.G. Baird, *Polymer Processing and Properties*, G. Astarita and G.Nicolais Eds., Plenum Publishing Corp. NY., 215 (1984).

56. G. Menning, *Die Angew. Makromol. Chemie*, **185/186**, 179 (1991).

57. V.M. Nadkarni and S.R. Ayodhia, *Polym. Eng. Sci.*, **33**, 358 (1993).

58. S. Picarollo and M. Saiu, *Plast. Rubb. Process. Appl.*, **10**, 11 (1988).

59. S.C. Malguarnera and D.C. Riggs, *Polym. Plast. Tech. Eng.*, **17**, 193 (1981).

60. J.P. Trotignon and J. Verdu, *J. Appl. Polym. Sci.*, **34**, 1 (1987).

61. B. Fisa, *Composites Materials and Technology: Processes and Properties*, Chapt.7, Hanser Publishers, Munich (1988).

62. S. Piccarolo, A. Rallis and G. Titomanlio, *Int. Polym. Process.*, **2**, 137 (1988).

63. B. Heise, L. Klostermann and W. Woebcken, *Colloid. Polym. Sci.*, **260**, 487 (1982).

64. J.P. Trotignon, J.L. Lebrun and J. Verdu, *Plast. Rubb. Process. Appl.*, **2**, 247 (1982).

65. B.Z. Jang, D.R. Uhlman and J.B. Vander Sande, *J. Appl. Polym. Sci.*, **29**, 4377 (1984).

66. D.R. Fitchmun and Z. Mencik, *J. Polym. Sci., Part B: Polym. Phys.*, **11**, 951 (1973).

67. M.R. Kamal and F.H. Moy, *J. Appl. Polym. Sci.*, **28**, 1787 (1983).

68. V. Tan and M.R. Kamal, *J. Appl. Polym. Sci.*, **22**, 2341 (1978).

69. F.H. Moy and M.R. Kamal, *Polym. Eng. Sci.*, **20**, 957 (1980).

70. S.S. Katti and J.M. Schultz, *Polym. Eng. Sci.*, **22**, 1001 (1982).

71. D.P. Russel and P.W.R. Beaumont, *J. Mater. Sci.*, **15**, 197 (1980).

72. J. Mowman, *J. Mater. Sci.*, **16**, 1151 (1981).

73. M. Guo and J. Bowman, *J. Appl. Polym. Sci.*, **28**, 2341 (1983).

74. J. Bowman, N. Harris and M. Bevis, *J. Mater. Sci.*, **10**, 63 (1975).

75. M.R. Kantz, H.D. Newman and F.H. Stigale, *J. Appl. Polym. Sci.*, **16**, 1249 (1972).

76. C.M. Hsiung, M. Cakmak and J.L. White, *SPE Antec Tech. Papers*, **32**, 128 (1986).

77. S.Y. Hobbs, *Polym. Eng. Sci.*, **14**, 621 (1974).

78. A. Rallis, S. Piccarolo and G. Titomanlio, *Plast. Rubb. Process. Appl.*, **9**, 181 (1988).

79. J.P. Trotignon and J. Verdu, *J. Appl. Sci.*, **34**, 19 (1987).

80. D. Singh, H.G. Mosle, M. Kunz and W. Wenig, *J. Mater. Sci.*, **25**, 4704 (1990).

81. W. Wenig, D. Singh and H.G. Mosle, *Die Angew. Makromol. Chem.*, **179** 35 (1990).

82. U. Wendt, *Kunststoffe*, **78**, 123 (1988).

83. R.G. Bell and C.D. Cook, *Plast. Eng.*, **8**, 18 (1979).

84. R.M. Criens and H.C. Mosle, *Polym. Eng. Sci.*, **23**, 591 (1983).

85. R.M. Criens, *Material Chemistry and Physics*, **14**, 69 (1986).

86. P. Hubbauer, *SPE Antec Tech. Papers*, **24**, 302 (1978).

87. S.C. Malguarnera, *Plast. Eng.*, 5, **35** (1981).

88. S.C. Malguarnera, A. Manisali and D.C. Riggs, *Polym. Eng. Sci.*, **21**, 1149 (1981).

89. D. Singh and H.G. Mosle, *Makromol. Chem. Macrom. Symp.*, **20/21**, 489 (1988).

90. A. Meddad and B. Fisa, *unpublished work.*

91. A. Meddad, M.Sc.A. thesis, École Polytechnique de Montréal, April 1992.

92. B. Fisa and M. Rahmani, *Polypropylene - The Way Ahead*, International Conf., Madrid (Spain), November 9-10, 1989, Preprints published by the Rubber and Plastics Institute, London, 17 (1989).

93. J.W. Gillepsie, J.A. Vanderschuren and B. Pipes, *SPE Antec Tech. Papers*, **30**, 648 (1984).

94. A. Meddad and B. Fisa, *Polym. Eng. Sci.*, in press.

95. M. Rahmani, *Ph.D. Thesis*, École Polytechnique de Montréal, (1990).

96. R. Blanc, S. Philipon, M. Vincent, J.F. Agassant, H. Alglave, R. Müller and D. Froelich, *Int. Polym. Process.*, **2**, 21 (1987).

97. L.A. Goettler in: *Mechanical Properties of Reinforced Thermoplastics*, D. W. Clegg and A.A. Collyer Eds., Elsevier Applied Science Publishers, London, 1986.

98. L.A. Utracki, *Polym. Compos.*, **7**, 284 (1986).

99. L.A. Utracki, *Rubber. Chem. Technol.*, **57**, 507 (1984).

100. P.R. Hornsby and D.A.M. Russel, *J. Mater. Sci.*, **21**, 327 (1986).

101. L.E. Nielson, *Polymer Rheology*, Marcel Dekkers Inc., NEW YORK (1977).

102. M. Gosselin, *M.Sc.*, Thesis, École Polytechnique de Montréal (1988).

103. A. Bouti and B. Fisa, *SPE Antec Tech. Papers*, **37**, 2112 (1991).

104. F. Lalande, *SPE Antec Tech. Papers*, **37**, 404 (1991).

105. M. Akay and D. Barklay, *Plast. Rubb. Process. Appl.*, **20**, 137 (1993).

106. F. Bataille, T. Vu-Khanh and B. Fisa, *SPE Antec Tech. Papers*, **31**, 1174 (1985).

107. M. Rahmani and B. Fisa, *SPE Antec Tech. Papers*, **37**, 400 (1991).

108. A. Savadori, A. Pelliconi and D. Romanini, *Plast. Rubb. Process. Appl.*, **3**, 215 (1983).

109. P.R. Hornsby, I.R. Head and D.A.M. Russel, *J. Mater. Sci.*, **21**, 3279 (1986).

110. B.D. Favis, *Canadian. J. Chem. Eng.*, **69**, 619 (1991).

111. M. Xanthos, *Polym. Eng. Sci.*, **28**, 1392, (1988).

112. T.M. Liu, H.Q. Xie, K.J. O'Callaghan, A. Rudin and W.E. Baker, *J. Polym. Sci.: Part B: Polym. Phys.*, **31**, 1347 (1993).

113. L.A. Utracki and B.D. Favis, in *Handbook of Polymer Science and Technology: Composites and Speciality Applications*, **4**, N. P. Chereminisoff edt., Marcel Dekker, Inc. (1989).

114. C.R. Lindsay, D.R. Paul and J.W. Barlow, *J. Appl. Polym. Sci.*, **26**, 1, (1981).

115. R.C. Thamm, *Rubb. Chem. Tech.*, **50**, 24 (1977).

116. J. Karger-Kocsis and I. Csikai, *Polym. Eng. Sci.*, **27**, 241 (1987).

117. S. Fellahi, B.D. Favis and B. Fisa, submitted to *Polymer*.

118. B. Fisa, B.D. Favis and S. Bourgeois, *Polym. Eng. Sci.*, **30**, 1051 (1990).

119. E. Nolley, J.W. Barlow and D.R. Paul, *Polym. Eng. Sci.*, **20**, 364 (1980).

120. D.W. Bartlett, J.W. Barlow, D.R. Paul, *J. Appl. Polym. Sci.*, **27**, 2351 (1982).

121. L.S. Remaly and M.J. Sierodzinski, *SPE Antec Tech. Papers*, **27**, 724 (1981).

122. B. Brahimi and A. Ait-Kadi, *SPE Antec Tech. Papers*, **37**, 1129 (1991).

123. B. Brahimi, A. Ait-Kadi and A. Ajji, *Polym. Eng. Sci.*, in press.

124. S. Fellahi, B. Fisa and B.D. Favis, submitted to *J. Appl. Polym. Sci.*

125. E. Worden and S. Kushion, *SPE Antec Tech. Papers*, **37**, 2653 (1991).

126. G .Menning, *Kunst. Germ. Plast.*, **82**, 3 (1992).

127. G.W. Brewer, *SPE Antec Tech. Papers*, **33**, 252 (1987).

128. Elf Atochem, *Mod. Plast. Intl.*, **8**, 49 (1992).

129. J. Swoboda, G. Lindenschmidt and C. Bernhardt, *Germ. Pat.*, 4,224,419 (1980).

130. I. Duvdevani, *US. Pat.*, 4,407,998 (1983).

131. P.Y. Liu and D.E. Overton, *US. Pat.*, 4,532,282 (1985).

132. S.K. Gaggar, *US. Pat.*, 5,128,409 (1992).

133. B.D. Dean and K.A. Geddes, *US. Pat.*, 4,740,555 (1988).

134. M. Fukuda, Y. Ichikawa, T. Katto and T. Nitoh, *JPX. Pat.*, 4,935,473 (1990).

135. J.L. Derudder, F.J. Traver and I.C.W. Wang, *US. Pat.*, 4,939,205 (1990).

136. I.C.W. Wang, *US. Pat.*, 5,045,595 (1991).

137. C.F. Pratt, S.V. Phadke and O. Errol, *US. Pat.*, 4,965,111 (1990).

138. C.F. Pratt, S.V. Phadke and O. Errol, *US. Pat.*, 5,026,776 (1991).

139. R.A. Garcia, J.A. Kosin, G. Mooney and M.E. Tarquini, *US. Pat.*, 5,037,580 (1991).

140. J.F. Herten and B. Louies, *Kunstst. Germ. Plast.*, **75**, 743 (1985).

141. R.J. Curran, *US. Pat.*, 4,191,158 (1980).

142. J.E. Fayal, *US. Pat.*, 4,209,558 (1980).

143. J.W. Davis and E.D. Mannherz, *US. Pat.*, 4,403,933 (1983).

144. C.L. Grendol, *US. Pat.*, 4,540,534 (1985).

145. T. Ishida and Y. Ishida, *JPX. Pat.*, 4,560,342 (1985).

146. A.S. Tobolsky, *US. Pat.*, 4,677,006 (1985).

147. M.L. Vermilye, *US. Pat.*, 4,722,821 (1988).

148. N. Wakewfield, *Plast. Rubb. News*, **3**, 9 (1985).

149. W.H. Walker, *SPE Antec Tech. Papers*, **40**, 1880 (1994).

150. G. Gardner and R. Malloy, *SPE Antec Tech. Papers*, **40**, 626 (1994).

151. G. Gardner and C. Cross, *Plast. Eng.*, **2**, 29 (1993).

152. B. Miller, *Plast. World*, **11**, 28 (1990).

153. S.S. Oleelsky and L.G. Mohr, *Handbook of Reinforced Plastics*, Reinhold Publish. Corp., NEW YORK, 526 (1977).

154. W. Michaeli and S. Galuschka, *SPE Antec Tech. Papers*, **39**, 534 (1993).

155. K.T. Nguyen, D.M. Gao, P. Girard and G. Salloum, *Executive Conference Management, Molding 1994*, Anaheim, California, March (1994).

156. D.B. Kirby and O.W. Heybey, *US. Pat.*, 4,399,093 (1983).

157. H. Becker, Malterdington, G. Fisher and U. Miller, *Kunsts. Germ. Plast.*, **83**, 3 (1993).

158. GTS Process, *British. Plast. Rubber*, 2, 1992.

159. SCORIM, Anonymous.

160. K. Tomari, H. Takashima and H. Hamada, submitted to *Adv. Polym. Tech.*

161. P.S. Allen and M.J. Bevis, *Plast. Rubb. Process. Appl.*, **7**, 3 (1987).

162. J.R. Gibson, P.S. Allan and M.J. Bevis, *Composites Manuf.*, **1**, 183 (1990).

163. S. Piccarolo, F. Scargiali, G. Grippa and G. Titomanlio, *Plast. Rubb. Process. Appl.*, **19**, 205 (1993).

164. S. Parekh, S. Desai and J. Brizzolara, *SPE Antec Tech. Papers*, **39**, 530 (1993).

165. R. Malloy, G. Gardner and E. Grossman, *SPE Antec Tech. Papers*, **39**, 521 (1993).

166. S. Parekh, S. Desai and J. Brizzolara, *SPE Antec Tech. Papers*, **40**, 621 (1994).

167. D.O. Kazmer, *SPE Antec Tech. Papers*, **40**, 631 (1994).

168. K.M.B. Jansen and A.A.M. Flaman, *Executive Conference Management, Molding 1994*, Anaheim, California, March (1994).

169. C.J. Aloisio and R.R. Cammons, *US. Pat.*, 4,434,120 (1984).

170. M. Jaffe and Z. Ophir, *US. Pat.*, 4,457,962 (1984).

171. M.A. Williams, B.D. Bauman, D.R. Rupresht and P.D. Marsh, *US. Pat.*, 4,752,428 (1988).

172. T. Kousai, Y. Moriushu and T. Ishida, *US. Pat.*, 4,830,805 (1989).

173. *Design of Molds for Test Specimens of Plastic Molding Material*, ASTM standard Practice Norm D-647-68.

174. G. Menges and P. Mohren, How to Make Injection Molds, Hanser Publisher, Munich (1986).

175. M.J. Bozarth and J.L. Hamill, *SPE Antec Tech. Papers*, **30**, 1091 (1984).

CHAPTER 2

MORPHOLOGICAL STABILITY IN INJECTION MOLDED HDPE/PA6 BLENDS

SOMMAIRE

La morphologie des mélanges polymères immissibles moulés par injection reste encore un domaine de recherche vierge. La présence de ligne de soudure dans les objets moulés par injection est un défaut reconnu depuis longtemps, ce qui limite leur domaine d'application. Cette faiblesse est plus accentuée encore avec les mélanges polymères. Dans ce travail, une étude morphologique très détaillée des mélanges polyéthylène haute densité/polyamide-6 (25/75 vol%) avec et sans compatibilisant, est entreprise avec un fort accent sur la zone de ligne de soudure plus particulièrement. Un insert est utilisé pour générer la ligne de soudure anisi que des expérience de short-shot afin de suivre l'évolution de la morphologie pendant le remplissage du moule.

Une analyse morphologique très détaillée de la peau et de la région de la zone de soudure a été réalisée grâce à un microscope électronique à balayage et un système d'analyse d'image. Les points essentiels de ces résultats sont les suivants : a) existence d'un effet peau/coeur important, b) diminution de l'épaisseur de la peau et de la largeur de la ligne de soudure avec l'ajout d'un compatibilisant et c) une absence apparente de la phase dispersée au niveau de la peau ainsi que dans la ligne de soudure. L'existence d'une variation de morphologie à travers l'épaisseur de l'échantillon (une phase dispersée

très orientée dans la sous-peau et sphérique dans le coeur) a été démontrée clairement dans cette étude.

Afin de vérifier la validité de l'observation mentionnée ci-dessus concernant le semblant absence de la phase dispersée au niveau de la peau et de la ligne de soudure, la spectroscopie photoélectrons à rayons X (XPS) et l'analyse calorimétrique (DSC) d'échantillons microtomés de la surface ont été utilisées comme techniques additionnelles pour caractériser quantitativement la composition de la surface des plaques ainsi que celles du front d'écoulement. Les résultats montrent que la composition de la surface et celle de la ligne de surface est très proche de celle du mélange d'origine (25/75% vol). La phase dispersée est bien présente dans la peau. La microscopie à transmission électronique (TEM) révèle la présence dans la peau d'une phase dispersée très fine avec des dimensions 10 fois plus petite que dans le coeur de l'échantillon.

L'agent interfacial utilisé, un ionomère à base d'acrylate d'isobutyle et d'acide méthacrylique de polyéthylène, avait pour effet de réduire la taille de la phase dispersée, l'épaisseur de la peau et la largeur de la ligne de soudure. Les dimensions des régions contenant une phase dispersée très fine (peau et ligne de soudure) correspondent bien avec celles observées dans le front d'écoulement analysé à partir des échantillons de short-shot. Il a été observé moins de coalescence et une morphologie plus stable.

Le mécanisme responsable de cette importante réduction de la taille de la phase dispersée observée au niveau du front d'écoulement, de la peau et de la ligne de soudure a été attribué à une rupture des particules à cause de l'écoulement élongationnel et à la déformation biaxiale subie par les particules de la phase dispersée au niveau du front d'écoulement.

2.1 INTRODUCTION

During this last decade, there has been an intense activity to tailor new plastic materials in the form of blends or alloys using melt processing machinery. This approach has considerable cost advantages over the development of materials in polymerization reactors. There are approximately 4500 patents produced annually with respect to polymer blends and alloys. Blends have an annual growth rate of about 10% compared to about 3% for plastics alone[1].

Polymer blends are mixtures of homopolymer or copolymers of different molecular structure. Immiscible polymer blends possess a minor phase which may undergo severe deformation and acquire an anisometric configuration during melt processing. This will result in a structure characterised by a distribution of shape factor ratios, concentration and orientation of the dispersed phase throughout the thickness of a molded article. Most industrial polymer blends are immiscible. Consequently the introduction of a compatibilizer either as a third component or developed in-situ through

reactive processing[2,3,4] at a reduced concentration level is necessary to reduce the interfacial tension, the dispersed phase size, improve the adhesion and subsequently improve the mechanical properties[5]. This will normally result in a more stable morphology[6,7,8].

Blends of non-polar polyolefins with polar polyamides are an example of materials where the dissimilarity of components dictates the use of a suitable compatibilizer. There have been several studies of the polyolefin/polyamide system[9,10,11,12,13]. White et al.[9] have studied the rheology and the morphology of extruded PP/PA, they have considered in particular the influence of melt temperature and PE viscosity[8] and the development of different types of morphologies[10]. A comparative morphological study between compression and injection molded non-compatibilized HDPE/PA6 blends[14] where the mold temperature, the annealing time inside the mold and the injection speed were varied, revealed the presence of the usual skin/core structure, with an oriented skin, an intermediate zone where the anisotropy is maximum and an isotropic core. It was found that the dispersed phase forms plaques or oriented lamellas in the machine direction.

Factors influencing the morphology of polyolefin/polyamide blends have been studied extensively in this laboratory[15,16,17,18]. The influence of interfacial modification through the use of a polyethylene methacrylic acid isobutyl acrylate ionomer in such systems has been considered[16,17,19]. It was found that chemical bonding occurs at the interface through amide formation between the carbonyl group of the ionomer and the

terminal amine of polyamide. It has been shown that interfacial modification in these systems can significantly diminish the phase size/volume fraction dependence. Hence coalescence effects are reduced and morphological stability is enhanced[1,3,5]. Despite this work and others[14] on polyolefin/polyamide blends, very few studies have considered the morphology developed during injection moulding.

Injection molding is a well-known process in the plastics industry. It is characterized by a complex and non-isothermal flow in a closed and cooled mold cavity. This will generally result in an anisotropic skin/core structure. The filling of the mold cavity is achieved through fountain flow. During the injection of the molten material inside the cavity, a velocity profile is established. Since the mold wall is cooled, the plastic in contact with it will freeze immediately to form what is known as the skin where the shear will be at a maximum. Dispersed, deformable polyethylene particles will be elongated in the direction of flow. The hot core will be less deformed, and has sufficient time to relax. The final result of this complex process is the so-called skin/core morphology.

2.1.1 Weldlines

When two separate polymer flow fronts come into contact, there is formation of a zone having a morphology and properties different from the rest of the material. This zone is called a "weldline or knit line". Fisa et al.[20] state that weldlines produced by the

separation and recombination of the flow around an insert represent the most frequently encountered situation in industrial parts.

Weldlines in homopolymers is a well documented subject[20-28]. The quality of a weldline is associated with the flow field which arises as the two fronts reunite. A possible explanation for the weakness engendered by this reunion is the trapped air at the interface between the two opposing fronts, leading to the formation of a V-notch which may act as a stress concentrator[21,22]. Tadmor[23] proposed that the above two flows generate molecular orientation that is predominantly along, rather than across the weld interface because of a fountain-like flow. Two processes that most likely precede the weld healing are stress relaxation, which results in a loss of this orientation, and molecular re-entanglement, which is a self diffusion phenomena. A stress relaxation mechanism has been invoked by Tomari et al.[24], while the latter process has been adopted by De Gennes[25] and Wool et al.[26], to explain the healing phenomena. Finally, Titomanlio et al.[27] have used the volume shrinkage approach to explain the weakness due to the presence of a weldline.

Weldlines in injection molded polymer blends is not a well documented subject. Injection molded EPDM/PP systems with a weldline obtained with a double gated mold were studied by Thamm et al.[29]. They reported an absence of the minor phase (EPDM) in the weldline region. When the viscosity of the EPDM was lower than that of the PP, the former was found to migrate to the surface. Similar results were reported later by

Malguarnera et al.[28]. They attributed the absence of the dispersed EPDM in the weldline region to a deficiency in the flow front region although this was never supported experimentally. Paul et al.[30] have studied the effect of a compatibilizer on the mechanical properties of several systems with and without weldline obtained in a double gated mold. Karger-Kocsis et al.[31] studied the structure/properties relationship, and the phenomena causing rupture of injection molded blends of EPDM/PP with and without a weldline obtained by double gate feeding. The usual skin/core structure was found. In the skin two zones were observed; a thin PP layer on the surface, and a subskin with highly elongated rubber particles. The core was rich in rubber particles. This effect was attributed to the existence of a concentration gradient due to crystallization of the front in contact with the mold surface. During crystallization the polypropylene apparently rejects the rubber particles instead of engulfing them.

Preliminary morphological observations were also carried out in studies on HDPE/PA-6 compatibilized with an ionomer[32,33]. It was reported that significant morphological and concentration variations existed throughout the thickness of the plaque. A deficiency of the minor phase in the skin and weldline region was reported[33].

One of the main concerns in the processing of polymer blends is the stability of the morphology. It is generally believed that the addition of an interfacial modifier leads to a better stabilisation of the morphology. Despite this fact, little detailed work has

been undertaken on the morphology of both compatibilized and non-compatibilized blends during injection molding and including weldlines.

The objective of the present work is to consider the effect of a polyethylene methacrylic acid isobutyl acrylate ionomer on the morphological characteristics of injection molded HDPE/PA-6 systems including weldlines. A detailed morphological analysis of the skin and weldline will be undertaken by scanning electron microscopy (SEM), transmission electron microscopy (TEM), and image analysis. Since both the skin and the weldline region originate from the flow front, a morphological analysis of the latter will also be carried out. X-ray photoelectron spectroscopy (XPS) and differential scanning calorimetry (DSC) of microtomed layers from the surface, will be used as additional techniques to characterize qualitatively and quantitatively the surface and the flow front composition of the plaques.

2.2 EXPERIMENTAL

2.2.1 Materials

The polyamide-6 (PA-6) is a Zytel 211 from E.I. Dupont de Nemours Inc. with a number average molecular weight, M_n = 25000 g/mole. The high density polyethylene (06153C) is from Dow Chemical Canada having a melt flow index (MFI), 6.3 g/10 min, M_n = 20200 g/mole and M_w = 81300 g/mole. The compatibilizing agent is an ionomer

(Surlyn 9020, from E.I. du Pont de Nemours & Co. Inc.) a terpolymer consisting of 80% of ethylene and 20% mixture of methacrylic acid and isobutyl acrylate. The methacrylic acid is 70% zinc neutralized, having a molecular weight, M_n = 25000 g/mole (obtained from the supplier). The polyethylene is stabilized with 0.2% antioxidant (Irganox 1010 of Ciba Geigy).

2.2.2 Compounding

The first operation consists of mixing polyethylene (HDPE) with 0.2 wt% antioxidant (Irganox) in a single screw extruder. Then, using a twin-screw extruder 10% ionomer (I), based on the weight of the dispersed phase, was mixed with the stabilized PE. Finally, 25 vol% of PE with (PEIPA) or without compatibilizer (PEPA), was mixed with 75 vol % of polyamide (PA-6). Prior to a typical mixing operation, the sample mixture was dried overnight at 90°C under vacuum to minimize hydrolytic degradation of the polyamide during processing. The polymer blending was carried out on a ZSK-30 (Werner-Pfleiderer) intermeshing, co-rotating twin-screw extruder with a screw length to diameter ratio, L/D of 40. Feeding was performed under nitrogen and vacuum was applied in the decompression zone. The blending conditions are shown in Table 2.1. Rod-shaped extrudates were kept for SEM observation.

Table 2.1 - Compounding conditions

	PE/antioxidant 25 kg-PE 50 g- antioxid single-screw		PE/Ionomer 10 kg-PE 1.11 kg-I twin-screw		(PE/I)/PA 12 kg - PA6 3.083 kg-PE/I twin-screw		PE/PA 2.793 kg-PE 10.87 kg-PA twin-screw	
T_1 (°C)	Fixed 160	Obs 146	Fixed 160	Obs 152	Fixed 185	Obs 180	Fixed 185	Obs 180
T_2	170	165	185	188	235	232	235	235
T_3	180	170	190	203	250	245	250	235
T_4	175		195	212	250	250	245	233
T_5	180		195	192	245	240	245	233
T_6	190		200	201	250	240	250	230
RPM	80		300		300		200	
Flow rate (g/min)	90		170		180		100	
Torque (%)			65		65		50	
Feeding under N_2	No		Yes		Yes		Yes	
Degassing	No		Yes		Yes		Yes	

2.2.3 Rheology

The viscosity of all neat materials (HDPE, ionomer, and PA6) and the two prepared formulations (PE/PA-6 and PE-Ionomer/PA-6) were measured at 200, 230,

250°C using 3 dies having different L/D ratios: 10, 20, 40, on an Instron capillary viscosimeter. Only data at L/D:40 and 250°C will be reported here.

2.2.4 Injection molding

The injection molding machine used was a Battenfeld type BA-C 750/300, with a clamping force of 80 tons. A conventional mold equipped with interchangeable cavities of rectangular shape (127 mm x 76 mm x 4 mm) was used. It is equipped with a 2 mm deep flash gate fed with a trapezoidal duct having a section varying from 30 to 50 mm^2 (Fig. 2.1A). To produce plaques with weldlines, an insert having 12 mm diameter is installed in the cavity (Fig. 2.1B).

4 types of experiments were performed: full plaques and short shots both with and without insert, using the previously prepared formulations. The injection molding conditions are:

Thickness of the plaque: 4 mm, insert diameter: 12 mm, shot weight: 50.2 g

Total cycle time: 42 s, cooling time: 20 s and hold time: 10 s

Nozzle temperature: 250°C and mold temperature: 65°C

Injection pressure: 150 Bars and hold pressure: 100 Bars

screw RPM: 50, injection speed: 100 mm/s

Materials were dried in an air circulating oven at 80°C.

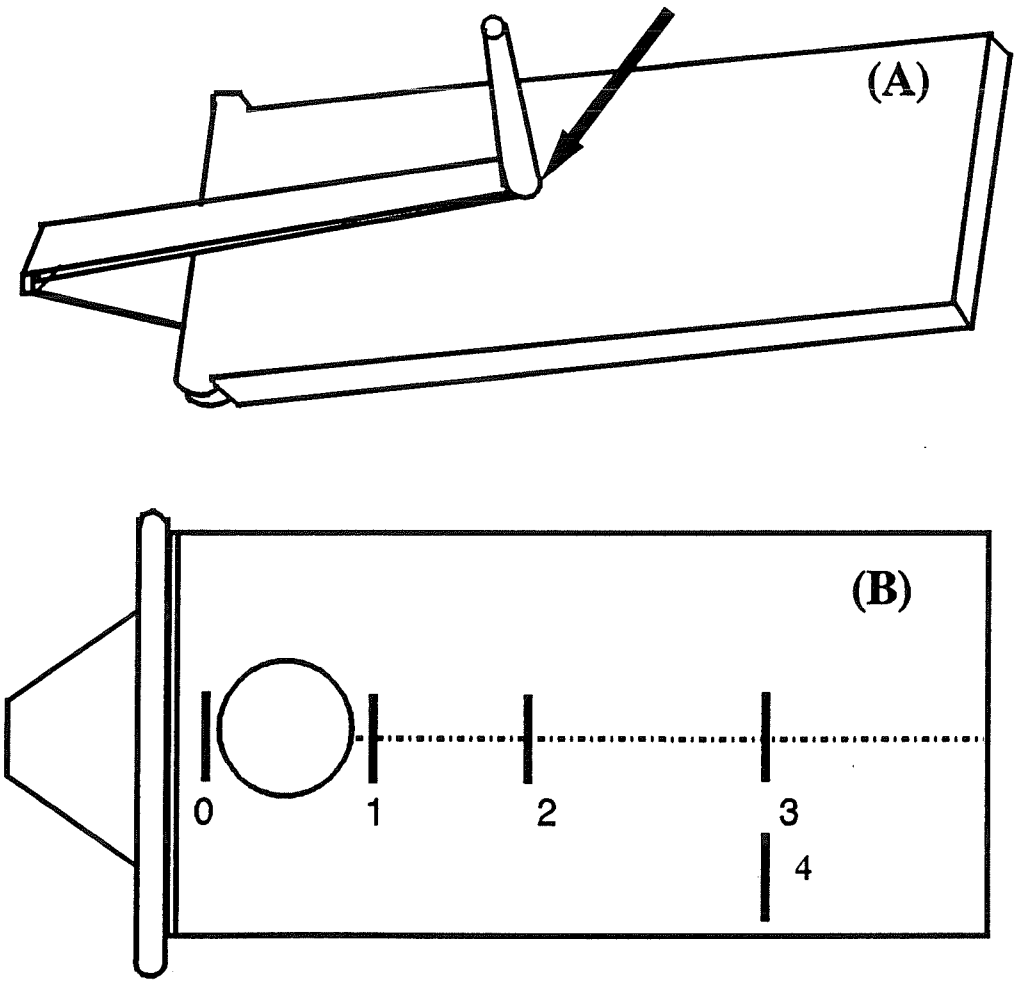

Figure 2.1 - Injection molded plaques, shape and positions at which samples were taken

2.2.5 Morphological analysis

2.2.5.1 Electron microscopy

In addition to the twin-screw extrudates, samples were taken at different positions from complete injection molded (transversally and longitudinally to flow direction) and short-shot plaques as indicated in Fig. 2.1B, according to the preceding conditions. Only formulations of (25/75) PE/PA-6 with and without compatibilizer were studied. Morphological preparation can proceed in two ways:

- Freeze-fracture: a small circular or rectangular strip from each sample is placed in liquid nitrogen for 10-15 min, and then fractured manually.
- Microtoming: rectangular samples (1 x 1.5 x 0.5 cm) are cut. A Reichert Jung Supercut 2050 microtome equipped with a glass knife is used. First each sample is frozen in liquid nitrogen for 15 min. During the cutting operation, the temperature is kept at approximately -100°C to reduce the extent of surface deformation. The microtomed samples were immersed for 1 hour in decalin at 120°C to dissolve the polyethylene (minor phase). Following the extraction the samples were dried in a vacuum oven for 24 hours to remove the solvent. Freeze-fractured or microtomed surfaces were then treated with a gold-palladium layer and examined in a Jeol 8645 type scanning electron microscope.

2.2.5.2 Image analysis

The semi-automatic image analyzer used to measure the diameters of the dispersed phase was the Jandel digitizing tablet controlled by the Jandel Sigma-scan system. For each sample, up to approximately 300 diameter measurements on one run were obtained from the SEM micrographs. The experimental error is approximately $\pm 10\%$. When the same measurements are carried out successively on the same micrograph, the difference is less than 10%. A correction was applied to the distribution of diameters for each sample according to the Saltikov method. The mathematical particle corrections account for two phenomena: (a) the fact that the observed diameter of a given particle, after microtoming or fracture, is usually less than the true diameter of the original spherical particle; and (b) materials with large dispersed particle size distributions result in an average diameter value that overestimates the contribution of large particles[34].

2.2.5.3 Transmission electron microscopy (TEM)

Slices of less than 80 nm thickness were cut using an ultramicrotome type RMC-MT-7 at a 30° angle of inclination, and a cutting speed of 2 mm/s from the skin region in both directions (transverse and longitudinal to flow) of PA-6, HDPE and PEPA plaques to a depth not exceeding 80 μm. They were then observed under a Jeol 2000FX transmission electron microscope with a voltage of 200 kV.

2.2.6 Differential scanning calorimetry (DSC)

A Dupont 900 differential scanning calorimeter was used with a scanning rate of 20°C/min. Samples from neat HDPE, neat PA6 and PEPA blend were microtomed from the surface of the plaques to a depth not exceeding 100 μm.

2.2.7 X-ray photoelectron spectroscopy (XPS)

Samples (5 mm x 5 mm) were cut from neat HDPE, PA6, PEPA, Surlyn and PEIPA plaques, as well as from the flow front on a non-compatibilized blend. They were then surface analyzed using X-ray photoelectron spectroscopy (XPS). XPS studies were carried out on a VG Escalab MKII instrument. An X-ray beam (Mg K α at 1253.6 eV) was used to produce the photoemission of electrons from core and valence levels of the surface atoms. About 60 Å of depth are probed, when the detector is perpendicular to the surface. The analyzed surface was 2 x 3 mm. All peak positions were corrected for adventitious carbon, at 285.0 eV in binding energy, to adjust for charging effect. The results obtained with this technique are reported[35] to be accurate within $\pm$ 5%.

2.3 RESULTS AND DISCUSSION

2.3.1 Rheology

From Figure 2.2, it can be seen that the polyamide (PA-6) has a somewhat higher viscosity than the polyethylene (PE) over the range of shear rates considered. Since the viscosity ratio at high shear rates is slightly less than 1, this should ensure a fine dispersion[36]. It can be noticed that the compatibilizer (Surlyn) has a higher viscosity than the other components.

In Figure 2.3, the viscosity of the PE/PA-6 blend, shows a negative deviation with respect to that of pure PA-6. The presence of HDPE causes a drastic reduction in the PA-6 viscosity. When a compatibilizer is used, the system PE/I/PA-6 shows a positive deviation from additivity at low shear rates (below 100 s^{-1}) and a negative one at higher shear rates with respect to PA-6. The increase in viscosity is attributed to interfacial interactions[16].

2.3.2 Morphology

In the following discussion, morphological results on samples taken from extrudates (twin screw extrusion), sprue area and inside the mold cavity (injection molding) will be presented.

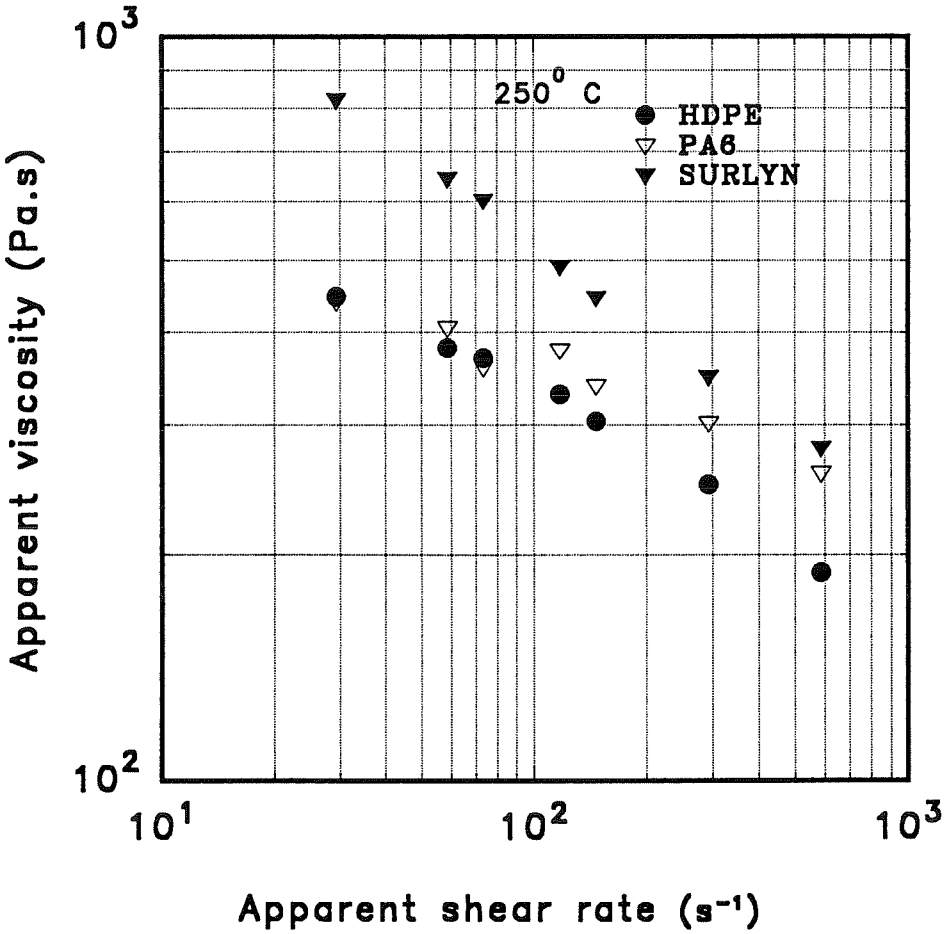

Figure 2.2 - Apparent viscosity vs shear rate of neat HDPE, PA-6 and Surlyn

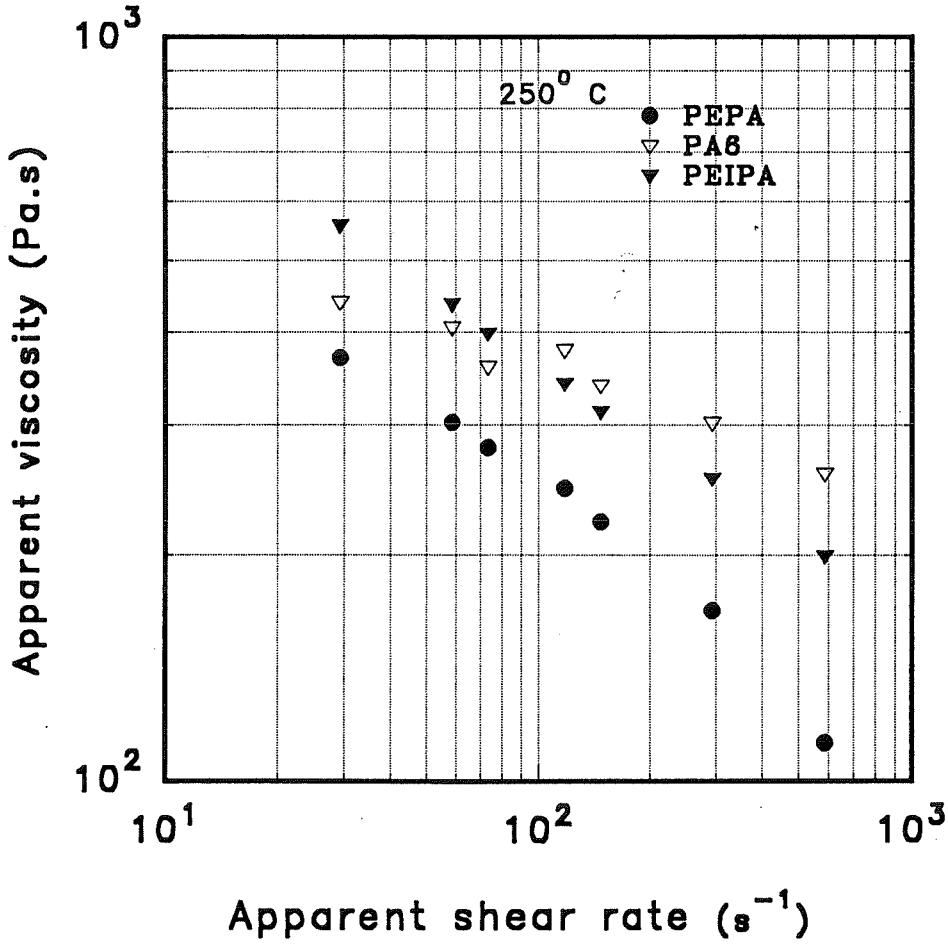

Figure 2.3 - Apparent viscosity vs shear rate of neat PA-6, uncompatibilized (PEPA) and compatibilized (PEIPA)

2.3.2.1 Twin screw extrusion

Table 2.2 shows the influence of twin-screw processing on the size of the dispersed phase. Twin screw extrudates display small particles located at the skin (d_v = 1.60 μm), while the core of the sample consists of coarser particles (d_v = 5.0 μm) for the non-compatibilized blend. When a compatibilizer is added, the size of the dispersed phase is reduced in both the skin (d_v = 1.40 μm) and core (d_v = 1.20 μm), a more uniform distribution of the dispersed phase throughout the sample cross-section is observed.

Table 2.2 - Comparison of the dispersed phase size (μm): d_n and d_v

		NC*			C*		
		d_n	d_v	d_v/d_n	d_n	d_v	d_v/d_n
Twin screw extruder (extrudate)	skin	1.0	1.60	1.60	0.91	1.40	1.50
	core	2.70	5.0	1.8	0.91	1.20	1.3
Injection molding (sprue)	skin	2.50	4.0	1.6	0.30	0.40	1.3
	core	2.60	3.90	1.20	0.71	0.90	1.3

*NC:HDPE/PA6
C:HDPE/COMPATIBILIZER/PA6

2.3.2.2 Injection molding

2.3.2.2.1 Sprue area

In the sprue area (position indicated in Figure 2.1): a uniform distribution of the dispersed phase is observed. The shear rate in the gate is between 300-400 s^{-1}. The sprue area is not cooled except at its bottom and the sample to be analyzed was cut at this position. When the extruded compound is injection molded a cross-section of freeze fractured sprue reveals a finer skin and a coarser core for both blends as compared to the twin screw extruded samples. Results are shown in Table 2.2. Overall, the injection molding step causes an additional but slight reduction of the dispersed phase size, which might be attributed to the high shear rate level developed in the sprue region. For the non-compatibilized blend a coarse structure throughout the cross-section (d_n = 2.50 μm and d_v = 4.0 μm) is observed. When a compatibilizer is added, the structure is much finer in both the skin (d_n = 0.30 μm and d_v = 0.40 μm) and the core (d_n = 0.71 μm and d_v = 0.90 μm). When the system is compatibilized, a much finer dispersion is observed and this is attributed to interfacial interactions[16].

2.3.2.2.2 Inside the mold cavity

i) Skin/core Region

Inside the mold cavity, the usual skin/core morphology is found. As the molten material enters the cavity in a parabolic profile, and the material in the front is deposited on the wall undergoing considerable stretching, it solidifies instantaneously forming an immobile frozen layer. The additional molten material will flow inside this envelope. It is well-known that the velocity is at a maximum in the core and nil at the wall. The shear stress shows the opposite tendency, a maximum at the skin and a minimum in the core[23]. Because of the high shear encountered in this process, the material is highly pseudoplastic meaning that the velocity profile is quite flat, and, only a thin region in the vicinity of the frozen layer (subskin) will be highly elongated[37]. The core region will be the last to solidify, and may even relax[20] (Fig. 2.4). The skin region was also observed at higher magnification (x 10 000) on the SEM, however no dispersed phase was evidenced. Selective solvent dissolution of the sample indicates that the skin is apparently composed of pure PA-6 (Fig. 2.5 and 2.6). The subskin is rich in PE where apparently shear induced coalescence has taken place. For the non-compatibilized systems (Fig. 2.5) the skin and the subskin are approximately 300 and 600 μm thick respectively. A highly oriented subskin region and shear induced coalescence are observed (Fig. 2.5b). When a compatibilizer is used, the morphology is more stable, and less elongation is observed (Figs. 2.6a, b and c) in the subskin region. The skin and

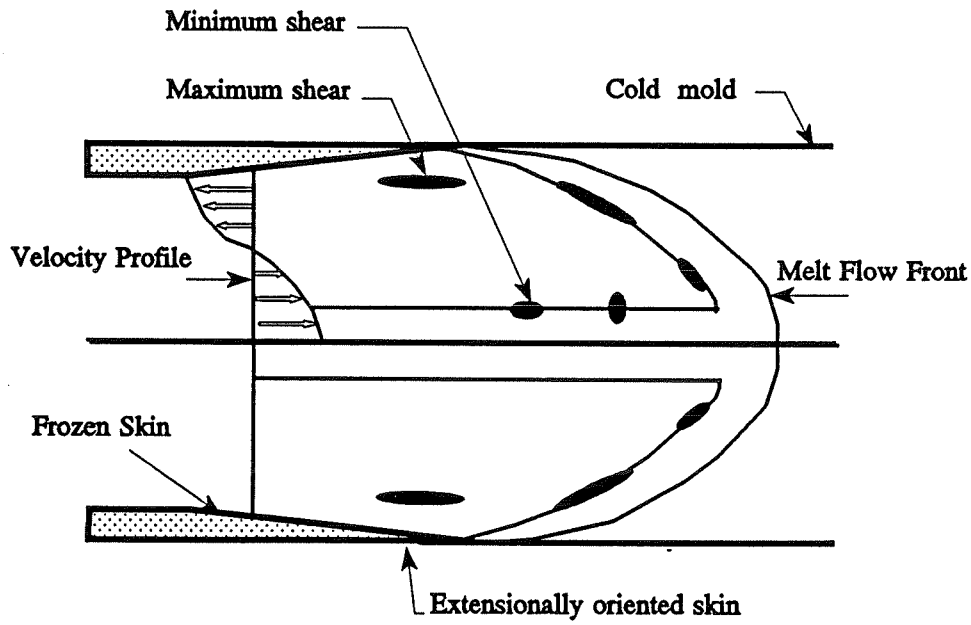

Figure 2.4 - Schematic representation of the fountain flow

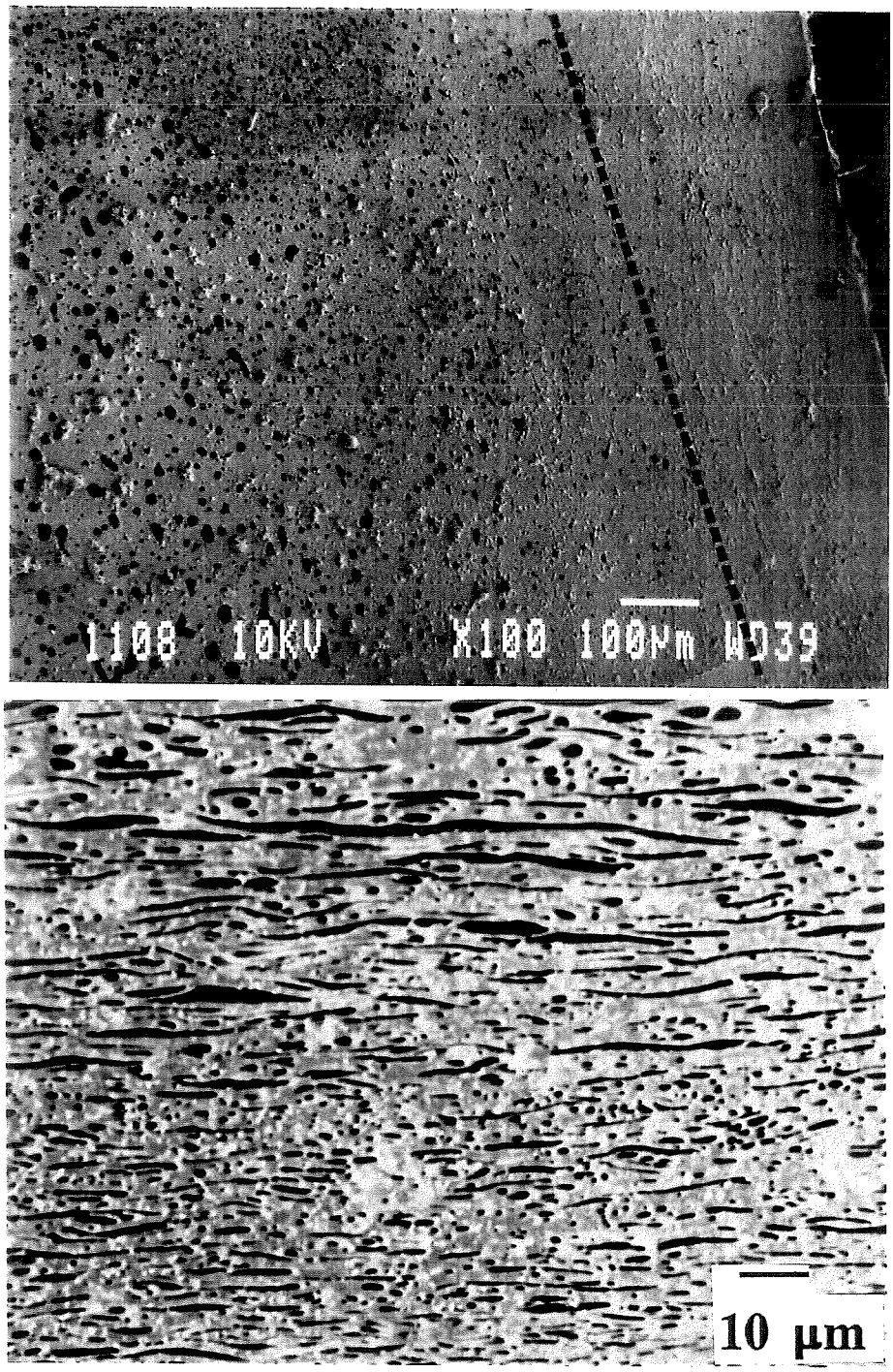

Figure 2.5 - Morphology of non-compatibilized sample - a) morphological change throught the thickness in complete sample at position 4 (parallel to flow view), b) shear induced coalescence in the subskin region of a non-compatibilized sample (perpendicular to flow view)

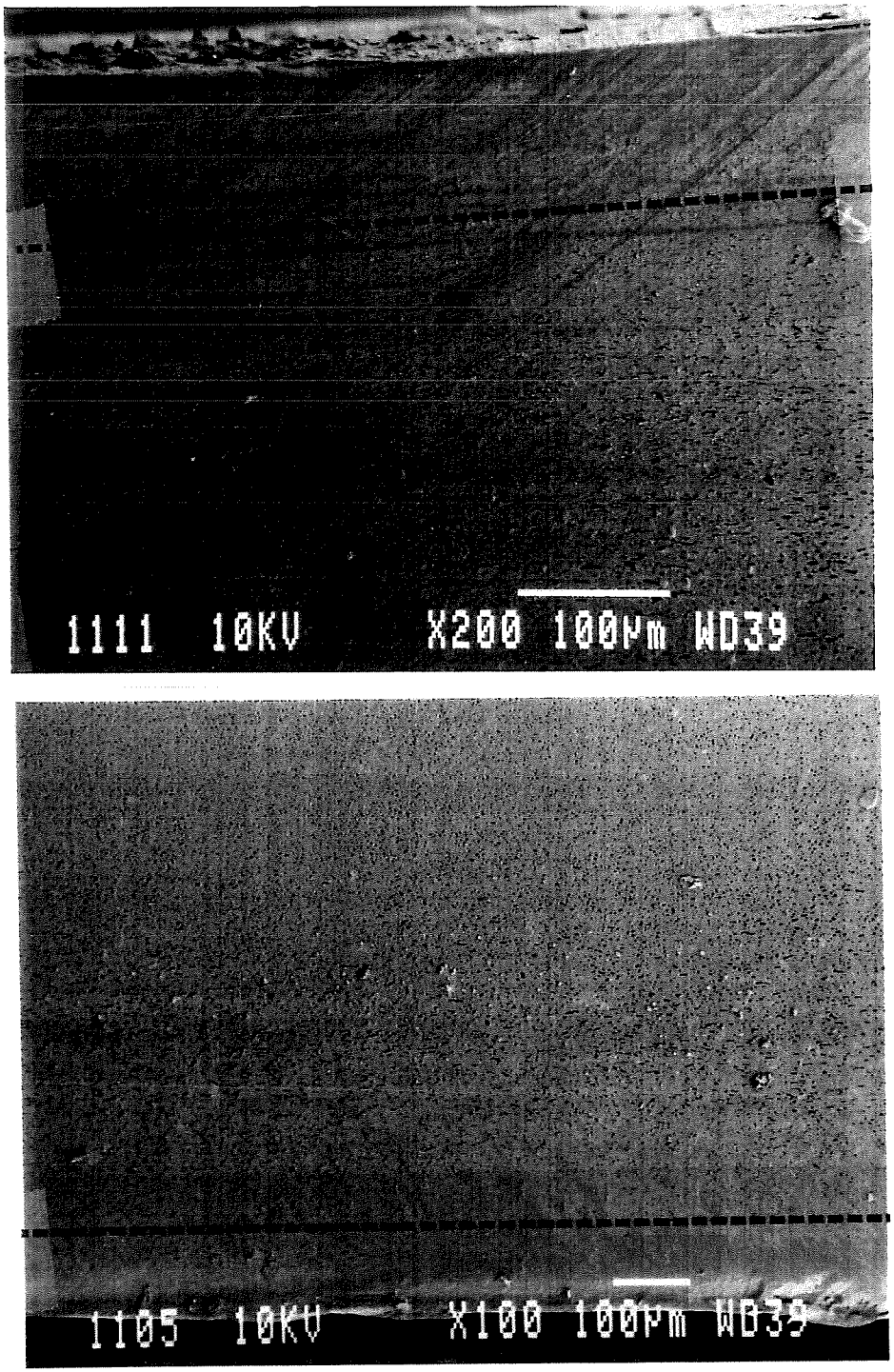

Figure 2.6 - Morphological change throughout the thickness - a) compatibilized complete sample at position 4 (parallel to flow view), b) compatibilized complete sample at position 2 (perpendicular to flow view)

c)

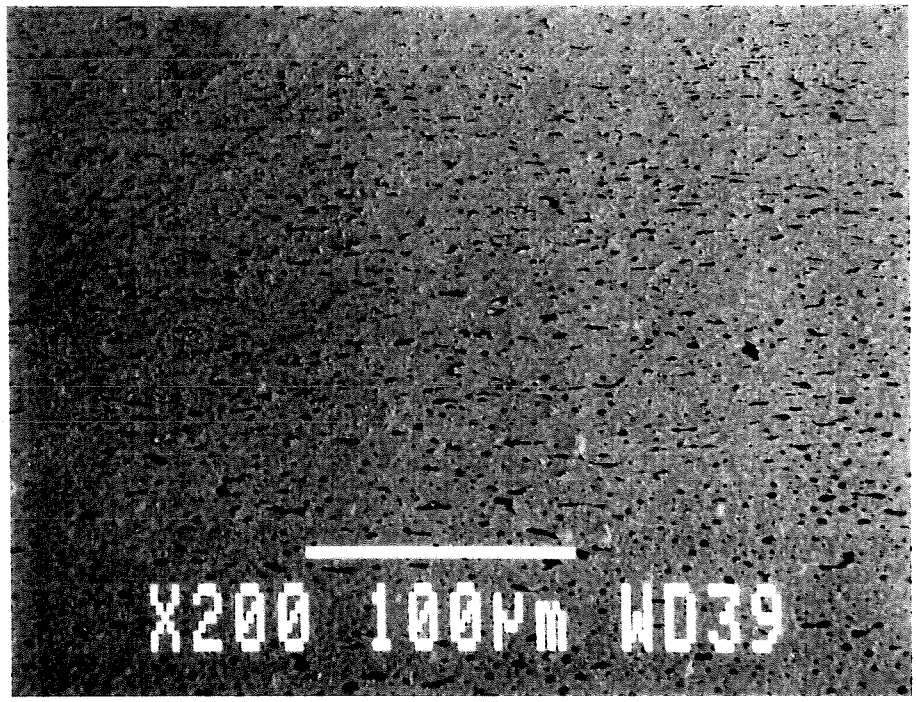

Figure 2.6 - Cont'd
c) magnification in the subskin region of Fig. 2.6b

the subskin in this blend are approximately 100 and 400 μm thick respectively. The delineation between the different zones is relatively simple. It is based on the discontinuity between very small (in the skin and weldline region) and very large particles elsewhere (subskin and core). A detailed schematic representation of the observed morphology for both blends is illustrated in Fig. 2.7. The principal features of the above micrographs are the following:

- significant skin/core effect observed for non-compatibilized blends displaying a morphological variation with respect to the thickness i.e dispersed phase is very fine in the skin, highly oriented in the subskin and spherical in the core;
- diminution of the thickness of the skin and weldline regions with interfacial modification displaying a reduced minor phase size;
- apparent absence of the minor phase in the skin even at higher SEM magnification.

To check the validity of the above observation related to the apparent absence of dispersed phase; DSC thermograms of microtomed slices from the skin, transmission electron microscopy (TEM) as well as X-ray photoelectron spectroscopy of the surface of the blends, Surlyn and neat resins were performed. If the skin of the plaques made of the non-compatibilized blend as already reported above is made of pure PA-6, then when an 80 μm layer is microtomed from this region and analyzed by DSC, it should reveal only the presence of a PA-6 melting peak (220°C). As shown in Fig. 2.8 this was

not the case. Both phases are clearly present in the skin. The test was repeated several times to ensure reproducibility, and it is evident that, in the skin, the dispersed phase is present (T_{melt}:130°C) which apparently contradicts the SEM results. Thermograms of samples taken from the skin region for neat HDPE, PA-6 and the blend are shown in Fig. 2.8 curves 1, 2 and 3 respectively. The areas under their respective peaks, indicates that approximately the same proportions (21.7 wt%/78.3 wt%) of HDPE/PA-6 exist in the blend skin as in the original, as prepared, compound (20.4/79.6 wt%). The area under the peak in neat HDPE is 168 J/g and in neat PA-6 is 72 J/g. For the non-compatibilized blend (PEPA) under investigation, the area under the peak corresponding to PE is estimated to be 29 J/g while that for PA-6 is 44 J/g. To predict the % composition of the blend skin a rule of mixtures approach was applied to the area under the peaks.

In order to verify the surface composition of the blend via another technique, X-ray photoelectron spectroscopy (XPS) was carried out. This is a technique also known as Electron Spectroscopy for Chemical Analysis (ESCA) and is widely used to investigate the chemical composition of surfaces. Surface analysis by XPS involves irradiating a solid in vacuo with mono-energetic soft x-rays and analysing the emitted electrons by energy. The spectrum is obtained as a plot of the number of detected electrons per energy interval versus their binding energy. The detected electrons originate from only the top few atomic layers, making XPS a unique surface-sensitive technique for chemical analysis[38]. Since the % of carbon atoms of pure HDPE and nylon are different, the %

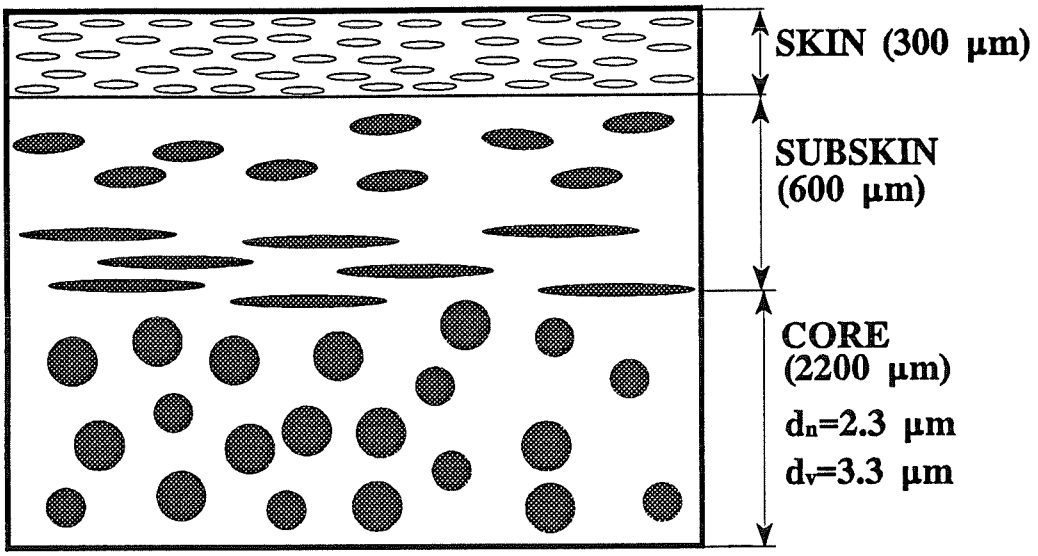

a)

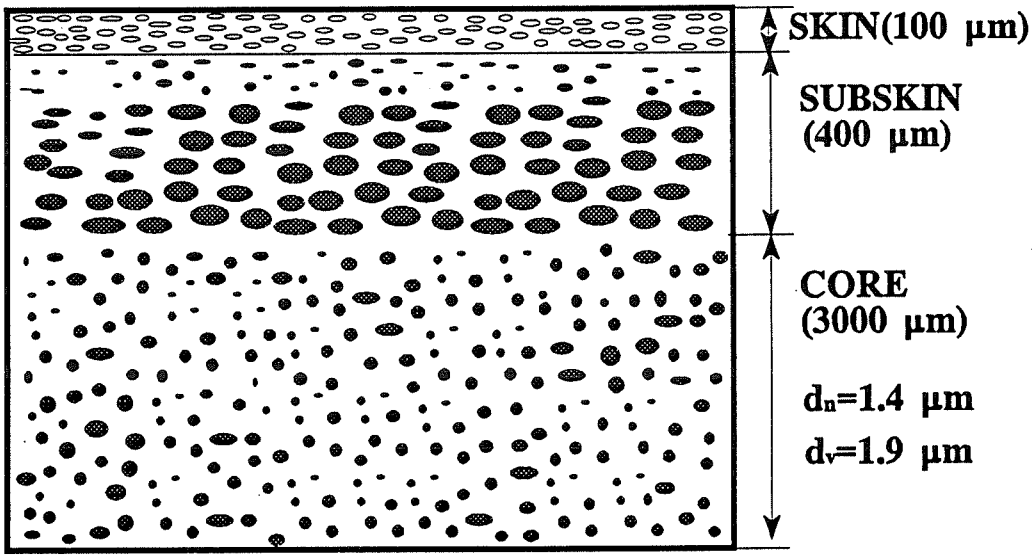

b)

Figure 2.7 - Schematic of the skin/core structure of injection molded parts - a) non-compatibilized blend, b) compatibilized blend

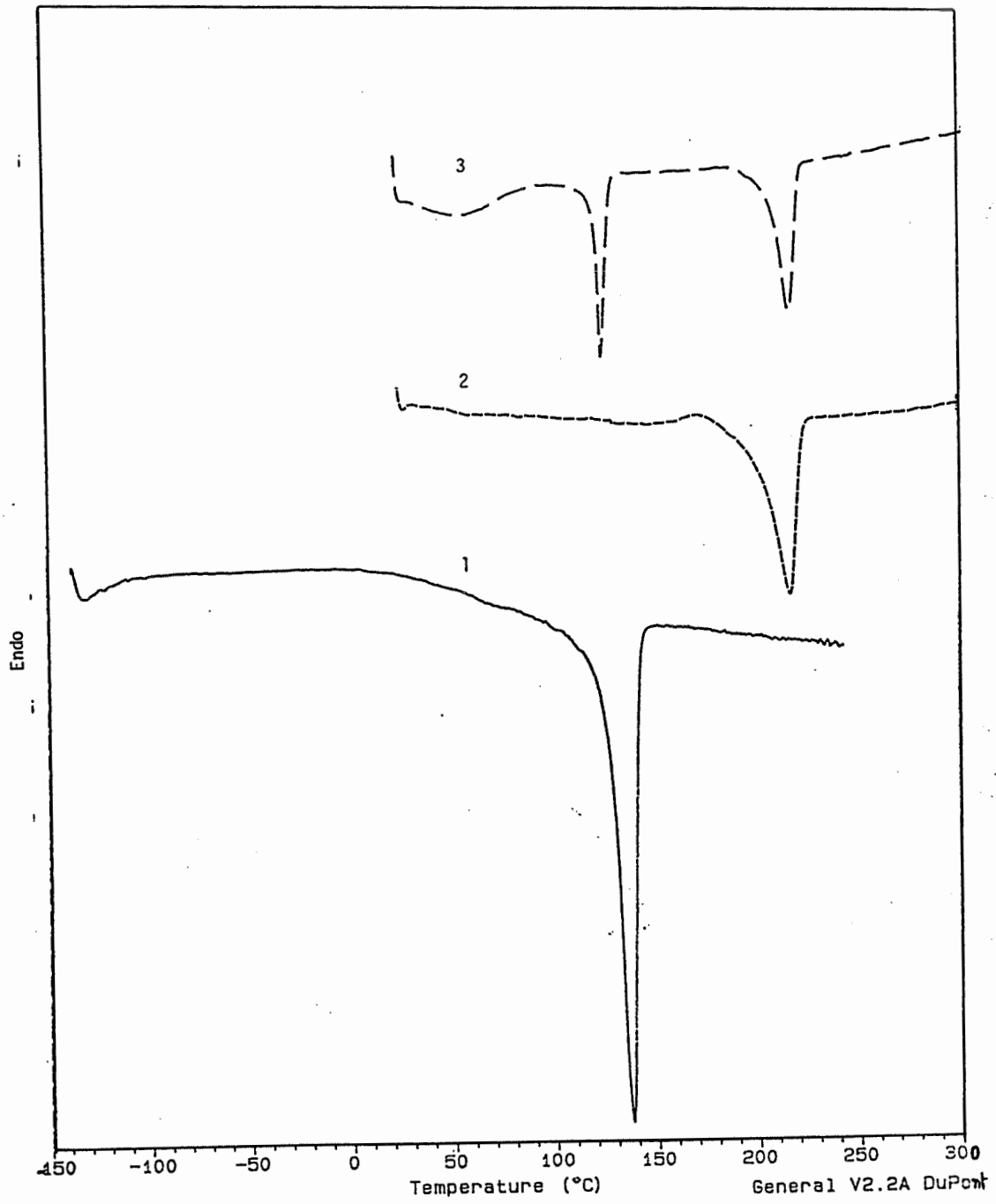

Figure 2.8 - DSC thermograms for: HDPE (1), PA-6 (2) and PEPA (3) (samples taken from the skin)

of carbon atoms obtained by XPS can give an indication of the relative proportion of a given component. The spectrum of neat HDPE, PA-6 and surlyn are shown in Fig. 2.9, while those of the blends are shown in figures 2.10 and 2.11. The results are summarized in Table 2.3. It can be seen that the number of carbon atoms is 71.9% (the % stands for atomic per cent) for neat PA-6 and 92% for neat HDPE. The lower per cent value for PA-6 is related to the presence of other atoms such as nitrogen and oxygen in PA-6. In neat HDPE, there is 6.2% oxygen. This can be attributed to carbonyl groups formed during the polymerization reaction. The non-compatibilized blend reveals the presence of 77.8% carbon (C) atoms, 7.1% nitrogen (N) atoms and 13.1% oxygen (O) atom. Knowing the % C, N and O for the neat components as well as that for the blend, the blend skin composition can be estimated via a rule of mixtures approach. These results confirm that the skin exists as a blend at approximately the same composition (24.4 wt% HDPE/75.6 wt% PA-6) as in the original, as prepared, blend (20.4 wt% HDPE/79.6 wt% PA-6). Similar observations also hold true for the compatibilized system. No segregation of individual blend components occurs. The XPS data therefore confirms the DSC results.

Finally, TEM observations on very thin slices (80 nm) cut from the skin region of the plaque in the direction perpendicular to flow (Fig. 2.12a) and longitudinally (Fig. 2.12b) revealed the presence of highly oriented HDPE particles, having an average diameter less than 0.5 μm and a length comprised between 5-10 μm. These results therefore indicate the presence of a very fine and elongated dispersed phase in the skin.

The TEM studies of the non-compatibilized system indicate the presence of very fine dispersed phase structures of less than 0.5 μm thickness. It should be noted that these dimensions are almost one order of magnitude smaller than that observed in the core of the sample. The transverse section (taken perpendicular to the flow direction) illustrates that ribbon-like structures exist in the skin and demonstrates the presence of significant biaxial stretching.

Table 2.3 - Composition (atom %) of the surface of the plaques as revealed by X-ray Photoelectron Spectroscopy (XPS)

	Carbon (atom %)	Nitrogen (atom %)	Oxygen (atom %)
PA6	71.9	8.4	16.1
HDPE	92.0	0.8	6.2
SURLYN	76.2	4.2	16.6
PEPA	77.8	7.1	13.5
PEPA-front	78.6	1.8	12.6
PEIPA	79.8	7.0	12.0

It is clear therefore that the apparent absence of dispersed phase as observed by SEM and shown in Figs. 2.5 and 2.6 can be attributed to the very fine size of the dispersed phase in the skin relative to the core. During SEM analysis typical magnifications used to evidence the core structure are not sufficiently high enough to

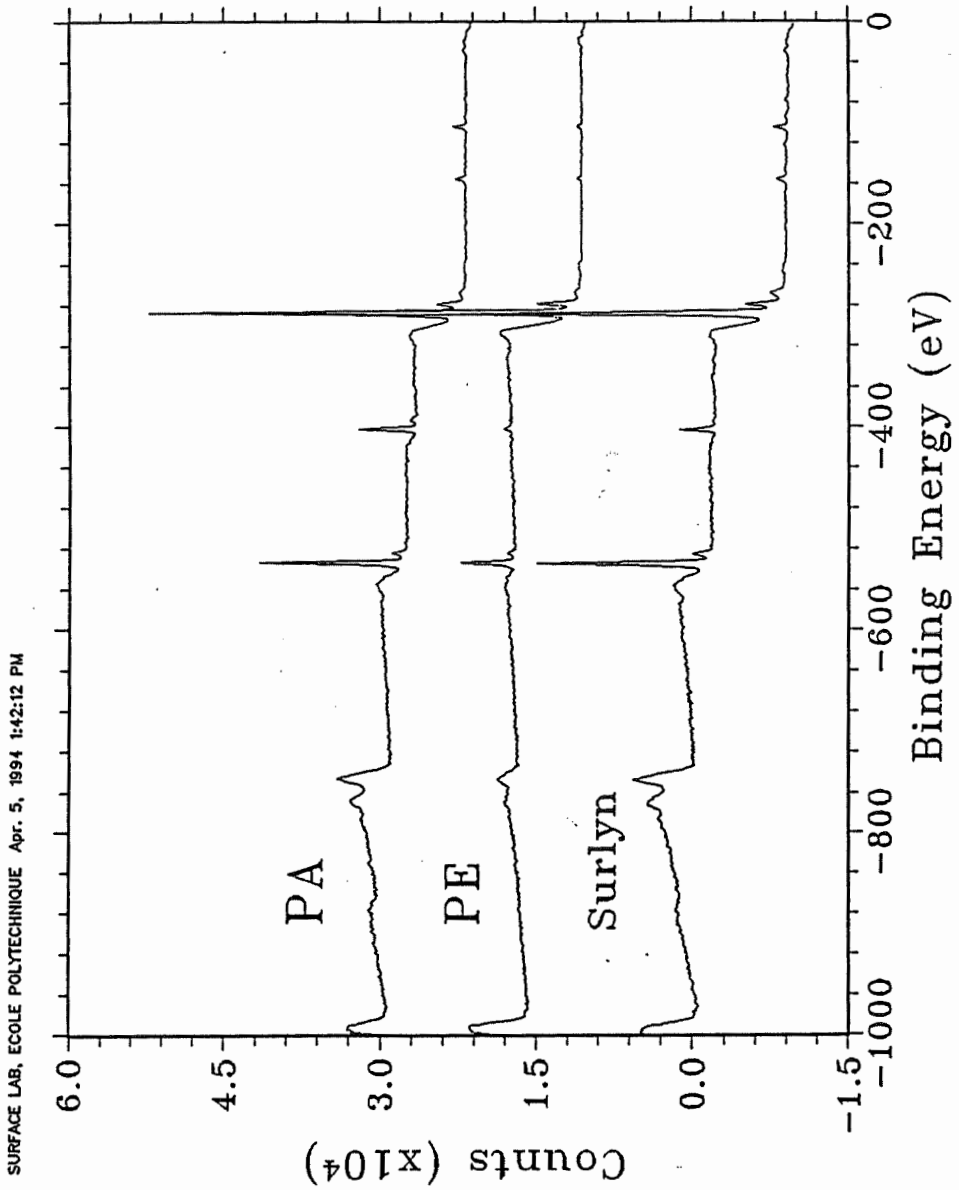

Figure 2.9 - XPS spectrums from the surface of: PA-6 (1), HDPE (2) and Surlyn (3) plaques

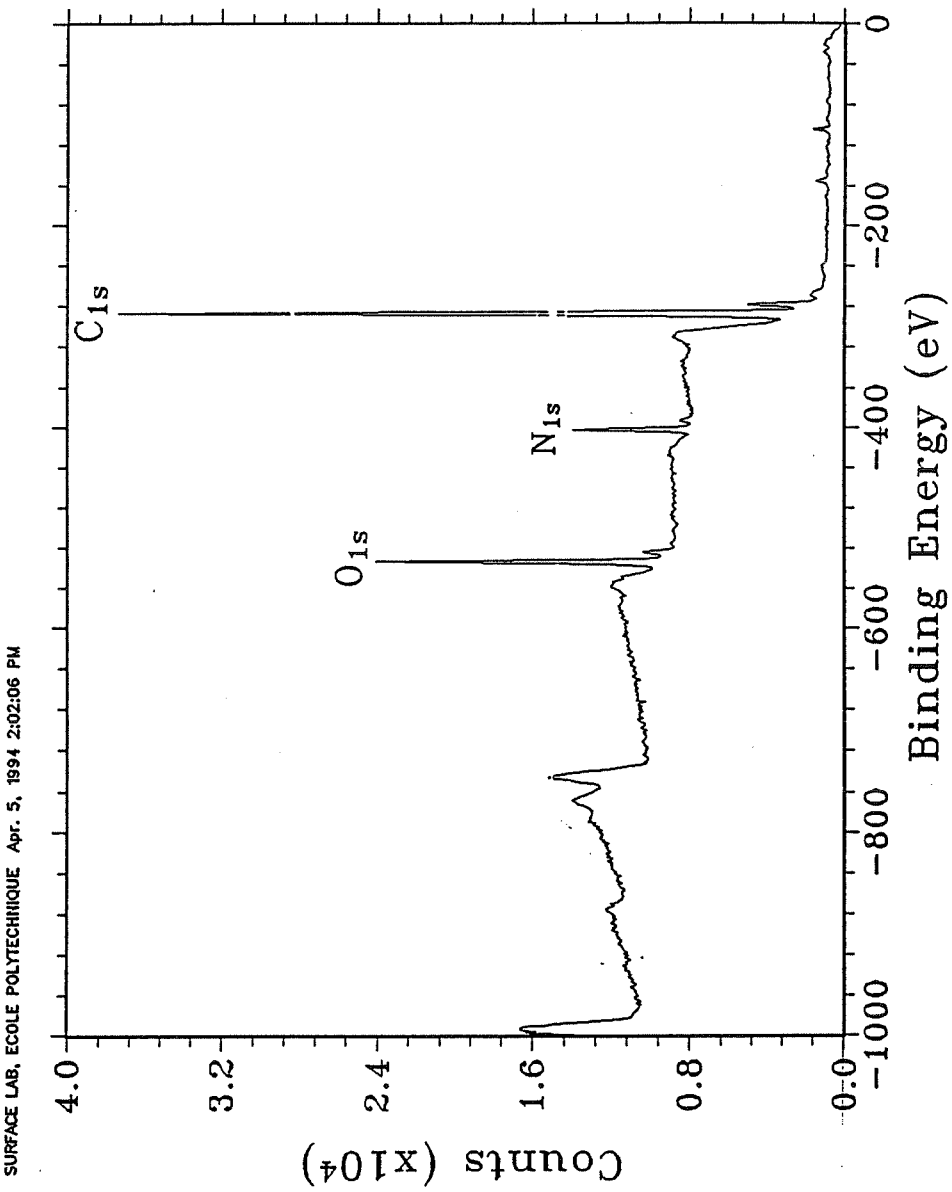

Figure 2.10 - XPS spectrum from the surface of non-compatibilized blend

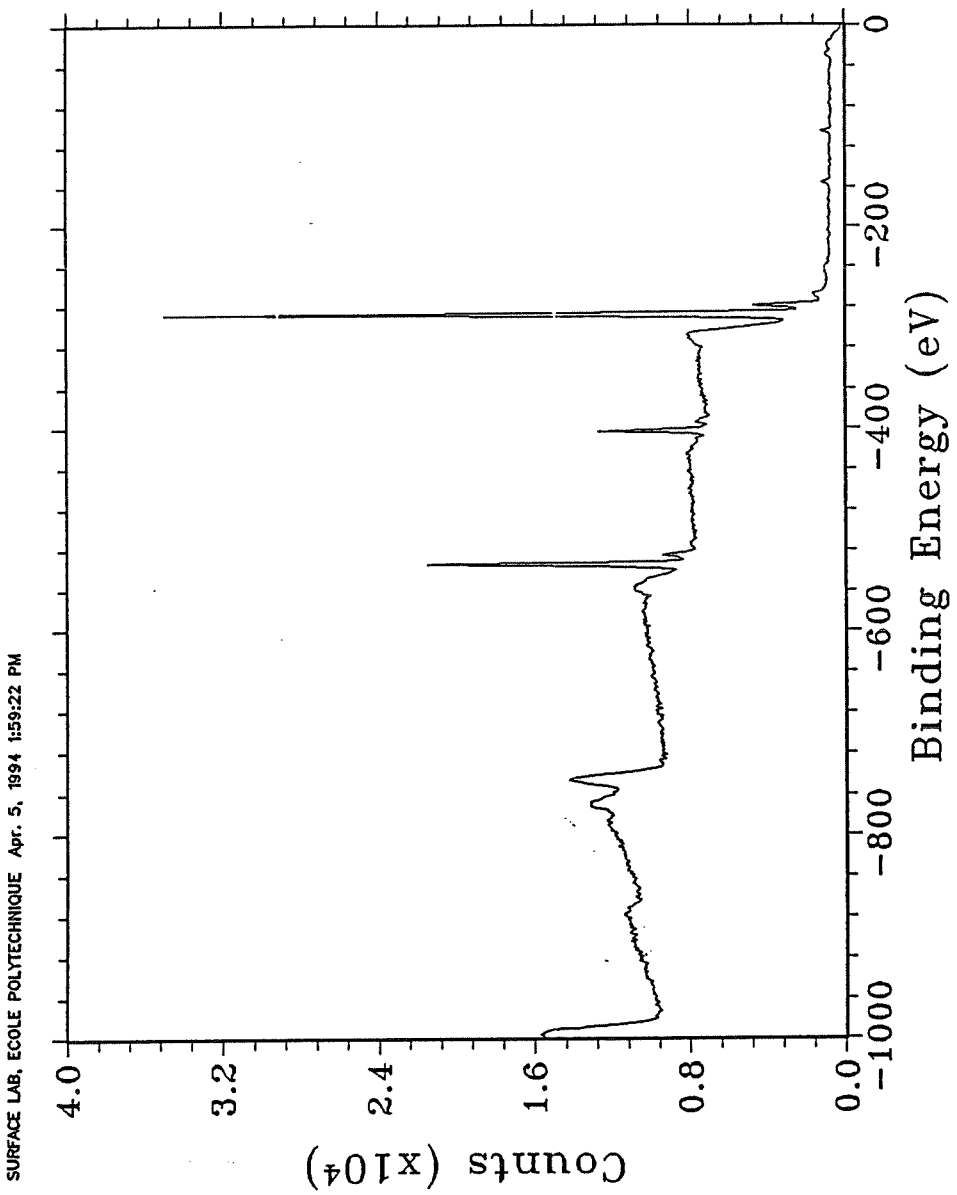

Figure 2.11 - XPS spectrum from the surface of compatibilized blend

allow visualization of the skin region. In fact DSC and XPS results show the surface composition of the dispersed phase to be very close to the original, as prepared, composition. Transmission electron microscopy further illustrates that the dispersed phase in the skin is very small and highly elongated.

ii) Core

The core represents approximately 50% of the whole sample in the non-compatibilized blend and 75% in the compatibilized one. The dispersed phase particles are more spherical than elsewhere, due to relaxation occurring during the cooling process. The structure of the core is coarser (d_n = 2.30 μm and d_v = 3.30 μm) with loose particles and is 2200 μm thick for the uncompatibilized blend. The compatibilized blend displays a finer dispersed phase (d_n = 1.40 μm and d_v = 1.95 μm), well adhered to the matrix and with a 3000 μm thick core (Fig. 2.7).

iii) Weldline morphology

In this study, a detailed examination was carried out to analyze the dispersed phase structure at the weldline region (Fig. 2.13a and b). A much finer morphology compared to the rest of the sample, and an apparent reduction in the concentration of the dispersed phase are observed. The overall behaviour is similar for systems both without (Fig. 2.13a) and with (Fig. 2.13b) compatibilizer, although there is a difference in the size of

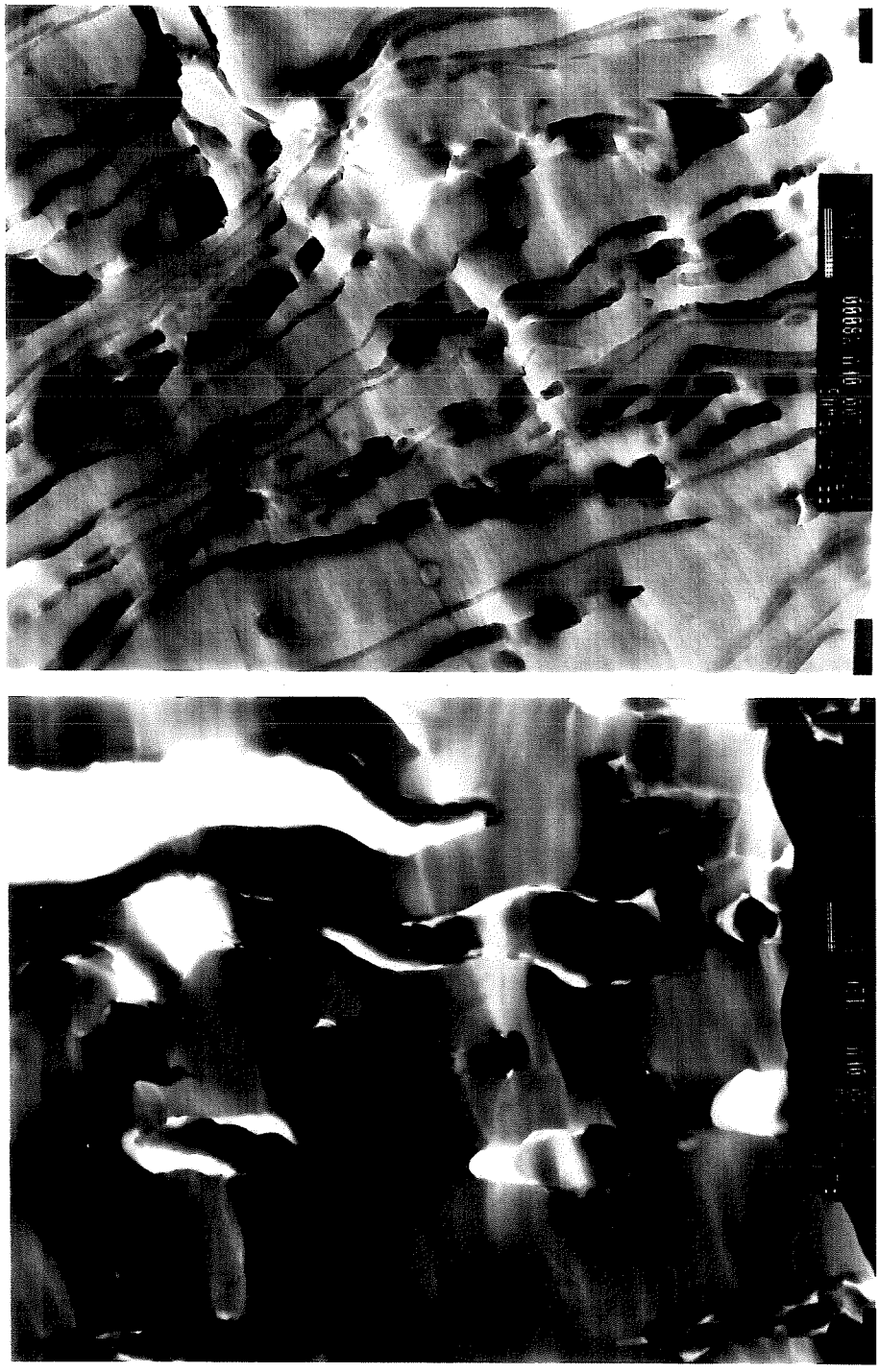

Figure 2.12 - TEM micrographs of samples taken from the skin region of: a) PEPA transverse view, b) PEPA longitudinal view

the dispersed phase, and the width of the weld line region. The micrograph in Fig. 2.13a for non-compatibilized blends, shows a weldline with a variable width, around 200 μm in the skin, and roughly 600 μm in the subskin. The micrograph of Fig. 2.13b of the compatibilized blends gives a weldline width of approximately 200 μm. The compatibilizer leads to a reduction of the dispersed phase size (d_n = 0.90 μm and d_v = 1.20 μm) and a narrowing of the weldline region compared to the weldline in the non-compatibilized blend (d_n = 1.60 μm and d_v = 4.70 μm). The surface of etched microtomed samples reveals a skin, and a weldline region made apparently of essentially pure PA-6 as was observed for the skin region. The weldline does not appear to be straight, but is deformed in the subskin region where the shear is at a maximum. It is well-known that the weldline is formed after two separated flow fronts meet. In other words it is formed from the skin region of two flow fronts. It will be shown in the next section that the width of the weldline region is approximately twice the thickness of the skin in the advancing melt front. A sketch representing the microstructure of the weldline in both blends without and with compatibilizer is shown in Fig. 2.14a and b respectively. The delineation between the weldine and non-weldline region is relatively straight forward and is based on the discontinuity between very small and very large particles.

iv) Analysis of the flow front

It is well accepted that in injection molding, the mold filling is based on a fountain flow approach[23] which consists of the successive deposition of the material generated in the flow front on the mold wall forming the skin. If the melt front is separated by an insert or through a double feeding system, the reunification of the fronts will result in the formation of a weldline. Consequently the thorough analysis of the melt front will lead inevitably to a precise knowledge of the composition and morphology of both the skin and the weldline regions. For this reason short-shot experiments were performed and the results of the morphological and XPS analysis of the melt front will be presented.

From micrograph, Fig. 2.6b (with compatibilizer) corresponding to positions 2, the skin of the flow front is roughly 100 μm thick. It appears that this structure is maintained all along the specimen length. If it is assumed that the skin is deposited from the melt front due to fountain flow, then a 100 μm thick skin on short-shot samples should be observed. Micrograph 15a, shows the front in the short-shot sample having a skin of approximately 100 μm thickness.

If a complete sample taken at position 4, Fig. 2.5a (without), and Fig. 2.6a (with compatibilizer) are compared, then for the former, the skin is approximately 300 μm thick as was mentioned previously, but the latter is around 100 μm thick. The ionomer has caused a drastic reduction in the skin thickness. By way of comparison, the front

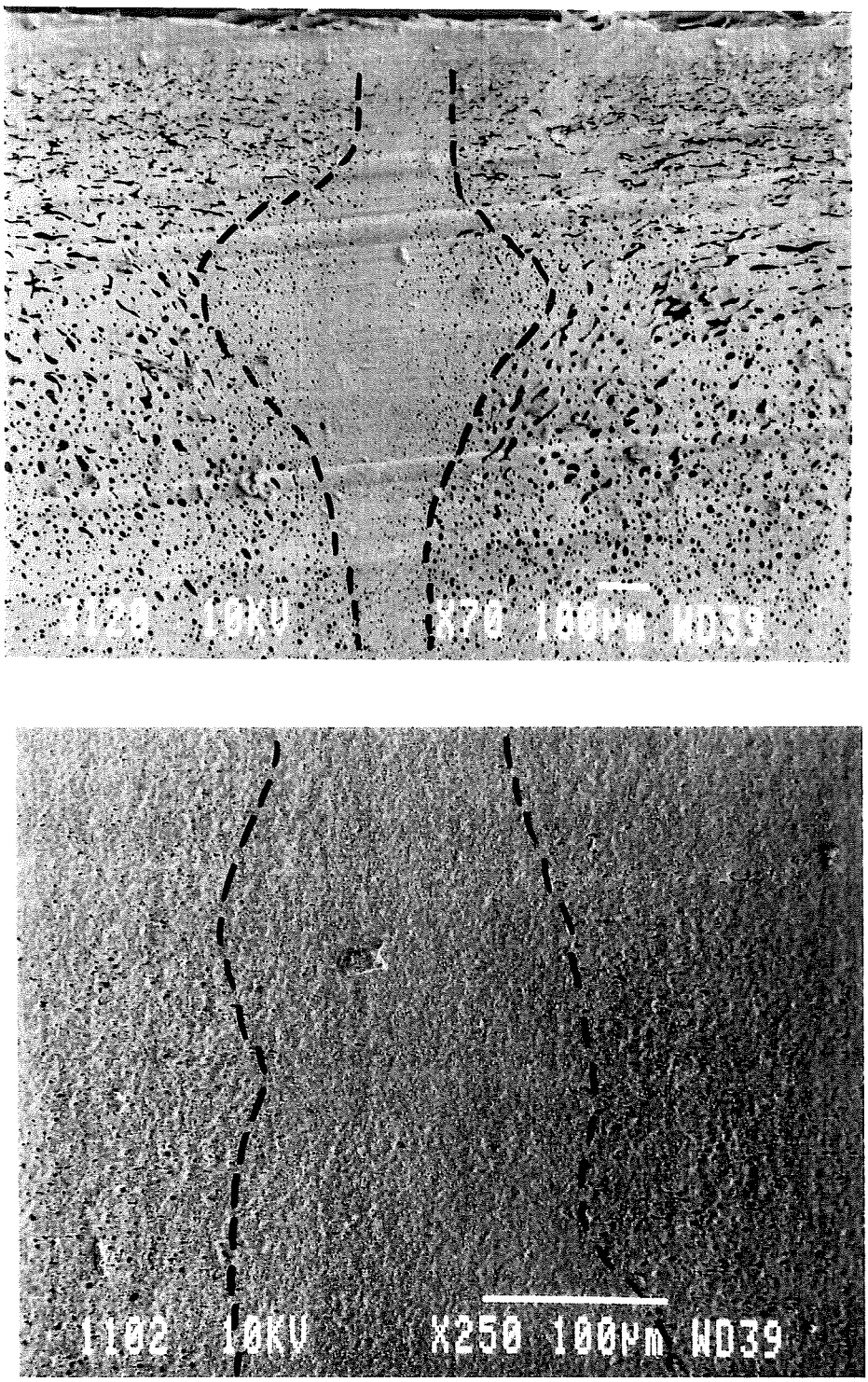

Figure 2.13 - SEM micrographs of samples containing a weldline (perpendicular to flow view) - a) non-compatibilized blend, b) compatibilized blend

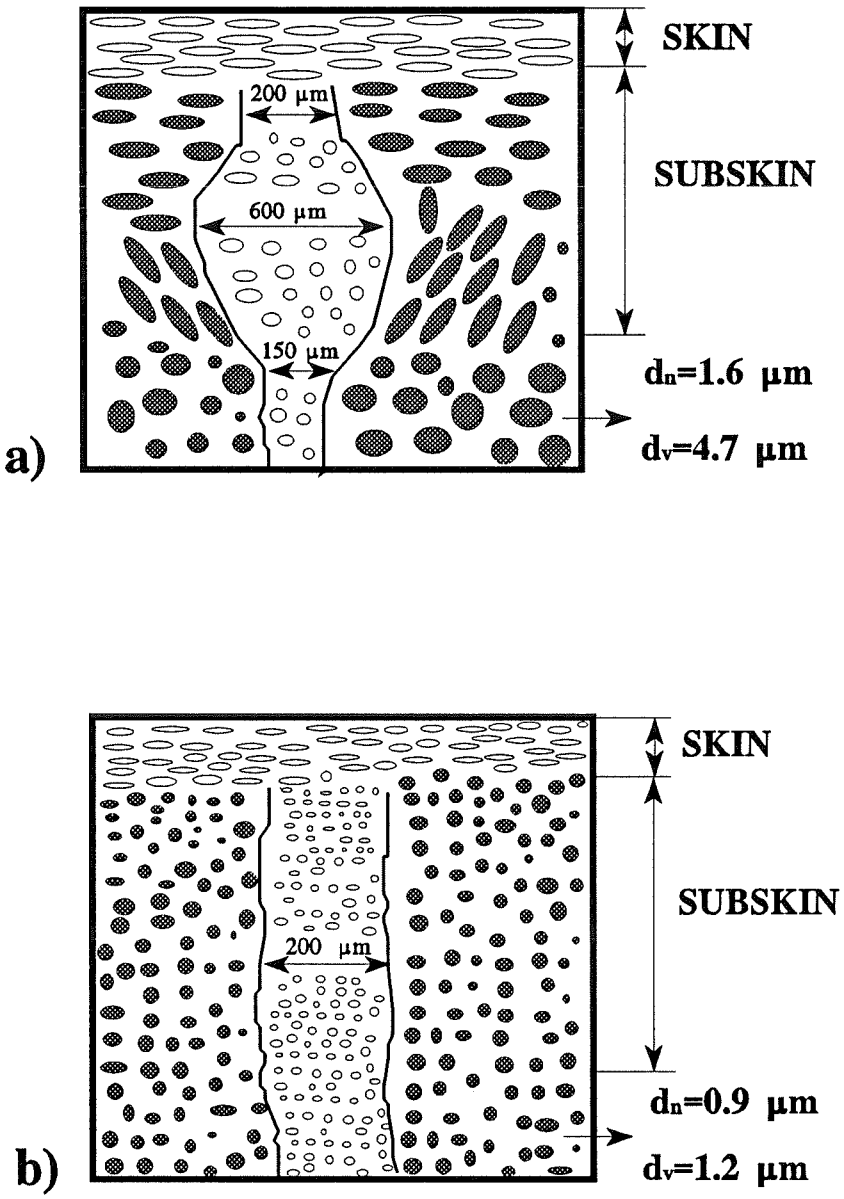

Figure 2.14 - Schematic representation of weldline structure - a) non-compatibilizer blend, b) compatibilized blend

in the non-compatibilized short-shot samples (Fig. 2.15b) shows the presence of a skin of roughly 250 μm thickness. It is astonishing to observe that the skin thickness in the flow front does not appear to depend on position along the plaque. This implies a steady depletion and reconstitution of the skin in the melt front as it advances throughout the mold. It should also be noted that the SEM observations (Fig. 2.15) again reveal an apparent absence of the minor phase in the skin of the flow front. The delineation of the skin thickness is based on the discontinuity between very small and very large particles.

It is well-known that both the weldline and the skin regions are formed from the deposition of material originating from the melt flow front[23]. The melt front as it expands in a "mushroom-like fashion" will be deposited on the cold surface of the mold forming a frozen skin. The rejoining of opposing or adjacent melt fronts leads to the formation of a weldline. An XPS test was run on a short-shot sample i.e. front (non-compatibilized blend). The spectrum is shown in Fig. 2.16 and the results are shown in Table 2.3. The amount of carbon atoms measured (78.6% carbon atom) on the surface of a short-shot sample is similar to that found on the surface of a complete PE/PA sample (77.8%). Then again using the rule of mixtures as before, one can easily predict the amount of carbon atoms in the flow front (76%) which is close to the initial, as prepared, amount of carbon atoms (78.6%). The composition of the skin in the flow front therefore is 35wt% PE/ 65wt% PA-6. The larger discrepancy observed here as compared to the original, as prepared composition (20.4/79.6 wt%), can be attributed to experimental errors because the surface analyzed in this case was very small.

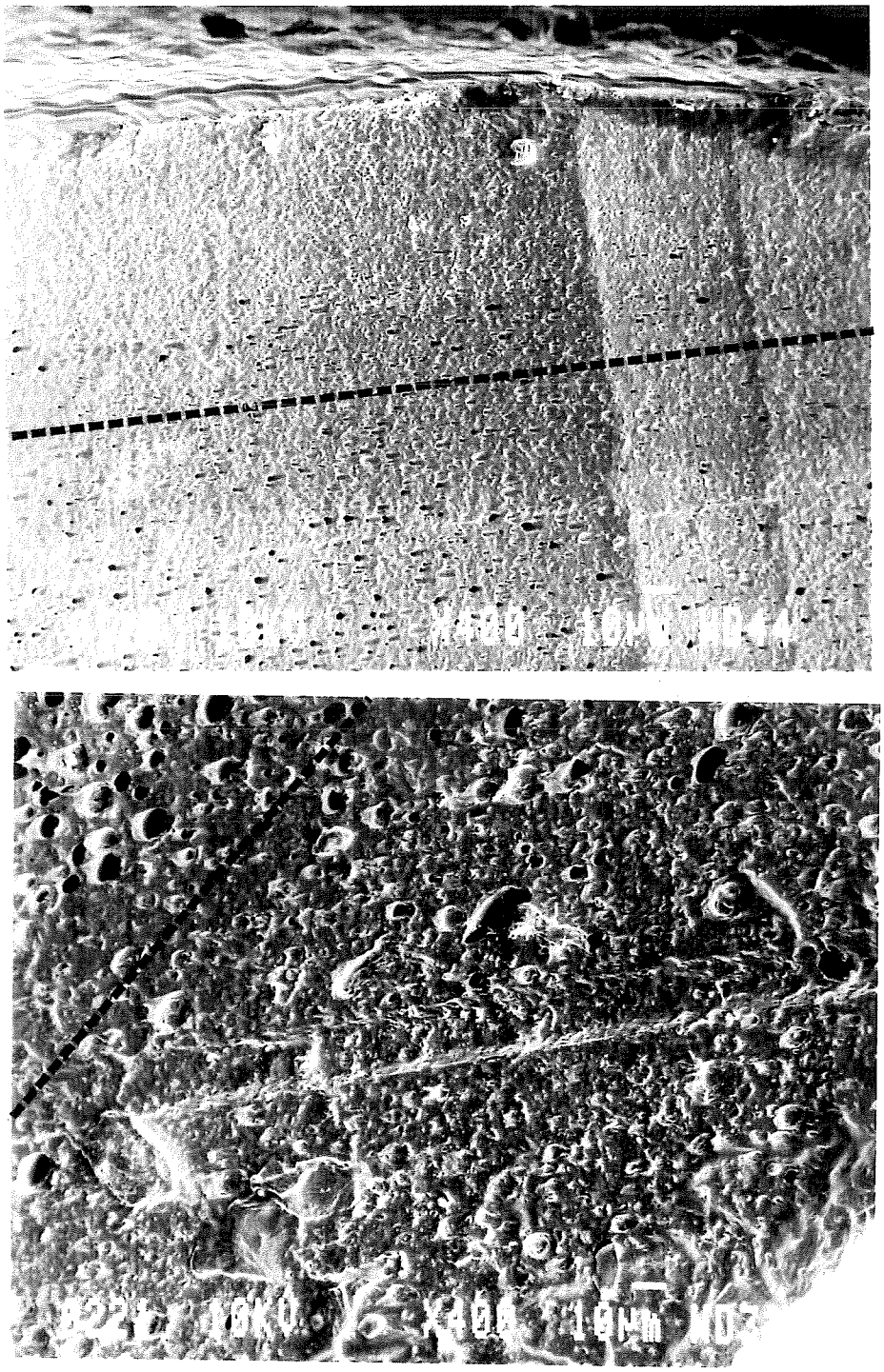

Figure 2.15 - SEM micrographs of short-shot samples taken at position 1, and showing the skin thickness in the flow front (perpendicular to flow view): a) with compatibilizer, b) without compatibilizer

Nevertheless, the results clearly confirm the significant presence of dispersed phase. Since both the weldline region and the skin originate from the melt front as suggested by Tadmor[23], these data can be directly applied to the weldline region. In other words, both phases (HDPE and PA-6) are present in the melt front as well as in the plaque skin of a PEPA sample as already mentioned. If it is assumed that the weldline region is the result of the contact between two melt fronts, then, the melt front itself is essentially a copy of the weldline. This is convenient since it is difficult to obtain XPS measurements directly at the weldline. It is evident from the above results therefore that the HDPE dispersed phase is present in the weldline region. Figure 2.17a and b shows SEM micrographs taken at the same magnification inside and outside the weldline. Inside the weldline region, the dispersed phase particles are very fine but in view of the above XPS results apparently exist at elevated concentrations as elsewhere in the sample.

These results are of significance since it has been reported on several occasions in the literature that the skin of injection molded polymer blends is composed of one pure component[28,29,31,32,33]. This work strongly indicates that great caution must be taken in the interpretation of SEM photomicrographs. In this study, it is shown that the dispersed phase is present in the skin and the weldline regions, but at significantly reduced particle dimensions. At magnification levels normally used to visualize the coarser core region, the dispersed particles in the skin become essentially invisible.

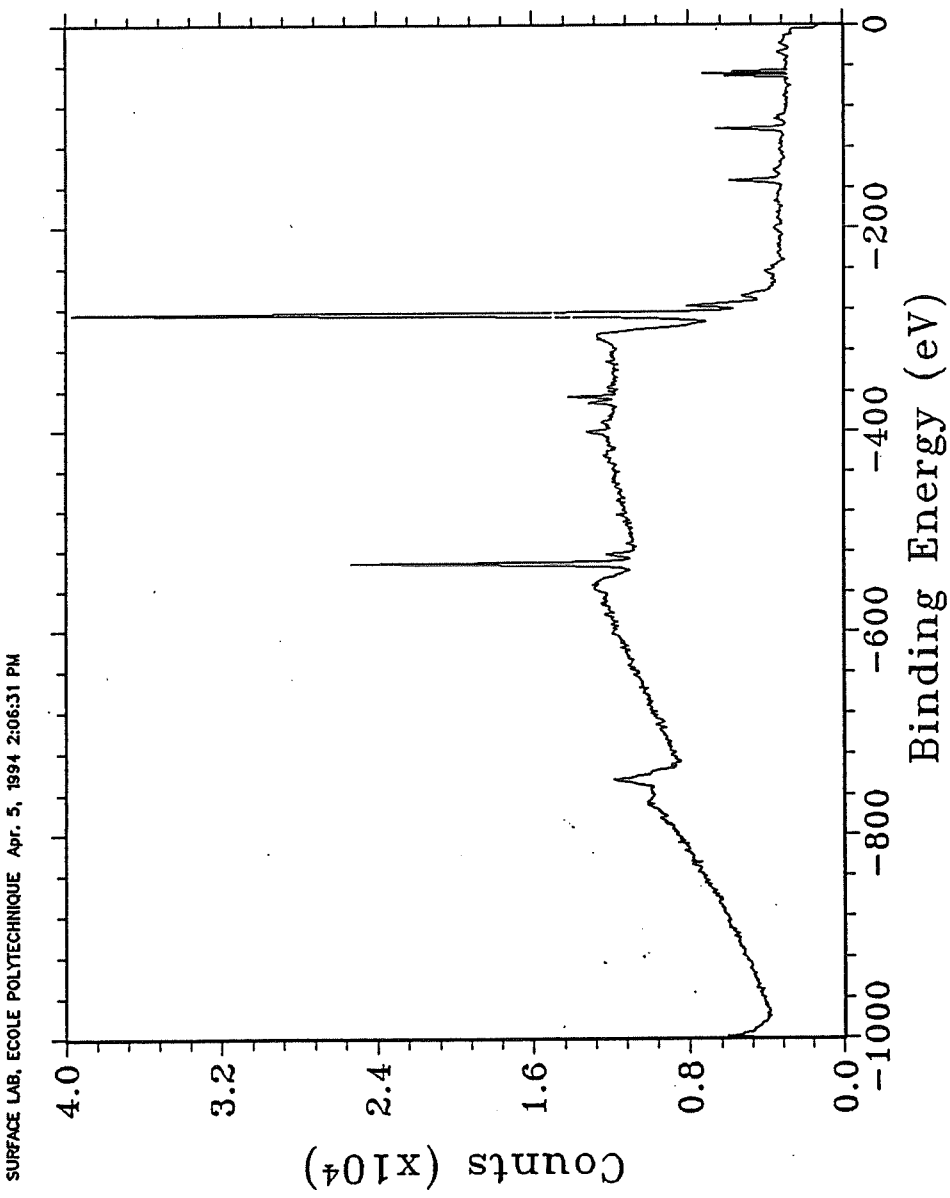

Figure 2.16 - XPS spectrum of the flow front surface of PEPA blend

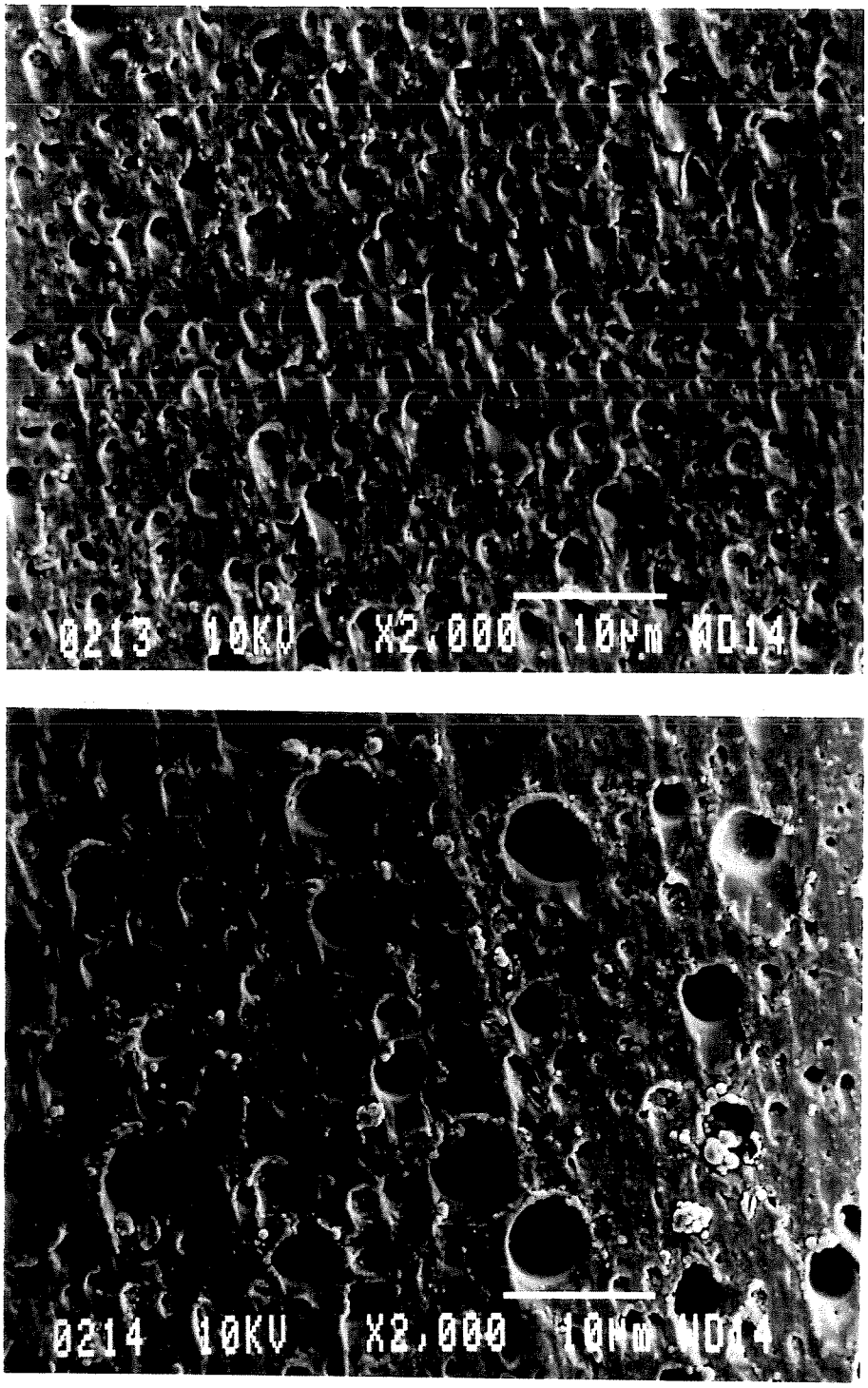

Figure 2.17 - SEM micrographs of the weldline region in non-compatibilized blend - a) inside the weldline, b) outside the weldline region

The following discussion will attempt to address the nature of the mechanism resulting in the significantly reduced size of the minor phase in both the skin and the weldline regions, as well as the morphological variations observed throughout the sample thickness. It is possible that the dispersed phase size reduction observed in the flow front and in the skin region may be attributed to particle break up resulting from the elongational flow and biaxial stretching that the particles undergo in the melt front. This is mainly based on the "fountain flow" effect which was introduced by Tadmor[23] to describe how polymer melts flow into an injection mold cavity. This is an inside-out flow pattern where melt streamlines in the middle of the channel, advance to the flow front, then turn outward towards the cavity wall. A schematic diagram of the flow model is shown in Fig. 2.4. The melt front is stretched extensionally which creates an oriented frontal layer that freezes upon contact with the mold surface. The fountain flow occurs in the region behind the melt front, as shown by the curved streamlines in Fig. 2.4. Well behind the frontal region is laminar shear flow as shown by the parabolic velocity profile; the highest velocity being in the centre of the cavity, the lowest velocity is under the laid-down frontal layer. This velocity profile is coupled with a shear profile with a maximum shear zone located near the wall and a minimum shear zone at the middle of the channel[38].

According to this model, the orientation at the surface of the molded part comes from the extensional orientation of the melt front and not from shear flow at the wall. Such a hypothesis would be supported by the results of this study since a very fine

dispersed particle size was found not only in the skin, but also in the weldline region and flow front samples. The diagram depicted in Fig. 2.4 shows that the melt elements that proceed to the very front come from the centermost streamlines where shear is at a minimum. Thus, these elements undergo an abrupt change from minimal deformation to highly stretched[37]. Similar findings have been also reported by Schmidt[39]. In addition, the theory of particle break up seems to support the above mechanism. The critical parameters that control the particle deformation and break up are the viscosity ratio (η_r), the shear stress ($\eta_m\dot{\gamma}$), the particle diameter (d) and the interfacial tension (σ). The basic principle of droplet deformation is that as soon as the disruptive stress due to the viscous drag of the medium is able to overcome the cohesive effect of surface tension, the drop bursts. In previous studies on newtonian systems it has been reported that at a high viscosity ratio ($\eta_r = 20$) the drop still bursts in an extensional flow field, whereas in uniform shear flow the drop would not burst even at the highest possible speeds. An extensional flow field is very effective for droplet break up and the limiting viscosity ratio range is much greater than that for uniform shear flow[5].

2.4 CONCLUSION

The morphological study of injection molded HDPE/PA-6 blends based on SEM and image analysis reveals: the existence of a significant skin/core effect for the non-compatibilized blend manifested as a morphological variation with respect to the thickness i.e. dispersed phase is highly oriented in the subskin and spherical in the core.

Interfacial modification results in a more stable morphology displaying a reduced dispersed phase size as well as the diminution of the thickness of the skin and weldline region. An apparent absence of the minor phase in the skin and weldline regions was observed for both uncompatibilized and compatibilized blends.

To verify the validity of the above observation related to the apparent minor phase deficiency in both the skin and weldline regions; differential scanning calorimetry (DSC) thermograms of microtomed slices from the skin, transmission electron microscopy (TEM) as well as X-ray photoelectron spectroscopy (XPS) analysis of the surface of the blends, Surlyn and neat resins were performed. This detailed compositional analysis reveals the presence of both components (HDPE and PA-6) on the surface of the plaques as well as on the melt front obtained through short-shot experiments, at approximately the same composition as in the original, as prepared, blend. When an interfacial modifier is used, XPS analysis reveals values for the surface composition similar to the unmodified case.

The apparent absence of dispersed phase as observed by SEM was attributed to the very fine size of the dispersed phase in the skin relative to the core. The nature of the mechanism governing the significantly reduced size of the minor phase in both the skin and weldline region is thought to be related to particle break up resulting from the elongational flow and biaxial stretching that the particles undergo in the melt front.

2.5 REFERENCES

1 Utracki L.A., *Polymer Alloys and Blends: Thermodynamics and Rheology*, Hanser Publishers, Munich, 1989, Chap I.

2 Baker W.E. and Saleem M., *Polym. Eng. Sci.*, 1987, **27**, 1634.

3 Xanthos M., *Polym. Eng. Sci.*, 1987, **28**, 1392.

4 Liu T.M., Xie H.Q., O'Callaghan, Rudin A. and Baker W.E., *J. Polym. Sci.*, part B: *Polym. Phys.*, 1993, **31**, 1347.

5 Favis B.D., *Can. J. Chem. Eng.*, 1991, **69**, 619.

6 Chen C.C. and White J.L., *Polym. Eng. Sci.*, 1993, **33**, 923.

7 Padwa A.R., Presented at the 11th NRCC/IMI Symposium "Polyblends-91", Oct. 29-30, 1991, Boucherville, Québec, CANADA.

8 Min K., Endo S., White. J.L., Kyu T., and Fellers J.F., *SPE ANTEC Tech. Papers*, 1985, **31**, 530.

9 Liang B.R., White J.L., Spruiell J.E. and Goswani B.C., *SPE ANTEC Tech. Papers*, 1983, **29**, 92.

10 Min K., White J.L. and Fellers J.F., *Polym. Eng. Sci.*, 1984, **24**, 1327.

11 Chen C.C., Fontan E., Min K. and White J.L., *Polym. Eng. Sci.*, 1988, **28**, 69.

12 Fairley G. and Prud'homme R.E., *Polym. Eng. Sci.*, 1987, **27**, 1495.

13 Serpe G., Jarrin J. and Dawans F., *Polym. Eng. Sci.*, 1990, **30**, 553.

14 Ghiam F. and White J.L., *Polym. Eng. Sci.*, 1991, **31**, 76.

15 Van Gheluwe P., Favis B.D. and Chalifoux J.P., *J. Mat. Sc.*, 1988, **23**, 3910.

16 Willis J.M., Favis B.D. and Lavallée C.J., *J.Mat. Sci.*, 1992, **27**. p.

17 Favis B.D., Lavallée C. and Derdouri A., *J. Mat. Sci.*, 1992, **27**, 4211.

18 Willis J.M. and Favis B.D., *Polym. Eng. Sci.*, 1988, **28**, 1416.

19 Macknight W.J., Lenz R.W., Musto P.V., and Somani R.J., *Polym. Eng. Sci.*, 1985, **25**, 1124.

20 Fisa B., SPI, 46th conference preprints, 1991, Session 9-C.

21 Gilmore G.D. and Spencer R.S., *Modern Plastics*, 1951, **4**, 117.

22 Hagerman E.D., *Plast. Eng.*, 1973, **10**, 67.

23 Tadmor Z., *J. Appl. Polym. Sci.*, 1974, **18**, 1753.

24 Tomari K., Harada T., Maekawa Z., Hamada H., Iwamoto M. and Ukai A., *Polym. Eng. Sci.*, 1993, **33**, 996.

25 De Gennes P.G., *The Journal of Chemical Phys.*, 1971, **55**, 572.

26 Wool R.P., Yuan B.L. and McGarel O.J., *Polym. Eng. Sci.*, 1989, **29**, 1340.

27 Titomanlio G., Piccarolo S. and Rallis A., *Polym. Eng. Sci.*, 1989, **29**, 209.

28 Malguarnera S.C., Riggs D.C., *Polym. Plast. Tech. Eng.*, 1981, **17**, 193.

29 Thamm R.C., *Rubb. Chem. Tech.*, 1977, **50**, 24.

30 Nolley E., Barlow J.W. and Paul D.R., *Polym. Eng. Sci.*, 1980, **20**, 364.

31 Karger-Kocsis J. and Csikai I., *Poly. Eng. Sci.*, 1987, **27**, 241.

32 Fisa B., Bouti A., Favis B.D and Lalande F., *SPE ANTEC Tech. Papers*, 1991, **37**, 1135.

33 Fellahi S., Favis B.D. and Fisa B., *SPE ANTEC Tech. Papers*, 1993, **39**, 211.

34 Favis B.D. and Therrien D., *Polym.*, 1991, **32**, 1475.

35 Poulin D., Diawara Y., Currie J.F., Yelon A., Gujrathi S.C. and Petrova-Koch V., *Mat. Res. Soc. Sym. Proc.*, 1993, **283**, 88.

36 Favis B.D. and Chalifoux J.P., *Polym. Eng. Sci.*, 1987, **27**, 1591.

37 Fritch L., *Plast. Eng.*, 1979, **5**, 68.

38 Moulder J.F. et al., *Handbook of XPS* edited by J. Chastain Perkin-Elmer, 1992, Chap. I.

39 Schmidt L.R., *Polym. Eng. Sci.*, 1974, **13**, 797.

CHAPTER 3

WELDLINE STRENGTH IN INJECTION MOLDED HDPE/PA6 BLENDS: INFLUENCE OF INTERFACIAL MODIFICATION

SOMMAIRE

La plupart des objets moulés par injection contiennent des défauts connus sous le nom de ligne de soudure. Ce défaut peut introduire une faiblesse pouvant affecter leur performance. La présence de ligne de soudure est plus problématique dans le cas de systèmes multiphasés où la situation peut être aggravée par l'incompatibilité des composants des deux côtés de l'interface qui résulte en un affaiblissement additionnel en l'absence d'adhésion entre les différentes phases. En plus, le comportement des lignes de soudure est influencé par des effets morphologiques et d'orientation. Ce travail a pour but d'établir la relation entre la structure et les propriétés mécaniques des mélanges polyéthylène haute densité/polyamide-6 moulés par injection. L'effet de la ligne de soudure est étudié en détail. Deux types de moules ont été utilisés : le premier moule (type I) permet d'obtenir des éprouvettes correspondant au type (M-I) de la norme ASTM D638M, en utilisant deux seuils d'alimentation. Le deuxième moule (type II) à cavité rectangulaire muni d'un seuil en nappe. De plus, un insert peut être installé dans la cavité pour diviser le front d'écoulement en deux, conduisant à la formation d'une ligne de soudure. Deux formulations contenant 25% PE/75 vol % PA-6 avec et sans compatibilisant ont été préparées. Dans le cas des éprouvettes du type I, la phase

dispersée est orientée parallèlement à l'écoulement. Dans le coeur qui représente uniquement 10 % de l'épaisseur de l'échantillon, la phase dispersée adopte une forme plus sphérique. La morphologie de la ligne de soudure est très similaire à celle de la peau de l'éprouvette, les structures allongées sont orientées parallèlement au plan de la ligne de soudure. L'effet du compatibilisant sur les propriétés mécaniques (sans ligne de soudure) des éprouvettes moulées directement est mineure : il est masqué par l'orientation induite par l'écoulement. En présence d'une ligne de soudure, une réduction de 40 % dans les propriétés mécaniques du système non compatibilisé est observée. L'addition d'un compatibilisant permet au matériau de récupérer sa capacité à s'écouler et les propriétés mécaniques sont très proches de celles des échantillons sans ligne de soudure. Pour le deuxième type de moule (plaque), l'effet de la ligne de soudure est moins prononcé ainsi que l'effet de la distance après l'insert est négligeable. L'anisotropie est très prononcée avec le matériau non compatibilisé. Dans le cas où il est compatibilisé, toutes les propriétés mécaniques ne sont pas affectées par la présence de ligne de soudure, exception faite pour les plaques de 2 mm d'épaisseur dans la position très proche de l'insert. Les propriétés dans la direction longitudinale (parallèle à l'écoulement) sont similaires à celles des échantillons du type I et ne sont pas affectées par une augmentation de l'épaisseur de la plaque. Par conséquent, on peut questionner l'utilité des éprouvettes moulées directement pour étudier les différents aspects reliés aux propriétés mécaniques des systèmes multiphasés où la structure générée par ce type d'écoulement est très différente de celle rencontrée dans des pièces «réelles» moulées par injection.

3.1 INTRODUCTION

There is a strong relationship between the morphology and properties of immiscible polymer blends. The size and the shape of the minor phase affects many properties namely the impact strength, the ductility, barrier properties as well as the flow behavior. The morphology of the dispersed phase can be influenced to varying degrees by interfacial modification, viscosity and elasticity ratios, composition and by the processing history[1,2,3].

During processing of these materials both phases can be deformed and oriented. When processed by the injection molding process the flow of the molten polymer inside a cold mold generates a complex morphology throughout the thickness[4]:

- two outside "skin" layers are formed by the expansion and rapid solidification of the melt front;
- two subskin "shear" layers influenced by the high shear rate;
- a central "core" layer which, having undergone less shearing during flow inside the mold and taking longest time to solidify, has a structure closest to that obtained under quiescent solidification.

Injection molded parts may also contain defects known as weldlines or knitlines. They result from the union of two separated flow fronts. Weldlines in injection molded

polymer blends are not well documented. In his review paper on the application of polymer blends, Robeson[5] reported that in complex molds, the elimination of weldlines is virtually impossible, and very poor retention of strength (specially impact strength) is observed. Weldlines have been referred to as being the "Achilles's heel" of immiscible polymer blends. Loss of strength and toughness due to the presence of weldlines may be a problem in some homogeneous materials as well, but in multiphase materials such as polymer blends, filled and reinforced polymers, or liquid crystal polymers, the strength loss is usually much more pronounced. The weldline region is known to be structurally different from the rest of the material[6,7].

Evaluation of immiscible blends by measure of the ductility, the impact strength always shows a negative departure from additivity rule[8]. Addition of an appropriate compatibilizer helps to recover the lost strength and ductility and is often accompanied by some loss of the yield strength and of the stiffness[9,10,11,12]. In order to evaluate the performance of such systems, samples for mechanical testing must be prepared. Different approaches are available:

- direct injection molding of samples required by the method (e.g. tensile samples defined by ASTM D638) standard;
- machining samples from molded plaques or from molded parts.

Undoubtedly because of the convenience the mechanical properties of plastics are most often studied using directly molded dogbone shaped tensile specimens. The flow induced structure has a profound effect on the mechanical behaviour of these samples. For instance, as was reported earlier[13], during tensile and tensile impact loading, failure is initiated in the shear zone along the skin-core boundary. Because of the difference in flow encountered the directly molded samples and the ones machined from plaques, one might expect differences in their behavior. For instance, Fisa et al.[14] reported a similar comparative study on non-compatibilized polypropylene/polycarbonate blends. The hypothesis of flow induced orientation can be used to explain the differences observed between the properties of the samples machined from plaques and those directly molded into the tensile samples. The machined samples exhibit lower stiffness and strength. In the end-gated tensile sample cavity the melt convergence, as it enters the narrower section, must impart additional orientation and elongation to the dispersed phase. Fracture occurs in the area where the melt exits from the narrow section, where the diverging flow starts to orient the elongated structures in the direction perpendicular to flow[14].

Injection molded polymer blends containing weldlines is not as well documented a subject as its counterpart in virgin homopolymers. Injection molded EPDM/PP systems with a weldline obtained with a double gated mold were studied by Thamm et al.[15]. They reported an absence of the minor phase (EPDM) in the weldline region. Similar results were reported later by Malguarnera et al.[16]. They attributed the absence of the

dispersed EPDM in the weldline region to a deficiency in the flow front region although this was never supported experimentally. Paul et al.[8,9,10] have studied the effect of a compatibilizer on the mechanical properties of several systems with and without weldline obtained in a double gated mold. Karger-Kocis et al.[13] studied the structure/properties relationships, and the phenomena causing rupture of injection molded blends of EPDM/PP with and without weldline. The usual skin/core structure was found. In the skin two zones were observed; a thin PP layer on the surface, and a sub-skin with highly elongated rubber particles. The core was rich in rubber particles. This effect was attributed to the existence of a concentration gradient due to crystallization of the front in contact with the mold surface. During crystallization the polypropylene rejects the rubber particles instead of engulfing them. Similar morphological observations were carried out in this laboratory in a preliminary study on HDPE/PA6 compatibilized with an ionomer[17], although a crystallization mechanism was not considered.

In this work we study the mechanical behavior of injection molded HDPE/PA6 blends with and without a weldline, as well as the influence of a compatibilizer. The detailed study of the morphology of these materials is being published separately[20]. The principal conclusions are:

- At a microscopic level the morphology of the weldline zone differs significantly from the rest of the material. For example in 4 mm thick plaques three distinct layers are observed away from the weldline. A skin originating

from the expansion of the melt front is about 100 μm thick in the compatibilized blend and 300 μm in the non-compatibilized one.

- The minor phase in the skin region is so finely divided as to be invisible by scanning microscopy. However, the measurements by calorimetry (DSC) and by X-ray photoelectron spectroscopy (XPS), and solvent extraction reveal that the concentration is relatively constant throughout the molded part[18]. In the subskin, the morphology is much coarser due to shear-induced coalescence. In the core a spherical morphology predominates.

- The morphology gradient observed throughout the thickness, i.e. fine dispersion in the skin, coarse in the subskin (shear) layer and intermediate in the core is also found as one moves away from the weldline to the bulk of the molded part. The width of the weldline zone is roughly twice that of the skin suggesting again that in these blends the weldline is formed by the meeting of two laterally expanding melt fronts. Consequently, the weldline region shows a very similar morphology to that observed in the skin.

In spite of the immense technological importance of polymer blends, little work has been published on both compatibilized and non-compatibilized blends during injection molding, and particularly in the presence of a weldline. The objective of the present paper is to consider the mechanical characteristics including those of weldlines, of two

injection molded polymer blends and its relationship to morphology. Directly molded tensile samples and those machined from rectangular plaques are used. The parameters to be investigated are the thickness of the plaque and the flow path length.

3.2 EXPERIMENTAL

3.2.1 Materials

The polyamide-6 (Zytel 211 from Dupont Canada Inc.) with a number average molecular weight of M_n = 25000 was used. A high density polyethylene from Dow Chemical Canada (Dow 06153C) having a melt flow index of 6.3 g/10 min, M_n = 20200, and M_w = 81300 was selected as a minor phase. The compatibilizing agent is an ionomer (Surlyn 9020, Dupont Canada Inc) terpolymer consisting of 80% of polyethylene and 20% mixture of methacrylic acid and isobutyl acrylate. The methacrylic acid is 70% zinc neutralized. The polyethylene is stabilised with 0.2% antioxidant (Irganox 1010 of Ciba Geigy). Glass beads (untreated and silane treated), obtained from Potters Ballotini were used as fillers in complementary experiments. The average bead diameter is about 45 μm.

3.2.2 Compounding

The first operation consists of mixing the polyethylene with 0.2 wt% antioxidant in a single screw extruder. Then, using a twin-screw extruder, 10 vol % of the ionomer (I) are admixed to the stabilized PE. Finally, 25 vol % polyethylene (PE) with or without compatibilizer, or 25 vol % of glass beads, were incorporated into polyamide-6 (PA6). Prior to a typical mixing operation, the sample mixture was dried overnight at 90°C under vacuum to minimize hydrolytic degradation of the polyamide during processing. The polymer blending was carried out on a ZSK-30 (Werner-Pfleiderer) intermeshing, co-rotating twin-screw extruder with a screw length to diameter ratio, L/D of 40. Feeding was performed under nitrogen and vacuum was applied in the decompression zone. The blending conditions can be found in refs[19,20]. Neat PA6 has been twin screw extruded to give it the same thermal history as the PA6 in the blends.

3.2.3 Injection Molding

The injection molding machine used is a Battenfeld type BA-C 750/300, with a clamping force of 80 tons. Two experimental molds, both with interchangeable cavities were employed. A rectangular plaque (127 mm x 76 mm x 2, 4 and 6 mm cavity depth) is used. It is provided with a 2 mm deep flash gate fed with a trapezoidal duct having a section varying from 30 to 50 mm^2. Tensile test bars were cut at different locations and termed as type II specimens (Fig. 3.1). To produce plaques with weldlines a 6, 12

or 18 mm diameter circular insert is installed in the cavity. Directly molded 3 mm dogbone tensile bars (type I in Fig. 3.1) were molded using one or two gates to make samples with or without weldline. As received neat PA6, HDPE, as well as the prepared compounds were injection molded. The molding conditions are the same for both types and are reported elsewhere[19,20].

3.2.4 Tensile Testing

Prior to testing all samples were conditioned at 23°C and 50% R.H. for several days. The ASTM D638 standard was followed. Type I samples were tested directly while a special dogbone shaped sample was designed to make the best use of the type II plaques. Samples were machined transversally at different positions (B, M and E) and longitudinally (L) from plaques with and without weldline as illustrated in Fig. 3.1. A universal tensile machine was used with a cross head speed 5 mm/min, and 2.5 kN maximum load, to generate both ultimate tensile properties, and the secant modulus at 0.2%. For the latter case, an MTS extensometer (632.13C.20) with a 10 mm gage length was used. The load and axial extension were recorded using a data acquisition software.

To study local stiffness variations along the sample, the extensometer was placed either on or outside the weldline at positions 1, 2 and 3 as indicated by the numbered arrows in the Fig. 3.1. Directly molded dogbone specimens were used in this test.

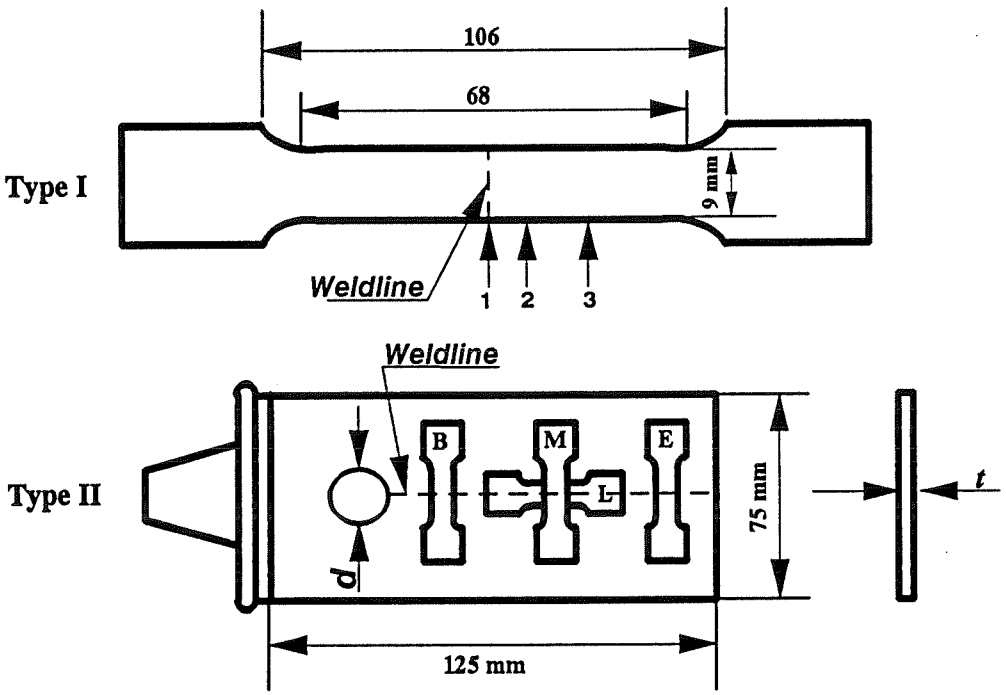

Figure 3.1 - Mold cavities used in this work. Type I - directly molded tensile specimens. Type II - rectangular plaque with locations at which samples were machined. Plaques thickness: (t): 2, 4 and 6 mm, insert diameter (d): 6, 12 and 18 mm

3.2.5 Tensile Dilatometry

The tensile test was carried out according to ASTM D638 M. The volume change measurement was carried out during the tensile test using the above mentioned axial extensometer, and an Instron transverse extensometer model 2640.007. It is assumed that the deformation in the thickness is equal to that in the width[21]. Both extensometers were attached to the specimen. Lateral and axial extension were recorded simultaneously on a PC using a data acquisition software. From the axial strain (ϵ_a), and the transverse strain (ϵ_T) one can compute the volume strain ($\Delta V/V_0$) as:

$$\Delta V/V_0 = (1 + \epsilon_a)\,(1 + \epsilon_T)^2 - 1 \qquad (3.1)$$

3.2.6 Scanning Electron Microscopy

Samples with and without compatibilizer were studied and were prepared as follows:

- Freeze-fracture: a small rectangular strip from each sample is placed in liquid nitrogen for 10-15 min, and then fractured manually.

- Microtoming and solvent extraction: rectangular samples (1 x 1.5 x 0.5 cm) are cut. A Reichert Jung Supercut 2050 microtome equipped with a glass knife is used. First each sample is frozen in liquid nitrogen for 15 min. During the cutting operation, the temperature is kept at approximately -100°C to reduce the extent of surface deformation. The microtomed samples were immersed for 1 hour in decalin at 120°C to dissolve the polyethylene (minor phase). Following the extraction the samples were dried in a vacuum oven for 24 hours to remove the solvent.

- Fracture surfaces of samples broken in a tensile test.

Samples surfaces, after being coated with a layer of Gold/Palladium, were examined under a Jeol 8645 type scanning electron microscope at 10 Kv.

3.3 RESULTS AND DISCUSSION

3.3.1 Double Gated (Type I Mold)

In neat polyamide and in the compatibilized blend, the weldline is invisible to the naked eye except for a V-notch of a variable depth. The depth of the V-notch is related to the distance from the vents which are located in the middle of the cavity (along the weldline area). The side of the sample which coincides with the mold parting line does

not have a V-notch while, at the opposite side, the V-notch is almost 100 μm deep. This observation confirms the role that trapped air, compressed by the expanding melt fronts, plays in the formation of the V-notch[22,23,24]. In the non-compatibilized blend the weldline region is more opaque than the rest of the sample. It was observed that the higher opacity of the weldline area, which is predominantly located in the core of the weldline, develops during the later part of the cooling cycle. The presence of this more opaque zone indicates that the residual stresses, resulting from the non-isothermal solidification during the cooling stage, are sufficient to induce debonding of the matrix-minor phase interface[25]. The higher opacity is evidently related to the presence of microvoids in the weldline zone.

The morphology of the non-compatibilized blend is shown in Fig. 3.2. Away from the weldline (Fig. 3.2A) the minor phase particles are elongated and oriented parallel to flow in the skin and subskin regions. The orientation is particularly pronounced in the skin where the polyethylene particles are stretched into sheet like formations. In the core, which represents only about 10% of the sample thickness, spherical shape predominates. The section of the weldline area is shown in the Fig. 3.2B. It is obvious that the morphology of the weldline is closely related to that of the skin. The weldline, having been formed by the collision of two opposing melt streams, also shows the minor phase keeping the shape and orientation it acquired during the melt front expansion. In Fig. 3.2B a 50 μm thick layer, where the minor phase is more finely divided, separates the two melt fronts. The morphology of the compatibilized blend is

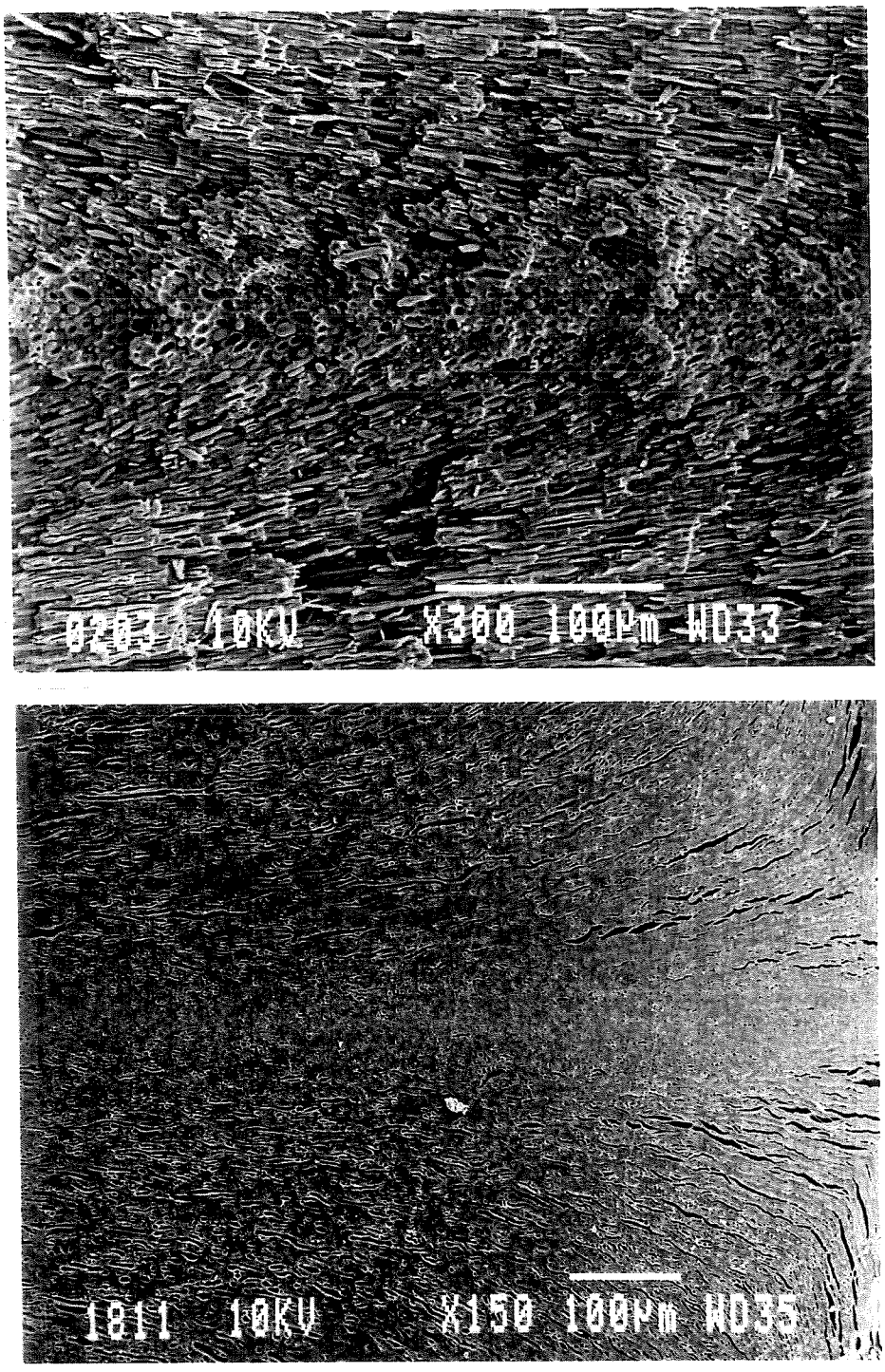

Figure 3.2 - Micrographs of type I non-compatibilized blend (NC) - perpendicular to flow view. A) no weldline B) with weldline

quite similar to that of its non-compatibilized counterpart. The main difference between the blends is the size of the minor phase formations - the compatibilized blend exhibits a much finer morphology[1,2].

The results of the tensile tests on these directly molded samples are summarized in the Table 3.1. The stress vs apparent strain curves are shown in Fig. 3.3. To draw the curves in Fig. 3.3 (as well as those shown in the Figs. 3.12, 3.13 and 3.14 for type II specimens), the strain was simply assumed to be proportional to the crosshead displacement. The neat polyamide-6 is not affected by the presence of the weldline. Its behavior is similar to that reported for other semicrystalline, ductile plastics such as polyamide 66, polypropylene, high density polyethylene etc.[26,27]. In this study it was found that the mechanical properties of polyamide-6 are somewhat affected by the passage through the twin screw extruder. For this reason the property values given for neat polyamide-6 are those of the extruded polymer. It is believed that partial devolatilization of the plasticizer may be the cause of the slightly higher stiffness of the twin screw extruded and injection molded samples (compared to those made by molding of as received pellets).

The effect of the compatibilizer appears negligible in samples without the weldline: both materials follow the same path (curves C and NC, Fig. 3.3) until well beyond the yield point, the only difference being a higher elongation at break of the compatibilized sample (250% versus 100% for the non-compatibilized blend). In both

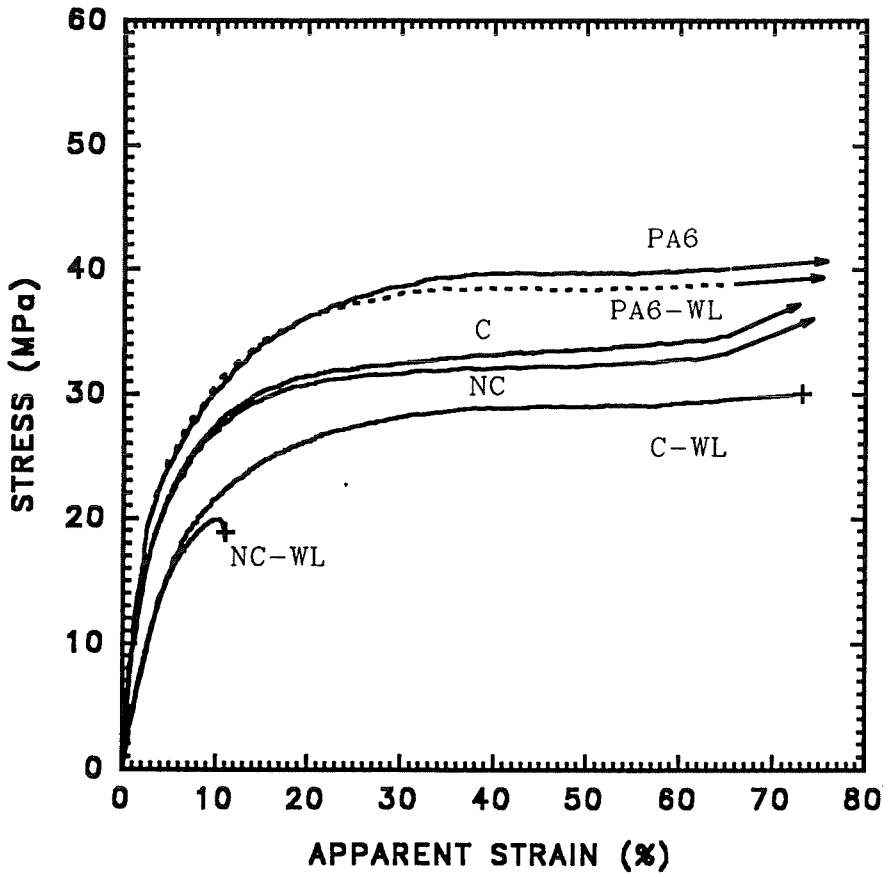

Figure 3.3 - Stress/strain curves of type I samples with (WL) and without weldline PA6, compatibilized (C) and non-compatibilized (NC) blends

Table 3.1 - Tensile properties for type I samples; NC-without compatibilizer, C-with compatibilizer, NC-WL: with weldline, and C-WL: with weldline. Standard deviations are: modulus, E-3%; yield stress, σ_y-3%; stress-at-break, σ_b-5%, elongation at yield, ϵ_y-15%; and elongation at break, ϵ_b-25% of reported values. NA:not available. (*):PA6 twin screw extruded.

Material	E (GPa)	σ_y (MPa)	ϵ_y (%)	σ_b (MPa)	ϵ_b (%)
PA6	0.90/1.4*	39	45	62	220
PA6-WL	0.90	39	35	59	200
NC	1.20	32	40	40	100
NC-WL	1.10	no yield	no yield	20	10
C	1.20	33	40	58	270
C-WL	.90	29	45	32	80
PA6NTGB	1.70	19	2.2	NA	NA
PA6TGB	2.0	25	NA	NA	NA

blends, the post-yield deformation occurs via homogeneous yielding of the entire gage length as is the case of neat nylon 6. The effect of the compatibilizer is much more visible in samples with weldlines (curves C-WL and NC-WL, Fig. 3.3). Although at small strains both materials also follow the same path, the non-compatibilized sample breaks at the weldline before the onset of yield. The addition of the compatibilizer has restored the ability of the material to yield in the presence of a weldline, but the sample still ends up breaking in the weldline at an overall strain of 80%. Considering the structure of the weldline area as shown in Fig. 3.2B one would expect the fracture to develop along the elongated structures oriented parallel to the weldline. This does not

seem to be the case. The overall view of the fracture surface is shown in Fig. 3.4. In the outer zone which represents about 75% of the cross-sectional area, the matrix exhibits significant microstretching (Fig. 3.5A). In the inner zone the fracture occurred in a brittle manner (Fig. 3.5B). Most of the PE particles in this zone are loose and do not show any evidence of plastic deformation. As mentioned above, the PE particles in the core which is under tensile stress generated during cooling probably separated from the matrix before the test had even begun. Occasionally an amoeboid PE formation (Fig. 3.5C) can be found but these are clearly in a minority. Thamm reported similar structures oriented perpendicular to flow[15]. Fracture surfaces of compatibilized samples are analogous to that of their non-compatibilized counterparts. In the outside layer the PE particles have deformed along with the matrix (Fig. 3.6A) while the core reveals the presence of well adhered, but undeformed polyethylene particles (Fig. 3.6B). As with the non-compatibilized blend the fracture surface of the core shows little evidence of ductility. It appears that the fracture starts in the sample interior where the material is under triaxial stress rather than at the V-notch, and consequently it cannot yield as already reported in the literature[13]. Following the fracture of the core, the material near the surface is able to stretch as evidenced by the appearance of fracture surfaces.

Comparison of various materials used in this work at small strains provides a very valuable insight into their behavior. The stress vs axial strain curves are shown in the figures 3.7, 3.8, 3.9 and 3.10. To draw these curves the strain was assumed to be identical to the extensometer displacement. Fig. 3.7 shows the stress-strain curves of

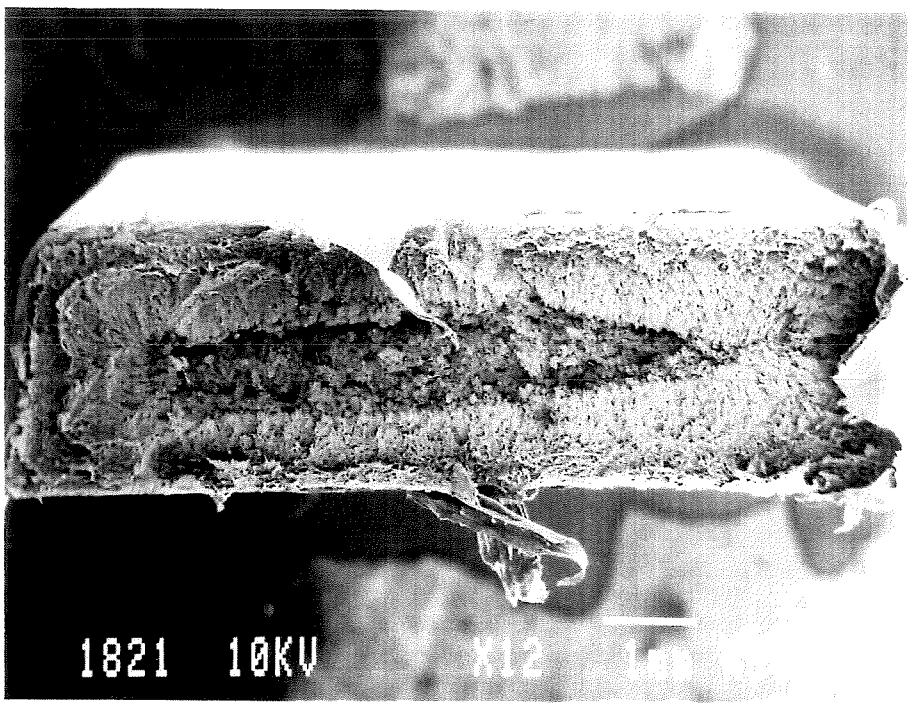

Figure 3.4 - Micrograph of non-compatibilized (NC) blends type I specimens. Fracture surface at the weldline. General view perpendicular to flow

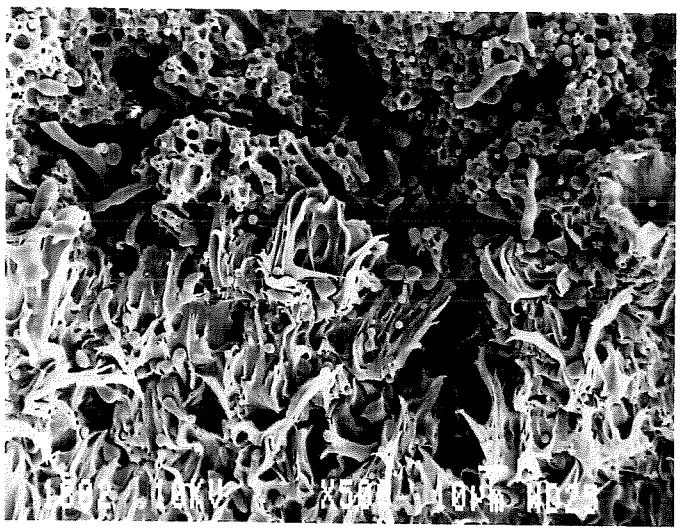

A

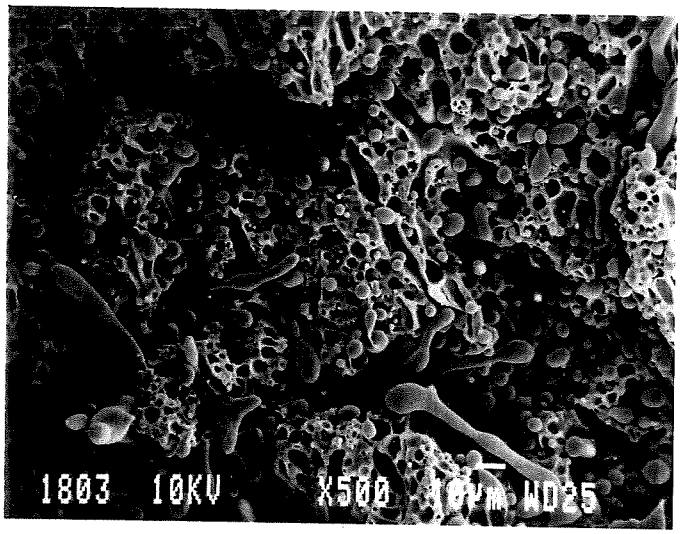

B

Figure 3.5 - Micrographs of fractures surfaces of tested type I non-compatibilized (NC) specimens containing a weldline (perpendicular to flow view). A) skin, B and C) core

C

Figure 3.5 - Cont'd
C) core

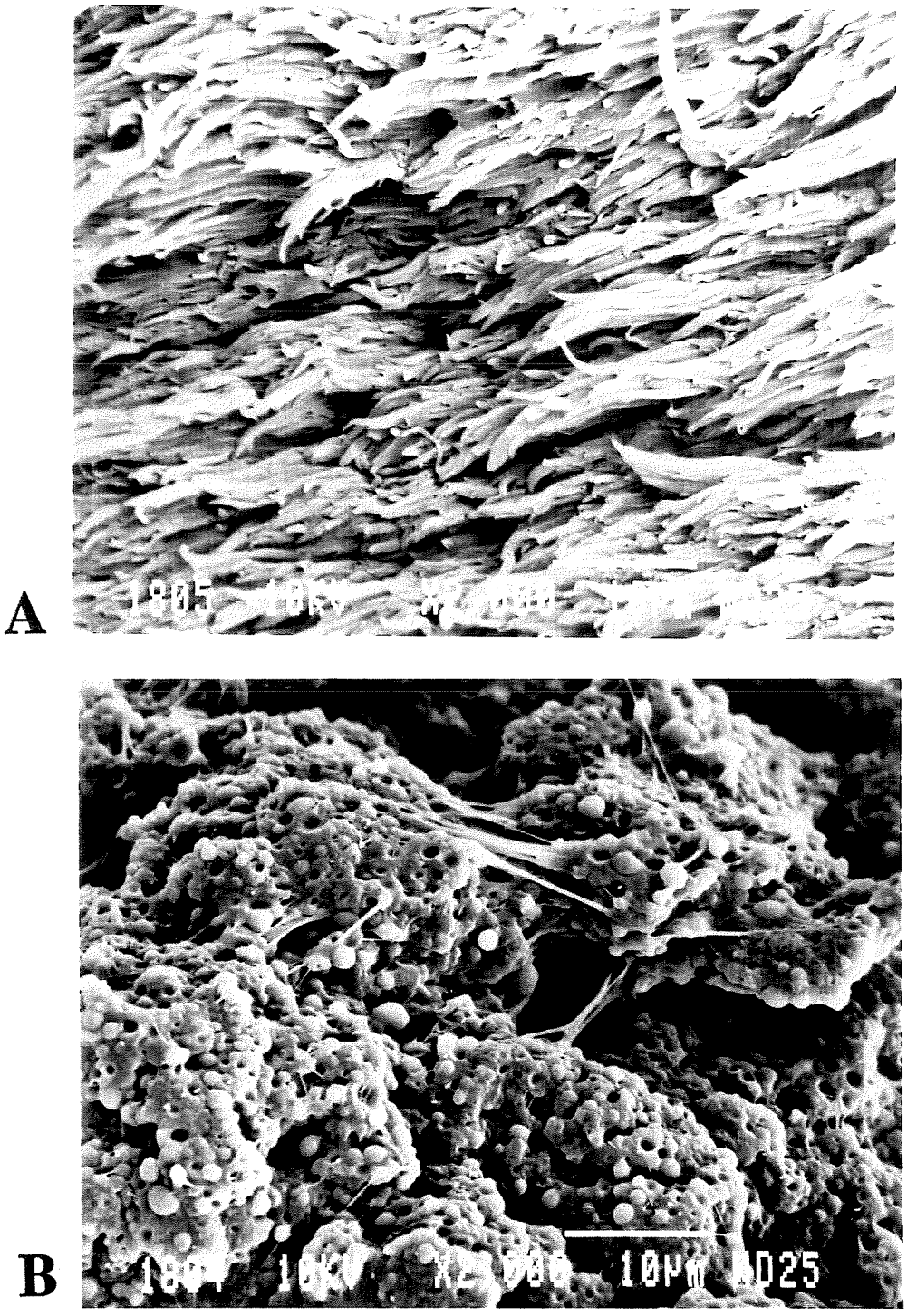

Figure 3.6 - Micrographs of fractures surfaces of compatibilized (C) blends type I specimens containing a weldline (perpendicular to flow view). A) skin, B) core

both blends, of the polyamide-6 filled with 25 vol% of glass beads; (untreated and silane treated), as well those of both starting materials (PE and PA6). In the polyamide containing poorly adhering glass beads (curve GB-NT), the stress reaches a maximum at about 2% strain. The yield stress of this material is approximately equal to that of the unfilled polyamide reduced by the factor representing the area occupied by glass beads[28]. It was shown that at yield essentially all the glass beads debonded from the matrix[28]. When glass beads are treated with silanes little or no debonding takes place in the range of strains considered[28], and the stress borne by the material at a given strain exceeds that of the neat PA6 (curve GB-T). The curves of both blends show an appearance similar to that of treated glass bead filled PA6. Both curves (C and NC) follow very closely that calculated using the rule of mixtures:

$$\sigma_b = \sigma_{PA}\,\Phi_{PA} + \sigma_{PE}\,\Phi_{PE} \qquad (3.2)$$

This curve is identified as Eq. 3.2 in Fig. 3.7 where σ_b, σ_{PA} and σ_{PE} are stresses measured at a given strain in the blends, neat PA6 and in neat HDPE, respectively while Φ_{PA} and Φ_{PE} are their volume fractions (0.75 and 0.25 respectively).

This result shows that in both blends tested under these conditions the dispersed phase bears its share of stress. This may seem surprising in light of the data obtained by the tensile dilatometry (Fig. 3.8). The volume strain recorded with the compatibilized blend

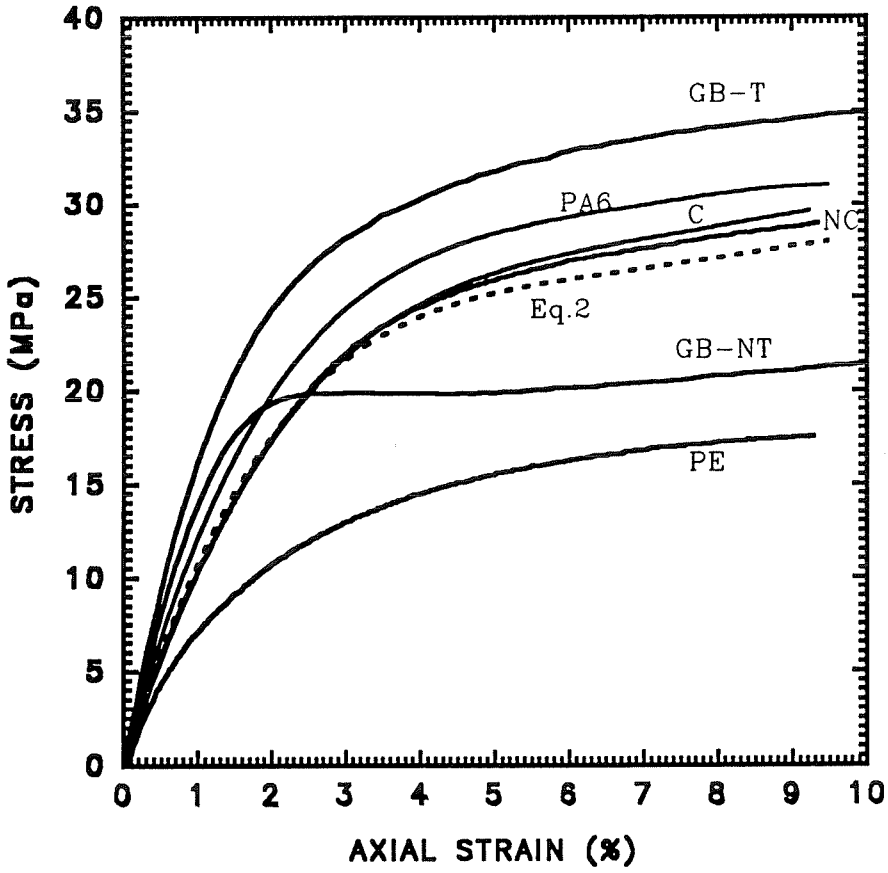

Figure 3.7 - Stress vs axial strain curves of type I samples. Neat HDPE (PE), PA6, compatibilized (C) non-compatibilized (NC), filled PA6 with treated (GB-T) and untreated (GB-NT) glass beads and (---) equation 3.2

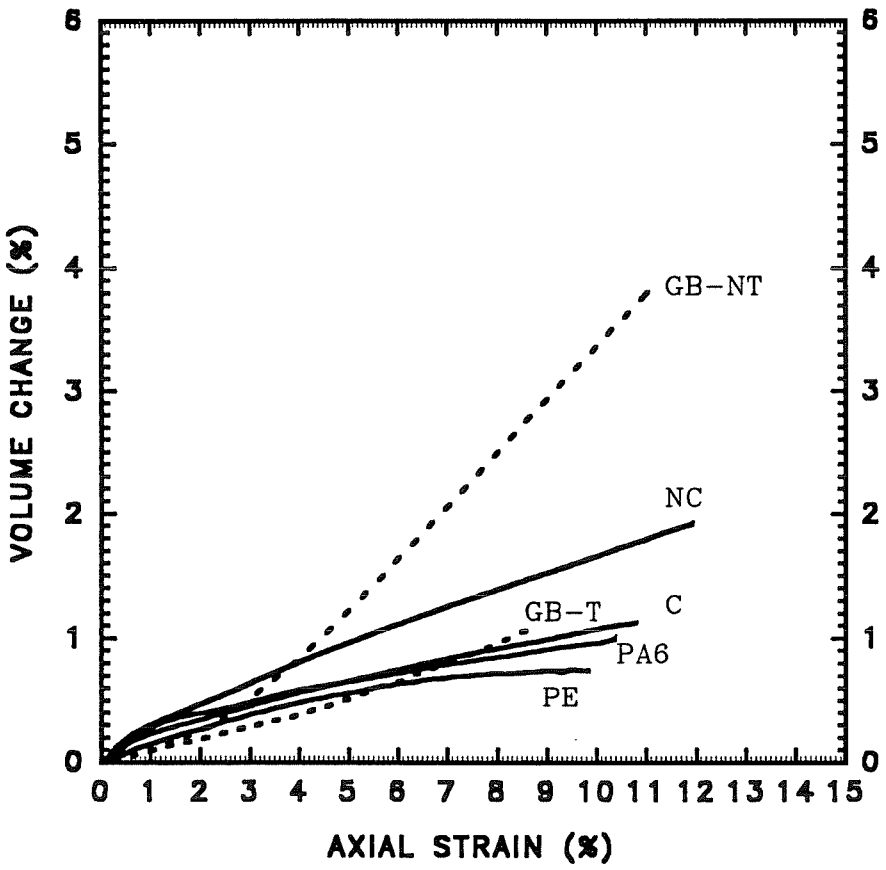

Figure 3.8 - Volume change versus axial strain of type I specimens (notation same as in Fig. 3.7)

is small. In fact it is similar to that recorded for both that of the neat polymer as well as the polymer filled with treated glass beads. With untreated glass beads and with the non-compatibilized blend (NC) the interfacial debonding begins at about the same level of strain i.e. 1.5%. However, the material filled with untreated beads dilates at a faster rate than the uncompatibilized blend. Despite the debonding, the dispersed phase of the non-compatibilized blend can bear the same load as in its compatibilized counterpart. This observation suggests that with this sample shape the mechanical behavior is dominated by the flow-induced morphology. An elongated particle of variable cross-section and shape (see also Fig. 3.5) trapped in the matrix has no choice but to deform along with the matrix in spite of the lack of interfacial adhesion. Consequently one can question the utility of the directly molded tensile specimens to study various aspects of the mechanical behavior of multiphase materials where the flow generated structure is very different from that which is found in "real" injection molded parts.

Conventional methods used to evaluate the weldline strength consist of dividing the yield stress (breaking stress in the absence of yield) of the weldline sample by that of a sample without the weldline[34]. This approach indicates the strength loss of 40% for the non-compatibilized sample and of 10% in the compatibilized one. Monitoring tensile properties by placing extensometers on and away from the weldline and by studying how the strain develops during the constant strain rate test sheds a slightly different light on the situation. With the non-compatibilized blend (Fig. 3.9) the stress strain curve of the weldline area overlaps that measured away from the weldline up to a stress of about

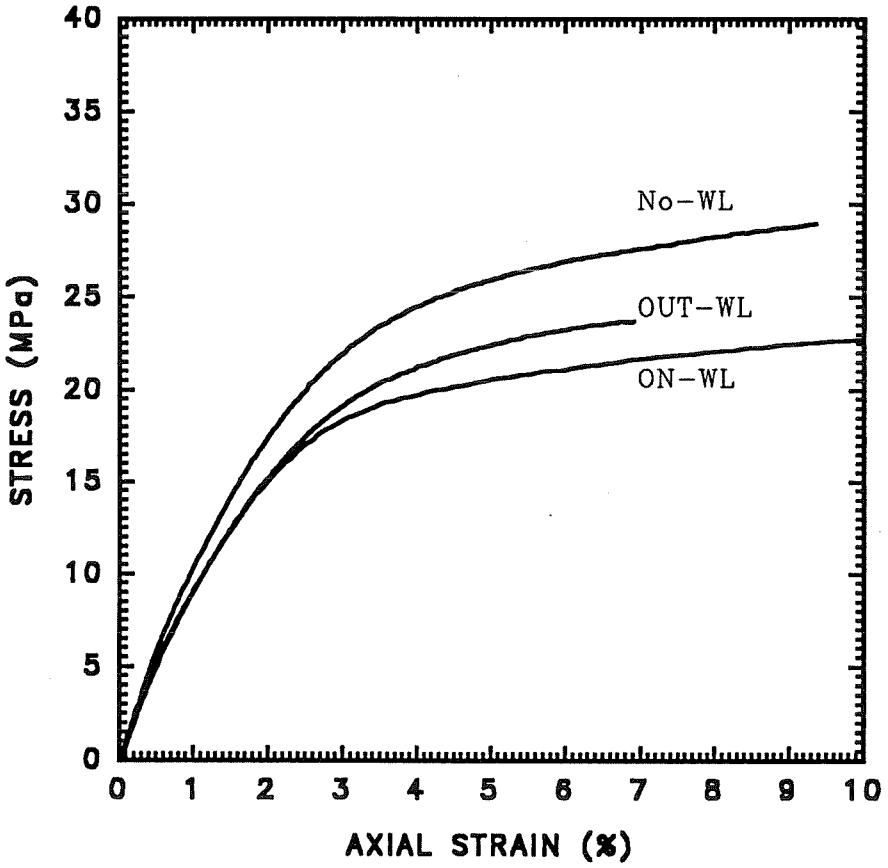

Figure 3.9 - Effect of the weldline and of the extensometer location for type I specimens of non-compatibilized blends; without position 1 (NC), with position 1 (NC-WL), with but outside the weldline positions 2 and 3 (NC-OUT-WL)

15 MPa. Above 15 MPa the weldline area starts to deform at a faster rate and the sample breaks at 20 MPa, when the strain away from the weldline is only about 6.5%. Similar behavior has been observed for glass filled polyamide-6[26].

Fig. 3.10 shows the results obtained with the compatibilized blend. In this case the curves are identical. It can be said therefore that in the compatibilized blend the behavior of the weldline area is identical to that of the material away from the weldline and consequently the weldline effect is negligible.

It is now necessary to consider the differences between the samples molded with the weldline (two gate cavity) and without the weldline (one gate). Figures 3.3, 3.9, 3.10, and Table 3.1 show that the initial stiffness is lower when the cavity has two gates not only in the weldline, but also away from the weldline. Since the injection rate is identical for all these samples (0.42 cm^3/s), the melt velocity in the cavity when one gate is used is twice that of the two gate cavity. Complementary experiments in which the injection rate was doubled (with the two gate cavity) were performed to determine the effect of melt velocity on the stress strain curves. The results show that this effect is negligible. Other workers have also reported that melt velocity in the cavity does not affect the tensile properties (stiffness and stress)[11]. It appears therefore that the morphology and the mechanical properties of both blends are affected by the overall thermomechanical history of the measured area. With one gate the melt flows through the entire cavity length and the melt front penetrates the wider cavity area opposite to the

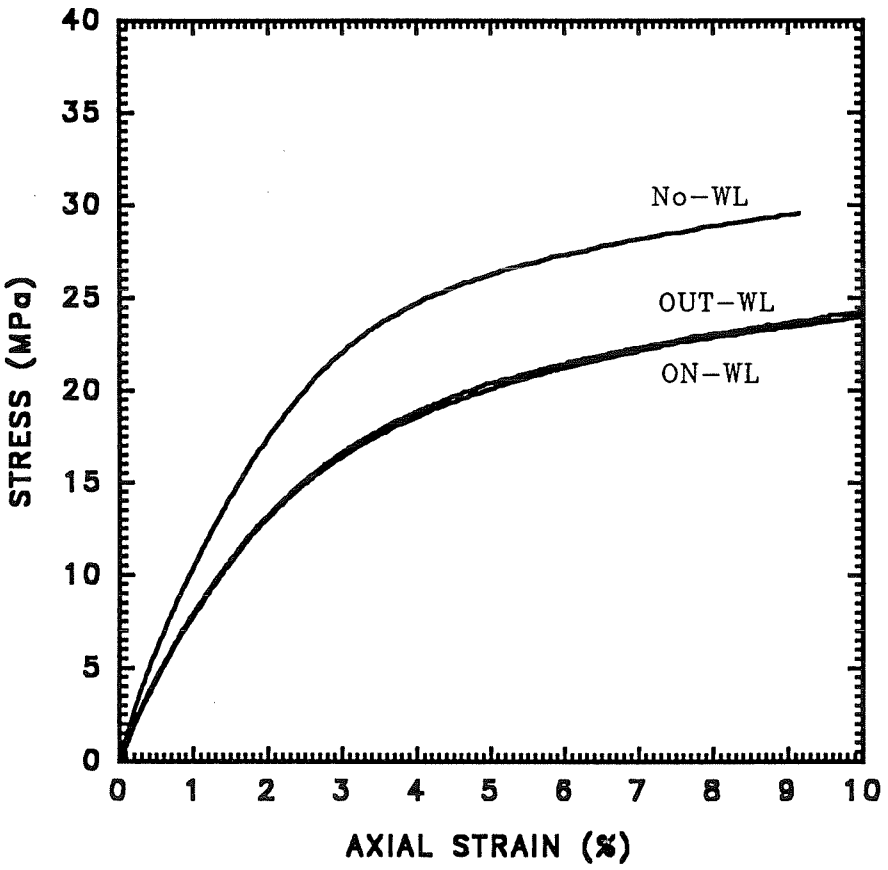

Figure 3.10 - Effect of the weldline and the location of the extensometer on the stress/strain curves of type I specimens of compatibilized (C) blends (notation same as in Fig. 3.9)

gate. Intuitively one would expect the orientation to be higher than in the case of the two gate mold where the tested area comprises two immobilized melt fronts in the weldline and material that travelled a shorter distance and was at a higher temperature at the end of the mold filling stage.

Finally, it is worth noting that the elastic moduli for samples without weldline are not affected by addition of the compatibilizer. Similar results have been reported for other multiphase systems[29,30].

3.3.2 Plaques (Type II)

Although the weldlines are nearly invisible to the naked eye in plaques molded using cavities with an insert and although one would like to believe that the molten polymer forgets the insert at a certain distance behind it, this is not the case with the blends used in this work. Differences in the mold filling patterns can be evidenced by short-shot experiments. Fig. 3.11 shows the short shots obtained with the matrix, and with the compatibilized blend. With PA6 (Fig. 3.11A) (and with HDPE), the junction of the two melt fronts vanishes at a short distance behind the insert and the melt front recovers a straight profile. With both blends, the junction persists during the entire mold filling stage (Fig. 3.11B). This unexpected mold filling behavior has been also reported with fiber and platelet filled PP[31] and glass fiber reinforced PA6,6[26]. It indicates that as with other multiphase systems the melt in the weldline zone advances at a slower pace

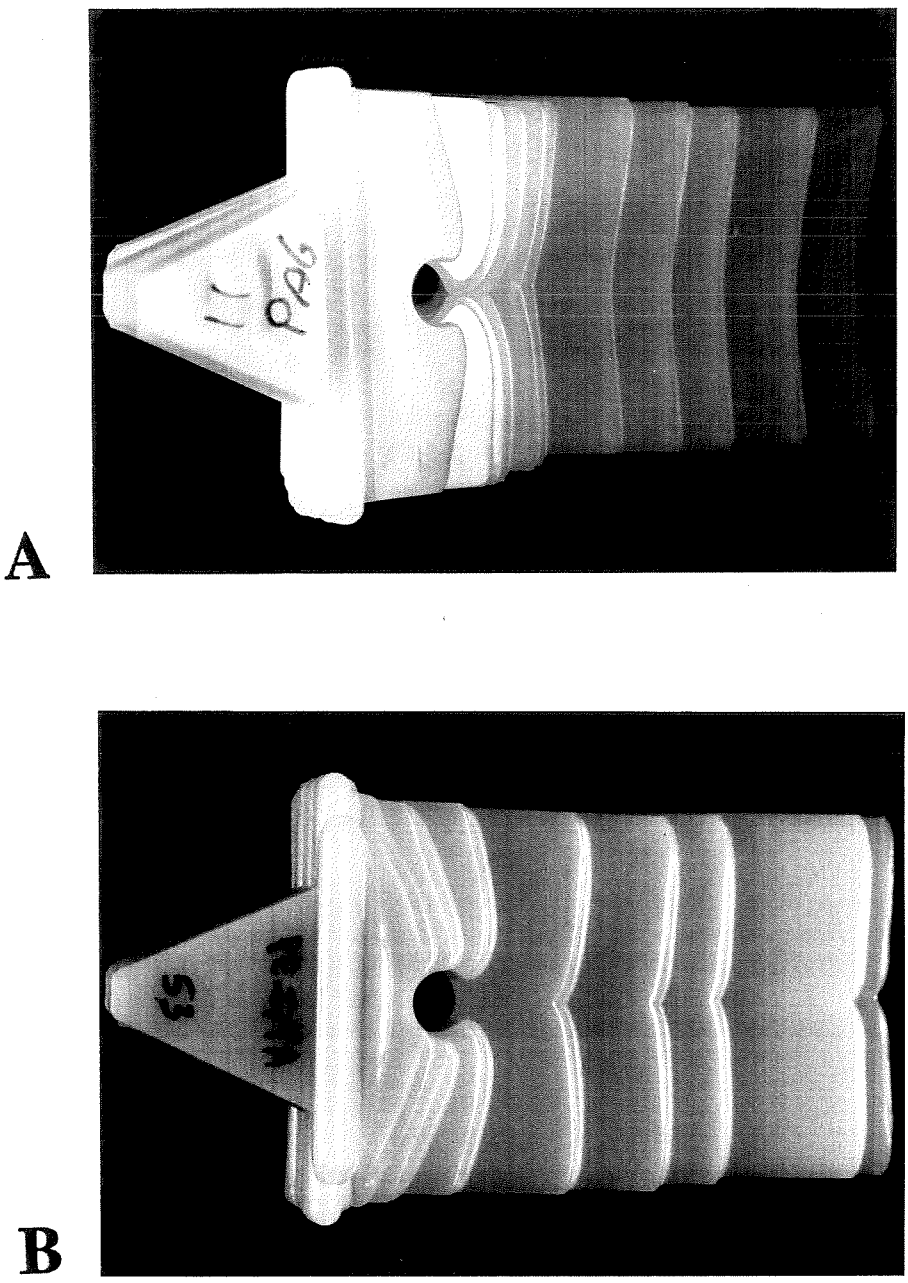

Figure 3.11 - Short-shots of type II mold with 4 mm thickness and 12 mm insert diameter, obtained with: A) neat PA6 and B) compatibilized blends (HDPE/Ionomer/PA6)

than in other areas of the plaque suggesting that the local viscosity of the melt behind the insert is higher than elsewhere offering more resistance to flow. One of the consequences of the higher viscosity and of the slower melt advancement is that the weldline plays a role similar to that of the wall and at the weldline is formed by adjacent melt fronts depositing onto each other. Yokoi et al.[32] have studied the evolution of the angle between the melt front with the distance from the insert. They stated that when the "weldline vanishing angle value" is reached the weldline has effectively disappeared.

The mechanical behavior of uncompatibilized and compatibilized blends (2, 4 and 6 mm thick samples cut transversally to flow with (for 4 mm only) and without weldline is shown in Figs. 3.12 and 3.13 respectively. For samples cut longitudinally to flow their results are gathered in Fig. 3.14. Tensile properties are presented in the Table 3.2. The results can be summarized as follows:

- The effect of the weldline on the properties is much less pronounced than indicated by the directly molded samples (type I).

- In non-compatibilized blends (Table 3.2), the yield stress is reduced by only about 15% in position B, immediately behind the insert when compared to a sample without a weldline. This difference becomes even smaller for positions farther away from the insert (Fig. 3.12).

Table 3.2 - Tensile properties of type II samples as functions of positions B, M, E, and L (see Fig. 3.1); sample thickness - t; C and NC with and without compatibilizer respectively. In each column the first/second values are for samples with and without weldlines respectively. The average standard deviations are similar to those reported in Table 3.1.

Position	t(mm)	σ_y (MPa)		ϵ_y (%)		σ_b (MPa)		ϵ_b (%)	
		NC	C	NC	C	NC	C	NC	C
B	2	18/21	26/26	14/18	55/34	19/20	26/34	15/100	60/230
	4	21/26	34/30	14/75	40/35	27/23	33/33	25/150	140/140
	6	26/29	34/32	20/27	55/34	30/30	34/35	55/65	100/130
M	2	20/20	26/26	20/11	31/22	17/21	31/34	47/56	180/230
	4	23/23	31/31	13/21	42/22	26/28	34/35	75/140	180/140
	6	25/27	34/33	46/20	31/32	31/32	38/34	85/85	140/110
E	2	19/21	26/25	19/21	33/30	19/21	38/38	38/59	210/260
	4	25/26	33/30	49/85	25/28	25/31	36/40	50/160	130/210
	6	28/28	33/32	32/30	33/30	29/33	37/38	60/110	170/180
L	2	29/28	29/29	31/42	21/34	47/45	48/>50	140/220	190/>250
	4	28/28	34/34	27/37	18/26	48/45	50/54	140/120	140/260
	6	30/28	34/34	51/40	21/26	46/38	51/47	100/130	150/240

- In non-compatibilized blends there is significant strength anisotropy- the yield stress recorded in the direction parallel to flow (position L, Table 3.2) is about the same as that recorded in type I samples (i.e $\approx$ 30-33 MPa). In addition the yield stress parallel to flow is independent of the plaque thickness except for the 2 mm case. The yield stress perpendicular to flow (e.g. position M) is only about 20 MPa for the 2 mm plaques. It is about 25 MPa when the thickness is 4 mm. At 6 mm thickness the yield stress anisotropy disappears. The effect of the thickness on the yield stress is more pronounced in this direction (i.e. transverse to flow) as shown in Figs. 3.12 and 3.14. Menges

et al.[33] have attributed this phenomenon to the competition between flow induced orientation and crystallinity. In the thinner plaque, the effect of orientation on the yield stress predominates while in the thicker ones it is a crystallization effect which prevails.

The initial slopes of the stress strain curves are relatively independent of both the plaque thickness and of the direction (Figs. 3.12, 3.13 and 3.14). The curves start to deviate at the onset of yield. This suggests that yielding coincides with the beginning of the debonding process.

- In compatibilized blends the weldline effect essentially disappears, all tensile properties are unaffected by the presence of the weldline. The only exception to this are the 2 mm thick plaques in the position close to the insert where the weldline sample breaks without appreciable yielding. The weldline free sample, however, undergoes significant homogeneous yielding. The yield stress is independent of the plaque thickness and orientation except for the 2 mm thick plaque (Figs. 3.13 and 3.14).

- The effect of insert diameter on the yield strength has been found to be negligible in both blends.

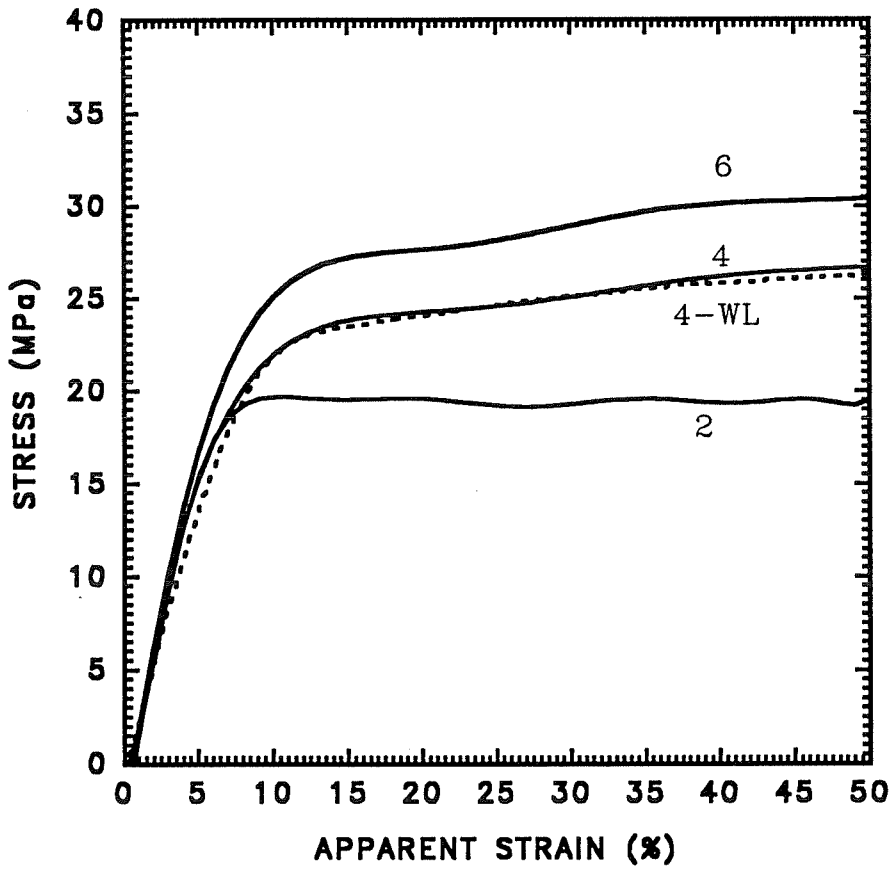

Figure 3.12 - Stress/strain curves for non-compatibilized blends (NC) type II specimens. Plaque thickness: 2, 4 and 6 mm, insert diameter: 12 mm. Transverse direction (M). Weldline in the 4 mm thick plaque: 4-WL

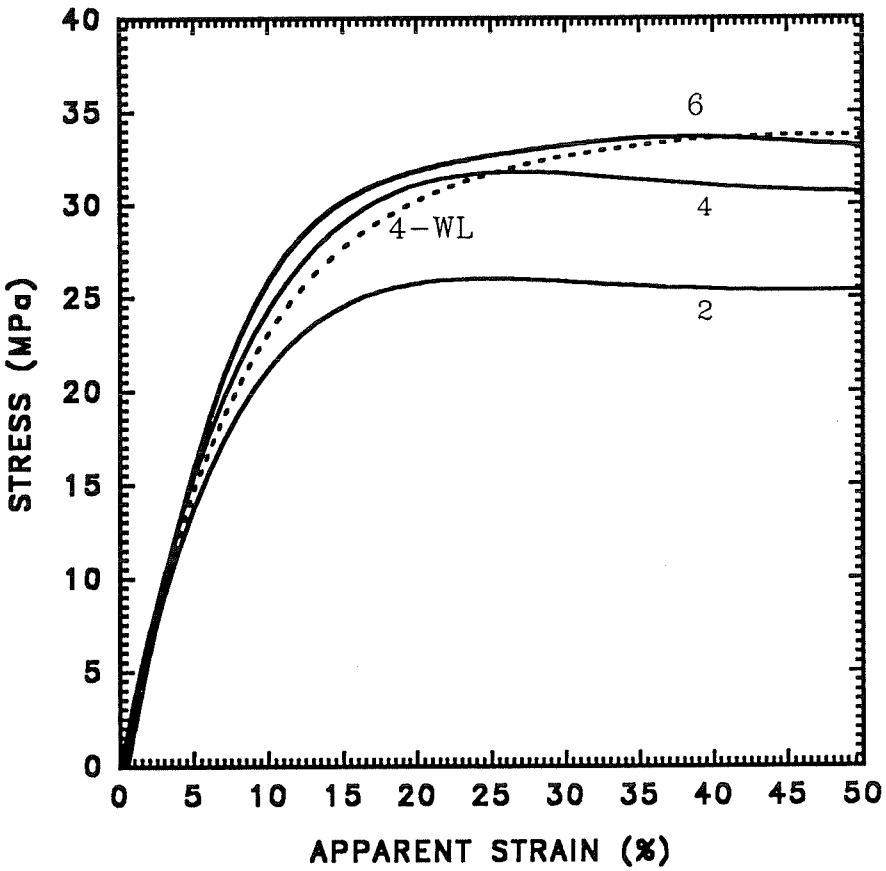

Figure 3.13 - Stress/strain curves for compatibilized blends type II specimens. Plaque thickness: 2, 4, 6 mm, insert diameter: 12 mm. Weldline in the 4 mm thick plaque: 4-WL

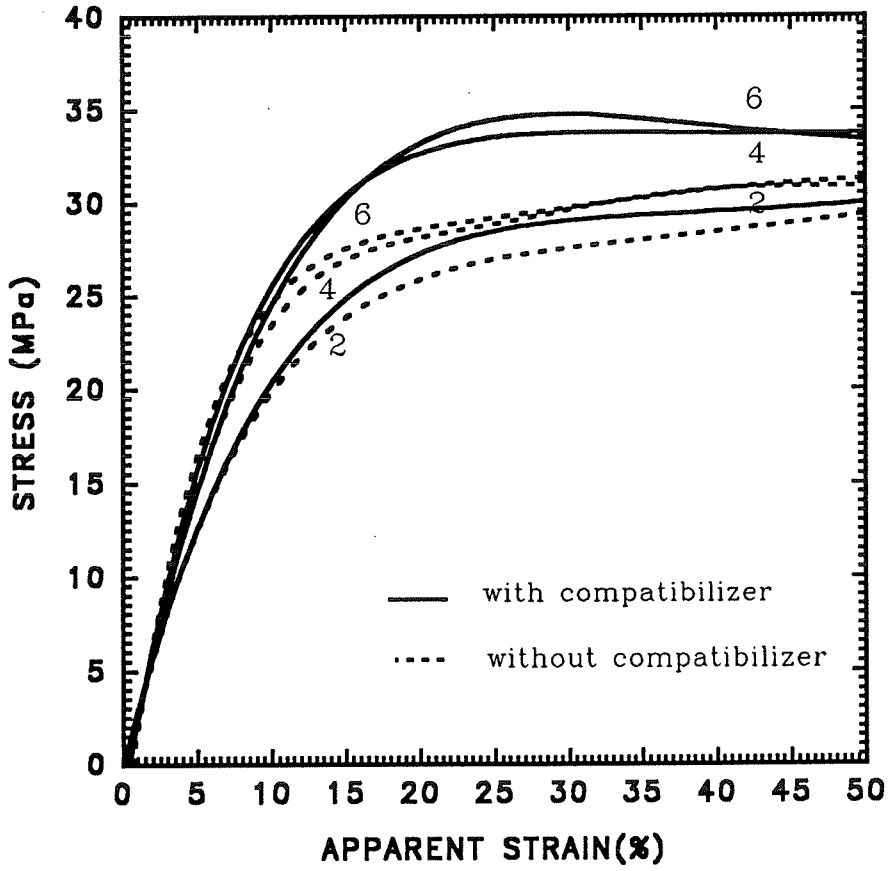

Figure 3.14 - Stress/strain curves for non-compatibilized (NC) and compatibilized (C) blends type II specimens. Plaque thickness: 2, 4 and 6 mm. In the longitudinal direction (—— with compatibilizer, ---- without compatibilizer

The effect of the compatibilizer on interfacial adhesion is shown in the Fig. 3.15. These pictures were obtained by fracturing the samples at liquid nitrogen temperature. In the non-compatibilized blend (Fig. 3.15A) the fracture surface exhibits loosely held, completely debonded, PE particles. With the compatibilized blend (Figs. 3.15B and C) the fracture path went through the dispersed phase. It is very interesting to note that the surface of the broken polyethylene particles in the compatibilized blend contains small ($\approx$ 0.2 μm) spherical formations. The most likely explanation for this observation is that some of the compatibilizer contained in the polyethylene exuded as the material was brought to room temperature.

Micrographs of fracture surfaces of tested samples of both blends are shown in Figs. 3.16 and 3.17. In the non-compatibilized blends the bulk of the minor phase appears undeformed through the entire thickness. Despite the fact that the material deformed by 70% the fiber-like formations in the outer layers and the spherical ones in the core are well separated from the matrix. Only occasionally in the outer layer do the fibers show evidence of cold drawing (see arrows Fig. 3.16B). This observation and the fact that the yield stress is generally lower than that predicted by the rule of mixtures shows that the debonding occurred well before the onset of yield. The transition between the core where the polyethylene is spherical and the outer layers where elongated predominate is clearly visible.

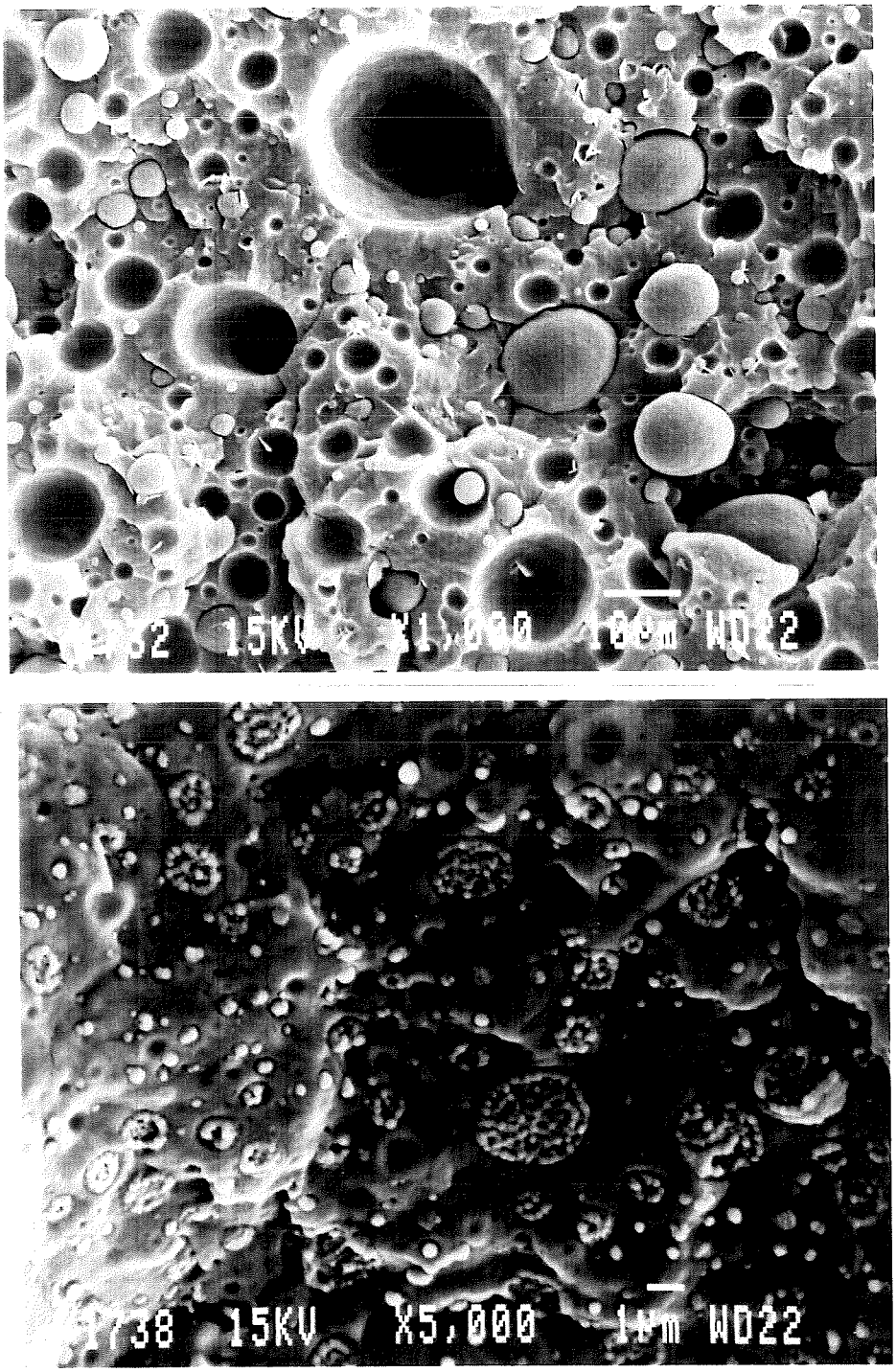

Figure 3.15 - Micrographs of freeze fractured untested 4 mm thick samples. A) non-compatibilized (NC) parallel to flow view, B) compatibilized (C) blend perpendicular to flow view.

C

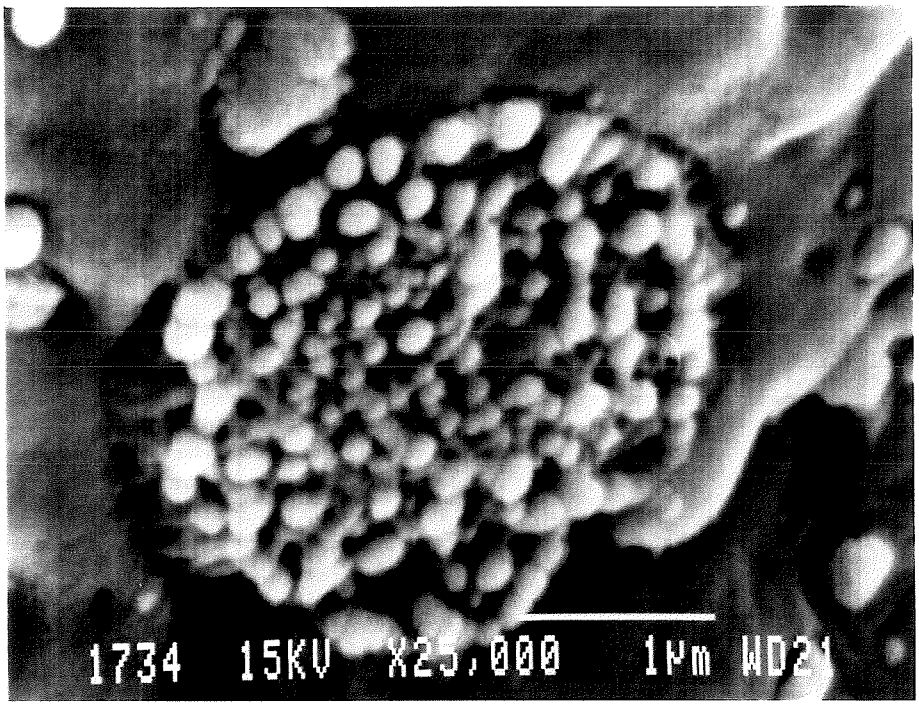

Figure 3.15 - Cont'd
C) magnification of B (x 25000)

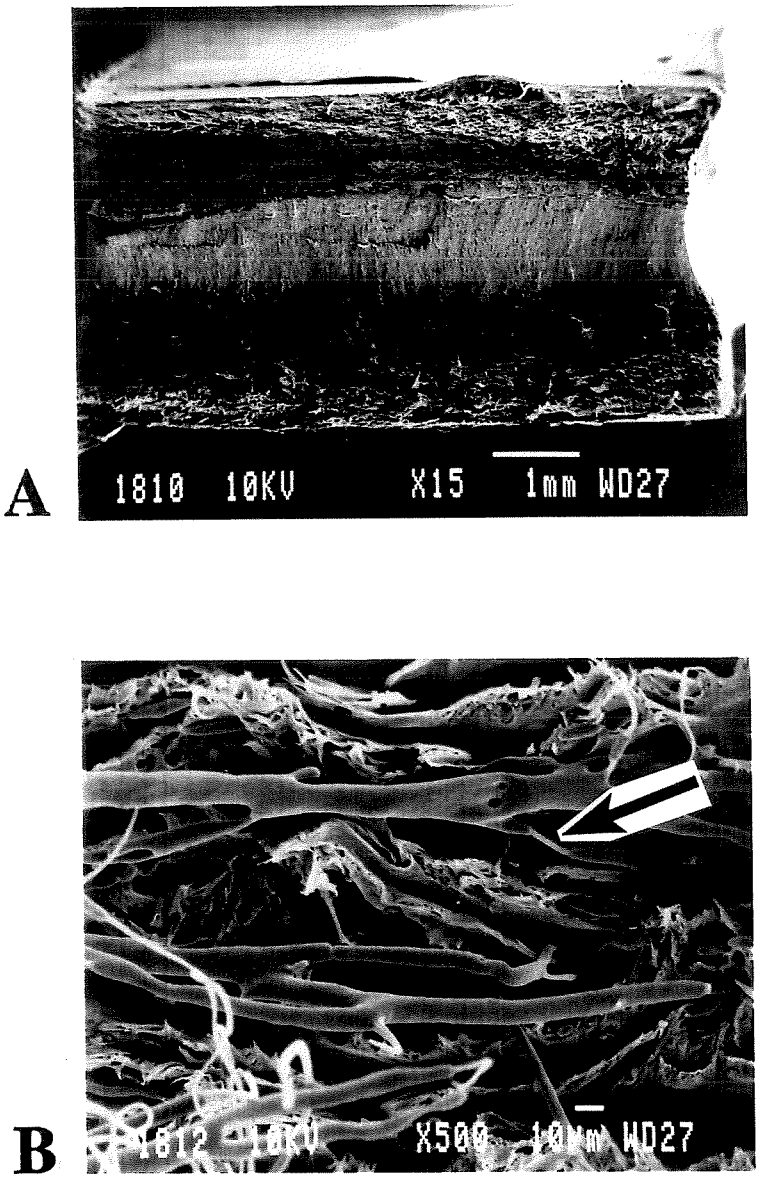

Figure 3.16 - Micrographs of rupture surfaces (perpendicular to flow view) of tested non-compatibilized type II specimens containing a weldline (position M). A) whole cross-section, B) skin

C

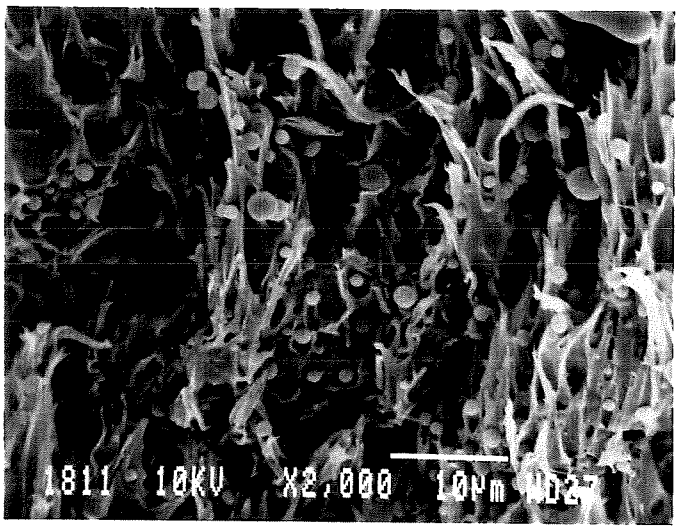

Figure 3.16 - Cont'd
C) core

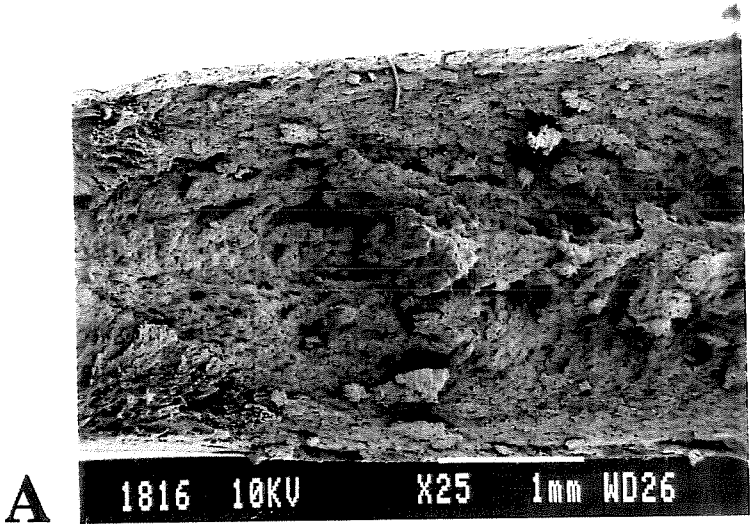

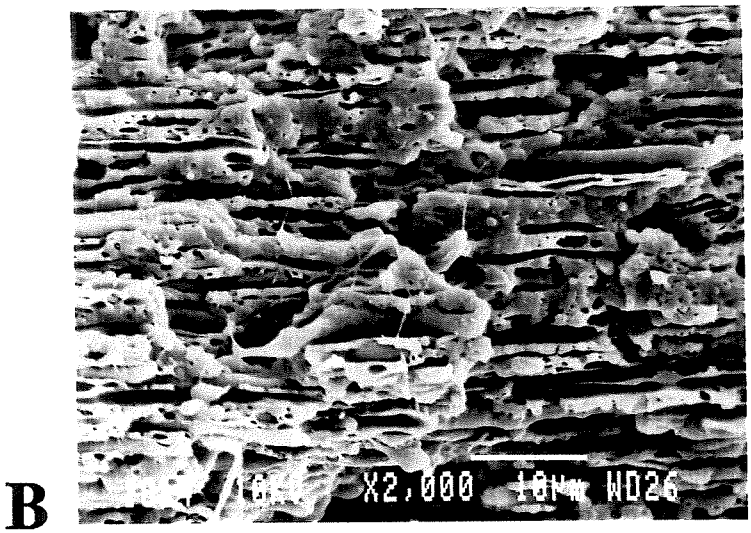

Figure 3.17 - Micrographs of fracture surfaces (perpendicular to flow view) of tested compatibilized blends type II specimens containing a weldline at position M. A) whole cross-section, B) skin

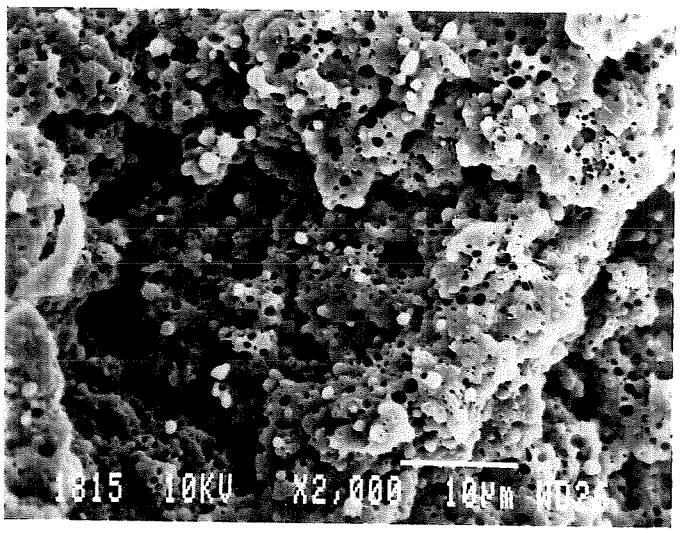

Figure 3.17 - Cont'd
C) core

With the compatibilized blends (Fig. 3.17), the fracture surfaces do not show evidence of microstretching. A highly oriented subskin is shown in Fig. 3.17B. In the core the dispersed phase is spherical and much finer (Fig. 3.17C). The yield stress is about the same as the one observed in type I samples. This confirms that in the compatibilized blend the dispersed phase adhesion to the matrix is sufficient to prevent significant debonding until at least the yield point.

3.4 CONCLUSION

The measured effect of the compatibilizer on the mechanical properties of injection molded high density polyethylene/polyamide-6 depends greatly on the mold shape and on testing direction. In directly molded tensile samples without weldline, the highly stretched polyethylene particles oriented parallel to the applied stress bear their fraction of stress and the yield stress is independent of the presence of the compatibilizer. The strength loss due to the presence of the weldline is about 40% in the absence of the compatibilizer in directly molded tensile samples but becomes negligible when the compatibilizer is added.

When test specimens are machined from molded plaques in which the weldline was produced by placing a circular insert to divide the flow, the weldline effect is much less pronounced. In the absence of the compatibilizer a strength loss of about 15% is recorded (compared to samples machined from the plaque without an insert). In

addition, the uncompatibilized blend exhibits significant flow anisotropy. The compatibilized blend is essentially isotropic and maintains the same strength in the presence of the weldline.

3.5 REFERENCES

1. L.A. Utracki, *Polymer Alloys and Blends: Thermodynamics and Rheology*, Hanser Publishers, Munich, Chap I. (1989).
2. B.D. Favis, *Can. J. Chem. Eng.*, **69**, 619-625 (1991).
3. P. Van Gheluwe, B.D. Favis, J.-P. Chalifoux, *J. Mat. Sci.*, **23**, 3910 (1988).
4. Z. Tadmor, *J. Appl. Polym. Sci.*, **18**, 1753 (1974).
5. C. Robeson, *Polym. Eng. Sci.*, **27**, 1591 (1987).
6. B. Fisa, in "*Composites Materials and Technology, Processing and Properties*, P.K. Mallick and Newman, eds., chap. 9, p. 265-320, Hanser Publishers, Munich (1990).
7. R. Boukhili, R. Gauvin, *Plast. Rubber Process. and Appl.*, **11**, 17-22 (1989).
8. E. Nolley, J.W. Barlow, D.R. Paul, *Polym. Eng. Sci.*, **20**, 364 (1980).
9. D.W. Bartelett, J.W. Barlow, D.R. Paul, *J. Appl. Polym. Sci.*, **27**, 2351-2360 (1982).
10. C.R. Lindsay, D.R. Paul, J.W. Barlow, *J. Appl. Polym. Sci.*, **26**, 1-8 (1981).
11. B. Brahimi, A. Ait-Kadi and A. Ajji, *SPE ANTEC Tech. Papers*, **37**, 1129 (1991).

12. R. Armat and A. Moet, *Polym.*, **34**, 977 (1993).

13. J. Karger-Kocsis, I. Csikai, *Polym. Eng. Sci.*, **27**, 241 (1987).

14. B. Fisa, B.D. Favis, S. Bourgeois, *Polym. Eng. Sci.*, **30**, 1051 (1990).

15. R.C. Thamm, *Rubb. Chem. Tech.*, **50**, 24 (1977).

16. S.C. Maguarnera and D.C. Riggs, *Polym. Plast. Tech. Eng.*, **17**, 193 (1981).

17. B. Fisa, A. Bouti, B. Favis and F. Lalande, *SPE ANTEC Tech. Papers*, **37**, 1135 (1991).

18. S. Fellahi, Ph.D. thesis, Mech. Eng. Dept., École Polytechnique de Montréal (1994).

19. S. Fellahi, B. Fisa, B.D. Favis, *SPE ANTEC Tech. Papers*, **39**, 211 (1993).

20. S. Fellahi, B.D. Favis and B. Fisa, to be published.

21. S.Y. Hobbs, M.E.J. Dekkers and V.H. Watkinson, *J. Mat. Sci.*, **23**, 1225 (1988).

22. G.D. Gilmore and R.S. Spencer, *Modern Plastics*, **4**, 117 (1951).

23. L.R. Schmidth, *Polym. Eng. Sci.*, **14**, 797 (1974).

24. E.D. Hagerman, *Plast. Eng.*, **10**, 67 (1973).

25. P.G. Charalambides, *J. Am. Ceram. Soc.*, **73**, 1674 (1990).

26. A. Meddad and B. Fisa, *Polym. Eng. Sci.*, in press.

27. J.P. Trotignon, J.L. Lebrun and J. Verdu, *Plast. Rubb. Proc. Appl.*, **2**, 1249 (1982).

28. A. Meddad, S. Fellahi, M. Pinard and B. Fisa, *SPE ANTEC Tech. Papers*, **40** (1994).

29. P. Vollenberg, D. Hienkens and H.C.B. Ladan, *Polym. Comp.*, **9**, 382 (1988).

30. E.A.A. Van Hartingsvelt, Ph.D. thesis, Delft university, The Netherlands (1987).

31. B. Fisa and M. Rahmani, *Polym. Eng. Sci.*, **31**, 1330-1336 (1991).

32. H. Yokoi, H. Watanabe and K. Oka, *SPE Antec Tech. Papers*, **37**, 367 (1991).

33. G. Menges, A. Troost, J. Koske, H. Ries and H. Stabrey, *Kunstst. Ger. Plast.*, **78**, 806 (1988).

34. R.M. Criens and H.C. Mosle, *Polym. Eng. Sci.*, **23**, 591 (1983).

CHAPTER 4

TENSILE DILATOMETRY OF INJECTION MOLDED HDPE/PA6 BLENDS

SOMMAIRE

Afin de mieux comprendre le mécanisme de déformation des mélanges HDPE/ PA-6 (25 vol%/75 vol%) (compatibilisé ou non) moulés par injection, le changement de volume a été mesuré grâce à la technique de dilatométrie durant un test de traction. Des éprouvettes de traction (dog-bone) ont été soit découpées à partir de plaques soit moulées directement. Il faut noter que ces mélanges ainsi que les matériaux vierges qui les constituent ont été testés.

Pour les éprouvettes moulées directement, tous les matériaux considérés dans cette étude : PA-6, HDPE et leurs mélanges dans les même proportions que ci-dessus, se déforment par écoulement par cisaillement. La nature de la phase dispersée a permis de mettre en évidence l'effet de l'orientation induite par l'écoulement. Dans le cas d'une phase dispersée souple (HDPE), elle n'a d'autres choix que de se déformer en supportant une part des contraintes appliquées et l'effet du compatibilisant est masqué par cette orientation. Par contre, dans le cas d'une phase dispersée rigide (billes de verre) dans les même proportions qu'avant, l'effet du traitement de l'interface est très évident. On passe d'un mode cavitation (45 %)/écoulement par cisaillement à un processus de déformation presque par pur écoulement en cisaillement (85 %).

Pour les éprouvettes découpées à partir de plaques de PA-6 ou HDPE, elles se déforment principalement par écoulement par cisaillement. Dans la direction transversale à l'écoulement et pour le mélange non compatibilisé, le mécanisme de déformation est un mélange de cavitation (55 %)/écoulement par cisaillement; par contre, dans la direction longitudinale, c'est un mécanisme par écoulement par cisaillement (80 %). Ceci peut être attribué à l'orientation induite par l'écoulement comme mentionné ci-dessus. L'addition d'un compatibilisant transforme le mécanisme de déformation en écoulement par cisaillement (85 %). Le même comportement est observé dans la direction longitudinale pour les deux mélanges avec ou sans compatibilisant. L'épaisseur de la plaque semble avoir un effet appréciable sur le processus de déformation.

Le comportement dilatationnel dépend énormément du type de morphologie engendrée par l'orientation induite par l'écoulement. Le rapport peau/coeur, qui est une indication de la proportion de la phase dispersée orientée par rapport à celle non orientée, joue un rôle déterminant dans le mécanisme de déformation mis en jeux.

4.1 INTRODUCTION

Polymer blends represent an area of growing interest to both scientific and industrial communities. These materials are physical blends of two or more polymers most often compatibilized through the introduction of a third agent or developed in-situ through reactive processing[1-4].

In order to assess the mechanical performance in tension, it is standard procedure to rely on the usual stress/strain curve to obtain the stress at break and yield, the elongation at break and yield, the modulus, and Poisson's ratio. However, through the combined use of longitudinal and transverse extensometers much more information can be obtained. In the latter case the volume strain of the sample can be monitored and subsequently related to the various processes of deformation which may take place during the course of the experiment.

Injection molded parts are known to exhibit a three layer structure: skin/subskin/and a core. Depending on the thickness of the part, the size of each layer may vary due to orientation, cooling and/or crystallization considerations[5,6]. This is expected to have a profound effect on the mechanism of deformation in such systems.

Volume strain can be a useful indicator of the various processes which may occur during the course of the usual stress-strain experiment. Prior to yielding, there is primarily an elastic volume dilatation, normally expressed as the Poisson's ratio. After yielding, the volume behaviour reflects the relative extent of phenomena which do not display any volume change (shear yielding, shear band deformation and cold drawing), as compared to cavitational phenomena (crazing, microvoiding). In the literature different methods have been developed to study dilatational phenomena: 1) liquid displacement dilatometer[7-11], 2) use of two or three extensometers[12-16], 3) use of strain gauges[17].

The dilatometry technique was initially developed to obtain information on deformational mechanisms:[7,10-16,18-21]. Bucknall and co-workers[12] were the first to introduce this approach, to evaluate quantitatively, the deformation mechanism responsible for toughening. This technique was used to study craze formation in rubber-modified plastics during a creep experiment. The rate of volume change can be related directly to the rate of crazing. Bucknall and Clayton[22] applied this technique to compression molded HIPS during a creep test. Three deformation steps were observed: 1) an instantaneous dilatation attributed to an elastic response, 2) a slow dilatation, 3) a rapid dilatation. Steps 2 and 3 are attributed to crazing. In a recent paper, Naqui and Robinson[16] applied tensile dilatometry to polymethylmethacrylate (PMMA) and talc-filled polypropylene (PP). The engineering constants: tensile modulus and lateral contraction ratio were measured and found to be viscoelastic. The volume strain response revealed a significant cavitation-type mechanism in the case of talc-filled PP, whereas PMMA showed a shear yielding mechanism. The volume strain was found to be directly related to the bulk modulus for these materials. The authors suggest a new method of presenting the results: volume strain versus stress.

Other authors have used tensile dilatometry to assess interfacial bonding in multiphase systems[7,11,23-25]. The technique has been applied to polystyrene (PS)/low density polyethylene (LDPE) blends by Coumans et al.[7] to measure the sample volume change. It was found that Poisson's ratio was highly dependant on the presence of the

compatibilizer. The authors also reported that shear banding increases with the level of compatibilizer.

The volume change of injection and compression molded high density polyethylene (HDPE)/polystyrene (PS) and (HDPE/polyether copolymers (PEC))/PS compatibilized with various amounts of a triblock copolymer (SEBS) based on styrene-butadiene was studied during uniaxial mechanical straining[11]. A reduced volume dilatation on adding SEBS, was observed, indicating better interfacial adhesion between the components of the first blend. The dilatational behavior of the second blend was substantially less suggesting more effective compatibilization. Microscopy results confirmed the above findings by showing the existence of good interfacial adhesion. Compression molded samples behaved differently, and these differences were attributed to morphological phenomena. In some cases, the authors reported that the volume dilatation peaks at the yield stress but decreases after yielding as a result of reduced load on the sample.

Despite a certain body of literature on the subject of tensile dilatometry, no detailed work has been undertaken to elucidate the mechanism of deformation involved in injection molded parts with variable geometry. This lack of information becomes even more crucial when it comes to multiphase systems in general and polymer blends in particular. It is therefore the aim of the paper to consider the use of tensile dilatometry to investigate the process of deformation involved in injection molded HDPE/PA-6 and

glass beads filled PA-6. The role of interfacial modification on both systems in affecting the mechanism of deformation will also be shown. As well, the influence of the geometry of the mold cavity to emphasize molecular and dispersed phase orientation and its influence on the deformation mechanism, will also be considered.

4.2 EXPERIMENTAL

4.2.1 Materials

The polyamide-6 (PA-6) is a Zytel 211 from E.I. Dupont Inc. with a number average molecular weight, M_n = 25000 g/mole. A high density polyethylene from Dow Chemical Canada (Dow 06153C) having a melt flow index of 6.3 g/10 min, M_n = 20200 g/mole, and M_w = 81300 g/mole was selected as a minor phase. The compatibilizing agent having M_n = 25000 g/mole is an ionomer (Surlyn 9020, Dupont Canada Inc.) a terpolymer consisting of 80% of ethylene and 20% mixture of methacrylic acid and isobutyl acrylate. The methacrylic acid is 70% zinc neutralized. The polyethylene is stabilised with 0.2% antioxidant (Irganox 1010 of Ciba Geigy). Glass beads (untreated and silane treated), obtained from Potters Ballotini were used as fillers in complementary experiments. The average bead diameter is about 45 μm.

4.2.2 Compounding

The first operation consists of mixing the polyethylene with 0.2 wt% antioxidant in a single screw extruder. Then, using a twin-screw extruder, 10 vol% of the ionomer (I) are admixed to the stabilized PE. Finally, 25 vol% polyethylene (PE) with or without compatibilizer, or 25 vol% of glass beads, were incorporated into polyamide-6 (PA6). Prior to a typical mixing operation, the sample mixture was dried overnight at 90°C under vacuum to minimize hydrolytic degradation of the polyamide during processing. The polymer blending was carried out on a ZSK-30 (Werner-Pfleiderer) intermeshing, co-rotating twin-screw extruder with a screw length to diameter ratio, L/D of 40. Feeding was performed under nitrogen and vacuum was applied in the decompression zone. The blending conditions can be found in refs[26,27]. Neat PA6 has been twin-screw extruded to give it the same thermal history as the PA6 in the blends.

4.2.3 Injection Molding

The injection molding machine used is a Battenfeld type BA-C 750/300, with a clamping force of 80 tons. Two experimental molds, both with interchangeable cavities were employed. A rectangular plaque (127 mm x 76 mm x 2, 4 and 6 mm cavity depth) is used. It is provided with a 2 mm deep flash gate fed with a trapezoidal duct having a section varying from 30 to 50 mm^2. Tensile test bars were cut at different locations and termed as type II specimens (Fig. 4.1). Directly molded 3 mm dogbone tensile bars

(type I in Fig. 4.1) were produced. As received neat PA6, HDPE, as well as the prepared compounds were injection molded. The molding conditions are the same for both types and are reported elsewhere[26,27].

4.2.4 Tensile Testing

Prior to testing all samples were conditioned at 23°C and 50% R.H. for several days. The ASTM D638 standard was followed. Type I samples were tested directly while a special dogbone shaped sample was designed to make the best use of the type II plaques. Samples were machined transversally at different positions (B, M and E) and longitudinally (L) from plaques as illustrated in Fig. 4.1. A universal tensile machine was used with a cross-head speed of 5 mm/min, and 2.5 kN maximum load, to generate the stress-strain curves. For the latter case, an MTS extensometer (632.13C.20) with a 10 mm gage length was used. The load and axial extension were recorded using a data acquisition software.

4.2.5 Tensile Dilatometry

The tensile test was carried out according to ASTM D638. The volume change measurement was carried out during the tensile test using the above mentioned axial extensometer, and an Instron transverse extensometer model 2640.007. It is assumed that the deformation in the thickness is equal to that in the width[24]. Both extensometers

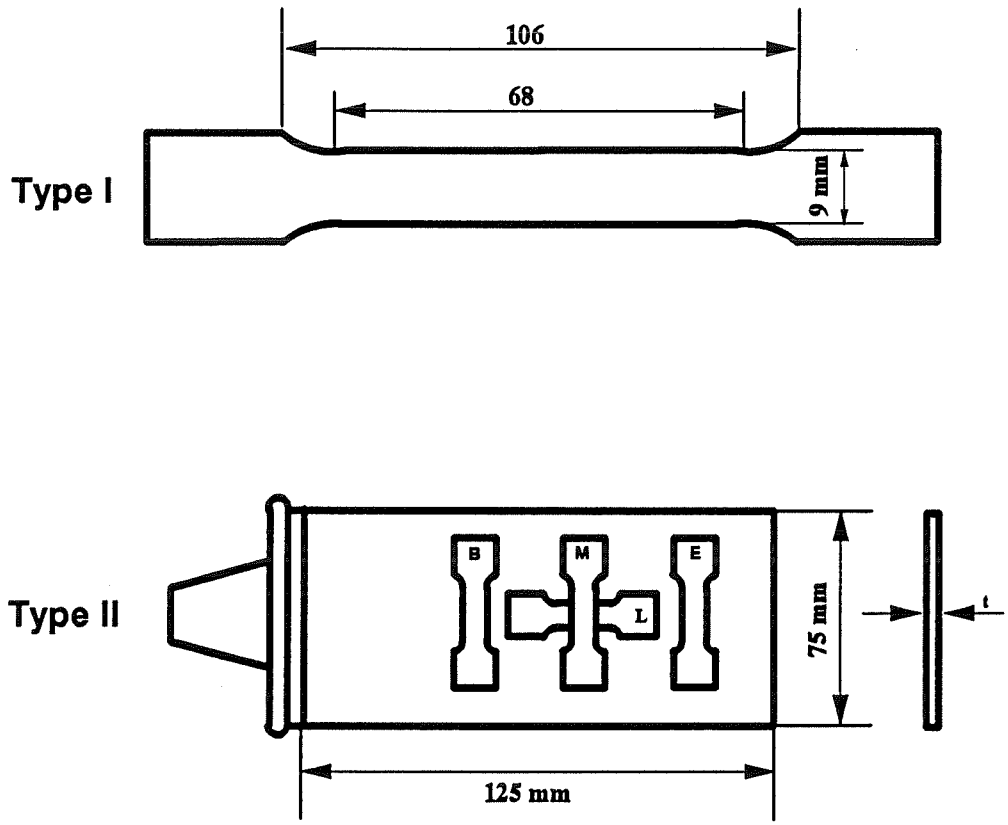

Figure 4.1 - Mold cavities used in this work. Type I molded tensile specimens. Type II- rectangular plaque with location at which samples were machined.

were attached to the specimen. Lateral and axial extension were recorded simultaneously on a PC using a data acquisition software. From the axial strain (ϵ_a), and the transverse strain (ϵ_T) one can compute the volume strain ($\Delta V/V_0$) as:

$$\Delta V/V_0 = (1 + \epsilon_a)(1 + \epsilon_T)^2 - 1 \tag{4.1}$$

and Poisson's ratio as:

$$\nu = -\frac{\epsilon_T}{\epsilon_a} \tag{4.2}$$

Note that ϵ_T assumes a negative value. In addition to that, in a plot of ($\Delta V/V_0$) versus (ϵ_a), a postyield slope of one indicates that the mechanism of deformation is due to pure crazing, while for a nil postyield slope, the mechanism which prevails is pure shear yielding with no volume change. A mixed mode mechanism of deformation will situate itself between the two extremes.

4.2.6 Scanning electron microscopy

The surfaces of samples which had been deformed up to 15% axial strain, were freeze fractured, coated with a layer of gold/palladium, and observed under a Jeol 820 scanning electron microscope at 10 kV.

4.3 RESULTS AND DISCUSSION

Most of the published literature concerning the mechanical properties of injection molded articles reports on the use of a directly molded dog-bone type specimen. In actual applications however a plaque-type mold is more representative. For this reason a comparison was carried out between the two specimen types. Another advantage in using plaques is that the mold thickness can be varied hence allowing one to modify the skin/core ratio and evaluate the influence of orientation. Plaque specimens also allow for the measurement of the transverse properties.

4.3.1 Directly molded dogbone specimens (type I)

Influence of a rigid or deformable minor phase

Neat Polymers

The behavior of PA-6 can be described as follows: in the range of strains studied ($< 10\%$) the PA-6 stress-strain curve has not reached a maximum (Fig. 4.2). However during the first elastic stage which is observed at (0-1%) the Poisson ratio is 0.48. It is worth noting that the volume change versus axial deformation is almost linear after the initial increase due to the elastic effect, as shown on Fig. 4.3. The ΔV is essentially negligible, and the mechanism of deformation which prevails is shear yielding (post-yield

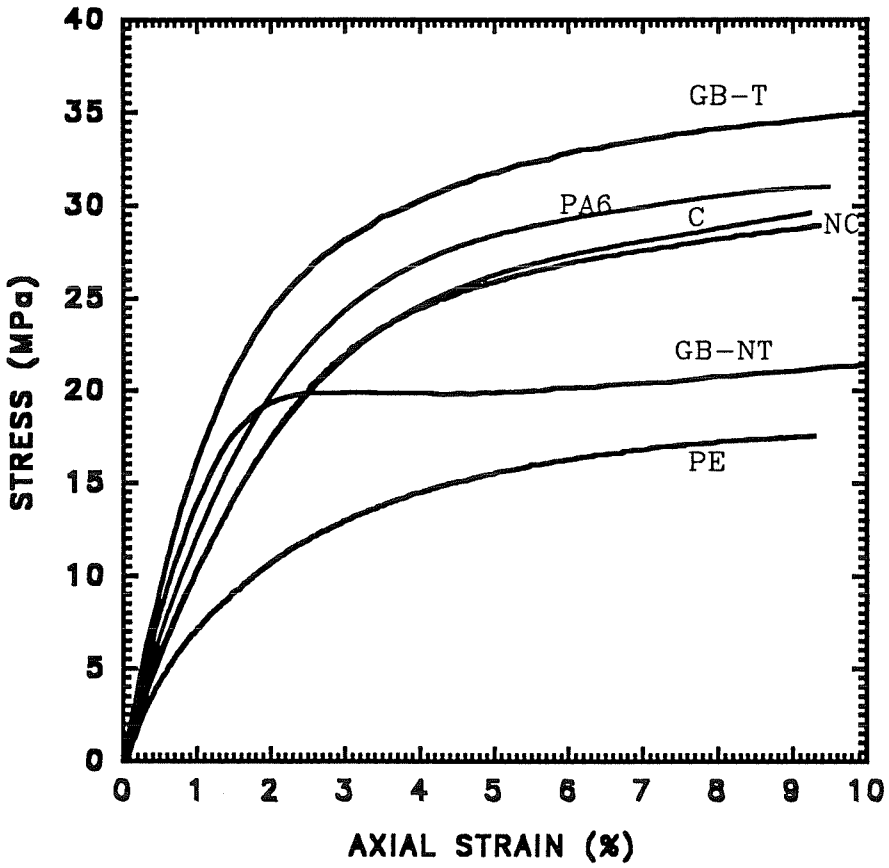

Figure 4.2 - Stress versus strain curves for type I specimens for different materials: PA-6; HDPE; GB-T: treated glass beads filled PA-6; GB-NT: untreated glass-beads filled PA-6; C and NC: with and without compatibilizer respectively for HDPE/PA-6

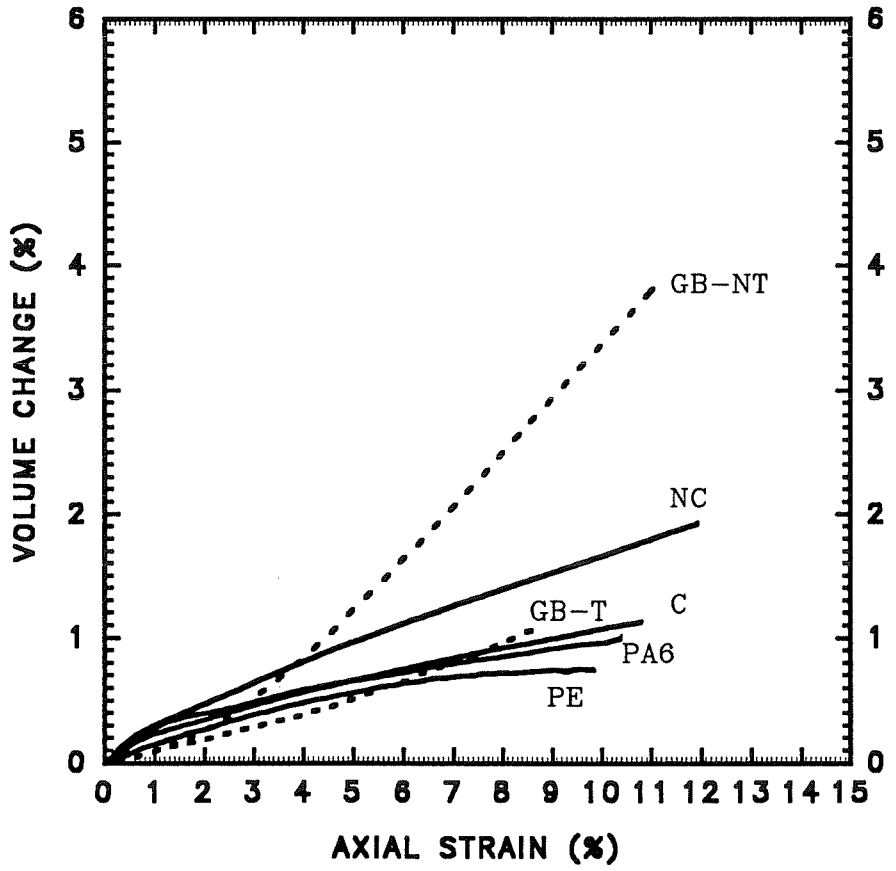

Figure 4.3 - Volume change versus axial strain of type I specimen. Same notation as in Fig. 4.2

slope: 0.06 as shown in Table 4.1), as already reported in the literature[24].

With respect to the behavior of HDPE there is a ΔV increase of approximately 0.5% up to the yield point due to elastic deformation, and beyond that no volume change is observed (Fig. 4.3). This indicates a shear yielding process of deformation (Table 4.1).

Table 4.1 Post-yield slope and Poisson ratio (ν) at 0.5% axial deformation. Directly molded (Type I) specimens. (C and NC): with and without compatibilizer respectively. (*): 25 vol% glass bead filled PA-6, (T) treated and (NT) non-treated.

Materials	Slope	Poisson ratio
PA-6	0.06	0.47
HDPE	0.04	0.42
NC	0.16	0.45
C	0.10	0.465
25-NT*	0.45	0.46
25-T*	0.15	0.47

Blend with rigid dispersed phase

The comparison of various materials used in this work at small strains provides a very valuable insight into their behavior as shown in Fig. 4.2. To draw the stress/strain curves, the strain was assumed to be identical to the extensometer

displacement. Fig. 4.2 shows the stress-strain curves of both blends, of the polyamide-6 filled with 25 vol% of glass beads; (untreated and silane treated), as well as those of both neat starting materials (PE and PA6). In the polyamide containing poorly adhering glass beads (curve GB-NT), the stress reaches a maximum at about 2% strain. The yield stress of this material is approximately equal to that of the unfilled polyamide reduced by the factor representing the area occupied by glass beads. This confirms work in a previous study where it was shown that at yield essentially all the glass beads debonded from the matrix[28]. With untreated glass beads and with the non-compatibilized blend (NC) the interfacial debonding begins at about the same level of strain i.e. 1.5%. However, the material filled with untreated beads dilates at a significantly faster rate (0.45 slope) than the uncompatibilized blend (0.16 slope) as shown in Fig. 4.3 and Table 4.1. SEM observations of the untreated glass beads filled PA-6 shown in Fig. 4.4a and taken after mechanical testing clearly shows debonding and significant cavitation.

Blend with deformable dispersed phase

When 25% vol of HDPE is added to PA6 a slight decrease in the tensile stress (Fig. 4.2) is recorded. This decrease has been reported in the literature[29] and is attributed to the poor interface, but it is apparent that the PE minor phase appears to bear its share of stress since the non-treated HDPE/PA-6 blend displays similar behavior as neat PA-6. In addition, as seen in Fig. 4.3 for the untreated blend, an increase in ΔV with axial strain is observed. The dependence of ΔV is linear and reaches 2% at 12%

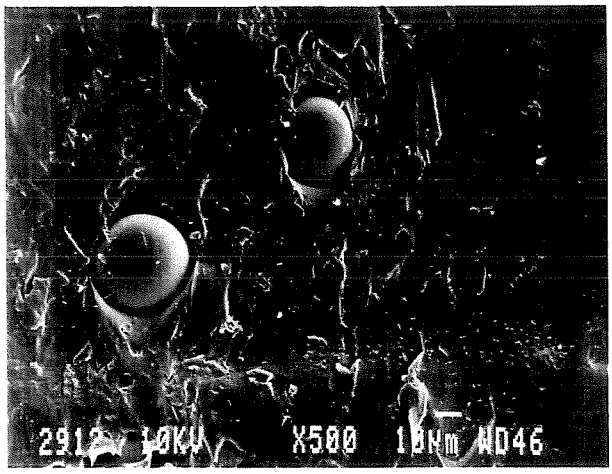

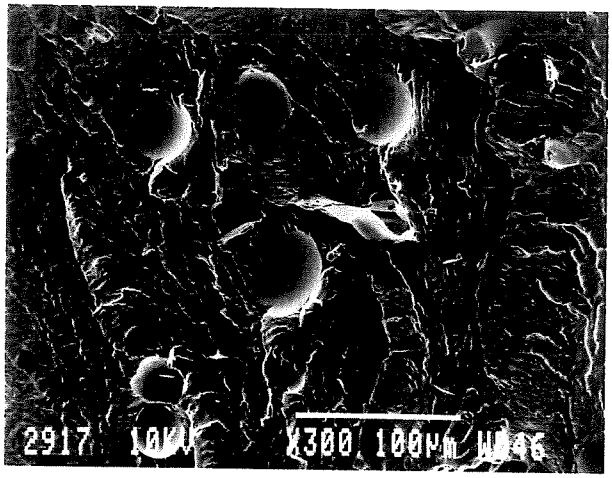

Figure 4.4 - Micrograph of fracture surface of type I glass bead filled PA-6 (transverse to flow view) - a: untreated; b: treated glass beads

axial strain. Some stress whitening was observed on the specimen. The mechanism which prevails is predominantly shear yielding (slope 0.16). When compared to neat PA6, with a postyield slope of 0.06 the difference is very small (Table 4.1). SEM observations for the non-treated HDPE/PA-6 blend clearly show extensive dispersed phase orientation in the sample. Fig. 4.5 was taken to display differences between the core and the subskin region. In fact detailed study of the skin, subskin/core ratio shows it to be 30/1. These samples therefore are essentially highly oriented except for a narrow portion in the middle.

In summary, PA-6 filled with a rigid dispersed phase shows significant differences in both the stress-strain and dilatometric behavior (increased cavitational phenomena) when compared with neat PA-6. With untreated glass-beads as the minor phase, there is no chance for them to deform. Under loading, glass beads debond leading to loss of strength and formation of voids or cavitation. PA-6 with a deformable HDPE minor phase however displays much less variation with respect to neat PA-6. Morphological observations demonstrate significant cavitation at the interface for non-treated glass-beads filled PA-6 (Fig. 4.4a) and significant orientation of the dispersed phase in HDPE/PA-6 blends with a skin/core ratio equal to 30/1 (Fig. 4.5). These results strongly indicate that dispersed phase orientation plays a predominant role in determining the mechanism of deformation (cavitation/shear yielding) for non-compatibilized systems. This supposition will be examined in more detail later in the paper.

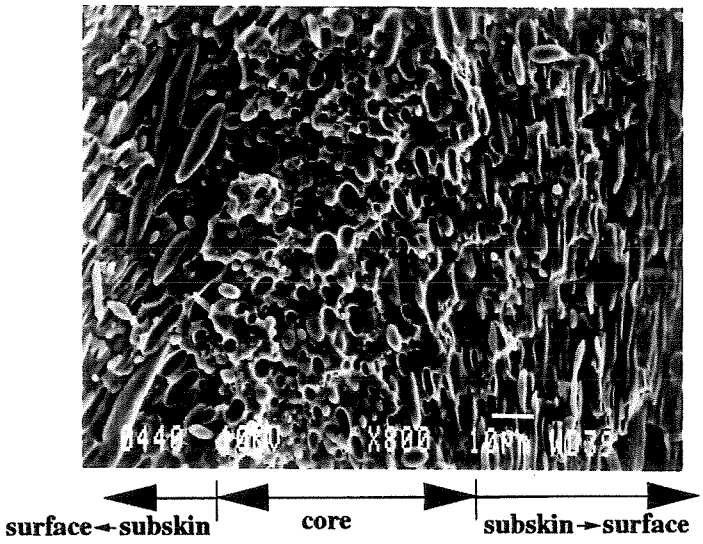

Figure 4.5 - Micrograph of fracture surface of type I non-compatibilized blend (transverse to flow view)

Effect of interfacial modification

Blend with a rigid dispersed phase

The stress-strain curve of treated glass beads filled PA-6 is shown in Fig. 4.2. When glass beads are treated with silanes little or no debonding takes place in the range of strains considered[28], and the stress borne by the material at a given strain exceeds that of the neat PA6 (curve GB-T). The rate of volume change in this system is very slow (slope: 0.15) indicating the good interfacial adhesion achieved through the use of silanes (Figs. 4.2 and 4.4). Fig. 4.4 illustrates the effect of surface treatment. While the matrix debonded from untreated beads creating elongated cavities (Fig. 4.4a), the treated beads appear to be solidly anchored to the matrix (Fig. 4.4b). This results in a more compact structure with no chance of debonding and the mechanism of deformation which prevails is shear yielding (Fig. 4.3 and Table 4.1).

Blend with a deformable dispersed phase

As shown in Fig. 4.2, the addition of a compatibilizer to the HDPE/PA-6 blend results in tensile properties very similar to the non-compatibilized case in the range of strains considered. The compatibilizer also has little effect on the dilatometric behaviour as observed in Fig. 4.3 and Table 4.1. The volume strain recorded with the compatibilized blend (postyield slope 0.10) is small. In fact it is very similar to that

recorded for both that of the neat polymer (postyield slope 0.06) as well as the polymer filled with treated glass beads (postyield slope 0.15).

This result shows that in both blends tested under these conditions the dispersed phase bears its share of stress. This may seem surprising in light of the data obtained by the tensile dilatometry (Fig. 4.3). Despite some debonding, the dispersed phase of the non-compatibilized blend can bear the same load as in its compatibilized counterpart. An elongated dispersed phase particle of variable cross-section and shape trapped in the matrix appears to deform along with the matrix in spite of the lack of interfacial adhesion. It is apparent from these results that the influence of flow induced orientation mimics the effect of compatibilization.

4.3.2 Machined from plaque (type II) specimens

Effect of HDPE minor phase

For the case of the plaque specimen, Fig. 4.6 shows that in the transverse as well as in the longitudinal direction, neat PA6 deforms by pure shear yielding (a nil postyield slope). A rapid volume increase up to 1.5% axial strain, due to the Poisson effect, is followed by a very slow volume increase suggesting isotropic properties for neat PA6. When PE is added, and after 3-4% axial deformation which corresponds to the onset of yielding, a drastic volume increase can be observed in the transverse direction. A post-

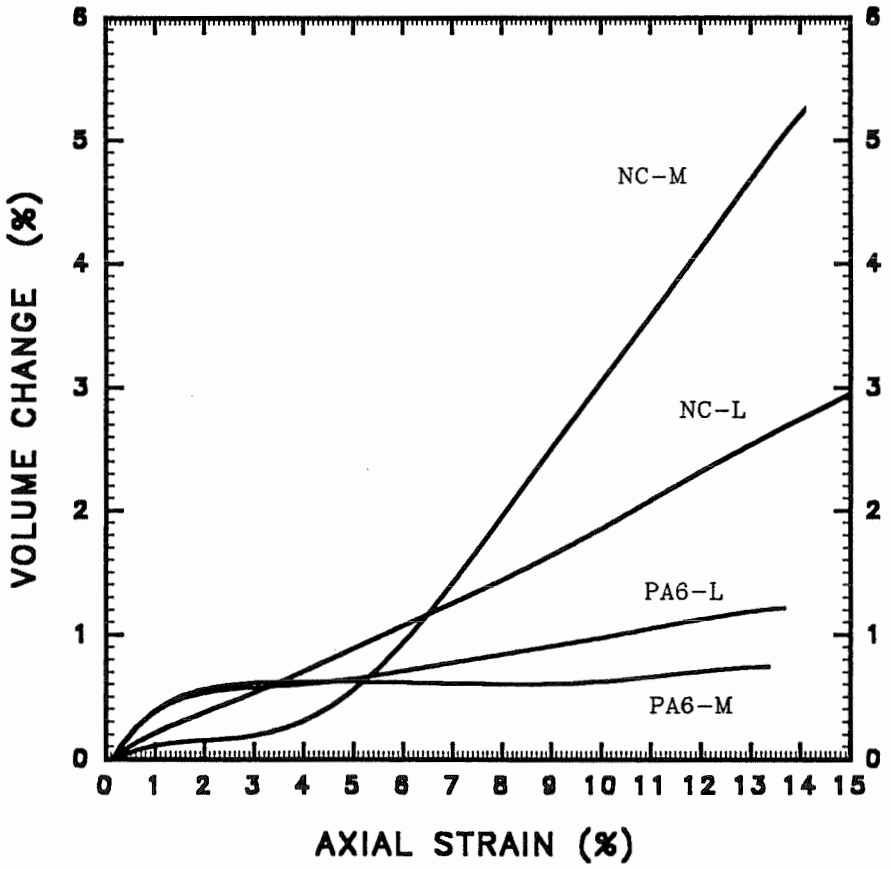

Figure 4.6 - Volume change versus axial strain for 4 mm type II specimens. Neat PA6 and non-compatibilized (NC) are compared in the transverse (at position M) and the longitudinal direction (L)

yield slope of 0.55 is obtained, indicating a mixed mechanism of deformation with 55% cavitation contribution, the remainder is due to shear yielding (Table 4.2). The volume increase is related to the poor interface and is also due to the fact that the specimen is tested perpendicular to the direction of flow. Excessive whitening is observed. In the longitudinal direction the addition of PE causes a linear volume increase up to 2.8% at an axial strain of 15% leading to 0.18 post-yield slope, greater than for neat PA6 (slope 0.007). This may be attributed to the poor interface between the components of the blends, favouring more void formation[11].

Effect of interfacial modification

Fig. 4.7 illustrates the influence of adding a compatibilizer in a 4 mm thick sample. In the longitudinal direction the addition of a compatibilizer has little effect on the dilatometric behavior, because the non-compatibilized sample experiences significant dispersed phase orientation and mimics the compatibilizing effect as discussed before (curves NC-L and C-L). The orientation phenomena is shown by SEM observations in Figs. 10a, and b. In the transverse direction, the effect of interfacial modification is more evident, since a drastic reduction in ΔV is observed. This supports previous findings[1,11], a better interface is achieved, although it can be affected by other factors such as crystallinity[30,31]. The volume increase reaches 2% at an axial strain of 15%. The postyield slope as shown in Table 4.2, changes from 0.55 for the non-compatibilized blend to 0.12 for the compatibilized one, indicating the profound effect of interfacial

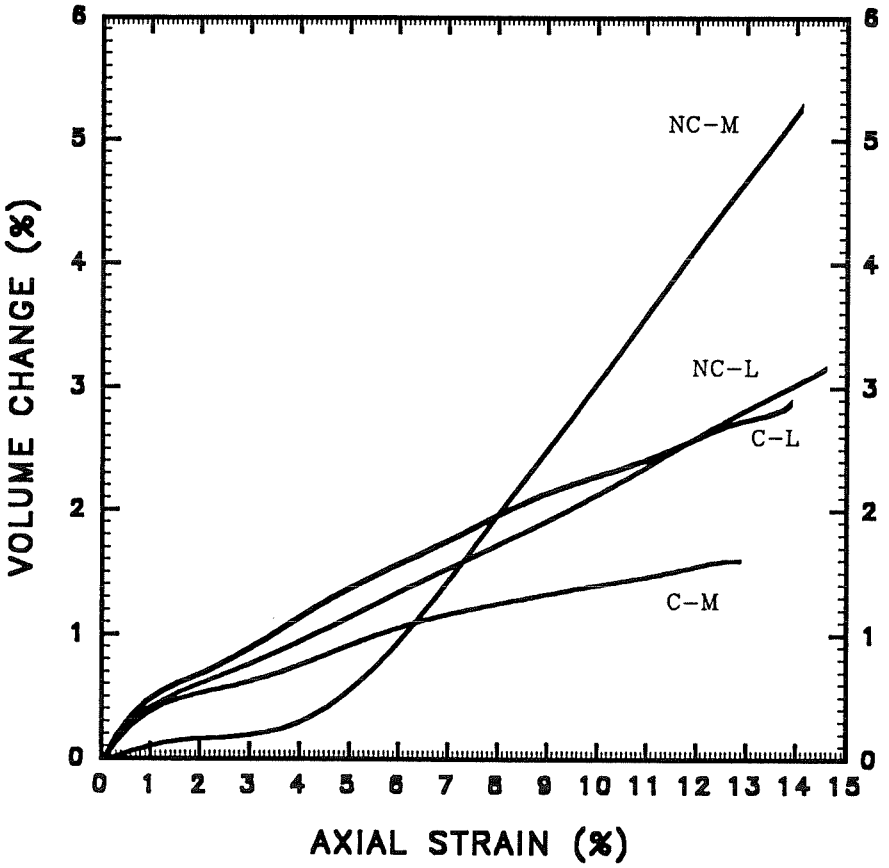

Figure 4.7 - Volume change versus axial strain of 4 mm thick type II specimens. Compatibilized (C) and non-compatibilized (NC) are compared in the transverse (at position M) and the longitudinal direction (L)

modification on the mechanism of deformation of such blends in the transverse direction. Poisson's ratio (Table 4.2 is slightly increased upon addition of the compatibilizer indicating a better interface[7].

Table 4.2 Post-yield slope and Poisson ratio at 0.5% axial deformation for Type II specimens with 2, 4, 6 mm thickness. (C and NC): with and without compatibilizer respectively. Samples were taken longitudinally (L) and transversally at position (B,M,E).

Materials	Slope	Poisson ratio
PA-6 (M)	0.007	0.48
PA-6 (L)	0.007	0.48
2-NC (M)	0.35	0.47
2-NC (L)	0.15	0.42
4-NC (M)	0.55	0.45
4-NC (L)	0.18	0.41
6-NC (M)	0.45	0.42
6-NC (L)	0.32	0.48
4-NC (B)	0.45	0.48
4-NC (E)	0.40	0.48
4-C (M)	0.12	0.45
4-C (L)	0.15	0.40

Effect of specimen position

The volume change versus axial deformation of non-compatibilized 4 mm thick specimens taken longitudinally (L) and transversally at positions B, M, E as shown on Fig. 4.1, is plotted in Fig. 4.8. A similar volume increase (starting at approximately 3% axial strain) can be observed for the samples cut transversally (position B, M, and E). This corresponds as already mentioned to the onset of yielding. Overall the effect of position is negligible, and the dilatational properties are not highly affected (see post-yield slopes in Table 4.2). Finally, the longitudinal specimen displays a linear volume increase (up to 3% at 15% axial deformation) right from the beginning. This can be attributed to orientation considerations. The anisotropy in the sample is clearly visible as well as the close relationship between the structure developed during processing and the resulting mechanical properties.

Effect of plaque thickness

The influence of plaque thickness was carried out for type II specimens with 2, 4 and 6 mm thickness, analyzed transversally (at position M) and longitudinally (L). The results are illustrated in Fig. 4.9. Generally speaking, after yielding, the volume change in the transverse direction is significantly greater than that in the longitudinal direction (post-yield $slope_T > slope_L$ as shown in Table 4.2). After a constant volume change up to 2-3% axial deformation corresponding to the limit of elasticity, ΔV starts rising

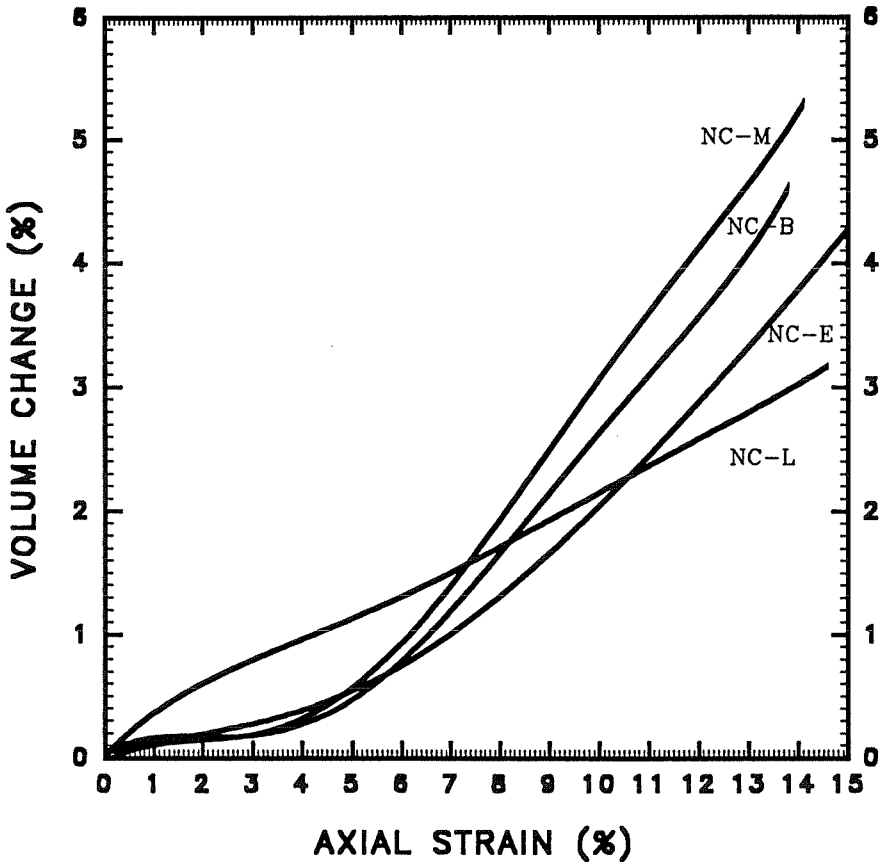

Figure 4.8 - Volume change versus axial strain of 4 mm thick type II specimens. Non-compatibilized (NC) samples taken at positions: B, M, E, L (see Fig. 4.1)

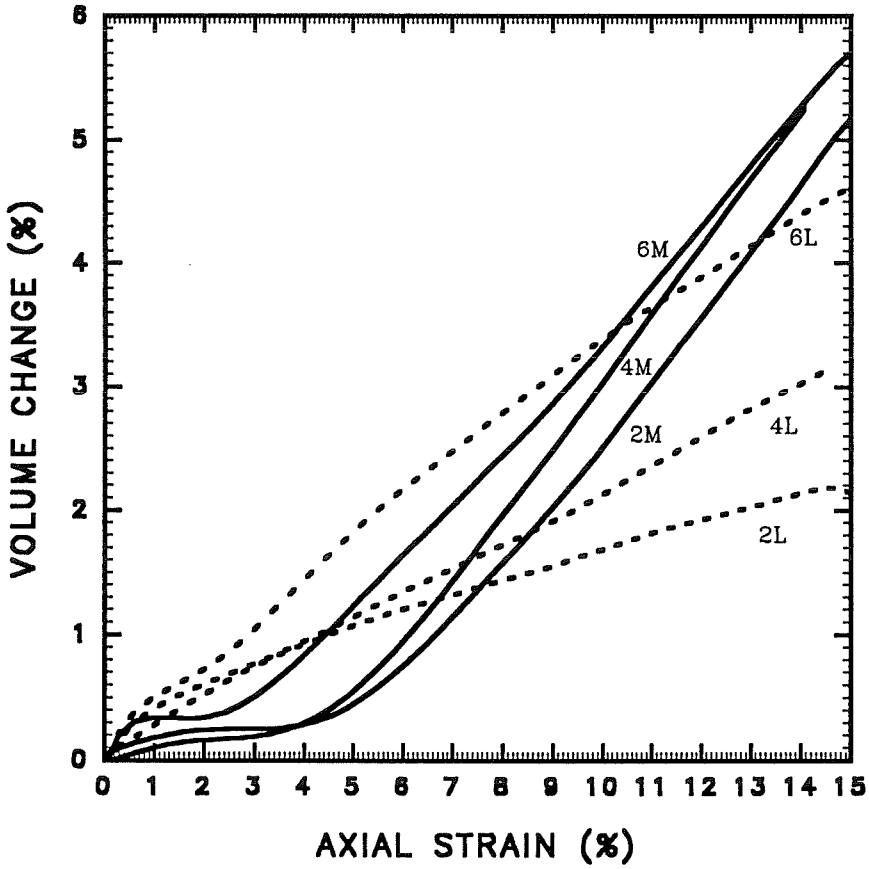

Figure 4.9 - Volume change versus axial strain of non-compatibilized (NC) type II specimens with variable plaque thickness (2, 4, 6 mm) compared in the transverse direction (at position M) and longitudinally (L)

drastically. This is in contrast to the longitudinal direction where the ΔV is linear right from the beginning. In the transverse direction, the volume changes at a given axial strain can be classified as follows: 2 mm < 4 mm < 6 mm, although the difference with respect to specimen thickness is minimal. In the longitudinal direction, the volume difference is much more noticeable with the same order as before (2 mm < 4 mm < 6 mm). For the thick specimen, the core region is larger leading to more internal cavitation as opposed to the highly oriented skin as shown in (Fig. 4.10). This will lead evidently to a higher volume change at a given axial strain. It appears that the skin to core ratio plays a major role in this case. SEM observations of samples with variable thickness concluded that the 2 mm thick specimen is composed of 150 μm core and 1850 μm skin (including subskin), the 4 mm thick sample is composed of a 2000 μm core and a 2000 μm skin (subskin included), while in the 6 mm thick sample, the core as expected is larger reaching 4000 μm leaving a skin (with subskin) of 2000 μm. The ratio of the oriented zone (skin) to the non-oriented zone (core) equals 10 for 2 mm, 1 for the 4 mm and 0.5 for the 6 mm (Fig. 4.10d,e). This clearly supports the previous findings that longitudinal dispersed phase orientation incurred during injection molding plays a strong role in determining the mechanism of deformation.

Influence of mold type

SEM studies illustrate a skin/core ratio of 30/1 for the 3 mm dogbone specimen (Fig. 4.4). For the case of the plaque (type II specimen) the skin/core ratios as discussed

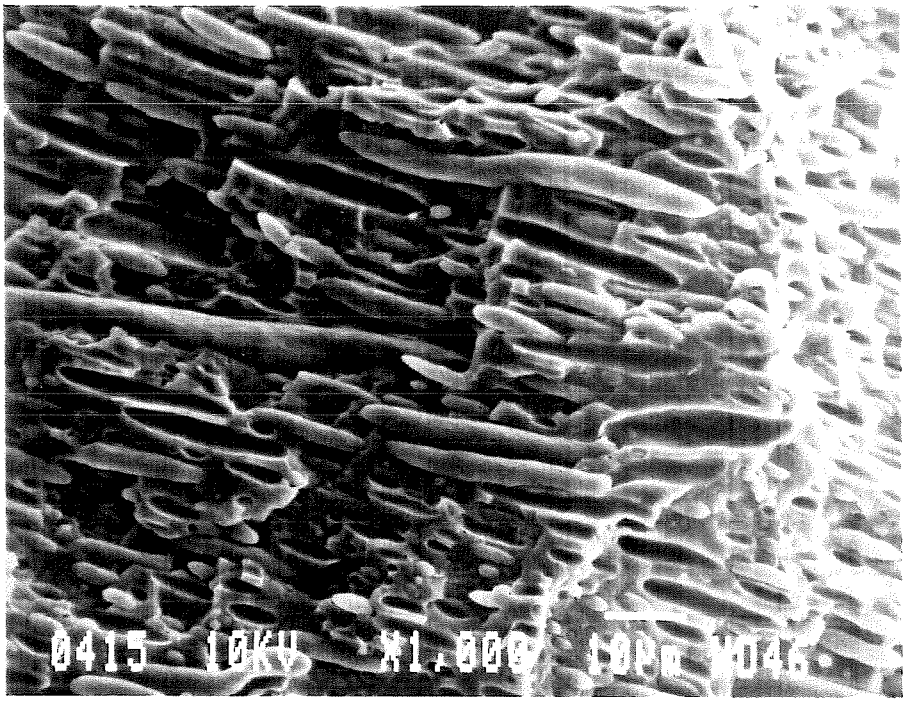

Figure 4.10 - Non-compatibilized type II samples (longitudinal to flow view) - a) in the skin; b) subskin

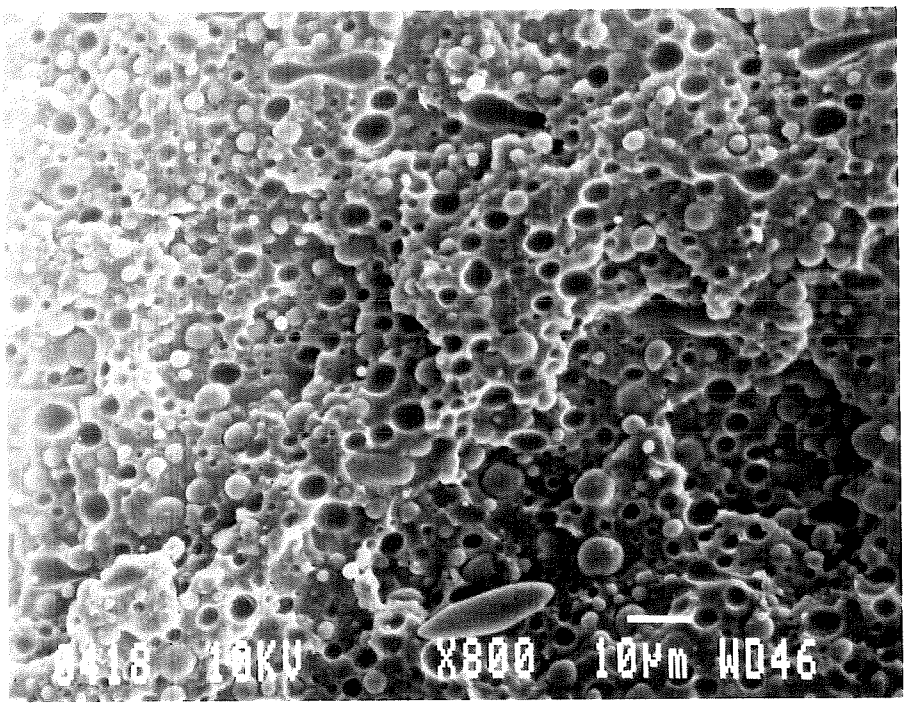

Figure 4.10 - Cont'd
c) core

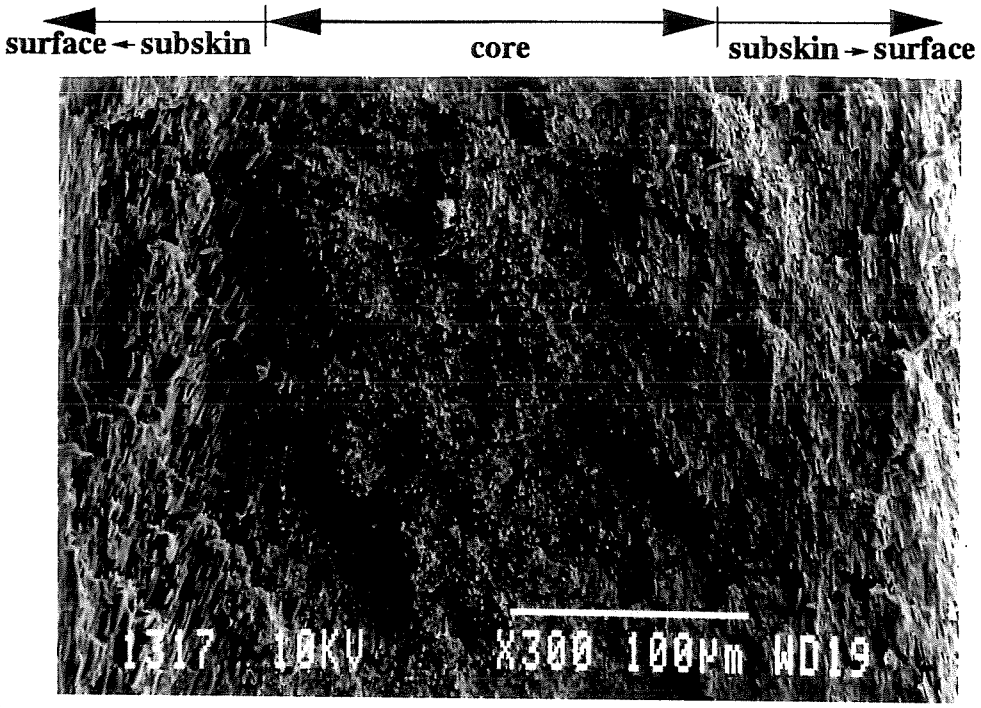

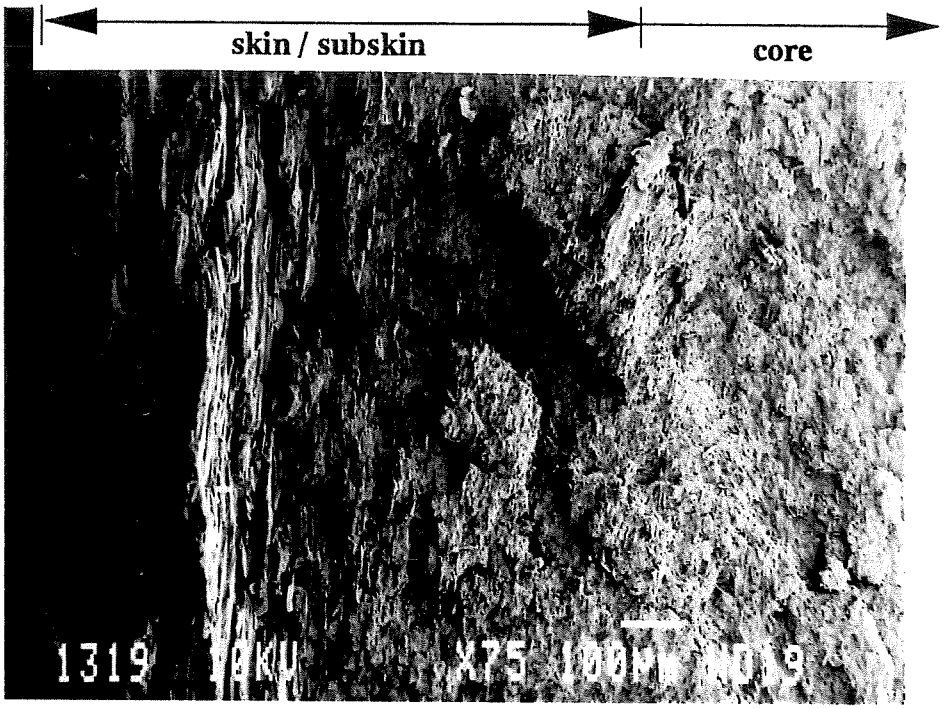

e)

Figure 4.10 - Cont'd (transverse to flow view)
d) and e) fracture surfaces of a 2 mm and 4 mm thick samples

previously were evaluated to be 0.5/1 for 6 mm, 1/1 for 4 mm and 10/1 for 2 mm thick specimens (Fig. 4.10d,e). Despite these differences, very little variation is observed in the longitudinal direction during tensile dilatometry between type I and type II specimens (Fig. 4.11). However this study has shown that the non-compatibilized blend, analyzed in the transverse direction, due to high levels of longitudinal orientation displays significantly increased cavitation behavior (slope of 0.55 in the transverse direction vs 0.18 for the longitudinal one) as shown in Fig. 4.7 and Table 4.2. This emphasizes the need to consider both longitudinal and transverse directions and illustrates the benefit of using plaques as opposed to directly molded dogbone specimens. The compatibilized blends showed little differences in their slopes (0.12 for the transverse vs 0.15 for the longitudinal case).

The most striking results in this study indicate that the deformation mechanism in injection molded non-compatibilized blends is largely controlled by orientation phenomena. Tensile dilatometry experiments taken in the direction of orientation display a predominantly shear yielding process and mimic the behavior of compatibilized systems. The importance of orientation is confirmed in studies varying the plaque thickness where the skin/core ratio is modified and also by the significant difference in longitudinal vs transverse properties. SEM micrographs clearly show the significant orientation in these systems. This phenomena appears to be principally related to the orientation of the dispersed phase since neat PA-6 behaves in an isotropic fashion.

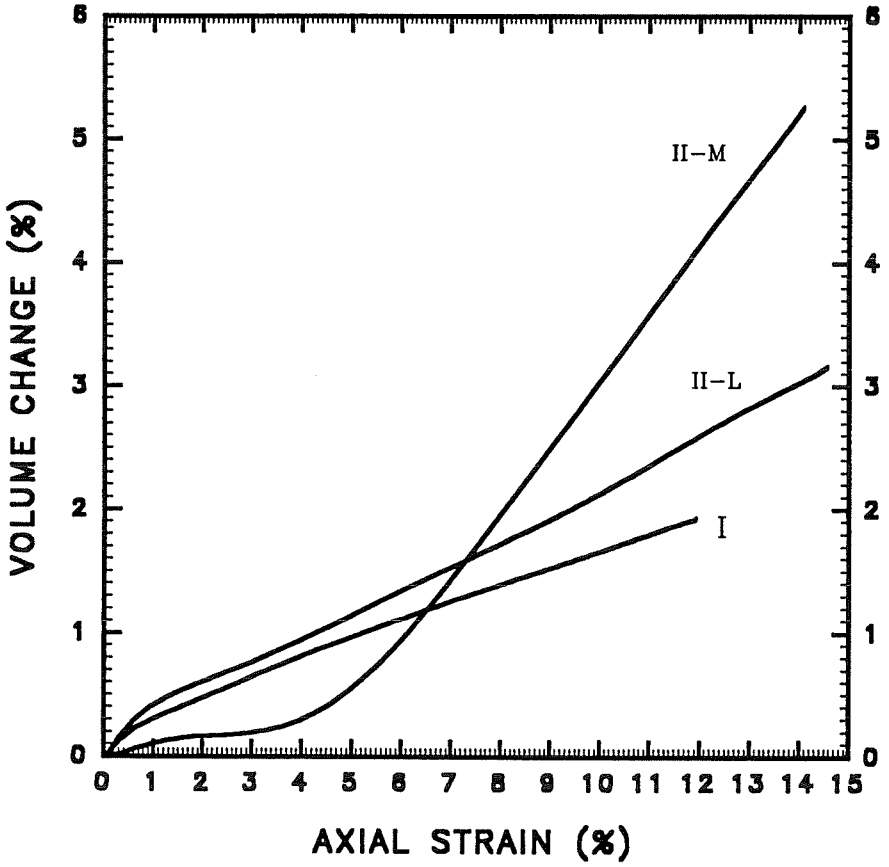

Figure 4.11 - Volume change versus axial strain of non-compatibilized (NC) blends. Comparison between type I and type II specimens (4 mm thick) taken at position M and L

4.4 CONCLUSION

Tensile dilatometry has been carried out for injection molded HDPE/PA6 blends. Directly molded (type I) and machined from plaques (type II) tensile bars were used. In type II specimens cut transversally to the flow direction, the addition of HDPE to PA6 dramatically transforms the deformation from essentially a pure shear yielding process to a mixed mode cavitation/shear yielding type mechanism. In type II cut longitudinally as well as type I specimens the flow induced orientation mimics the effect of the compatibilizer and the mechanism of deformation which prevails is almost pure shear yielding. The minor phase in the uncompatibilized blend bears its share of stress despite the debonding. This effect is even more evident when a rigid minor phase (glass beads) is substituted for HDPE where significant mechanical loss and increased cavitation is observed. The addition of interfacially modified glass beads results in a return to a predominantly shear yielding type mechanism. The most significant result in this study demonstrates a correlation between dispersed phase orientation and dilatational phenomena. Significant orientation in the longitudinal direction appreciably reduces the extent of cavitation in the unmodified blends in these samples. In fact the oriented but unmodified blends closely resembles the performance of interfacially modified samples. The dilatational behavior of the samples appears to be highly dependent on the skin/core thickness ratio.

4.5 REFERENCES

1. B.D. FAVIS, *Can. J. Chem. Eng.*, **69** (1991) 619.
2. L.A. UTRACKI, "Polymer Blends and Alloys: Thermodynamics and Rheology" (Hanser Publishers, Munich, 1989).
3. A. PLOCHOCKI, in "Polymer Blends", Edited by D.R. PAUL and S. NEWMAN, (Academic Press, New York, 1978), Vol. 1, Chap. 21, p. 319.
4. T.M. LIU, H.Q. XIE, A. O'CALLAGHAN, A. RUDIN and W.E. BAKER, *J. Polym. Sci., part B: Polym. Phys.*, **31** (1993) 1347.
5. B. FISA and M. RAHMANI, *Polym. Eng. Sci.*, **31** (1991) 1330.
6. B. FISA and A. MEDDAD, *Polym. Eng. Sci.*, in press.
7. J.W. COUMANS, D. HEIKENS, S.D. SJOERDSMA, *Polymer*, **21** (1980) 103.
8. M.E.J. DEKKERS and D. HEIKENS, *J. Appl. Polym. Sci.*, **30** (1985) 2389.
9. R.W. TRUSS and G.A. CHADWICK, *J. Mater. Sci.*, **11** (1976) 111.
10. L.G. CESSNA, *Polym. Eng. Sci.*, **14** (1974) 696.
11. M.C. SCHWARZ, H. KESKULLA, J.W. BARLOW, and D.R. PAUL, *J. Appl. Polym. Sci.*, **35** (1988) 653.
12. C.B. BUCKNALL and D. CLAYTON, *Nature*, **231** (1971) 107.
13. R.J.M. BORGGREVE, R.J. GAYMANS and H.M. EICHENWALD, *Polymer*, **30** (1989) 79.
14. D.S. PARKER, H.J. SUE and A.F. YEE, *Polymer*, **31** (1990) 2267.
15. M.A. MAXWELL, A.F. YEE, *Polym. Eng. Sci.*, **21** (1981) 205.

16. S.I. NAQUI and I.M. ROBINSON, *J. Mater. Sci.*, **28** (1993) 1421.

17. S.Y. HOBBS and M.E.J. DEKKERS, *J. Mater. Sci.*, **24** (1989) 1316.

18. I.T. BARRIE, D.R. MOORE and S. TURNER, *Plast. Rubb. Proc. Appl.*, **3** (1983) 365.

19. J.M. POWERS and R.M. CADDEL, *Polym. Eng. Sci.*, **12** (1972) 432.

20. D.C. LEACH and D.R. MOORE, *Composites*, **16** (1985) 113.

21. S.Y. HOBBS, M.E.J. DEKKERS and V.H. WATKINSON, *J. Mater. Sci.*, **23** (1988) 1219.

22. C.B. BUCKNALL and D. CLAYTON, *J. Mater. Sci.*, **7** (1972) 202.

23. A.F. YEE and R.A. PEARSON, *J. Mater. Sci.*, **21** (1986) 2462.

24. E.A.A. VAN HARTIGSVELDT, *Ph.D. Thesis*, University of Delft-Holland (1987).

25. H. BERTILSON, B. FRANZEN and J. KUBAT, *Plast. Rubb. Process. Appl.*, (1991).

26. S. FELLAHI, B.D. FAVIS and B. Fisa, *SPE Antec Tech. Papers*, **39** (1993) 211.

27. S. FELLAHI, B.D. FAVIS and B. FISA, submitted to *Polymer*.

28. A. MEDDAD, S. FELLAHI, M. PINARD and B. FISA, *SPE Antec Tech. Papers*, **40** (1994) 2284.

29. R. ARMAT and A. MOET, *Polymer*, **34** (1993) 977.

30. D.W. BARTLETT, J.W. BARLOW and D.R. Paul, *J. Appl. Polym. Sci.*, **27** (1982) 235.

31. G. MENGES, A. TROOST, J. KOSKE, H. RIES and H. STABREY, *Kunstst. Germ. Plast.*, **78** (1988) 22.

FINAL CONCLUSIONS

The morphological investigation of injection molded HDPE/PA-6 based on SEM, image analysis, XPS, DSC and TEM has clearly demonstrated the existence of a significant skin/core effect for the non-compatibilized blend manifested as a morphological variation with respect to the thickness i.e very fine dispersed phase particles in the skin, highly oriented in the subskin and spherical in the core. A detailed compositional analysis reveals the presence of both phases (HDPE and PA-6) on the surface of the plaques as well as on the melt front obtained through short-shot experiments, at approximately the same composition as in the original, as prepared blend. Interfacial modification results in a more stable morphology displaying a reduced dispersed phase size as well as the diminution of the thickness of the skin and the weldline region. The apparent absence of the dispersed phase in both the skin and weldline region as observed by SEM, is only an artefact and is demystified in this study. The very fine structure in these regions (skin and weldline) is thought to be related to particle break up resulting from the elongational flow and biaxial stretching that the particles undergo in the melt front.

The measured effect of the compatibilizer on the mechanical properties of injection molded HDPE/PA-6 blends depends greatly on the mold shape and on testing directions. In directly molded tensile samples without weldline, the highly stretched PE particles oriented parallel to the applied stress bear their fraction of stress and the yield

stress is independent of the presence of the compatibilizer. This leads to question the utility of this type of mold in evaluating the effect of a compatibilizer in a blend with a deformable and orientable dispersed phase. The strength loss due to the presence of the weldline is about 40% in the absence of the compatibilizer but becomes negligible when the compatibilizer is added. In type II mold (plaque) which represents the situation in "real parts", the weldline effect is much less pronounced for both blends. Using directly molded samples to study the effect of the weldline in molded parts, might lead to erroneous conclusions concerning material performance.

Tensile dilatometry has been carried out to study the mechanism of deformation of injection molded HDPE/PA6 blends. Directly molded (type I) and machined from plaques (type II) tensile bars were used. In type II specimens cut transversally to the flow direction, the addition of HDPE to neat PA6 dramatically transforms the deformation from essentially a pure shear yielding process to a mixed mode cavitation/shear yielding type mechanism. In type II cut longitudinally as well as type I specimens the flow induced orientation mimics the effect of the compatibilizer and the mechanism of deformation which prevails is almost pure shear yielding. The minor phase in the non-compatibilized blend bears its share of stress despite the debonding. Tensile dilatometry appears to allow for more insight into this behavior, and the effect of the compatibilizer is more evident. This result indicates that tensile dilatometry is a powerful tool, to study the effect of interfacial modification in polymer blends with a ductile matrix. The effect of a compatibilizer especially evidenced through reduced

cavitation phenomena when samples taken in the transverse direction are compared. When a rigid minor phase (glass beads) is substituted for HDPE, significant mechanical loss and increased cavitation is observed. The addition of interfacially modified glass beads results in a return to a predominantly shear yielding type mechanism. The most significant result in this study demonstrates a correlation between dispersed phase orientation and dilatational phenomena. Significant orientation in the longitudinal direction appreciably reduces the extent of cavitation in the unmodified blends in these samples. In fact the oriented but unmodified blends closely resembles the performance of interfacially modified samples. The dilatational behavior of the samples appears to be highly dependent on the skin/core thickness ratio. In this study a relationship between morphology and mechanical properties has been clearly established.

RECOMMENDATIONS FOR FUTURE WORK

From the review on the effect of weldline in injection molded parts, it is clear that the topic of the effect of the weldline in polymer blends in particular is the least documented. More investigation is therefore clearly needed. The welding aspect of two interfaces is to be considered from both experimental and theoretical sides. Experimentally, the effect of processing parameters (T_{Melt}, T_{mold}, M_w) that favor diffusional phenomena are to be considered. This should be coupled with rheological measurements (complex moduli and viscosity) to determine the relaxation time of each polymer. This information should then be used to develop the theoretical side of the welding process using Wool's approach in order to predict the strength of weldline containing parts.

The other recommendation as a continuation of the present study, is to couple tensile dilatometry with fractography to discriminate between the various cavitational phenomena reported here for injection molded HDPE/PA-6 blends.

Finally, since the weldline region is structurally different from the rest of the material, it is recommended to consider it as such. Using a Charpy test on notched samples, where the notch is placed in the weldline zone, it is possible to evaluate the strength of the weldline region. By the same token, the toughening capability of the

ionomer in injection molded HDPE/PA-6 blends can be evaluated using notched and unnotched samples without weldline.

BIBLIOGRAPHY

AGASSANT, J.F., AVENAS, P., and SERGENT, J.P., *La mise en forme des matières plastiques, Technique & Documentation* - Lavoisier, Paris (France), 96 (1986).

AKAY, M., and BARKLAY, D., *Compos. Struct.*, **3**, 269 (1985).

AKAY, M., and BARKLAY, D., *Plast. Rubb. Process. Appl.*, **20**, 137 (1993).

ALLEN, P.S., and BEVIS, M.J., *Plast. Rubb. Process. Appl.*, **7**, 3 (1987).

ALOISIO, C.J., and CAMMONS, R.R., *US. Pat.*, 4,434,120 (1984).

ANONYMOUS, Celstran Application Profile, Internal Product Information, Hoechest AG, Frankfurt (1990).

ANONYMOUS, European Patent Application EP 0 120 003 B1, Bayer AG, Leverkusen, (1989).

ARMAT, R., and MOET, A. *Polymer*, **34**, 977 (1993).

ATOCHEM, E., *Mod. Plast. Intl.*, **8**, 49 (1992).

AVRAMOVA, N., *Polymer*, **34**, 1905 (1993).

BAKER W.E., and SALEEM M., *Polym. Eng. Sci.*, **27**, 1634 (1987).

BARRIE, I.T., MOORE, D.R., and TURNER, S., *Plast. Rubb. Proc. Appl.*, **3**, 365 (1983).

BARTLETT, D.W., BARLOW, J.W., PAUL, D.R., *J. Appl. Polym. Sci.*, **27**, 2351 (1982).

BATAILLE, F., VU-KHANH, T., and FISA, B., *SPE ANTEC Tech. Papers*, **31**, 1174 (1985).

BECKER, H., MALTERDINGTON, FISHER, G., and MILLER, U., *Kunsts. Germ. Plast.*, **83**, 3 (1993).

BELL, R.G., and COOK, C.D., *Plast. Eng.*, **8**, 18 (1979).

BERTILSON, H., FRANZEN, B., and KUBAT, J., *Plast. Rubb. Process. Appl.* (1991).

BLANC, R., PHILIPON, S., VINCENT, M., AGASSANT, J.F., ALGLAVE, H., MÜLLER, R., and FROELICH, D., *Int. Polym. Process.*, **2**, 21 (1987).

BORGGREVE, R.J.M., GAYMANS, R.J., and EICHENWALD, H.M., *Polymer*, **30**, 79 (1989).

BOUKHILI, R., GAUVIN, R., and GOSSELIN, M., *SPE Antec Tech. Papers*, **35**, 1566 (1989).

BOUKHILI, R., GAUVIN, R., and GOSSELIN, M., *J. Thermoplast. Compos. Mater.*, **2**, 78 (1989).

BOUKHILI R., and GAUVIN, R., *Plast. Rubb. Process. Appl.*, **11**, 17 (1989).

BOUTI, A., and FISA, B., *SPE Antec Tech. Papers*, **37**, 2112 (1991).

BOWMAN, J., HARRIS, N., and BEVIS, M., *J. Mater. Sci.*, **10**, 63 (1975).

BOZARTH, M.J., and HAMILL, J.L., *SPE Antec Tech. Papers*, **30**, 1091 (1984).

BRAHIMI, B., and AIT-KADI, A., *SPE Antec Tech. Papers*, **37**, 1129 (1991).

BRAHIMI, R., AIT-KADI, A., and AJJI, A., *Polym. Eng. Sci.*, in press.

BREWER, G.W., *SPE Antec Tech. Papers*, **33**, 252 (1987).

BRUEHL, B., and DELPY, U., *Kunstst. Germ. Plast.*, **77**, 439 (1987).

BUCKNALL, C.B., and CLAYTON, D., *Nature*, **231**, 107 (1971).

BUCKNALL, C.B., and CLAYTON, D., *J. Mater. Sci.*, **7**, 202 (1972).

BUCKNALL, C.B., *Pure and Appl. Chem.* (IUPAC), **58**, 999 (1986).

CESSNA, L.G., *Polym. Eng. Sci.*, **14**, 696 (1974).

CHEN, C.C., and WHITE, J.L., *Polym. Eng. Sci.*, **33**, 923 (1993).

CHEN, C.C., FONTAN, E., MIN, K., and WHITE, J.L., *Polym. Eng. Sci.*, **28**, 69 (1988).

CHRISTIE, M., *Plast. Eng.*, **7**, 41 (1986).

CLOUD, P.J., McDOWELL, F., and GERARAKIS, S., *Plast. Technol.*, **22**, 48 (1986).

COUMANS, J.W., HEIKENS, D., SJOERDSMA, S.D., *Polymer*, **21**, 103 (1980).

CRAWFORD, R.J., and BENHAM, P.P., *J. Mech. Eng. Sci.*, **16**, 178 (1974).

CRIENS, R.M., and MOSLE, H.C., *Polym. Eng. Sci.*, **23**, 591 (1983).

CRIENS, R.M., *Material Chemistry and Physics*, **14**, 69 (1986).

CURRAN, R.J., *US. Pat.*, 4,191,158 (1980).

DAVIS, J.W., and MANNHERZ, E.D., *US. Pat.*, 4,403,933 (1983).

DEAN, B.D., and GEDDES, K.A., *US. Pat.*, 4,740,555 (1988).

DE GENNES, P.G., *Journal of Chem. Phys.*, **55**, 572 (1971).

DEKKERS, M.E.J., and HEIKENS, D., *J. Appl. Polym. Sci.*, **30**, 2389 (1985).

DERUDDER, J.L., TRAVER, F.J., and WANG, I.C.W., *US. Pat.*, 4,939,205 (1990).

Design of Molds for Test Specimens of Plastic Molding Material, ASTM standard Practice Norm D-647-68.

DUVDEVANI, I., *US. Pat.*, 4,407,998 (1983).

ENGBERG, K., KNUTSSON, A., WERNER, P.E., and GEDDE, U.W., *Polym. Eng. Sci.*, **30**, 1620 (1990).

FAIRLEY, G., and PRUD'HOMME, R.E., *Polym. Eng. Sci.*, **27**, 1495 (1987).

FAVIS, B.D., *Can. J. Chem. Eng.*, **69**, 619 (1991).

FAVIS, B.D., LAVALLÉE, C., and DERDOURI, A., *J. Mat. Sci.*, **27**, 4211 (1992).

FAVIS, B.D., and THERRIEN, D., *Polym.*, **32**, 1475 (1991).

FAVIS, B.D., and CHALIFOUX, J.P., *Polym. Eng. Sci.*, **27**, 1591 (1987).

FAYAL, J.E., *US. Pat.*, 4,209,558 (1980).

FELLAHI, S., FAVIS, B.D., and FISA, B., *SPE Antec Tech. Papers*, **39**, 211 (1993).

FELLAHI, S., FAVIS, B.D., and FISA, B., submitted to *Polymer*.

FELLAHI, S., FISA, B., and FAVIS, B.D., submitted to *J. Appl. Polym. Sci.*

FISA, B., and RAHMANI, M., *Polym. Eng. Sci.*, **31**, 1330 (1991).

FISA, B., DUFOUR, J., and VU-KHANH, T., *Polym. Comp.*, **8**, 408 (1987).

FISA, B., and RAHMANI, M., *Polym. Eng. Sci.*, **31**, 1330 (1991).

FISA, B., and RAHMANI, M., *Composites-90*, IMI, November, 23 (1990).

FISA, B., SANSCHAGRIN, B., and GAUVIN, R., *SPI, 46th conference preprints*, Session 9-C (1991).

FISA, B., *Composites Materials and Technology: Processes and Properties*, Chap. 7, Hanser Publishers, Munich (1988).

FISA, B., and RAHMANI, M., *Polypropylene - The Way Ahead*, International Conf., Madrid (Spain), November 9-10, 1989, Preprints published by the Rubber and Plastics Institute, London, 17 (1989).

FISA, B., FAVIS, B.D., and BOURGEOIS, S., *Polym. Eng. Sci.*, **30**, 1051 (1990).

FISA, B., SPI, 46th conference preprints, Session 9-C (1991).

FISA, B., BOUTI, A., FAVIS, B.D, and LALANDE, F., *SPE ANTEC Tech. Papers*, **37**, 1135 (1991).

FITCHMUN, D.R., and MENCIK, Z., *J. Polym. Sci., Part B: Polym. Phys.*, **11**, 951 (1973).

FRITCH, L., *Plast. Eng.*, **5**, 68 (1979).

FUKUDA, M., ICHIKAWA, Y., KATTO, T., and NITOH, T., *JPX. Pat.*, 4,935,473 (1990).

GAGGAR, S.K., *US. Pat.*, 5,128,409 (1992).

GARCIA, R.A., KOSIN, J.A., MOONEY, G., and TARQUINI, M.E., *US. Pat.*, 5,037,580 (1991).

GARDNER, G., and MALLOY, R., *SPE Antec Tech. Papers*, **40**, 626 (1994).

GARDNER, G., and CROSS, C., *Plast. Eng.*, **2**, 29 (1993).

GENNARO, A., *Plast. Rubb. Process. Appl.*, **13**, 251 (1990).

GHIAM F., and WHITE J.L., *Polym. Eng. Sci.*, **31**, 76 (1991).

GIBSON, J.R., ALLAN, P.S., and BEVIS, M.J., *Composites Manuf.*, **1**, 183 (1990).

GILLEPSIE, J.W., VANDERSCHUREN, J.A., and PIPES, B., *SPE Antec Tech. Papers*, **30**, 648 (1984).

GILMORE, G.D., and SPENCER, R.S., *Modern Plastics*, **4**, 117 (1951).

GOETTLER, L.A. in: *Mechanical Properties of Reinforced Thermoplastics*, D. W. Clegg and A.A. Collyer Eds., Elsevier Applied Science Publishers, London (1986).

GOSSELIN, M., *M.Sc.*, Thesis, École Polytechnique de Montréal (1988).

GRENDOL, C.L., *US. Pat.*, 4,540,534 (1985).

GTS PROCESS, *British. Plast. Rubber*, 2 (1992).

GUO, M., and BOWMAN, J., *J. Appl. Polym. Sci.*, **28**, 2341 (1983).

HAGERMAN, E.D., *Plast. Eng.*, **10**, 67 (1973).

HALL, M.M., JAMES, D.I., and WATKINSON, K.M., *SPE ANTEC Tech. Papers*, **24**, 369 (1978).

HALL, W.J., and BURK, R.D., *SAE Special Publications*, **SP-710**, 49 (1987).

HEISE, B., KLOSTERMANN, L., and WOEBCKEN, W., *Colloid. Polym. Sci.*, **260**, 487 (1982).

HERTEN, J.F., and LOUIES, B., *Kunstst. Germ. Plast.*, **75**, 743 (1985).

HOBBS, S.Y., and DEKKERS, M.E.J., *J. Mater. Sci.*, **24**, 1316 (1989).

HOBBS, S.Y., DEKKERS, M.E.J., and WATKINSON, V.H., *J. Mater. Sci.*, **23**, 1219 (1988).

HOBBS, S.Y., *Polym. Eng. Sci.*, **14**, 621 (1974).

HODGKINSON, J.M., *Polym. Preprints, ACS*, **29**, 143 (1988).

HORNSBY, P.R., and RUSSEL, D.A.M., *J. Mater. Sci.*, **21**, 327 (1986).

HORNSBY, P.R., HEAD, I.R., and RUSSEL, D.A.M., *J. Mater. Sci.*, **21**, 3279 (1986).

HSIUNG, C.M., CAKMAK, M., and WHITE, J.L., *SPE Antec Tech. Papers*, **32**, 128 (1986).

HUBBAUER, P., *SPE Antec Tech. Papers*, **24**, 302 (1978).

ISHIDA, T., and ISHIDA, Y., *JPX. Pat.*, 4,560,342 (1985).

JAFFE, M., and OPHIR, Z., *US. Pat.*, 4,457,962 (1984).

JANG, B.Z., UHLMAN, D.R., and VANDER SANDE, J.B., *J. Appl. Polym. Sci.*, **29**, 4377 (1984).

JANSEN, K.M.B., and FLAMAN, A.A.M., *Executive Conference Management, Molding 1994*, Anaheim, California, March (1994).

JUD, K., KAUSCH, H.H., and WILLIAMS, J.G., *J. Mat. Sci.*, **16**, 204 (1981).

KAMAL, M.R., and MOY, F.H., *J. Appl. Polym. Sci.*, **28**, 1787 (1983).

KANTZ, M.R., NEWMAN, H.D., and STIGALE, F.H., *J. Appl. Polym. Sci.*, **16**, 1249 (1972).

KARGER-KOCSIS, J., and CSIKAI, I., *Polym. Eng. Sci.*, **27**, 241 (1987).

KATTI, S.S., and SCHULTZ, J.M., *Polym. Eng. Sci.*, **22**, 1001 (1982).

KAZMER, D.O., *SPE Antec Tech. Papers*, **40**, 631 (1994).

KIM, S.G., and SUH, N.P., *Polym. Eng. Sci.*, **26**, 1200 (1986).

KIRBY, D.B., and HEYBEY, O.W., *US. Pat.*, 4,399,093 (1983).

KOUSAI, T., MORIUSHU, Y., and ISHIDA, T., *US. Pat.*, 4,830,805 (1989).

KRASNECKY, D., *SPE Antec Tech. Papers*, **37**, 363 (1991).

KWEI, K.H., MALONE, M.F., and WINTER, H.H., *Polym. Eng. Sci.*, **26**, 1012 (1986).

KODAMA, M., and ABE, K., *Mat. Proces. Prod in interior trim, SAE special publ. #* 860 (1991).

LALANDE, F., *SPE Antec Tech. Papers*, **37**, 404 (1991).

LANTOS, P.R., *Polym. Plast. Technol. Eng.*, **26**, 313 (1987).

LEACH, D.C., and MOORE, D.R., *Composites*, **16**, 113 (1985).

LIANG, B.R., WHITE, J.L., SPRUIELL, J.E., and GOSWANI, B.C., *SPE ANTEC Tech. Papers*, **29**, 92 (1983).

LINDSAY, C.R., PAUL, D.R., and BARLOW, J.W., *J. Appl. Polym. Sci.*, **26**, 1, (1981).

LIU, T.M., XIE, H.Q., O'CALLAGHAN, A., RUDIN, A., and BAKER, W.E., *J. Polym. Sci., part B: Polym. Phys.*, **31**, 1347 (1993).

LIU, P.Y., and OVERTON, D.E., *US. Pat.*, 4,532,282 (1985).

MACKNIGHT, W.J., LENZ, R.W., MUSTO, P.V., and SOMANI, R.J., *Polym. Eng. Sci.*, **25**, 1124 (1985).

MALGUARNERA, S.C., and MANISALI, A.I., *Polym. Eng. Sci.*, **21**, 586 (1981).

MALGUARNERA, S.C., and MANISALI, A.I., *SPE Antec Tech. Papers*, **26**, 124 (1980).

MALGUARNERA, S.C., *Polym. Plast. Technol. Eng.*, **18**, 1 (1982).

MALGUARNERA, S.C., and RIGGS, D.C., *Polym. Plast. Tech. Eng.*, **17**, 193 (1981).

MALGUARNERA, S.C., *Plast. Eng.*, **35**, 5 (1981).

MALGUARNERA, S.C., MANISALI, A., and RIGGS, D.C., *Polym. Eng. Sci.*, **21**, 1149 (1981).

MALLOY, R., GARDNER, G., and GROSSMAN, E., *SPE Antec Tech. Papers*, **39**, 521 (1993).

MAVRIDIS, H., HRYMAK, A.N., and VLACHOPOULOS, J., *AICHE J.*, **34**, 403 (1988).

MAXWELL, M.A., YEE, A.F., *Polym. Eng. Sci.*, **21**, 205 (1981).

MEDDAD, A., FELLAHI, S., PINARD, M., and FISA, B., *SPE Antec Tech. Papers*, **40**, 2284 (1994).

MEDDAD, A., and FISA, B., *unpublished work.*

MEDDAD, A., M.Sc.A. thesis, École Polytechnique de Montréal, April 1992.

MEDDAD, A., and FISA, B., *Polym. Eng. Sci.*, in press.

MEKHILEF, N., *Ph.D. Thesis*, Laval University, Québec (1994).

MENGES, G., TROOST, A., KOSKE, J., RIES, H., and STABREY, H., *Kunstst. Germ. Plast.*, **78**, 22 (1988).

MENGES, G., SCHACHT, T., BECKER, H., and OTT, S., *Int. Polym. Process.*, **2**, 77 (1987).

MENGES, V.G., SCHACHT, T., and OTT, S., *Kunststoffberater*, **4**, 54 (1988).

MENGES, G., and MOHREN, P., How to Make Injection Molds, Hanser Publisher, Munich (1986).

MENNING, G., *Die Angew. Makromol. Chemie*, **185/186**, 179 (1991).

MENNING, G., *Kunst. Germ. Plast.*, **82**, 3 (1992).

MOY, F.H., and KAMAL, M.R., *Polym. Eng. Sci.*, **20**, 957 (1980).

MICHAELI, W., and GALUSCHKA, S., *SPE Antec Tech. Papers*, **39**, 534 (1993).

MILLER, *Plast. World*, **11**, 28 (1990).

MIN, K., ENDO, S., WHITE, J.L., KYU, T., and FELLERS, J.F., *SPE ANTEC Tech. Papers*, **31**, 530 (1985).

MIN, K., WHITE, J.L., and FELLERS, J.F., *Polym. Eng. Sci.*, **24**, 1327 (1984).

MOULDER, J.F. et al., *Handbook of XPS* edited by J. Chastain Perkin-Elmer, Chap. I. (1992).

MOWMAN, J., *J. Mater. Sci.*, **16**, 1151 (1981).

NADKARNI, V.M., and AYODHIA, S.R., *Polym. Eng. Sci.*, **33**, 358 (1993).

NAQUI, S.I., and ROBINSON, I.M., *J. Mater. Sci.*, **28**, 1421 (1993).

NGUYEN, K.T., GAO, D.M., GIRARD, P., and SALLOUM, G., *Executive Conference Management, Molding 1994*, Anaheim, California, March (1994).

NIELSON, L.E., *Polymer Rheology*, Marcel Dekkers Inc., NEW YORK (1977).

NOLLEY, E., BARLOW, J.W., and PAUL, D.R., *Polym. Eng. Sci.*, **20**, 364 (1980).

OLEELSKY, S.S., and MOHR, L.G., *Handbook of Reinforced Plastics*, Reinhold Publish. Corp., New York, 526 (1977).

PADWA, A.R., Presented at the 11th NRCC/IMI Symposium "Polyblends-91", Oct. 29-30, 1991, Boucherville, Québec, CANADA.

PAREKH, S., DESAI, S., and BRIZZOLARA, J., *SPE Antec Tech. Papers*, **39**, 530 (1993).

PAREKH, S., DESAI, S., and BRIZZOLARA, J., *SPE Antec Tech. Papers*, **40**, 621 (1994).

PARKER, D.S., SUE, H.J., and YEE, A.F., *Polymer*, **31**, 2267 (1990).

PICAROLLO, S., and SAIU, M., *Plast. Rubb. Process. Appl.*, **10**, 11 (1988).

PICCAROLO, S., RALLIS, A., and TITOMANLIO, G., *Int. Polym. Process.*, **2**, 137 (1988).

PICCAROLO, S., SCARGIALI, F., GRIPPA, G., and TITOMANLIO, G., *Plast. Rubb. Process. Appl.*, **19**, 205 (1993).

PISIPATI, R., and BAIRD, D.G., *Polymer Processing and Properties*, G. Astarita and G. Nicolais Eds., Plenum Publishing Corp. NY., 215 (1984).

PLOCHOCKI, A., in "Polymer Blends", Edited by D.R. PAUL and S. NEWMAN, (Academic Press, New York, 1978), Vol. 1, Chap. 21, p. 319.

POULIN, D., DIAWARA, Y., CURRIE, J.F., YELON, A., GUJRATHI, S.C., and PETROVA-KOCH, V., *Mat. Res. Soc. Sym. Proc.*, **283**, 88 (1993).

POWERS, J.M., and CADDEL, R.M., *Polym. Eng. Sci.*, **12**, 432 (1972).

PRAGER, S., and THIRREL, M., *J. Appl. Phys.*, **75**, 5194 (1981).

PRATT, C.F., PHADKE, S.V., and ERROL, O., *US. Pat.*, 4,965,111 (1990).

PRATT, C.F., PHADKE, S.V., and ERROL, O., *US. Pat.*, 5,026,776 (1991).

RAHMANI, M., *Ph.D. Thesis*, École Polytechnique de Montréal (1990).

RAHMANI, M., and FISA, B., *SPE Antec Tech. Papers*, **37**, 400 (1991).

RALLIS, A., PICCAROLO, S., and TITOMANLIO, G., *Plast. Rubb. Process. Appl.*, **9**, 181 (1988).

REMALY, L.S., and SIERODZINSKI, M.J., *SPE Antec Tech. Papers*, **27**, 724 (1981).

ROBESON, L.M., *Polym. Eng. Sci.*, **24**, 587 (1984).

ROSATO, D.V., and ROSATO, D.V., *Injection molding Handbook*, Chap. 18, Van Nostrand Reinhold, NY (1986).

RUSSEL, D.P., and BEAUMONT, P.W.R., *J. Mater. Sci.*, **15**, 197 (1980).

SAVADORI, A., PELLICONI, A., and ROMANINI, D., *Plast. Rubb. Process. Appl.*, **3**, 215 (1983).

SCHWARZ, M.C., KESKULLA, H., BARLOW, J.W., and PAUL, D.R., *J. Appl. Polym. Sci.*, **35**, 653 (1988).

SCHMIDT, L.R., *Polym. Eng. Sci.*, **14**, 797 (1974).

SCORIM, Anonymous.

SERPE, G., JARRIN, J., and DAWANS, F., *Polym. Eng. Sci.*, **30**, 553 (1990).

SINGH, D., MOSLE, H.G., KUNZ, M., and WENIG, W., *J. Mater. Sci.*, **25**, 4704 (1990).

SINGH, D., and MOSLE, H.G., *Makromol. Chem. Macrom. Symp.*, **20/21**, 489 (1988).

SWOBODA, J., LINDENSCHMIDT, G., and BERNHARDT, C., *Germ. Pat.*, 4,224,419 (1980).

TADMOR, Z., *J. Appl. Polym. Sci.*, **18**, 1753 (1974).

TAN, V., and KAMAL, M.R., *J. Appl. Polym. Sci.*, **22**, 2341 (1978).

THAMM, R.C., *Rubb. Chem. Tech.*, **50**, 24 (1977).

TITOMANLIO, G., PICCAROLO, S., and RALLIS, A., *Polym. Eng. Sci.*, **29**, 209 (1989).

TOBOLSKY, A.S., *US. Pat.*, 4,677,006 (1985).

TOMARI, K., TONAGAI, S., HARADA, T., HAMADA, H., LEE, K., MORII, T., and MAEKAWA, Z., *Polym. Eng. Sci.*, **30**, 931 (1990).

TOMARI, K., HARADA, T., MAEKAWA, Z., HAMADA, H., IWAMOTO, M., and UKAI, A., *Polym. Eng. Sci.*, **33**, 996 (1993).

TOMARI, K., TAKASHIMA, H., and HAMADA, H., submitted to *Adv. Polym. Tech.*

TROTIGNON, J.P., and VERDU, J., *J. Appl. Polym. Sci.*, **34**, 1 (1987).

TROTIGNON, J.P., LEBRUN, J.L., and VERDU, J., *Plast. Rubb. Process. Appl.*, **2**, 247 (1982).

TROTIGNON, J.P., and VERDU, J., *J. Appl. Sci.*, **34**, 19 (1987).

TRUSS, R.W., and CHADWICK, G.A., *J. Mater. Sci.*, **11**, 111 (1976).

TUSHIE, D.R., JENSEN, G.A., and BEASLY, N.F., *Engineered Materials Handbook*, **2**, Engineering Plastics, ASM International, Metals Park, OH (1988).

UTRACKI, L.A., *Polym. Compos.*, **7**, 284 (1986).

UTRACKI, L.A., *Rubber. Chem. Technol.*, **57**, 507 (1984).

UTRACKI, L.A., and FAVIS, B.D., in *Handbook of Polymer Science and Technology: Composites and Speciality Applications*, **4**, N. P. Chereminisoff edt., Marcel Dekker, Inc. (1989).

UTRACKI, L.A., *Polymer Alloys and Blends: Thermodynamics and Rheology*, Hanser Publishers, Munich, Chap I (1989).

VAN GHELUWE, P., FAVIS, B.D., and CHALIFOUX, J.P., *J. Mat. Sc.*, **23**, 3910 (1988).

VAN HARTIGSVELDT, E.A.A., *Ph.D. Thesis*, University of Delft-Holland (1987).

VERMILYE, M.L., *US. Pat.*, 4,722,821 (1988).

WAKEWFIELD, N., *Plast. Rubb. News*, **3**, 9 (1985).

WALKER, W.H., *SPE Antec Tech. Papers*, **40**, 1880 (1994).

WANG, I.C.W., *US. Pat.*, 5,045,595 (1991).

WATKINSON, K., THOMAS, A., and BEVIS, M., *J. Mat. Sci.*, **17**, 347 (1982).

WENDT, U., *Kunststoffe*, **78**, 123 (1988).

WENIG, W., SINGH, D., and MOSLE, H.G., *Die Angew. Makromol. Chem.*, **179**, 35 (1990).

WILLIAMS, M.A., BAUMAN, B.D., RUPRESHT, D.R., and MARSH, P.D., *US. Pat.*, 4,752,428 (1988).

WILLIS, J.M., FAVIS, B.D., and LAVALLÉE, C.J., *J. Mat. Sci.*, **27** (1992).

WILLIS, J.M., and FAVIS, B.D., *Polym. Eng. Sci.*, **28**, 1416 (1988).

WOOL, R.P., YUAN, B.L., and McGAREL, O.J., *Polym. Eng. Sci.*, **29**, 1340 (1989).

WOOL, R.P., and OCONNOR, K.M., *J. Appl. Phys.*, **52**, 5953 (1981).

WORDEN, E., and KUSHION, S., *SPE Antec Tech. Papers*, **37**, 2653 (1991).

XANTHOS, M., *Polym. Eng. Sci.*, **28**, 1392 (1988).

YEE, A.F., and PEARSON, R.A., *J. Mater. Sci.*, **21**, 2462 (1986).

YOKOI, H., KAMATA, S., and KANEMATSU, T., *SPE ANTEC Tech. Papers*, **37**, 358 (1991).

YOKOI, H., MURATA, Y., WATANABE, H., and OKA, K., *SPE Antec Tech. Papers*, **37**, 367 (1991).